CARDIFF UNIVERSITY
SCHOOL OF OPTOMETRY AND VISION SCIENCES

Aspects of a perimetric learning index

Aristeidis Chandrinos
Doctor of Philosophy

Cardiff University, 2017

Chandrinos Aristeidis
Doctor of Philosophy
Cardiff University,

Aspects of perimetric learning index

The purpose of this thesis was to develop further the Learning Index in perimetry and examine how it performs in different groups, with different algorithms and investigate different procedures of calculation.

The Learning Index calculated using concentric rings of visual field data, following the method of Olsson and colleagues (1997), facilitated in a MatLab environment. The used data included visual field assessment for 29 normal, 25 glaucoma and 25 ocular hypertensive individuals who followed perimetry for both eyes, for different strategies and for five consecutive visits once a week.

Alternative methods to evaluate the LI were used like the glaucoma hemifield test pattern. The influence of the different strengths of a variety of filters was also used, filtering the perimeter outcome in order to disassociate learning effect from real defects. Mean and Median filters were also used, and dissimilar Adaptive filters as well, that seemed to be robust filters that could help to establish a more sensitive Learning Index.

In automated perimetry the innovation of a Learning Index would consider and examine how individuals learn to perform better visual field tests during recurrent visits under different algorithms. The argument is if that Learning Index could allow clinicians performing visual field tests to administer their patients and control possible detected abnormality, after their first or second visual field test. In this way they will prevent development of the disease, confine patient's fatigue and provide quality of life and simultaneously financial savings for the state and private health organizations.

The carried out learning index calculations results were sufficiently encouraging for a next phase of a future index development and with likelihood in the future to be incorporated in automated perimeters algorithms.

ACKNOWLEDGMENTS

I would like to thank the following persons who helped and contributed for the completion of this thesis.

Firstly, I would like above all to thank my supervisor, Prof. John M. Wild, for his everlasting patience; his guidance; and not only his scientific, but also his personal support and encouragement.

Next I would like to express my sincere gratitude to my family, my wife Elpiniki and my lovely daughter Vasiliki, who had supported me to carry on all the difficulties throughout my project

Furthermore, I want to thank Dr. Tony Redmond for his excellent guidance and support to the final corrections of this thesis.

I am also grateful to Dr Carlo Knupp, Senior Lecturer at Cardiff School of Optometry and Vision Sciences, for the collaboration and the design of software for the calculations and Dr. Frank Rakenbrant, Mathematician, for his help in MatLab filters modulus development. Many thanks to my colleagues, Kholoud, Saleh and Eleni, have given me their friendship and, therefore, a favourable working environment.

Table of Contents

LIST OF TABLES

LIST OF FIGURES

Figure 3.13 The Total Deviation and Patterns Deviation numerical and probability plots of SITA SWAP algorithm, for right and left eye respectively, at 1st (top), 3rd (middle) and 5th visit (bottom), for OAG male patient aged 52. The reliability indices during the test show very good patient performance, and the variability Learning Index is likely to be due to the difficulty of blue on yellow strategy.

Figure 3.14 The Total Deviation and Patterns Deviation numerical and probability plots of SITA SWAP algorithm, for right and left eye respectively, at 1st (top), 3rd (middle) and 5th visit (bottom), for OHT female individual aged 71. The reliability indices during the test show poor test performance, and the high Learning Index is likely to be due to the difficulty of blue on yellow strategy and the fatigue effect that masks the learning effect.

Figure 3.15 The Total Deviation and Pattern Deviation numerical and probability plots of SITA Standard algorithm, for right and left eye respectively, at 1st (top), 3rd (middle) and 5th visit (bottom), for OHT female individual aged 53. The reliability indices during the test are in general acceptable. Although at visit 1 there appears a learning transfer from the right to the left eye, next visit illustrate high index to the left eye probably due to the fatigue from previous tests.

Figure 3.16 The Total Deviation and Pattern Deviation numerical and probability plots of SITA Fast algorithm, for right and left eye respectively, at 1st (top), 3rd (middle) and 5th visit (bottom), for OHT male individual aged 50. The reliability indices during the test are in general acceptable but the various Learning Index in both eyes is most likely due to the fatigue from previous tests.

Figure 3.17 The descriptive statistics (left panel), for the Learning Index for normal individuals (right eye), across the five visits, for each of the three algorithms. Box and Whisker plots (right panel), of the Learning Index distribution for the normal individuals (right eye), across the five visits, within algorithm for SITA Standard (top), SITA Fast (middle) and SWAP (bottom).

Figure 3.18. The descriptive statistics (left panel), for the Learning Index for OAG individuals (right eye), across the five visits, for each of the three algorithms. Box and Whisker plots (right panel), of the Learning Index distribution for the OAG individuals (right eye), across the five visits, within algorithm for SITA Standard (top), SITA Fast (middle) and SWAP (bottom).

Figure 3.19. The descriptive statistics (left panel), for the Learning Index for OHT individuals (right eye), across the five visits, for each of the three algorithms. Box and Whisker plots (right panel), of the Learning Index distribution for the OHT individuals (right eye), across the five visits, within algorithm for SITA Standard (top), SITA Fast (middle) and SWAP (bottom).

Figure 3.20 The descriptive statistics (left panel), for the Learning Index for normal individuals (left eye), across the five visits, for each of the three algorithms. Box and Whisker plots (right panel), of the Learning Index distribution for the normal individuals (left eye), across the five visits, within algorithm for SITA Standard (top), SITA Fast (middle) and SWAP (bottom).

Figure 3.21 The descriptive statistics (left panel), for the Learning Index for OAG individuals (left eye), across the five visits, for each of the three algorithms. Box and Whisker plots (right panel), of the Learning Index distribution for the OAG individuals (left eye), across the five visits, within algorithm for SITA Standard (top), SITA Fast (middle) and SWAP (bottom).

Figure 3.22. The descriptive statistics (left panel), for the Learning Index for OHT individuals (left eye), across the five visits, for each of the three algorithms. Box and Whisker plots (right panel), of the Learning Index distribution for the OHT individuals (left eye), across the five visits, within algorithm for SITA Standard (top), SITA Fast (middle) and SWAP (bottom).

Figure 3.23 Linear regression for mean LI against mean MD, as a function of algorithm, for right eye (left panel) and for left eye (right panel), at every visit for normal individuals

Figure 3.24 Linear regression for mean LI against mean MD, as a function of algorithm, for right eye (left panel) and for left eye (right panel), at every visit for glaucoma patients.

Figure 4.21. The descriptive statistics (left panel), for the Learning Index for OAG individuals (right eye), across the five visits, for each of the three algorithms, calculated with No-Eyelid pattern. Box and Whisker plots (right panel), of the Learning Index distribution for the OAG individuals (right eye), across the five visits, within algorithm for SITA Standard (top), SITA Fast (middle) and SWAP (bottom).

Figure 4.22. The descriptive statistics (left panel), for the Learning Index for OHT individuals (right eye), across the five visits, for each of the three algorithms, calculated with No-Eyelid pattern. Box and Whisker plots (right panel), of the Learning Index distribution for the OHT individuals (right eye), across the five visits, within algorithm for SITA Standard (top), SITA Fast (middle) and SWAP (bottom).

Figure 4.23. The descriptive statistics (left panel), for the Learning Index for normal individuals (left eye), across the five visits, for each of the three algorithms, calculated with No-Eyelid pattern. Box and Whisker plots (right panel), of the Learning Index distribution for the normal individuals (left eye), across the five visits, within algorithm for SITA Standard (top), SITA Fast (middle) and SWAP (bottom).

Figure 4.24. The descriptive statistics (left panel), for the Learning Index for OAG individuals (left eye), across the five visits, for each of the three algorithms, calculated with No-Eyelid pattern. Box and Whisker plots (right panel), of the Learning Index distribution for the OAG individuals (left eye), across the five visits, within algorithm for SITA Standard (top), SITA Fast (middle) and SWAP (bottom).

Figure 4.25. The descriptive statistics (left panel), for the Learning Index for OHT individuals (left eye), across the five visits, for each of the three algorithms, calculated with No-Eyelid pattern. Box and Whisker plots (right panel), of the Learning Index distribution for the OHT individuals (leftt eye), across the five visits, within algorithm for SITA Standard (top), SITA Fast (middle) and SWAP (bottom).

Figure 4.26. Bland and Altman plot of the difference between complete and No-Eyelid pattern method LI results (y axis) against the mean of both methods (x axis), for right eye (top) and left eye (bottom), for SITA Standard algorithm and normal individuals at visit 1 (left panel), visit 3 (middle panel) and visit 5 (right panel). The reference line for mean difference is the red line, the blue dot lines illustrate the 95% confidence lines (+/- 1.96xSD) and the green line is the linear regression line for the referenced R^2 value.

Figure 4.27. Bland and Altman plot of the difference between complete and No-Eyelid pattern method LI results (y axis) against the mean of both methods (x axis), for right eye (top) and left eye (bottom), for SITA Fast algorithm and normal individuals at visit 1 (left panel), visit 3 (middle panel) and visit 5 (right panel). The reference line for mean difference is the red line, the blue dot lines illustrate the 95% confidence lines (+/- 1.96xSD) and the green line is the linear regression line for the referenced R^2 value.

Figure 4.28. Bland and Altman plot of the difference between complete and No-Eyelid pattern method LI results (y axis) against the mean of both methods (x axis), for right eye (top) and left eye (bottom), for SITA SWAP algorithm and normal individuals at visit 1 (left panel), visit 3 (middle panel) and visit 5 (right panel). The reference line for mean difference is the red line, the blue dot lines illustrate the 95% confidence lines (+/- 1.96xSD) and the green line is the linear regression line for the referenced R^2 value.

Figure 4.29. Bland and Altman plot of the difference between complete and No-Eyelid pattern method LI results (y axis) against the mean of both methods (x axis), for right eye (top) and left eye (bottom), for SITA Standard algorithm and OAG individuals at visit 1 (left panel), visit 3 (middle panel) and visit 5 (right panel). The reference line for mean difference is the red line, the blue dot lines illustrate the 95% confidence lines (+/- 1.96xSD) and the green line is the linear regression line for the referenced R^2 value.

Figure 4.30. Bland and Altman plot of the difference between complete and No-Eyelid pattern method LI results (y axis) against the mean of both methods (x axis), for right eye (top) and left eye (bottom), for SITA Fast algorithm and OAG individuals at visit 1 (left panel), visit 3 (middle panel) and visit 5 (right panel). The reference line for mean difference is the red line, the blue dot lines illustrate the 95% confidence lines (+/- 1.96xSD) and the green line is the linear regression line for the referenced R^2 value.

Figure 4.31. Bland and Altman plot of the difference between complete and No-Eyelid pattern method LI results (y axis) against the mean of both methods (x axis), for right eye (top) and left eye (bottom), for SITA SWAP algorithm and OAG individuals at visit 1 (left panel), visit 3 (middle panel) and visit 5 (right panel). The reference line for mean difference is the red line, the blue dot lines illustrate the 95% confidence lines (+/- 1.96xSD) and the green line is the linear regression line for the referenced R^2 value.

ABBREVIATIONS

AAP = Achromatic Automated Perimetry

AGIS = Advanced Glaucoma Intervention Study

AMD = Age-related Macular Degeneration

ANOVA = Analysis Of Variance

ARA = Abnormal Response Area

ARTS = Absolute Relative Total Scotoma

AUC = Area Under the Curve

BL = Borderline

CAP = Computerised Automated Perimetry

CCT = Central Cornea Thickness

CDR = Cup to Disc Ratio

CFF = Critical Flicker Frequency

CI = Confidence Intervals

CLIP = Continuous Light Increment Perimetry

CPSD = Corrected Pattern Standard Deviation

CSFI = Combined Structure-function Index

DD = Diffuse defect

DIGS = Diagnostic Innovations in Glaucoma Studies

DLS = Differential Light Sensitivity

EGPS = European Glaucoma Prevention Study

EGS = European Glaucoma Society

EMGT = Early Manifest Glaucoma Trial

ERF = Error Related Factor

ETDRS = Early treatment of Diabetic Retinopathy Study

FDF = Flicker defined form

FDT = Frequency Doubling Technology

FDP = Frequency Doubling Perimetry

FL = Fixation Losses

FN = False Negative

FOS = Frequency Of Seen

FP = False Positive

FT = Full Threshold

HFA = Humphrey Field Analyser

HRP = High-pass Resolution Perimetry

HRT = Heidelberg Retinal Tomography

HTG = High Tension Glaucoma

GATE = German Adaptive Thresholding Estimation

GCP = Glaucoma Change Probability

GCPM = Glaucoma Change Probability Map

GHT = Glaucoma Hemifield Test

GPS = Glaucoma Probability Score

IQR = Inter Quartile Range

IOP = Intra Ocular Pressure

LD = Localised Defect

LED = Light-Emitting Diodes

LI = Learning Index

LTF = Long-Term Fluctuation

LPF = Luminance Pedestal Flicker perimetry

LV = Loss Variance

MAP = Motion Automated Perimeter

MD = Mean Deviation, Mean Defect

MDT = Motion Displacement Threshold

MRA = Moorefield's Regression Analysis

NFA = Nerve Fibre Analyser

NFL = Neural Fibre Layers

NHT = Neurological Hemifield Test

NTG = Normal Tension Glaucoma

OAG = Open Angle Glaucoma

OHT = Ocular Hypertension Treatment

OHTS = Ocular Hypertension Treatment Study

ONH = Optic Nerve Head

ONL = Outside Normal Limits

PD = Pattern Deviation

PFI = Pupillary Fatigue Index

PLR = Pointwise linear Regression

POAG = Primary Open Angle Glaucoma

PRLs = Prefered Retinal Loci

PSD = Pattern Standard Deviation

RBP = Rarebit Perimetry

RF = Reliability Factor

RGC = Retinal Ganglion Cell

RNFL = Retinal Neural Fibre Layers

ROC = Receiver Operator Characteristics

SAP = Standard Automated Perimetry

SD = Standard Deviation

SF = Short-term Fluctuation

SITA = Swedish Interactive Threshold Algorithm

SWAP = Short Wave Automated Perimetry

TAP = Tubingen Automated perimetry

TCA = Topographical Change Analysis

TD = Total Deviation

TMP = Temporal Modulation perimetry

TOP = Tendency Oriented Perimetry

VFI = Visual Field Index

WNL = Within Normal Limits

ZATA = Zippy Adaptive Threshold Algorithm

SECTION A: INTRODUCTION AND LITERATURE REVIEW

1 CHAPTER ONE - Review of Perimetry and Visual Field

1.1 The visual field

The ancients knew the existence of the field of vision and Hippocrates was the first who described hemianopias. In the 17th century, French physicist Mariotte described the physiological blind spot and related to it the optic nerve head. In the early 19th century, Young and Purkinje described and measured the limits of the visual field, and von Graefe was the first to use clinical measurement of the visual field in the 1850s (Johnson, 2013).

The differential light sensitivity (DLS) represents the reciprocal of the differential light threshold and is illustrated as ΔL/L. The differential light threshold is the luminance of the minimum stimulus, in opposition to a continuous luminance background. It is very essential in order to obtain a visual response and is expressed as L/ΔL, where L is the luminance background and ΔL is the luminance of the minimum stimulus. In order to evaluate the visual field, the differential light threshold must be measured at different locations within the field (Anderson and Patella, 1999; Schiefer, Patzold and Dannheim, 2005).

Visual field is the total area or the perceived “space” of peripheral vision, for an eye fixed on a stationary object and head and body preset on a particular position. The term “space” is used to highlight the fact that the eye is looking at a three-dimensional volume of space rather than a two dimensional area. The normal human visual field extends to approximately 60 degrees nasally to 100 degrees temporally (Fig. 1.1a) and approximately 60 degrees above

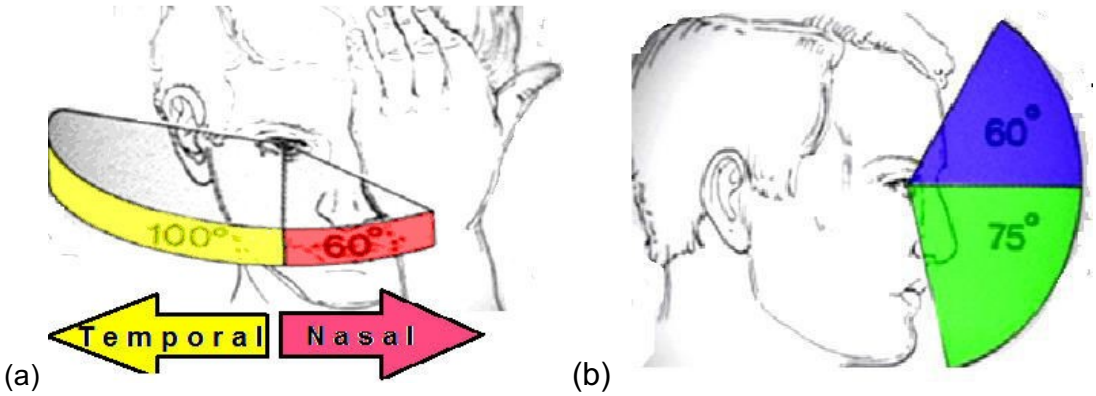

Figure 1.1. The extent of visual field, (a) temporal (yellow) and nasal (red) visual field and (b) superior (blue) and inferior (green) visual field

.

(superior) and 75 below (inferior) the horizontal meridian (Fig.1.1.b). Differences in visual field measurements obtained from individuals are related to the restriction of the nose and orbital bones around the eye. This is often noticed in patients with deep eyes and prominent brows (Henson, 1998; Stanojcic et al., 2010).

The physiological blind spot is the area that appears 15 degrees from the fixation point in the temporal visual field, and 1.5 degrees slightly below the horizontal meridian. It covers an area of 5.5 degrees horizontally and 7.5 degrees vertically (Schiefer, Patzold and Dannheim,, 2005; Rhodes, 2013). There are no rods or cones in this area and for this reason it does not record light and this area is known as the optic disc. Because the visual field diagram represents the field as the patient sees it, the blind spot appears to the right of fixation in the right eye and to the left of fixation in the left eye (Landers et al., 2006).

Traquair in 1927, for the first time proposed the concept of "an island of vision surrounded by a sea of darkness" in order to simulate the visual field (Fig. 1.2). Considering the visual field to be like a three-dimensional topographic map of an island or a hill, it makes interpretation easier. Traquair's representation sits on a base plane that stands for the horizontal and vertical dimensions of visual space, while the third dimension upwards signifies the differential light sensitivity (DLS), which is the capability of the visual system to identify spots of light that are brighter than the background, at each point of the field.

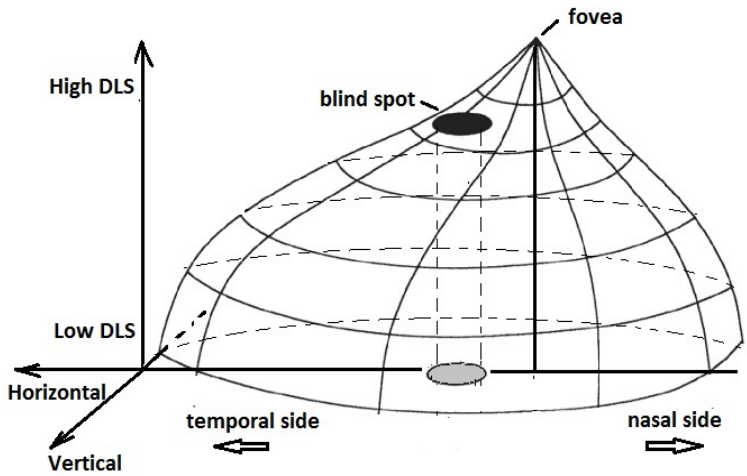

Figure 1.2. Three-dimensional representation of the differential light sensitivity of the visual field often referred to as the "hill of vision" or the "island of vision in the sea of blindness." The *black oval* represents the physiologic blind spot. The drawing represents left eye. (Modified after Johnson, 2006)

1.2 Kinetic and Static Perimetry

Commonly, there are two basic techniques for visual field assessment used in clinical practice. Depending on whether or not the stimulus moves, the

examination should be graded as kinetic or static (fig.1.3). Perimeters are also classified as manual or automated, depending on whether the stimulus is moved by hand, as in the Goldmann perimeter, or if the stimulus location is changed by a computerized mechanism incorporated into the instrument, as in the Humphrey Field Analyzer (HFA).

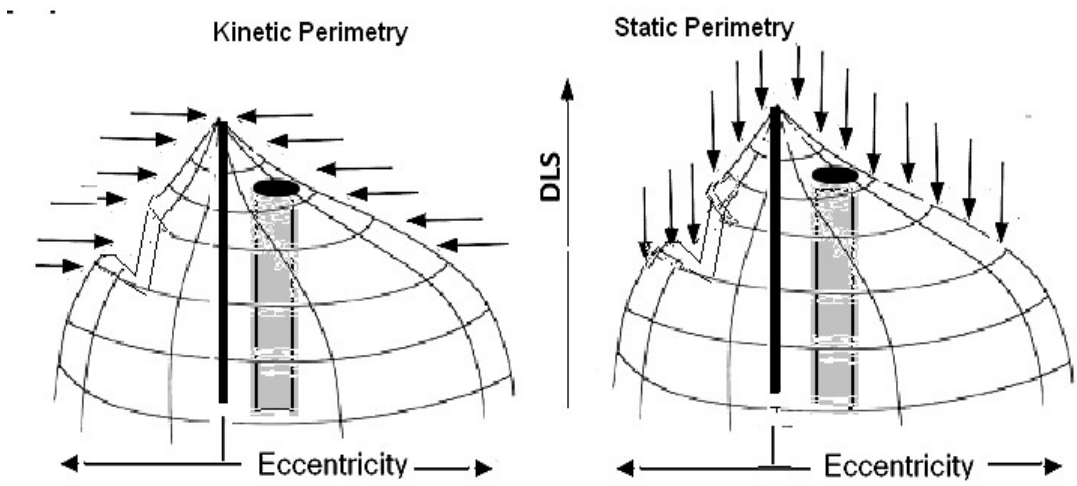

Figure 1.3 Three-dimensional illustrations of stimulus presentation in manual kinetic and static perimetry (Modified after Cubbidge, 2005)

In the late 1970s, computer technology was combined with visual field testing, resulting in the introduction of the first automated perimeters (Johnson, 2013). There are several detailed reviews of the history of visual field testing (Thompson and Wall, 2010; Johnson, Wall and Thompson, 2011; Johnson, 2013).

Although nowadays we have many different types of perimetric techniques and there have been many advances in this ophthalmic diagnostic test procedure, the basic test method has remained rather similar (Johnson, Wall and Thompson, 2011). Several automated visual field testing devices are on

the market, but the two most widely used systems are the Octopus perimeter developed by the Swiss firm Haag-Streit AG., and the Humphrey Visual Field Analyzer, marketed by Carl Zeiss Meditec, Inc. In fact, both perimeters mentioned have the capability of doing both static and kinetic tests, but in practice none of them can be used as a manual perimeter, because automated perimetry has mostly replaced manual perimetry in clinical practice (Werner, 2011).

Kinetic perimetry entails the detection of moving targets, while static perimetry involves the detection of a stationary target (Broadway, 2012). In kinetic perimetry a stimulus with constant size and luminance is presented from a non-seeing area to seeing area in the different meridians of the visual field, until the patient detects the stimulus, where those endings demonstrate the peripheral boundaries of the visual field. This line with the connected points is the isopter, which is plotted from the endpoints in each meridian. Normally each quadrant consists of no less than six radial lines with 15° separation. Each stimulus value and target size gives a different isopter size, which can be plotted on a single paper. The Goldmann hemispheric projection perimeter, which developed in 1945, is a common example of a manual perimeter for kinetic technique (Rowe and Rowlands, 2014).

The kinetic visual field has been classically interpreted by measuring one or more isopter field areas. However, more often than not measurement is limited to one isopter field area. As a result, there is not any information about the sensitivity of the target luminance (Christoforidis, 2011). For that, some automated kinetic perimeters have been developed to address the

disadvantages of the existing manual kinetic measurement techniques (Hirasawa et al., 2014).

In kinetic perimetry, shallow or small areas of visual field loss can be easily overlooked due to the movement of the stimulus and the resulting successive lateral summation. Therefore, the technique is not as sensitive as static perimetry (Heijl, 1976). However, kinetic perimetry is more useful than static perimetry for the examination of steeply bordered advanced loss and is currently more useful for the examination of the peripheral field (Vonthein et al., 2007). On the other hand, the process is restricted by the lack of standardisation of the stimulus velocity and by the reaction time of the patient, both of which can essentially influence the visual field size (Wall et al., 2013a).

In static perimetry, a constant size stationary stimulus is presented at a given location of the retina adjusted in specific levels of luminance and either increased, until a 'seen' response is obtained or decreased, until a 'not seen' response is obtained or both (Punjabi, Lin and Stampe 2006). Compared to manual kinetic perimetry, static perimetry is independent both of the patient's and the perimetrists' reaction time and, of course, of the stimulus velocity (Pineles et al., 2006, Christoforidis, 2011). The goal of the automated perimeter is to reduce testing time and to maintain standardised test conditions. The Goldmann perimeter was rarely used for static perimetry because of the tedious nature of the procedure (Henson, 1998, Pineles et al., 2006; Wall et al., 2013a).

The Humphrey perimeter, as the most used automated perimeter worldwide gained its standardisation over the Goldmann manual perimeter because of its new characteristics and became the new gold standard instrument for testing visual fields. During the visual field measurement, the background brightness (luminance) is held constant, while a test object of altering size, brightness, and position is projected onto it. In general, the slope of the visual field sensitivity contour is steeper for higher background luminance, and it is flatter for lower background luminance (Johnson, 2013).

1.3 Visual field loss

One of the main aims of perimetry is the assessment of the glaucomatous visual field. Glaucoma refers to a group of optic neuropathies leading to visual impairment and blindness. If glaucoma remains untreated, it may produce optic nerve damage, leading to vision loss. initially starting with unnoticeable scotomata at the periphery of the visual field, frequently are illustrated in the arcuate region showing progressively tunnel vision, and finally leading to blindness.

Consequently, visual field tests can be extremely valuable for glaucoma. At the same time, visual field assessment should be performed at baseline and periodically in the glaucoma follow-up or to monitor the effectiveness of adopted therapeutic schemes. On the other hand, visual field defects can adversely affect every day life activities such as reading or driving and should be taken into consideration when verifying degree of disability or planning rehabilitation strategies (Ghate et al., 2014).

The human visual pathway begins with the photoreceptors (rods and cones), which lie in the outer layers of the retina. These photoreceptors consist of photopigments sensitive to specific regions of electromagnetic spectrum that absorb photons of light. This light energy is transformed by photoreceptors into electrical signals, which are transmitted along the visual pathway. These signals pass from the photoreceptors through several retinal cell layers to the ganglion cells. While some photoreceptors may lose their sensitivity, a possible scotoma should develop in the specific area of the visual field (Kiernan and Rajakumar, 2014).

Axons from the retinal ganglion cells (RGC) then begin their route across the inner surface of the retina as the retinal nerve fibre layer and converge on and exit through the optic disc. This retinal nerve fibre layer lies just below the internal limiting membrane. Nerve fibres from the macular region run directly to the temporal side of the optic nerve head and are referred to as the "papillomacular bundle". Fibres from the nasal half of the retina come directly to the optic disc as superior and inferior radiating fibres. Fibres from the temporal retina arch above and below the macula and papillomacular bundle and run as superior and inferior arcuate fibres with a horizontal raphe in between (Fig.1.4). As the majority of these arcuate nerve fibres are more sensitive to glaucomatous damage and they stop at the horizontal raphe, this is a specific glaucomatous pattern (Prasad and Galetta, 2011).

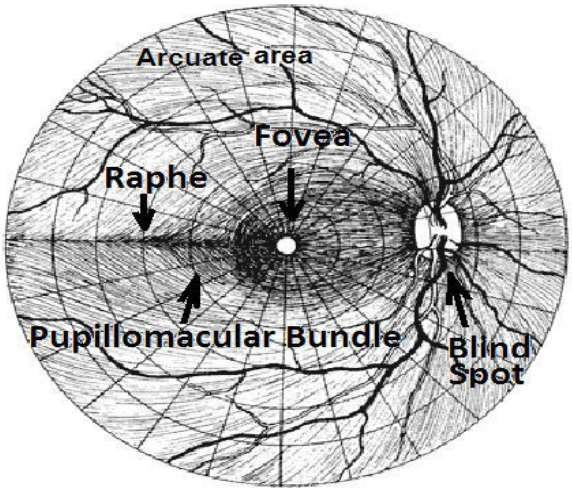

Figure 1.4. Retinal nerve fibre layer pattern demonstrates arching fibres above and below the papillomacular bundle. The arcuate area is the most common area of glaucomatous visual field defects. (Modified after Harrington and Drake, 1990)

The earliest changes indicative of glaucoma consist of increased variability of response in areas that afterwards develop defects (Kanski and Bowling, 2011). Alternatively, these alterations may be slight asymmetries between the two eyes. Classically, glaucomatous visual field defects are illustrated initially in the arcuate region within the central 30°. Defects in this area typically reflect the pattern of the arcuate nerve fibre layers (Fig. 1.4). However, with greater eccentricity from fixation the arcuate fibres gain a more linear orientation.

These differences in central and peripheral nerve fibre layer patterns influence the shape of glaucomatous visual field defects (Fig. 1.5). Since the defects respect the distribution of the retinal nerve fibre layer they come to an end at the horizontal midline, although deficiencies above and below the horizontal meridian are not aligned with each other.

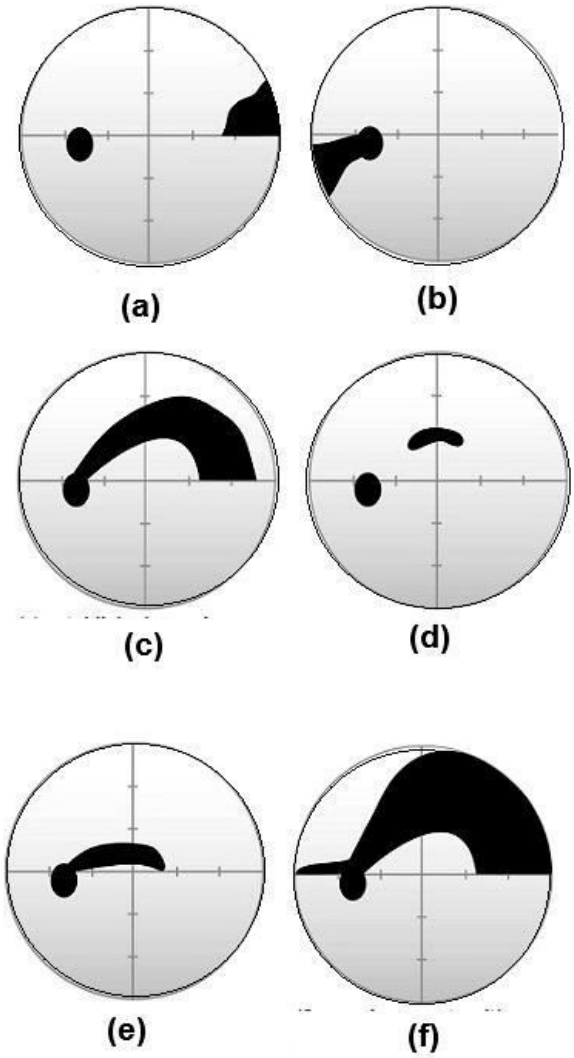

Figure 1.5 Schematic illustration of different types of glaucoma defect patterns.
(a) nasal step, (b) temporal wedge, (c) established superior arcuate defect (d) early superior paracentral defect at 10° (e) superior fixation-threatening paracentral defect (f) superior arcuate with peripheral breakthrough and early inferior defect.

Absolute scotoma is the visual field defect that can be classified as a blind area, where the perception of light is entirely lost. Damaged areas that retains some degree of differential light sensitivity and do not meet the above descriptions are classified as relative scotomata. Relative scotoma is a specific area of the visual field, where low luminance targets cannot be seen but larger or brighter ones are visible.

Paracentral and arcuate scotomata and nasal defects are examples of localized visual field loss. Arcuate or Bjerrum scotoma is a defect that develops between 10° and 20° of fixation in areas that constitute downward or more commonly upward extensions from the blind spot around fixation (Bjerrum area) to reach the horizontal line. If only a portion of the axons are involved and the fibres are likely to be of approximately equal length and originated only from a part of the arcuate segment, the defect is labelled as paracentral scotoma. A ring scotoma (or double arcuate scotoma) develops when arcuate defects in upper and lower halves of the visual field join together. Misalignment between the two often preserves the nasal step (Kanski and Bowling, 2011).

Nasal (Roenne) step represents a difference in sensitivity above and below the horizontal meridian in the nasal field, which results in an unequal loss of the inferior and superior arcuate nerve fibres across the horizontal raphe. It is a common finding usually associated with other defects. Early peripheral nasal steps have been described as “wedge-shaped” scotomata along the horizontal meridian. A temporal wedge is less common but has similar implications.

Generalized loss represents a small but significant loss in sensitivity across the whole visual field characterized by isopter contraction and a reduced mean sensitivity, commonly associated with cataract. It should be mentioned that very high brightness stimuli can cause light scatter and be seen by

functioning areas that lie peripheral to an absolute scotoma, leading to an incorrect classification of the defect as a relative scotoma (Prasad and Galetta, 2011).

As mentioned before, axons from the ganglion cells follow a specific topographic arrangement in the optic nerve and chiasm. The intracranial parts of the optic nerves extend posteriorly from the optic foramen and join at the optic chiasm. The extraocular part of the visual pathways starts at the optic nerve, passes through the optic chiasm, the optic tract, the lateral geniculate nucleus, the optic radiation and finishes at the nerve cells of the visual cortex.

Within the chiasm, fibres from the nasal retina of each eye cross into the contralateral optic tract, and fibres from the temporal retina pass uncrossed into the ipsilateral optic tract (Schiefer et al., 2007). Destruction of the optic chiasm causes bitemporal hemianopias resulting from tumours of the pituitary gland pressing upward from the sella turcica on the bottom of the optic chiasm. These visual field defects respect the vertical but not the horizontal meridian (Schiefer et al., 2007; Hitchings, 2009).

The optic tract consists of nerve fibres from one half of the visual field only, and bends the pathway around the brain stem. About 10 per cent of the fibres leave each half of the visual pathway and pass to the pretectal nucleus in the brain stem, which are responsible for the pupillary light reflex. The remainder of the optic tract ends at the lateral geniculate nucleus. Destruction of an optic tract cause homonymous hemianopsia.

The lateral geniculate nucleus (LGN) lies in the posterolateral aspect of the brain stem and next to the thalamus. In this area nerve fibres that originate from the retinal ganglion cells synapse with fibres that originate from cells in the visual cortex. The optic radiations continue the visual pathway from LGN to its ends at the neurons of the visual cortex. The fibres leave from the lateral part of LGN and spread out in a fan formation but preserving their retinotopic projection. Damage to the LGN causes contralateral homonymous quadrantanopsia.

The end point of the visual pathway is the visual cortex. In the visual cortex corresponding retinal points meet and become perfectly matched by location. Lesions in the visual cortex cause homonymous hemianopsia and usually have macular sparing.

1.4 Basic Principles of Perimetry

1.4.1 Stimulus size and intensity

In perimetry, the required stimulus size depends on the type of visual field examination. In automated perimetry it is common to refer to the size of stimulus using the size equivalent to one of those used in the Goldmann bowl perimeter. Normally, in automated perimetry, differential light sensitivity is verified by varying the brightness, not the size of the stimulus. It uses a standard white stimulus, with a range between 51 dB (or 0.08 apostilbs) that correspond to the minimum brightness or high retinal sensitivity, and 0dB (or 10000 apostilbs) that corresponds to the maximum brightness or non-retinal sensitivity (Heijl, Bengtsson and Patella, 2012).

Decibel (dB) is the unit used to measure differential retinal sensitivity. In practice, decibels are used to compare the intensity of light to the maximum possible light intensity the perimeter can produce. Decibels are usually specified as log units. The two are related by a factor of 10, where 1 log unit equals 10dB (Schiefer et al., 2005; Johnson, 2013).

Currently, static automated perimetry uses the Goldmann III target stimulus, which is a small circular increment of white light subtending 0.43^{o} of visual angle and is presented on a dimmer white background and all normal values are related to this stimulus size (Marin-Franch and Swanson, 2013). Larger stimulus sizes may be employed for individuals with poor visual sensitivity, like the Goldmann size V stimulus (1.72^{o} diameter, 64 mm^2) along with the Full Threshold testing strategy, because there is no SITA program currently

available for size V stimuli and its variability for individual test locations is substantially lower (Wall et al., 2013a).

The Original Goldmann set of stimuli includes 6 different sizes with a range from size 0 to size V, each step corresponding to a factor of 2 in diameter or a factor of 4 in area compared to the immediately previous smaller stimulus. Wall and colleagues found in a study the same number of abnormal locations with III, V, and slightly fewer for size VI (diameter 3.44^{o}), probably because increasing stimulus size results in a decrease in the number of abnormal test locations, as the bigger size of stimulus overlaps smaller defective areas (Swanson, 2013). Another undesirable consequence of using large stimulus sizes is a reduced detection of some hemianopic defects. Size VI appears slightly less sensitive for glaucoma with mild loss. However, using larger stimulus sizes has some distinct advantages. Variability is lower with larger sizes, often without a loss of signal and the effective dynamic range is greater (Wall et al., 2013a).

Newer instruments allow use of very different types of target stimuli (Fig.1.6), such as sinusoidal stimuli, flicker-defined forms, or moving lines. Novel types of perimetry, like Frequency Doubling Technology (FDT) utilizes a vertical sine wave grating with a size of 10° in diameter and a low spatial frequency (0.25 c/deg) that undergoes counterphase flickering at 25 Hz and FDT2 a size of 5° stimuli of a vertical cosine wave grating with a spatial frequency of 0.5 c/deg that undergoes counterphase flickering at 18 Hz. The flicker defined form (FDF) perimetry stimulus or Contour “Edge” Illusion is a circular stimulus 2–8°

in diameter, created by a phase reversal of black and white dots that flicker in counter-phase to the background dots (Wall et al., 2010; Francis et al., 2011).

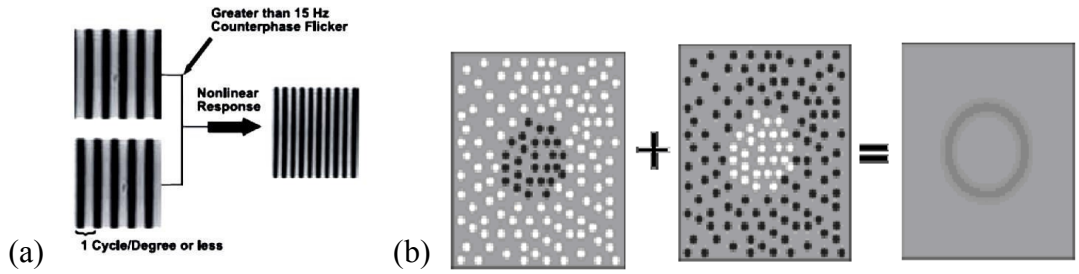

Figure 1.6. Sinusoidal stimuli for FDT (a) and dot flicker stimuli for FDF perimetry (b).

Between stimulus size and stimulus luminance there is a good relationship. For a range of small stimuli the effect of changing either size or intensity is proportionally the same, such that reducing the intensity of a stimulus at threshold by 50% means that the stimulus must be twice as large in order to reach threshold again. This relationship is commonly referred to as Ricco's law and describes complete spatial summation. However, this relationship becomes ineffective for larger stimuli and summation is said to be incomplete (Redmond and Anderson, 2011). When the stimulus area exceeds this critical area (known as "Ricco's area") then partial summation takes place.

Nevertheless, decrease in retinal effective illumination influences the stimulus relative visibility. In contrast, the lessened retinal image projection balances for this outcome; out to an eccentricity of 80º, the retinal illumination is more or less stable. Given that different perimeters have different types of stimuli, and even different definitions of sensitivity, the decibel scale is instrument dependent (Anderson, Johnson and Werner, 2011).

1.4.2 Background Illumination.

The island of vision can rapidly change due to fluctuations with the state of adaptation. Whenever the eye is light adapted (photopic), it will appear as a relatively low-elevation island with a peak at the centre- the fovea. In mesopic conditions it becomes flatter and in dark adaptation (scotopic) the peak of sensitivity at the foveal area is lost (Fig.1.7). The improvement of sensitivity in the dark-adapted retina is not the same at every location (Weijland et al., 2004).

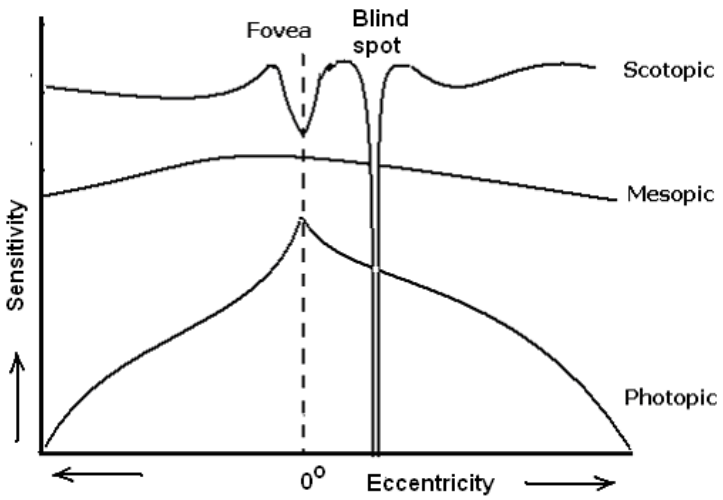

Figure 1.7 The island/hill of vision under Photopic, Mesopic and Scotopic adapted conditions.

Given that sensitivity reduces with age, Swanson and colleagues suggest that for a single background luminance, the retinal illumination produced in a young eye with a clear lens and 8-mm diameter pupil can be up to 20 times greater than the retinal illumination produced in an older eye with a 2-mm diameter pupil and typical density for an aged lens without cataract, although

illuminations produced by the background and stimulus are equally affected by pupil size and lens density (Swanson, Dul and Fischer, 2005; Swanson, 2013).

The background luminance of the perimeter carries out a significant role in retinal sensitivity determination and it must remain constant within an examination, since it confirms the state of retinal adaptation. It determines the state of light- versus dark-adapted retina. The Humphrey and Octopus perimeters generally use a background illumination of 31.5 asb or 10 cdm^{-2}. A background luminance of 10cdm^{-2} fulfils the necessity for minimum adaptation time for the patient from the general room illumination. Reducing the background illumination of a perimeter will increase the necessary time for the retina to adapt to the lower luminance (Anderson and McKendrick, 2007; Pan and Swanson, 2006; Redmond and Anderson, 2011).

The reason why at high background luminance the critical duration is reduced for large areas of stimulus is probably associated with the effect of background on spatial summation. As a consequence, the area over which there is complete spatial summation (Ricco's Law) turns out to be smaller at high background luminance, so that in order to accomplish maximal temporal summation the stimulus area must be smaller than Ricco's summation area, when increment threshold measurements are made, by contrast with the situation at absolute threshold when summation becomes unimportant (Davidson and Akingbehin, 1980; Todorova et al., 2013).

1.4.3 Stimulus Duration

The critical stimulus duration range in the normal population varies between 60 and 100ms (Greve, 1973; Saunders, 1975; Okuyama et al., 1999). Perimeters generally use a stimulus duration longer than the critical duration in order to minimize the effects of temporal summation that produce higher inter-individual variability (Greve, 1973; Carroll and Johnson, 2013). As a result, previous series of Octopus perimeters used stimulus duration of 100ms whilst the recent models of Octopus and the Humphrey Field Analyzers (HFA) use stimulus duration of 200ms. Short stimulus durations reduce the examination time and are useful for patients with poor fixation (Greve, 1973) but increase the variability of the threshold estimate (Rowe and Rowlands, 2014).

Temporal summation decreases with increasing stimulus size (Saunders, 1975) and increasing background luminance (Saunders, 1975; Daly and Normann, 1985; Garway-Heath et al., 2000a). Temporal summation also fluctuates physiologically not only between normal individuals but also in case of ocular disease (Garway-Heath et al., 2000b).

1.4.4 Stimulus generation

The stimulus generation method employed by automated perimeters varies between different types. Three different methods of stimuli generation have been employed: projection systems, fibre-optics or light-emitting diodes (LED).

LED and fibre-optics suffer from a series of restrictions, like the relative high-cost of fibre-optics.

The most common type of perimetric stimulus generation is the projection system that uses a single light source and permits the light pass through a system of condensing lenses, apertures and filters in order to be projected through a mirror system onto the bowl. The aperture and filter wheels control size and wavelength. Small stepper motors define stimulus location and give a maximum resolution of 0.2^{o} between adjacent stimuli (Fankhauser, 1979; Heijl, 1985; Swanson et al., 2014).

Projection system's advantages are the fine spatial resolution and the flexibility of the stimulus direction, but the noise created by stepper motors may lead to an increase of false positive responses due to patient audio clues. The Humphrey Field Analyzers and Octopus perimeter series, use a projection system of a halogen source (Weijland et al., 2004).

1.4.5 Stimulus configuration

During visual field examination, the most important effort is to balance the necessity to take full advantage of the possible visual field loss detection with that of a reasonable examination time. Without a doubt, the number of stimulus locations within any given visual field examination mostly defines the

duration of the test. On the other hand, the number of the stimuli and the extent of the separation between them, classifies the resolution with which the defect can be recognized (Henson, Chauhan and Hobley, 1988).

In any examination set of visual field tests the layout of stimulus locations is designated as a “Program”. The Program 32 first was introduced with Octopus perimeters in 1975. Later on, Humphrey Field Analyzers adopted the Program 32 and used it as a HFA 32-2 program. All Humphrey programs ending in -2 (e.g., 10-2, 30-2, 24-2,) are offset from the horizontal and vertical meridians. Programs 30-2 and 24-2, which use 6° spacing, are thus offset by 3° and the stimuli are introduced in terms of a square grid that is offset by 3°, equally from the horizontal and the vertical midlines, correspondingly, and in which the inter-stimulus separation is 6°.

One of the more commonly used tests is the standard Humphrey Program 30-2, which samples 76 locations with a uniform 6° grid extending to 27° from fixation (Fig. 1.8). As the distance from fixation increases, the normal sensitivity values decrease, with a analogous increase in the intratest and test-retest variability. One advance to shortening the test is to delete the outer row of locations (Fig. 1.8). Following this approach HFA established Program 24-2, which only tests out to 21°, except for preserving the important-nasal extent of Program 30-2. The resulting test contains 54 locations, a 29% reduction compared with the Program 30-2 grid, and considerably shortens the test duration. This represents an attractive trade off in patients who fatigue with additional testing.

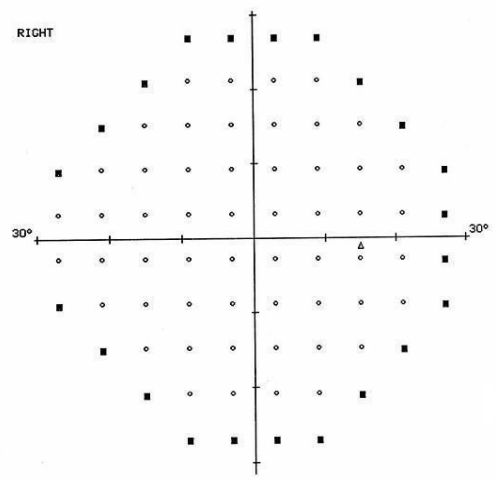

Figure 1.8. Program 24-2 and 30-2 test grids. Program 24-2 deletes the outer row (bold points) of the 30-2 test grid with the exception of the two nasal locations.

Programs 30-1 and 24-1 test a uniform 6° grid out to 30° and 24°, correspondingly, but are not offset from the horizontal and vertical meridians. Because scotomata centred on these meridians are difficult to classify (superior vs. inferior, nasal vs. temporal), and because the corresponding locations have a reduced amount of diagnostic value, these programs are rarely used.

There are supplementary programs permitting exploration of the peripheral visual field (beyond 30°), like the HFA Program 60-4 in standard static perimetry that extends the test out to 60°, with a uniform grid testing of 60 additional locations, when subject cooperation permits.

Advanced glaucoma patients demonstrate visual field defects often involving the central field. Program 10-2 provides a high-resolution test of the central

10°, with a fixed 2° grid and offset 1° from the meridians (Fig 1.9a). This strategy offers the benefit of testing more areas with quantifiable threshold and a total of 68 locations are used. For more objective and precise measurement of fixation characteristics, the use of Microperimetry has been employed. It has been widely used in clinical practice to document both retinal fixation and retinal sensitivity characteristics (Kulkarni, Chaudhurl and Jagathesan, 2013; Longhin et al., 2013).

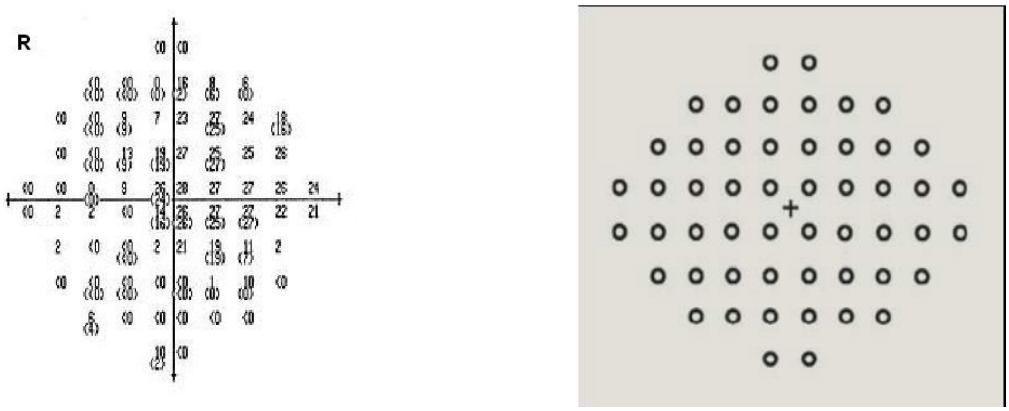

(a) (b)

Figure 1.9. (a) Program 10-2 grid uses 68 test points and 2° spacing with 1° offset from the meridians and tests out to 9° of visual field. (b) Microperimetry grids resembling the common 10-2 pattern but utilising 52 test points.

Microperimetry is a method in which retinal sensitivity is assessed while the fundus of the eye is directly inspected and it enables an exact correlation between macular pathology and corresponding functional defects (Midena, 2006; Ozturk et al., 2008).

Microperimeters incorporate the appropriate technology and facilities needed to consider components of residual visual function and functional vision. Residual visual function and functional vision after macular vision loss are principally defined by 3 most important components: scotoma characteristics, preferred retinal loci (PRLs) and oculomotor control. Microperimetry may demonstrate advantages as a method compared to standard automated perimetry (SAP) for residual visual function assessment (Markowitz and Reyes, 2013).

Microperimetry uses also a “10-2” grid pattern with a stimulus separation of 2° including stimulus locations at retinal eccentricities between 0° and 22°. (Fig.1.9b). Although typically the Goldman III stimulus size has been used, the size and colour of the stimuli and fixation target may be varied, and thresholds can be estimated using “4-2 dB” or “4-2-1 dB” staircase strategies (Acton and Greenstein, 2013).

1.5 Presentation of Perimetric Results

1.5.1 Numerical values of sensitivity

Each type of perimeter always includes a printout that contains a numerical display, where the threshold values of each tested point are listed. These values illustrate the threshold estimate at each stimulus location and are interpreted in terms of sensitivity, expressed in decibels.

Individuals with good peripheral vision can detect very faint stimuli, so the dimmer the stimuli the higher the threshold number. The higher the numbers of this plot, the greater the sensitivity at these visual field locations, and the

better the patient has performed on the test. With a number of threshold algorithms, the values of a second threshold estimate at any specified stimulus location are displayed underneath the initial value.

1.5.2 Greyscale printouts

The greyscale display, normally situated in the upper right corner of the printout, next to the numerical graph, assigns different shades of grey to different ranges of threshold sensitivity and gives a general idea of how a visual field looks. When showing and explaining test results to patients, the greyscale is very useful and easy for patients to understand (Dersu and Thaly, 2007; Chaglasian, 2013).

The greyscale graph converts the dB values to a "grey" tone scale. For example, values less than or equal to "0" are represented by solid black, meaning the patient did not respond to the brightest stimulus. Values above 40 dB are represented by total white, meaning that the patient could see the dimmest stimuli. The values in-between are represented as an interpolated grey scale, by varying shades of grey, made up of increasing densities of dots. The greyscale levels are regularly organized into groups of 5 dB in width. The greyscale range for the Humphrey Field Analyzers have a range from 0 to 51 dB, in 10 levels of grey. The scale at the bottom of the chart shows the corresponding values of the greyscale in apostilbs and decibels. Every change in the greyscale tone corresponds to a 5-decibel change in threshold.

The greyscale is neither age nor eccentricity corrected. By itself, the appearance of the grey scale in the normal eye darkens with increase in eccentricity. It furthermore darkens with increase in age, to reflect the reduction in the height and shape known as “peripheral steepening”. In early sensitivity loss the greyscale may show normality, mainly in the paracentral regions, but in the occurrence of severe loss, the greyscale becomes gradually more representative of the visual field as the general height correction (Asman, Wild and Heijl, 2004).

As a result of the dissimilarity in the magnitude of the normal values of sensitivity between standard automated perimetry and short-wavelength automated perimetry, the appearance of the greyscale for short-wavelength automated perimetry in the normal eye is darker than that for standard automated perimetry (Wild, 2001).

Nevertheless, as a consequence of the grid spacing, small defects can be missed when interpreting the result without reference to other information provided in the printout. Even if it permits the visualization of defective areas, the greyscale demonstration introduces values between authentic test locations and frequently conceals discrete scotomata. No diagnosis should be based on the greyscale alone, as these graphs turn out to be the least valuable information on the print out. The greyscale is intended to give just an impression and drive one's attention to an area that needs detailed examination.

1.5.3 Total Deviation and Pattern Deviation plots

The Total Deviation (TD) is a numerical plot that presents the deviation of the patient's raw sensitivity results from those of age-matched controls at each test location. The Pattern Deviation (PD) is a numerical plot similar to Total Deviation plot except that it is adjusted for any generalized depression, such as that caused by cataract or media opacities.

Correcting the seventh-best deviation value within the Program 24-2 test grid to zero deviation and adjusting the entire field by that value, the Pattern Deviation modifies the Total Deviation plots in an attempt to display any superimposed patterns of localized loss hidden under generalized depression. The Pattern Deviation plot should be carefully inspected for early detection or progression of glaucomatous visual field loss.

1.5.4 Total Deviation Probability maps

Variability depends upon test point location, general field status, and depth of visual field defects. Heijl and colleagues (1990) used these conclusions to estimate significance limits for change at each tested point as a function of the above factors, and knowledge of such limits to make possible the design of total deviation glaucoma change probability maps (Heijl, 1989; Heijl, Lindgren A and Lindgren G, 1990).

The total deviation symbol map illustrates the statistical significance likelihood of each calculated deviation from the normal age values at the specified location (i.e. $p<5\%$, $p<2\%$, $p<1\%$ or $p<0.5\%$) in terms of symbols, which rise in

the level of grey as the magnitude of the probability level becomes increasingly smaller. For instance, if a location is marked with the symbol for *p* < 1%, that means less than 1% of normal age-corrected fields have a threshold value that low (Werner, 2011). The darker the pattern (symbol) is, the more significant the deviation from the expected threshold (Wall et al., 2009),

1.5.5 Pattern Deviation Probability analysis

This additional probability analysis for the Humphrey Field Analyzer is displayed as the Pattern Deviation probability map in an identical manner to that for the Total Deviation map. The pattern deviation probability map separates the general reduction in sensitivity, which arises through media opacities, optical defocus or miosis from the localized sensitivity.

Pattern deviation maps show the significance of deviations from age-normal values after correcting for any generalized depression or elevation of sensitivity found in the normal portions of the field.

1.5.6 The Glaucoma Hemifield Test (GHT)

The Glaucoma Hemifield Test (GHT) is exclusively designed to identify localized glaucomatous visual field loss and is available for the Humphrey Field Analyzers (Asman and Heijl., 1992a; 1992b). It is evaluated by comparing the differences between the superior and inferior hemifield in the magnitude of the Pattern Deviation probability level either side of the midline. The power of GHT analysis to discover glaucoma damage derives from the predisposition of glaucomatous defects to affect the upper field differently from the lower field due to separation of upper and lower RGC axons at the optic disc (McCoy et al., 2014).

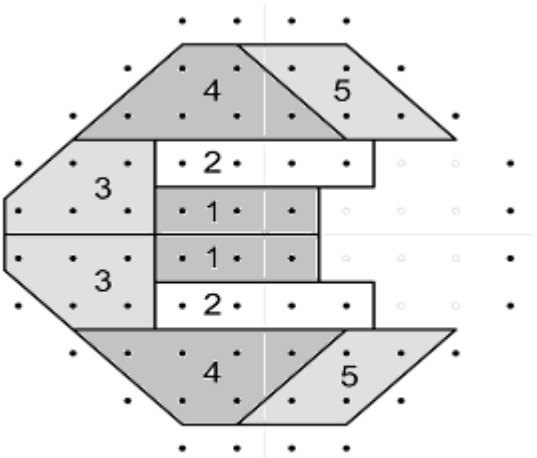

Figure 1.10 The GHT Pattern. The five superior clusters have five mirrored inferior clusters.

In an early glaucomatous patient visual field loss usually starts on one half of the field and it rarely crosses the horizontal meridian (Nouri-Mahdavi et al., 2011). As a result, the idea of the test is based upon the hypothesis that glaucomatous field loss is asymmetric between the superior and inferior hemi-

fields (Katz et al., 1995a; 1995b). Consequently, the GHT divides each of the upper and lower hemifields into 5 mirror-imaged zones (Fig. 1.10). Afterwards each zone is scored according to the number of Pattern Deviation probability values, and compared to its mirror image. The sum of the reciprocal of each of the given Pattern Deviation probability levels, is calculated as a probability score for every zone and then compared to the mirror image probability score (Asman and Heijl, 1992a; Katz, Quigley and Sommer, 1995; Katz, Quigley and Sommer, 1995b).

The result of the above comparison of the difference between the two hemifields is illustrated in qualitative terms on the printout. The GHT has three critical scales of classification of visual field: outside normal limits, borderline or within normal limits. These criteria based on the GHT may demonstrate high sensitivity and specificity with the intention of detecting early glaucomatous visual field changes (Johnson, Wall and Thompson, 2011; Boland and Quigley, 2011).

The label, under the GHT printout, named 'Outside Normal Limits' specifies a general asymmetry, which is statistically significant at $p<0.01$ or an asymmetry in one zone, which is statistically significant at $p<0.005$ and is displayed whenever at least one zone pair differs by an amount found in fewer than 1% of normal subjects.

The label 'Borderline' indicates that the asymmetry occurs with a probability level of $p<0.03$ found in fewer than 3% but more than 1% of normal subjects

and these visual fields are classified as normal. That is because the borderline classification indicates small differences between upper and lower hemi-fields.

The label ‘General Reduction of Sensitivity’ points to an overall reduction in sensitivity across the field, and these visual fields are classified as abnormal. A probability level of $p<0.005$ is displayed whenever even the best test point locations are so low as to be at levels seen in fewer than half a percent of normal subjects (Nouri-Mahdavi et al., 2011).

‘Abnormally High Sensitivity’ label occurs at a probability level of $p<0.005$ whenever the best test point locations are so high as to be at levels seen in fewer than half a percent of normal subjects and these visual fields are classified as normal (Katz, Sommer and Witt, 1991).

An analogous test to the GHT, labelled Neurological Hemifield Test (NHT) was developed to improve the detection of chiasmal and post-chiasmal visual field loss (Boland and Quigley, 2011). The NHT uses pointwise data from the pattern deviation analysis of the HFA instrument, much as the GHT compares pointwise pattern deviation data from mirror image clusters across the horizontal field meridian. The initial NHT compares one group of 16 points in the left hemifield to the mirror image of 16 points in the right hemifield, separated by the vertical midline. As a result, while the GHT compares any one or more of 5 clusters to each other, the NHT uses only a single, larger cluster for comparison (Boland and Quigley, 2011; McCoy et al., 2014).

1.6 Visual Field Global Indices

Assessment of a visual field involves clinical analysis of the pattern of field loss, looking for evidence of disease and/or progression depending on the clinical context. However as an addition to this, automated perimetry allows the field to be quantitatively analysed and described in numerical terms.

Visual field indices are also very important in evaluating visual field change over time. A wide variety of visual field indices have been developed for the Humphrey Analyzer to assess the data reduction at each stimulus location. Each type of index is a summary measure, which describes a specified feature of the visual field. The indices are optimally used in combination with spatial information, mainly that of the Pattern Deviation Maps (Cubbidge, 2005).

1.6.1 Mean Deviation (MD)

Mean Deviation (MD) simply is a weighted average deviation from the normal reference visual field. For the Humphrey Field Analyzer (HFA) a negative mean deviation represents loss in sensitivity and is a characteristic of visual field depression. In the presence of focal loss MD will also be more negative. It is essentially a condensed value that represents the average height of the entire hill of vision. In general, MD is relatively not very sensitive to localized defects but is strongly affected by generalized depression. Depending the type of perimeter used for the test, the MD polarity may be positive or

negative according to the way of subtraction of the average deviation from the normal reference data.

1.6.2 Pattern Standard Deviation (PSD)

Pattern Standard Deviation (PSD) reflects irregularities in the field, such as those caused by localized field defects and represents the unevenness of the surface of the hill of vision. PSD is calculated by taking a location-weighted standard deviation of all the threshold values.

PSD is insensitive to the overall average height and is strongly affected by localized defects. PSD is low or near zero when the visual field is normal and increases and peaks at moderate levels of localized field loss, but it turns low around zero in cases of high abnormality, because in this case there is rather a generalized loss.

1.6.3 Corrected pattern standard deviation

The corrected pattern standard deviation (CPSD) reveals a more accurate shape of the hill of vision by removing patient related factors and correcting the PSD by subtracting the Short term Fluctuation (SF) value. A high PSD value may be due to high SF, low patient reliability, actual visual field defect, or both (Yaqub, 2012).

1.6.4 Visual Field Index (VFI)

The Visual Field Index (VFI) is an index for the detection of progressive glaucomatous loss, used in any deterioration of specified visual field (therefore it was originally called Glaucoma Progression Index or GPI) and was developed to determine the age-corrected defect depth at stimulus locations that were recognized as significantly depressed by Pattern Deviation probability analysis (Bengtsson and Heijl, 2008).

The VFI is scored from 100%, which stands for a normal field to 0%, which represents absolute loss. Therefore, a sensitivity value, at any specified location, positioned within the normal range by Pattern Deviation probability analysis is scored as 100% and that of absolute loss is scored as 0%. On the other hand, it can be used as an indication of the severity of field loss at any specified visual field examination. A sensitivity value, at any specified location, showing a Pattern Deviation probability analysis of $p<0.05$ is expressed as a percentage, that is:

$$100 - [(\left| \text{Total Deviation} \right| / \text{age-corrected normal sensitivity}) \times 100].$$

The VFI is the mean of the weighted scores of the outcome at any specified location of the visual field, whereby the most inferior stimulus locations are weighted most highly. The main advantage of the VFI was that it would be mostly independent of media opacities (i.e. cataract) and would offer a more appropriate evaluation of progressive loss than the analogous Mean Deviation (Bengtsson and Heijl, 2008).

Nevertheless, the VFI has been known to improve in glaucoma patients with field loss after cataract extraction and IOL implantation. Ang and colleagues (2010) found that the improvement in the group mean VFI/deviation was 4.3% compared to 13.6% for the MD. In a study, 53 individuals with various types of cataract had undergone visual field tests and the VFI was left unaffected, whereas the postoperative MD demonstrated a statistically significant, but clinically insignificant improvement and the PSD a statistically significant but clinically insignificant worsening (Ang, Shunmugam and Azuaro-Blanco, 2010; Rao, Khanna and Payal, 2011).

Artes and colleagues (2011) believe that as the VFI measurement depends upon Pattern Deviation Probability values, a 'ceiling effect' is nearby which restricts the diagnostic sensitivity for recognition of progressive early defect (Artes et al., 2011).

The values of the VFI become highly variable in serial visual field tests with MDs crossing –20 dB, in comparison to those VFI values associated with MDs on either side of -20 dB. The likelihood for this effect is the change from use of pattern deviation probability value to total deviation probability value in points included in the calculation of VFI at - 20 dB of MD. The development of indices to measure VF rates that are free from this boundary effect in rather advanced glaucoma is desirable. In clinical practice and research settings, the decrease in VFI when MD crosses -20 dB of sensitivity can be highly variable (Rao, Khanna and Payal, 2011; Lee et al., 2014).

1.6.5 Cumulative defect curve (Bebie curve).

The cumulative defect curve, introduced in 1989 by Bebie et al., is a plot of defect classification, allowing an easy discrimination between diffuse and local visual field loss (Bebie, Flammer and Bebie, 1989; Buerki and Monhart, 2007). It represents the difference between the calculated threshold and age- corrected normal threshold for each one of the tested locations in the visual field. Former studies evaluating the cumulative defect curve suggested that the first third of the curve (dashed red line in figure 1.11A) is spared from increased variation in the early phase of glaucoma (Heijl, Lindgren and Olsson, 1987; Funkhouser, Fankhauser and Weale, 1992; Zulauf, Felhmann and Flammer, 1996). In the plot the abscissa corresponds to the extent of damage and the ordinate characterizes the size of the defect.

The normal range, included between the 5th and 95th percentiles is shaded light blue (Fig.1.11A). The left side of the curve that is parallel to the normal selection illustrates the generalized defect while the decrease on the right side characterizes the superimposition of the localized defect.

If the whole curve follows a depression in an even mode, diffuse loss is present (Fig. 1.11B). Henson et al., illustrated that in early glaucoma the first 10 ranks show decreased sensitivity and Asman further indicated that the volume of local sensitivity decline correlates with the level of Diffuse Defect (DD) (Henson, Chauhan and Hobley, 1988; Asman, Wild and Heijl, 2004). Nevertheless, Bebie curves are still useful for resolving the type of visual field loss present, although these curves cannot discriminate the glaucomatous

and non-glaucoma causes of localized or diffuse visual field loss (Bebie, Flammer and Bebie, 1989; Henson, Chauhan and Hobley, 1988).

.

1.6.6 Diffuse Defect (DD) index

Diffuse Defect (DD) and Localised Defect (LD) are available for the Octopus 300 and 900 perimeters (Monhart et al., 2006).

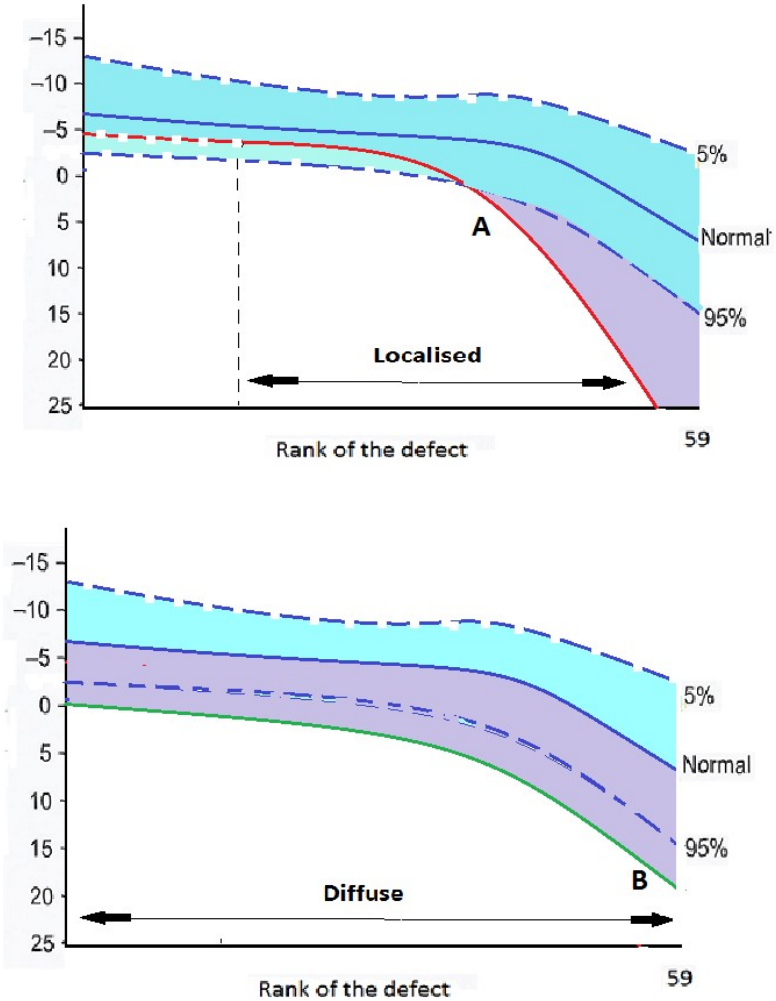

Figure 1.11. The red line (A) in the figure illustrates a Localized Defect (LD) curve and indicates that most of the field is normal but, to the right of the curved line, there are a few locations with deep focal defects. The green curve (B) in the figure, which runs parallel to the "normal" zone, illustrates the Diffuse Defect (DD) curve and indicates that the field has a uniform diffuse depression. A cataract or an artefact can cause such a result but it can also be an indication of early glaucomatous damage. The grey shaded area is the Abnormal Response Area (ARA). The number "59" represents the total number of locations tested (*modified after Monhart et al., 2006*).

Diffuse Defect (DD) index compares the magnitude of the 50th percentile of the distribution of the average normal age-corrected sensitivity, associated with particular ranked deviations in the Bebié curve (depending on the program used for the test), with the mean of the measured sensitivity at the related ranks. The DD Index as it is associated to TD can be either positive or negative (Monhart, 2009). This area (grey shaded) between the 50th percentile of the normal defect curve, shifted by DD, and the level of the subject's individual defect curve has in common an abnormal behaviour and has been labelled as abnormal response area (ARA) (Monhart et al., 2006).

1.6.7 Localised Defect (LD) Index

The Localised Defect (LD) is the area between the patient's defect curve and the 50th percentile of the defect curve when corrected for DD. The LD Index is similar to the PSD but the influence of false-positive responses is minimised due to the exclusion of the first 20% of the ranks in the calculation of the DD (Buerki and Monhart, 2007; Monhart, 2009).

Furthermore, Localised Defect (LD) is not used only in standard automated perimetry (SAP), but also is suggested as an early identifier for abnormal results in perimetry methods with higher between subject variability, such as blue/yellow (SWAP) or flicker perimetry. LD is expressed in dB and normalized to be comparable between different program patterns (Monhart et al., 2006; Monhart, 2009).

1.6.8 Reliability Indices

Reliability indices of the visual field are popular measures used in clinical practice to assess how well a subject has performed the test. A number of methods have been developed for estimating the reliability of the response from the patient during the visual field examination and these were built into most computerized perimeters (Bengtsson and Heijl, 2008 ; Rao, Khanna and Payal, 2014).

The reliability of a patient's examination results can be sampled in terms of the short-term fluctuation and the response to several quality control parameters, like fixation loss, false positive and false negative catch trials. These three considerations, commonly described as reliability indices, provide together an indication of how accurately the test has been performed and thus how significant the results might be (Benjumeda, 2006; Kocabeyoglu et al., 2013).

Unfortunately, during the formative years of automated perimetric testing, it was reported that a high percentage of glaucoma patients (45%) and healthy normal control participants (30%) had unreliable test results, and some continued to exhibit unreliable results on repeated testing. However, the use of standardized testing procedures, proper training to test administrators and the use of precise quality control procedures made it possible to dramatically reduce the number of unreliable visual fields (Johnson, 2013).

1.6.9 Fixation Loss

In visual field testing the most important step is to maintain fixation stability. Fixation can be supervised by a variety of high-tech methods, such as using the monitor of the perimeter, through the Heijl-Krakau method and by means of eye tracking (Heijl and Krakau, 1975a).

The Heijl-Krakau technique establishes the position of the blind spot within the visual field at the outset of the examination and monitors fixation by projecting a Goldmann size III stimulus into the blind spot location at various intervals throughout the examination (Heijl and Krakau 1975b; 1977). If the patient perceives the stimulus, a fixation loss is recorded or fixation is assumed to be correct if the patient does not respond. If the fixation losses number recorded by the Heijl-Krakau technique surpasses 20%, the examination is normally ranked as unreliable. In this case, a symbol (XX) will become visible next to the fixation losses to alert the technician that there is a reason for concern (Morrison and Pollack, 2003; Graves, 2013).

In order to prevent the incidence of pseudo fixation losses, initially it is important to map the correct position and size of the blind spot (Fankhauser, 1993). Optical effects, caused either by high positive or high negative corrective lenses can move the apparent position of the blind spot away from the planned location of fixation and it is very important to detect such problems early in the test (Sanabria, Feuer and Anderson, 1991; Chaglasian, 2013). If the patient places the head incorrectly on the instrument's chin rest,

the perimeter will use a different visual field point as the blind spot, and as a result the examination will be unreliable.

In the Humphrey Field Analyzer (HFA) 740 Series, a “gaze tracker” system was incorporated that uses the measured distance between the centre of the pupil and the first corneal reflex (Purkinje image), during a preset gaze of the fixation target. During the eye movement, the distance between the centre of the pupil and the corneal reflex increases, which is the deviation from the baseline. This deviation can be illustrated graphically as an upward deflection, truncated at an amplitude width of 10°. Deviations produced by head movements with an amplitude less than 1°, are not recorded by the system. On the other hand, tear film cracks or eye closure are represented by a downward deflection. In the Octopus version the test is automatically interrupted if fixation is lost during the test (Shaarawy et al., 2009).

A significant advantage of the Gaze tracker method, compared to the Hejl-Krakau technique, is that the quality control of fixation takes place throughout the whole examination and consequently makes the test less time consuming (Anderson, Shuey and Wall, 2009; Bergin et al., 2011; Nayak and Dharwadkar, 2014).

1.6.10 False positive catch trials

Automated perimetry uses two approaches to evaluate a false positive response. The original technique uses the catch-trial procedure, which implements a "non-presentation" of a stimulus during the testing process and

in conjunction with any mechanical noise associated with the stimulus presentation. A false positive response can occur when the patient either does not understand the evaluation process, or is impatient and anxious that they may miss any of the presented stimuli. An alternative process, is available in the Humphrey Field Analyzer 700 series, and is depended on the specific time at which a positive response will occur during the assessment period, when the patient is not expected to react (Olsson et al., 1992).

The response time method also may underestimate the frequency of errors caused, particularly among normal individuals (Artes et al., 2002; Newkirk et al., 2006; Wang and Henson, 2012).

A high false positive result indicates that patients are not concentrating on the test because they are under the impression that they must act rapidly. In the beginning, the criterion for an unreliable result of the examination of the field was 33% or more inaccurate answers of false positive catch trials. However, after the introduction of Swedish Interactive Threshold Algorithms (SITA) and the relative change in the way false positive responses were evaluated, the upper limit criterion has been reduced to less than or equal to 20% (Bengtsson and Heijl, 2008).

1.6.11 1.5.12.3 False negative catch trials

When a patient is does not react to a stimulus, which previously was seen at a lower luminance earlier in the examination, a false negative response is

recorded. In the Full Threshold and FASTPAC algorithms of the HFA, the stimulus luminance used for the false-negative catch trials at any given stimulus location, is 9 dB brighter than the initial value of sensitivity measured at an earlier period of the test (Wild et al., 1999a). On the other hand, the number of inaccurate answers to the false-negative catch trials is related to increasing severity of the field loss.

In Swedish Interactive Thresholding Algorithms (SITA) an adapted technique has been used to assess the false negative response, based upon the probability functions and upon a small number of specific false negative catch trials. Frequently, patients with visual field loss demonstrate a high number of incorrect responses to the false negative catch trials (Katz 1998; Bengtsson and Heijl, 2000). Extreme demonstration of such a result in the normal eye is related to the 'clover leaf ' field; practically characteristic pattern of a fatigue field with high false negatives and consequently the test has to be repeated (Olson, Purdie and Coleman, 2002; Nayak and Dharwadkar, 2014).

On the other hand, in particular areas of the visual field, the variability within-examination may be even greater than an increase of 9 dB. A rather high number of inaccurate responses to false negative catch trials for related reasons is often correlated to increased variability in sensitivity. Both short wavelength automated perimetry (SWAP) and the Heijl-Krakau technique for monitoring fixation, use a size III stimulus for catch trials testing. For a patient with severe visual field loss, a size V field may yield more data than a size III

field (Henson et al., 2000). A size III stimulus at 30 cm distance covers a retinal area of 4mm^2, and at the same time a size V stimulus covers a retinal area of 64 mm^2. In that case, the use of a larger stimulus may overlap the border of the blind spot that covers a retinal area of about 5 mm^2 (Swanson, 2013), and so a false response may be obtained. Thus, the maximum value of false response approval for false positive catch trials possibly has to be higher for SWAP, than for SAP (Bengtsson and Heijl, 2000; Denniss, McKentrick and Turpin, 2013).

As a result, clinicians should realize that False Negative response rates are important even when their frequencies are small. This finding may contribute to a visual field result incorrectly being classified as glaucomatous in a patient who otherwise has a normal physiological optic nerve head (Rao et al., 2014).

1.7 Methods of Threshold Estimation (Algorithms)

The technique used to determine the threshold sensitivity is called threshold algorithm (also named strategy). Normally, the visual threshold is described as a compilation of a frequency-of-seeing (FOS) curve, whereby the frequency of the percentage of seen responses (ordinate) is plotted as a function of the log of stimulus luminance (abscissa) and which has a 50% probability of detection of repeated presentations (Walsh, 1978; Chauhan et al., 1993b; Bengtsson and Heijl, 1998; Schiefer, Patzold and Dannheim, 2005). This curve, illustrated in Figure 1.12, is known as the psychometric frequency-of-seeing curve or FOS (Bebie, Fankhauser and Spahr,1976;

Chauhan et al., 1993b). For each location in the visual field, a frequency-of-seeing curve can be generated.

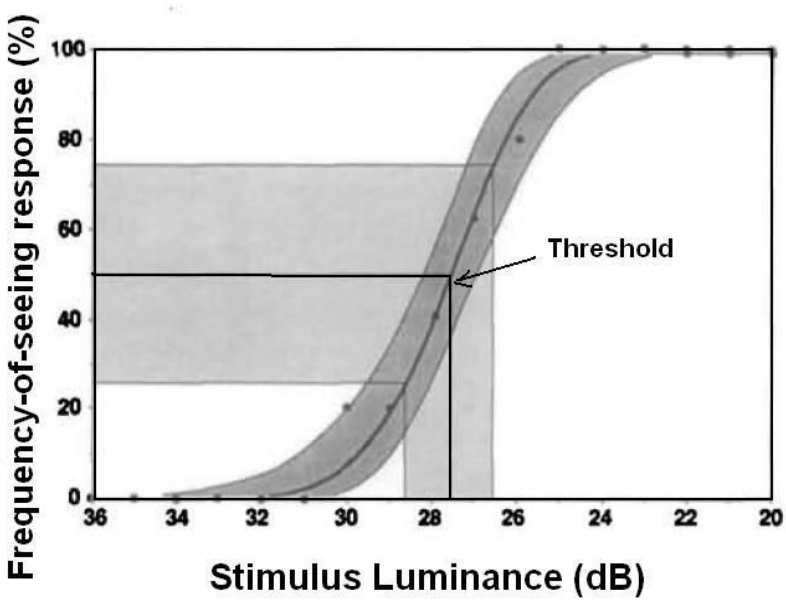

Figure 1.12. Illustrates an example of a frequency-of-seeing curve. Percentage of seen response, (ordinate) is plotted as a function of stimulus luminance (abscissa) The data points represent the raw data; the solid line, the fitted curve; and the shaded area around the curve, the 95% confidence interval. The threshold is the stimulus intensity corresponding to 50% frequency-of-seeing. The light grey shaded area is the interquartile range, which is an estimate of the slope of the curve and frequency-of-seeing (by Chauhan et al., 1993b)

The curve, in general, has a sigmoid (S-shaped) appearance with a linear part in the middle (Weber and Rau, 1992). The frequency of a 'seen' response is never 0% because of the presence of false-positive responses and never reaches 100% as a result of the presence of false-negative responses. Therefore, sufficiently dim stimuli will not be perceived, while sufficiently bright stimuli will. The boundary between perceptible and imperceptible stimuli is not

sharply defined and spans approximately 3 decibels for trained observers (Drance and Anderson, 1985).

The slope of the curve, as a measure of uncertainty in determining the threshold, is highly correlated to actual threshold or threshold deviation from age-appropriate normal values at a particular location and is an indication of the variability associated with the estimation of threshold. Consequently, a gradually flatter slope indicates increasing variability of the threshold estimate, whereas a progressively steeper slope indicates increasingly less variability (Walsh, 2011).

The slope magnitude is also frequently described in terms of the inter-quartile range and more precisely the difference between the sensitivity values corresponding to the 25% and 75% seen responses. The magnitude of the variability is dependent upon a number of factors. It rises with age and rises with increase in eccentricity of the stimulus location, but it varies also among individuals of the same age (Olsson et al., 1992; Schiefer, Patzold and Dannheim, 2005).

In perimetry a conventional method for estimating the differential light threshold adjusts the stimulus luminance in small intervals or steps either in an ascending or a descending manner until it is perceived with a probability of 50%. This method, known as the method of limits, is time consuming when the initial stimulus luminance is far from the threshold.

Currently, an adaptive mode has been used. The stimulus luminance varies in ascending and descending steps, until the threshold is estimated. This process is also known as staircase or bracketing (Turpin et al., 2003; Malik et al., 2006; Denniss, McKendrick and Turpin, 2013).

Generally in perimetry the commonly used algorithms utilize a double threshold crossing. If the initial stimulus is not seen, the luminance is increased in unit steps until a positive response is obtained. The stimulus luminance is then decreased in steps (which are half those used for the first estimation) until a negative response is obtained. The threshold is thereby crossed twice. The threshold can, of course, be approached from the opposite direction.

Wherever possible, the number of stimuli necessary to estimate the threshold is minimized with the intention of shortening the examination duration and thereby reducing the inherent variability in the threshold estimate arising from fatigue (Hudson, Wild and O'Neill, 1994; Gonzalez de la Rosa and Pareja, 1997; Anderson and McKendrick, 2007). Of course, this specific variability decreases with increase in the number of threshold crossings, with smaller step size and increase in the number of estimations.

By and large, in the last 40 years automated perimetry has used an assortment of threshold algorithms. This variety of algorithms can be classified, depending upon their date of introduction into early, second generation and current algorithms. The second generation algorithms exhibit a

reduction in examination duration, compared to that of the first invention, at the cost of some loss of accuracy of the threshold estimate whereas the current cohort of algorithms have employed advanced techniques taking advantage of increased computer processing speed to achieve a reduction in test duration without loss of accuracy in the threshold estimate.

1.8 The early algorithms

At late '70s, Octopus and Humphrey both adopted similar strategies for threshold estimation using the mean value of neighbouring stimulus locations combined with the slope of the age-corrected sensitivity gradient's data.

The Octopus series of perimeters initiate the examination at each of four 'principal' stimulus locations (termed anchor points) positioned near the centre of each quadrant of the visual field (Madea et al., 2000; Weijland et al., 2004). The primary luminance of each stimulus is the age-corrected normal value minus 4dB. If patient gives a negative response, the following stimulus luminance is increased by 6dB. The examination continues by increasing the stimulus luminance in steps of 8dB until a positive patient's response is achieved.

Subsequent to the threshold crossing, the stimulus luminance is reduced in steps of 4dB until the threshold is crossed for the second time. After the second crossing of threshold, the stimulus luminance is increased again in 2dB steps until the threshold is crossed for the third time. The last value is

adjusted by 1dB in the reverse direction to the last response (Weijland et al., 2004).

If the patient responds to the primary stimulus luminance positively, the luminance is decreased in steps of 2dB until a negative answer is achieved, after which the luminance is increased in 1dB steps until a positive reply again is gained. The estimated sensitivity at the four anchor points is applied to the former data of the slope of the age-corrected sensitivity gradient, to estimate the threshold of each of the nearby locations in the related quadrant.

The bracketing practice then continues in a similar fashion, in 4-2-1 dB steps. The primary luminance for the next set of following locations are calculated, in each case, from the median value of the three previously thresholded neighbouring localities and from the slope of the age-corrected sensitivity gradient (Zulauf, Felmann and Flammer, 1994; Weijland et al., 2004).

On the other hand, the Humphrey Field Analyzer uses the Full Threshold algorithm to acquire a threshold estimate crossing twice each of four stimuli (termed seed points) situated 9° from both the horizontal and vertical meridians, correspondingly (Artes et al., 2002).

Each one of these four seed points first luminance is 25dB and the threshold is crossed twice, in the order of 4dB and 2dB steps. The final 2dB crossing of threshold can take place in either an ascending or descending way. The threshold is calculated as the mean of the last positive and first negative

patient's reply. The original value for the immediate neighbouring stimulus points, obtained from sensitivity data at the primary locations and of the slope of the hill of vision, is 2 dB brighter than the expected value (Wild et al., 1999a).

1.8.1 Second generation algorithms

Through the decade of the '90s, Octopus and Humphrey implemented new algorithms in order to reduce the duration of an examination that produces fatigue to the patient and consequently creates less accurate test results.

1.8.2 Dynamic Strategy

Octopus perimeters put into operation the Dynamic Strategy algorithm that is still currently in use, despite the algorithm no longer being up to date. Dynamic Strategy reduces the examination duration by 30-40% in areas of normal sensitivity and by 40-50% in areas of severe loss, compared with the Threshold algorithm (Weber and Klimaschka, 1995; Anderson and Johnson, 2006).

The Dynamic Strategy algorithm uses luminance steps to adapt to the sensitivity at the specified stimulus location from data of the width of the FOS curve. When the visual field defect increases, then the step size increases too, from 2 dB to 10 dB, but threshold is crossed only once and the

approximation is calculated as the mean of the two most recent stimulus luminances (Weber and Klimaschka, 1995; Johnson, 2013).

For sensitivities in the normal range, the Dynamic Strategy algorithm demonstrates lower variability between-examination than the Threshold algorithm. Conversely, the short-term fluctuation of the Dynamic Strategy is higher than the Threshold algorithm, but the long-term fluctuation is similar (Zulauf, Felmann and Flammer, 1996). Obviously, the benefit of accuracy versus testing time is in favour of the Dynamic Strategy algorithm (Weber and Klimaschka, 1995; Anderson and Johnson, 2006; Johnson, 2013).

1.8.3 FASTPAC

The FASTPAC algorithm, introduced by Humphrey in 1991, applied a 3 dB step in either an ascending or a descending way correspondingly, and threshold is crossed only once (Flanagan, Wild and Trope, 1993). A major effort in the development of new perimetric strategies is to find a reasonable trade-off between testing time and accuracy to minimize patient stress and simultaneously to improve reliability of results (Glass, Shaumberger and Lachenmayr,1995).

A study by Glass and associates (Glass, Shaumberger and Lachenmayr, 1995) evaluated the properties of FASTPAC and compared FASTPAC to the standard 4-2 dB full-threshold procedure. Both procedures are staircase methods with predetermined step size for contrast variation.

A variety of clinical studies that evaluated the practical capability of both strategies have given opposing results.

The FASTPAC algorithm examination time is approximately 35% shorter than the Full Threshold algorithms test period, but is at the cost of an approximately 25% increase in the short-term fluctuation (within-test variability) and an apparent underestimation of focal loss in glaucoma (Glass, Shaumberger and Lachenmayr, 1995; Wild et al., 1999a; Barkana et al., 2006). This focal loss underestimation, combined with the larger short-term fluctuation is influenced by the magnitude of the difference between the starting value and the measured threshold. A positive difference leads to an overestimation of threshold whilst a negative difference leads to an underestimation of the threshold; this outcome is more prominent for the FASTPAC algorithm than for the Full Threshold algorithm (Glass, Shaumberger and Lachenmayr,1995; Barkana et al., 2006).

1.9 Current algorithms

1.9.1 SITA Algorithms

The Swedish Interactive Threshold Algorithms (SITA) include two available algorithms: the SITA Standard, which is analogous to the Full Threshold algorithm, and the SITA Fast, which is analogous to the FASTPAC algorithm, both introduced in 1997 for SAP with the HFA (Olsson, Asman and Heijl, 1997; Bengtsson et al., 1997; Bengtsson, Olsson and Heijl 1997; Bengtsson

and Heijl, 1998; Turpin et al., 2003; Bengtsson and Heijl, 2006; Punjabi, Lin and Stampe, 2006).

The SITA algorithm was designed to reduce testing time, while still providing a sufficient test of visual sensitivity, in order to increase attention and result in a more reliable test. SITA Standard uses 4 dB and 2 dB steps and was designed to replace the Full Threshold program (e.g. Full Threshold 30-2), and SITA Fast uses a 4dB step only and was designed to replace FASTPAC, which is a simplified Threshold program (Bengtsson et al., 1997; Bengtsson, Olsson and Heijl, 1997; Turpin et al., 2003).

Both algorithms reduce the examination duration in normal individuals: the SITA Standard algorithm is approximately 50% shorter compared to the Full Threshold algorithm, and the SITA Fast algorithm, 50% shorter compared to the FASTPAC algorithm. The SITA Fast algorithm is 41% shorter than the SITA Standard algorithm (Anderson and Patella, 1999; Wild et al., 1999a; Ng et al., 2009).

One may consider that a Full Threshold 30-2 visual field test on an eye, with significant pathology, might take 16 minutes to complete. The same test with SITA Standard would take about 8 minutes, and the same test with SITA Fast would take about 4.5 minutes. Running SITA with the 24-2 pattern instead of the 30-2 pattern can further reduce examination time. In addition, the 24-2 pattern gives adequate coverage for detecting and following glaucomatous field defects.

Both SITA algorithms make use of two Bayesian posterior probability functions (models) at each stimulus location. One function is a distribution of the probability of a seen response at any given value of sensitivity in the normal eye and the other function is a corresponding distribution in the glaucomatous eye (Olsson and Rootzen, 1994). The two probability models are based upon knowledge of the age-corrected threshold value, the between-individual variability in the estimation of threshold, the variation in the shape of the FOS curve between stimulus locations and the correlation of sensitivity between neighbouring stimulus locations. As the assessment continues each function is adjusted continuously (following the positive or negative response to each individual stimulus presentation), and the shape of each function repeatedly alters as the test progresses. The height of the function illustrates the most likely threshold at the given location and the width states the precision of the threshold estimation at any given moment in the examination (Wild et al., 1999b).

The procedure of threshold estimation at any given location is ended when a predetermined level of accuracy is obtained, as predefined by the Error Related Factor (ERF), (Bengtsson et al., 1997). The balance between accuracy and test time stands for the magnitude of the ERF at each stimulus location. The estimation of threshold with the SITA Standard algorithm cannot be finished, without at least one crossing of the threshold. On the other hand, with the SITA Fast algorithm the threshold estimation can be terminated at any given location without a crossing of threshold (Bengtsson et al., 1997;

Bengtsson and Heijl, 1998). The subsequent inter-stimulus interval is based upon the individual response time window and the SITA algorithms determine the response time to each stimulus presentation.

Every response that take place within a 'listen time' window of 180 ms (which immediately follows the onset of the stimulus presentation), and also those which occur within a further 'listen time' window (which commences at a fixed time, after the response window and which runs into the 'listen window' related to subsequent stimulus) are designated as False Positive responses (Olsson, Asman and Heijl, 1997).

The entire response information obtained during the examination has been used to recalculate the approximate sensitivity at each stimulus location at the termination of the examination (Bengtsson et al., 1997; McKendrick, 2005). In particular, this procedure allows the estimated thresholds at the beginning of the examination to be recalculated from all available response information. The procedure also identifies and excludes those responses, which take place within the 'listen time' window (the false-positive responses), providing better assessment of threshold.

By applying this practice, the necessity for the traditional false-positive catch trials is also avoided and therefore a slight reduction in the examination time duration is allowed. Generally, the rate of the false-positive responses appears on the printout. But the response time of the patient can be affected by the magnitude of the stimulus luminance and the stimulus location and may

vary during the examination (Wall et al., 1996; Artes et al., 2002). The resulting threshold estimation achieved by either SITA algorithm signifies the stimulus luminance matching to a 50% probability on the FOS curve (Bengtsson and Heijl, 1998).

Taken as a whole, the SITA Standard and SITA Fast algorithms demonstrate good sensitivity and specificity for the detection of glaucomatous visual field loss, and involve a significant reduction in the examination duration, in comparison to the older algorithms (Wild et al., 1999b; Sharma, et al., 2000; Budenz et al., 2002). However, the confidence limits for normality are greater for the SITA Fast algorithm than for the SITA Standard algorithm. The between-examination variability of the SITA Fast algorithm is also greater than that of the SITA Standard algorithm (Nordmann et al., 1998; Sekhar et al., 2000; Artes et al., 2002; Barkana et al., 2012). The mean sensitivity in the normal eye is larger for both SITA algorithms, compared to the Full Threshold algorithm. In the glaucomatous population, both algorithms create a marginally higher mean sensitivity, compared to Full threshold and STATPAC algorithms but with a statistically deeper defect depth (Wild et al., 1999a). For sensitivities above 25 dB the SITA Standard algorithm illustrates better test- retest variability than Full Threshold, but below 25 dB the SITA Fast shows slightly poorer test-retest variability. In general, this improvement of test-retest variability is credited to the reduction in perimetric fatigue effect due to decreasing the test duration (Artes et al., 2002).

Some practitioners are not comfortable using SITA Fast as a standard field test for glaucoma. They prefer to use SITA Standard as the default test and use SITA Fast in special situations. The SITA Fast test can be utilized for patients to "learn" on. Once the patient is comfortable with the testing procedure, it is better to switch to the SITA Standard test. The SITA Fast test can also be reserved for patients who cannot even tolerate the speed of the SITA Standard test. On the other hand, SITA algorithms cannot be used with the HFA 600 series due to the limited speed of the older processors and are only available for the HFA 700 series and later (Johnson and Samuels, 1997).

1.9.2 Zippy Adaptive Threshold Algorithm (ZATA)

In the 1980s a more efficient Bayesian approach was introduced to the methods of obtaining thresholds. One of the algorithms promoted (King-Smith, 1994; McKendrick, 2005) was called ZEST (Zippy Estimate by Sequential Testing). In the early 1990s the ZEST algorithm (Turpin et al., 2003) was used to develop ZATA (Zippy Adaptive Threshold Algorithm).

The Zippy Adaptive Threshold Algorithm (ZATA) was introduced for the Henson 8000 perimeter. Two versions of ZATA are available: Standard and Fast. Both algorithms use data from prior examinations to reduce the time for threshold estimation (McKendrick and Turpin, 2005).

They follow the same philosophy as the SITA test in the HFA but integrate a number of important improvements that increase the speed of the test and the accuracy of its threshold estimates (Denniss et al., 2013).

The first of these changes is that, when available, use is made of the findings from a previous test to set the starting intensity for each test location. This will reduce the number of presentations needed to find the threshold and hence speed up the test.

Alternatively, with the threshold algorithm the time taken to complete the test increases when there is a defect. This is because current threshold tests always start from normal age values rather than prior data. As soon as the test starts from the prior threshold estimates, testing time remains rather stable regardless of whether if the patient has a visual field defect or not. In cases where there is no prior data the test will start at the normal age values. Using prior data not only speeds up the test it also results in a more accurate threshold estimate. It extends the concept behind the development of the SITA tests, which is to use as much prior data as possible to optimise the test (Henson and Emuh, 2010; Denniss et al., 2013).

The algorithm reduces the examination duration in normal eyes and in eyes with severe field loss. However, at the time of submission of this thesis there are no any publications about the performance of these algorithms.

1.9.3 Tendency Oriented Perimetry (TOP)

The Tendency Oriented Perimetry (TOP) is a novel perimetric strategy, mainly designed to estimate the sensitivity of the visual field promptly, by using linear interpolation between test locations. TOP was initially introduced in 1996 for the Octopus perimeters (Gonzalez de la Rosa et al., 1996; Martinez et al., 1996; Scherrer et al., 2007).

This technique is based upon the correlation of sensitivity between neighbouring stimulus locations. A number of studies report that TOP is able to carry out accurate threshold determinations with a significantly reduced testing time (Gonzalez de la Rosa et al., 1996).

Additionally, some studies have shown that TOP was four times faster than the traditional full-threshold technique and was successful in detecting visual field abnormalities. On the other hand, TOP produces an underestimation of sensitivity for small visual field deficits (one or two stimulus locations) and decreases the slope of the boundary around visual field deficits. Defects with TOP tended to be smaller, shallower, and with softer edges than with the standard approach (Morales et al., 2000).

The TOP algorithm uses a subject's response at a specified point, not only to estimate the sensitivity at that point, but also to modify the sensitivity approximation of surrounding points within the visual field (Anderson, 2003). Gonzalez de la Rosa et al. reported that association between mean deviation

(MD) and loss variance (LV) for a conventional staircase procedure and the TOP algorithm were high, as assessed on a moderately sized group with mixed disease states (Gonzalez de la Rosa et al., 1996; Scherrer et al., 2007).

In the TOP technique, the visual field is divided into four overlapping sub-matrices, such that, in the case of Program 32, each sub-matrix comprises 19 stimulus locations with a between-stimulus separation of 15°. Each matrix is then examined in sequential order. The cycle is repeated for all locations in each of the four sub-matrices and the estimated sensitivity is recorded. The final adjustment recalculates the estimates based upon the established approximations between adjacent locations (Anderson, 2003).

1.9.4 German Adaptive Thresholding Estimation (GATE-i / GATE) strategy

German Adaptive Thresholding Estimation (GATE) is a new, fast threshold strategy, which is comparable to the Full Threshold staircase and the SITA Standard strategy. The GATE-i algorithm is similar to the GATE algorithm. The only difference is in the reference field that is based upon the age-corrected normal values rather than upon the previously determined thresholds for the given individual (Schiefer et al., 2009).

The GATE-i algorithm starts by determining the sensitivity at each of five predefined seed locations. At every seed location the measured sensitivity is compared to the matching age-corrected normal value. Subsequently, the

smallest deviation between the measured and age-corrected values of sensitivity is used to adjust the overall height of the expected visual field. The initial stimulus luminance at each subsequent stimulus location is slightly decreased compared to the expected value. If the stimulus is 'seen', the luminance is reduced in 4 dB steps until a 'non-seen' response is obtained, after which the luminance is increased until a 'seen' response is obtained. If the initial luminance is 'not seen', the subsequent stimulus is presented at the maximum luminance. If the latter is 'not seen', the thresholding procedure is terminated at the given location. If the maximum luminance is 'seen', the subsequent stimulus is presented at 4 dB brighter than the initial presentation and the luminance is increased in 4 dB steps until a 'seen' response occurs. The stimulus is then presented 2 dB dimmer than the level at which the 'seen' response occurred. Therefore, the threshold is defined as the mean of the dimmest 'seen' stimulus and the brightest 'not seen' stimulus.

The characteristics of the threshold recorded with the GATE-i and GATE algorithms can be compared satisfactorily with those obtained with the Full Threshold algorithm, despite the fact that the examination duration is approximately half that of the Full Threshold strategy (Schiefer et al., 2009).

1.9.5 Continuous Light Increment Perimetry (CLIP)

The Continuous Light Increment Perimetry (CLIP) is a fast threshold strategy using stimuli with constantly rising luminance, offered for use with the Oculus Easyfield perimeter. In the CLIP algorithm, threshold value is assigned the moment the stimulus is perceived.

CLIP follows a completely different path compared to other mentioned algorithms. Quite the opposite of the regular bracketing methods, CLIP makes use of test points with stimulus luminance continuously increased in smaller steps (usually 1 dB), from an infrathreshold level according to the patient's reaction time until it is seen. Measuring the average reaction time of the patient and selecting the appropriate incremental rate of the luminance can achieve a considerable decrease of the examination time achieved, without losing accuracy or reproducibility.

CLIP demonstrates a higher Mean Sensitivity than the 4-2 dB algorithm of the Easyfield perimeter in individuals with glaucomatous field loss and tends to underestimate the depth of deep focal loss. Wabbels and colleagues study demonstrated that the examination duration for CLIP was 5.6 minutes for 55 stimulus locations, compared to 8.9 minutes for the 4-2 dB algorithm (Wabbels, Diehm and Kolling, 2005).

Capris et al., found that mean point-wise sensitivity difference in individuals with glaucomatous field loss between the SITA Fast and the Full Threshold

(FT) algorithms of the Humphrey Field Analyzer (0.84 dB) was considerably lower than that found between CLIP and the 4-2 dB algorithm of the Easyfield perimeter and the Oculus FT strategy (1.71 dB). The mean test time duration for CLIP (450 ±100 sec.) and for SITA Fast (366±72 sec.) was significantly shorter than the corresponding FT strategies (Capris et al., 2008).

Consequently, test duration for the CLIP algorithm is considerably shortened. Moreover, reproducibility of the results is increased. Additionally, a convenient side effect, patient's satisfaction level is kept high due to the fact that a stimulus with increasing luminance in the end is always observed. The CLIP algorithm has also been found suitable for the examination of children above the age of 8 years (Wabbels and Wilscher, 2005). At the time of submission of this thesis, no detailed descriptions of these algorithms have been published.

1.9.6 SPARK Precision and SPARK Quick

SPARK is the name of the strategy (and not a acronym) that was produced by the form of the stimuli during perimetry with the Oculus Easyfield perimeter. The SPARK Precision strategy is considered to be fast and reliable threshold perimetry and a suitable visual field test for glaucoma patients that can be performed in less or about 3 minutes per eye (Gonzalez de la Rosa et al., 2013).

The large amounts of available statistical data makes possible fast and very precise measurements of the threshold values in the central visual field. The inventive modular structure of the method in four different phases, allows an expanded use of the SPARK strategy in clinical practice.

The SPARK Quick strategy is for follow-up or for screening examinations. In patients with a prior visual field examination, the quality of the results is similar to those of the SPARK Precision algorithm (Gonzalez de la Rosa et al., 2013) but with an additional decrease of examination duration of about 50%. In this way the examination can be reduced to almost 1.5 minutes per eye.

SPARK also includes a training strategy to reduce the effect of the learning effects in standard perimetry, which lasts approximately 40 seconds. At the time of this thesis submission no studies or publications are available about the performance of these algorithms against the more current established algorithms.

1.10 Novel techniques of perimetry

Over the past 15 years, an accumulation of studies have recognized that extensive damage of the retinal ganglion cell axons (RGCs) happens prior to the appearance of visual field loss obtained by standard automated perimetry (SAP), at least when the last is expressed in dBs (Harwerth, Smith and Chandler, 1999; Kerrigan-Baumrind et al., 2000; Harwerth et al., 2004; Malik, Swanson and Garway-Heath, 2012; Medeiros et al., 2012a; 2012b).

The first description for retinal ganglion cell loss, based upon histological proof, proposed that retinal ganglion cells with large diameter axons are preferentially damaged in early glaucoma (Quigley, Dunkelberger and Green, 1989; Glovinsky, Quigley and Dunkelberger, 1991). Later, histological data from monkey eyes, illustrated that perimetry defects may be present in early glaucoma manifestation for minimal amounts of ganglion cell loss (Harwerth et al., 1999; Morgan, Uchida and Caprioli, 2000).

Retinal ganglion cells of dissimilar sizes have different physiologic purpose. Small cells that project to the parvocellular layers of the lateral geniculate body belong to the "P pathway" or the "colour system," while large cells that project to the magnocellular layers, belong to the "M pathway" or the "luminance system" (Glovinsky, Quigley and Dunkelberger, 1991). Large optic nerve fibres selectively are lost in chronic human glaucoma (Quigley et al., 1987). Additionally, Glovinski and colleagues matched up the results of experimental glaucomatous eyes to the human glaucomatous eyes measurements, and validated that in studies of the midperipheral retina the large ganglion cells die faster (Glovinsky, Quigley and Dunkelberger, 1991).

A few years later, Johnson proposed that the idea of parallel M-cell and P-cell pathways is of clinical concern because of the likelihood that fussy eye diseases, like glaucoma, may preferentially affect one of these visual paths more than another, mainly in early phases of the disease development (Johnson, 1993). In that case it could be possible to use psychophysical tests

to examine selectively particular vision functions, like motion or colour. Later, Johnson introduced the «reduced redundancy hypothesis», as a substitute move towards the idea of early detection of functional defects (Johnson, 1993; Wall, 2004; Havvas et al., 2013).

Consequently, new methods has been developed to manipulate the “P pathway”, like Short Wavelength Automated Perimetry (SWAP) or High-pass Resolution Perimetry (HRP), to control the “M pathway”, such us Frequency Doubling Technology Perimetry (FDT) and Flicker Perimetry, to manage both “M and P pathways” like the Pulsar perimetry or by using minimum size of stimulus to avoid overlapping of ganglion cells receptive fields, such as Rarebit Perimetry (RBP).

1.10.1 Short Wavelength Automated Perimetry (SWAP)

Short Wavelength Automated Perimetry (SWAP) was used as a substitute technique, also known as “Blue on Yellow” perimetry that was developed to investigate K cell function in the 1980s and 1990s for the early identification of glaucomatous visual field loss (Hamill et al., 1984; Johnson et al., 1993a; Johnson et al., 1995; Keltner and Johnson, 1995; Wild, 2001).

SWAP is a type of visual field evaluation based on the approach that larger ganglion cells within the retina are selectively damaged throughout early glaucoma. Ten per cent of these larger ganglion cells belong to the blue-

yellow pathway: part of the koniocellular pathway (Dacey and Lee, 1994; McBride and Rowe, 2014).

The S- cone system (short wavelength cones) are isolated by blue-yellow conditions of SWAP and the participation of other cone systems (red – long wavelength and green – medium wavelength) are reduced and the rods activity saturated through the adaptation to yellow light so that the blue stimuli are seen principally by the blue cone system (Heijl, Bengtsson and Patella., 2012).

Originally, clinicians considered that SWAP could reveal glaucomatous visual field loss earlier than that obtained by standard automated perimetry (de Jong et al., 1990; Johnson et al., 1993a; 1993b). This verification period of SWAP for the detection of defects prior to that identified by standard automated perimetry lasted for more than a decade and recently was reviewed by Francis et al., (2011).

The obvious disadvantage of SWAP over standard automated perimetry was the increased between-individual normal variability (Wild, 2001) and to the greater than before within- and between-examination variability for SWAP relative to standard automated perimetry, in normal individuals (Blumenthal et al., 2003), in individuals with ocular hypertension and in individuals with open-angle glaucoma (Blumenthal et al., 2003). More recent research has not been able to confirm the early loss of visual field with SWAP or to monitor

progression in more advanced cases of glaucoma (Alencar and Medeiros, 2011).

On the contrary, SITA testing with standard white stimuli may detect just as much field loss in glaucoma as SWAP, (Bengtsson and Heijl, 2006) or at least as early. A recent comparison study between SAP and SWAP, after 5 years follow up to OHT patients, demonstrated that both SAP and SWAP detected early glaucoma, with confirmation when visual field loss was evident. It appeared that each method identified early glaucoma in a subset of patients and these subsets overlapped only partially (Havvas et al., 2013). On the other hand, FDT matrix perimetry had a higher sensitivity for detecting glaucoma than did SWAP at a comparable level of specificity (McBride and Rowe, 2014).

As a result of this high test-retest variability and the larger sensitivity to cataract, SWAP is no longer recommended for glaucoma management. In the future SWAP may instead find a place in maculopathy because during macula oedema the fluid primarily absorbs the blue light (Acton et al., 2010). An evaluation study between standard automated perimetry (SAP) and short wavelength automated perimetry (SWAP) for the central 10-2 visual test procedure in patients with age-related macular degeneration (AMD) illustrated that although not all patients were suitable for SWAP examinations, it remains of ample value as a tool in research studies of visual loss in AMD (Acton, Gibson and Cubbidge, 2012)

1.10.2 High-pass Resolution Perimetry (HRP)

High-pass Resolution Perimetry (HRP) is used as an alternative perimetric technique developed to examine the “P” ganglion cell sampling density (Frisén, 1987; 1993; Frisén and Nikolajeff, 1993). As expected, the HRP primarily

mirrored the function of the P cells, as was the case for SAP (Lennie, 1980; Livingstone and Hubel, 1987; 1988; Shapley, 1990). It is well known that P cells representation in the central retina is much greater than in the periphery. Unlike SAP, HRP verifies sensitivity by varying the size and not by varying the luminance intensity of the stimulus. The HRP threshold is associated with retinal ganglion cell density as a function of eccentricity and of age (Frisén 1988; 1993).

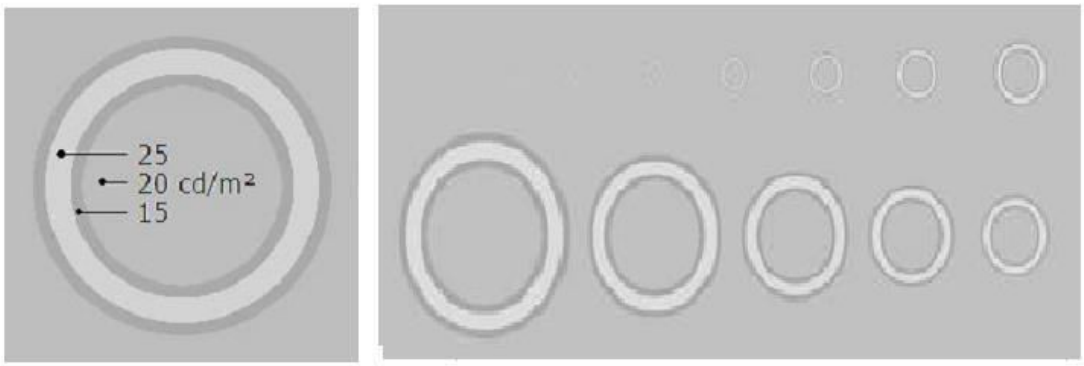

Figure 1.13 HRP test target consists of a bright circular core surrounded by dark borders. The dimensions and luminances are carefully calculated to make the target invisibly melt into the background if unresolved. Normal examination time is about 5 minutes. Fixation is monitored by occasionally projecting a target in the blind spot.

The stimulus is a series of 'ring' target stimuli that mostly contain high spatial frequencies with dark borders ($15cdm^{-2}$) surrounding a lighter centre

($25cdm^{-2}$) presented with duration of 165ms (Wall, 2004). The background luminance is $20cdm^{-2}$. The stimulus size is varied using an up-down staircase of variable steps over a range of 14 sizes of the stimulus, which changed with each stimulus being larger/ smaller than the previous stimulus by a factor of 1.26. The Ring program comprised 50 stimulus locations within the central visual field (Frisén 1986; 1987; 1993; Frisén and Nikolajeff, 1993)

The stimulus distribution of the HRP was thought to correspond with the arrangement of the ganglion cells. Therefore HRP could be superior to SAP in detection of visual field defects (Frisén 1986; 1987). Nevertheless, such a theory suggests that HRP thresholds are sampling-limited. This latter suggestion has been disproved (Ennis and Johnson, 2002) on the basis that the true level of resolution acuity in the periphery is probably underestimated as a result of the proportionately higher contrast in the periphery. Therefore, an HRP threshold is unlikely to be a direct measure of the underlying ganglion cell density.

Furthermore, although a few studies concluded that the HRP performed better than SAP (Frisén. 1993; Chauhan et al. 1993a; 1993b; 1999; Graham and Drance, 1995; Martinez, Sample and Weinreb, 1995; Meyer and Funk, 1995), other investigators have found that HRP performed less well (Lachenmayr et al., 1991a) or equally well (Lachenmayr et al., 1991b; Artes and Chauhan, 2005).

The HRP demonstrates less variability at visual field locations with reduced sensitivity than does SAP (Chauhan and House, 1991). The HRP may be associated with RNFL thickness (Airaksinen et al., 1990; Shirakashi et al., 1997; 1999) and the neuro-retinal rim area. Although It continues to be used in its country of origin, Sweden (Kalaboukhova, Fridhammar and Lindblom, 2006; Martin and Nilsson, 2007; Frisén and Jensen, 2008), and used for vision rehabilitation and lesion management, it has never achieved extensive recognition elsewhere (Sabel et al., 2011).

1.10.3 Rarebit Perimetry (RBP)

It is well known that Goldmann size III stimulus overlaps the visual field sampling, in a way that covers many ganglion cells receptive fields. As a consequence, the identification of abnormal function of any one fixed retinal ganglion cell is controlled, by those ganglion cells which remain functional and which produce normal receptive fields at the specified location of the stimulus.

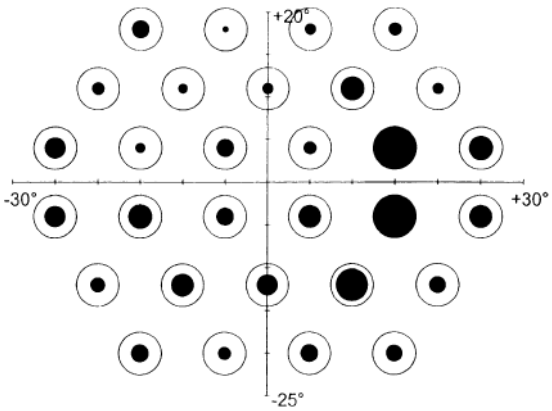

Figure 1.14 Size and distribution of test areas in rarebit perimetry. Outer, open circles represent size of test areas. Inner, closed circles represent any missed probes, as the percentage of probes shown.

An optional perimetric technique Rarebit Perimetry (RBP) was developed by utilizing a stimulus that presented a minimum of information (rare bits) with the purpose of locating very small spaces in the retinal neuronal matrix (Fig. 1.14) starting from dead (dysfunctional) or disconnected neurons (Frisén, 2002). Without a doubt, the stimuli used for RBP were to a large extent nearer in size to an individual ganglion cell receptive field in human (Hackett and Anderson, 2011).

The outcome of RBP was adversely affected by optical defocus (Salvetat et al., 2007) and by cataract (Salvetat et al., 2007; Nilsson et al., 2010). RBP exhibited also a similar learning effect to SAP between the first and the second or third examination and with lower between-examination variability for five examinations over a five-week period than that for standard automated perimetry (SAP) for both stimulus size I and size III (Vislisel et al., 2011).

Previous reports have found central vision tests useful for macular lesions but their performance with lesions of the anterior visual pathways has not been explored. On the other hand, in various studies the rarebit test appeared highly capable of detecting optic neuropathies and chiasmal lesions and its simplicity and short test duration indicated a useful tool in screening settings. Recently, a new computer-based quick test of neurovisual integrity was developed using segmented digits defined by rarebits, that is, receptive field – size bright dots briefly presented on a dark background (Frisén, 2013).

1.10.4 Frequency-Doubling technology perimetry (FDT)

The frequency doubling phenomenon was first described by Kelly over 40 years ago as the "frequency-doubling illusion" (Kelly, 1981). Frequency Doubling Perimetry (FDP) originally was a psychophysical test that consisted of the presentation of low spatial frequency sinusoidal gratings (<1cyc/deg) undergoing high temporal frequency counter-phase flicker at or above 15 Hz. Later versions of the Frequency Doubling Technology perimeter (Carl Zeiss Meditec, Inc., Dublin, CA), utilized a 0.25 cycles per degree sinusoidal grating, presented within a 10o x 10o stimulus square grid, which underwent counter phase flicker at 25Hz. Contrast was modulated until the grating was detected. With such stimulus parameters, the grating appeared to exhibit twice the spatial frequency (Kelly, 1981; Maddess and Ibbotson, 1992). A second- generation version of the Frequency Doubling Technology perimeter, the Humphrey Matrix perimeter, utilizes a 0.5 cycles per degree sinusoidal grating, presented within a 5° x 5° stimulus patch, which undergoes counter phase flicker at 18 Hz (Anderson et al., 2005). The dynamic range of the device seems to be compatible with that of the FDT perimeter (Anderson et al., 2005; Artes et al., 2005). The age-corrected stimulus is presented at one of two contrasts, which should be seen by 95% and 99%, respectively, of the corresponding age-corrected normal population (Johnson and Samuels, 1997; Johnson, 2008).

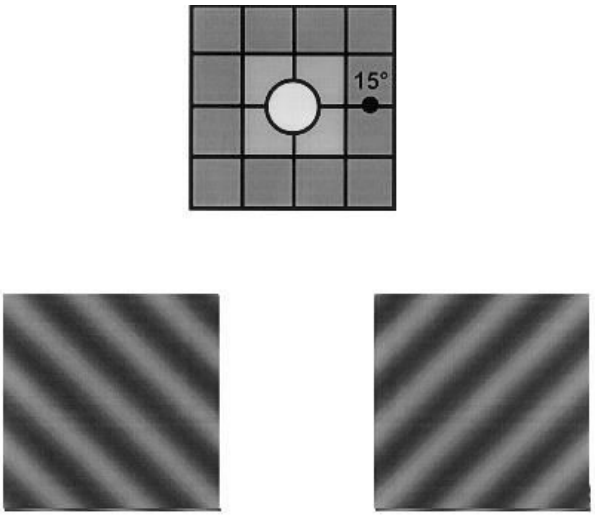

Figure 1.15. Schematic illustration of the FDT stimulus. Top: the 17-location stimulus configuration in the commercial FDT perimeter. Bottom: each stimulus has a 10° patch of sinusoidal grating oriented at 45° (right) or 135° (left).

The frequency-doubling phenomenon is considered to be hindered by a subset (five per cent) of ganglion cells within the magnocellular pathway called My cells (Sample et al., 2000). The My cells have larger diameter axons making them more prone to damage in early glaucoma (Quigley, Dunkelberger and Green, 1989). Since the magnocellular ganglion cells are distributed differently from parvocellular, the visual field topography produced by FDP may again differ from that seen with SAP (Anderson and Johnson, 2002). However, higher order cortical visual areas are also involved in the FDP processing (Zeppieri et al., 2008).

Initially, it was recommended that the original FDT perimeter demonstrated a higher sensitivity and specificity for the detection of open angle glaucoma (Johnson and Samuels, 1997; Casson et al., 2000; Cello et al., 2000; Serguhn

and Spiegel, 2001) compared to that of either SAP (Wu et al., 2001) or SWAP (Bowd et al., 2001).

However, optical defocus and forward light scatter influence negatively the outcome of FDT perimetry (Artes et al., 2003). The structure-function relationship has also been investigated for FDT and HRT by Iester and colleagues, who found better correlation to SAP than to FDT (Iester et al., 2002).

More recent studies suggested that the outcome of the Humphrey Matrix perimeter is similar to that for SAP in the detection of glaucomatous abnormality (Anderson et al., 2005; Spry et al., 2005; Brusini et al., 2005; Hong et al., 2007; Racette et al., 2008; Redmond et al., 2013), particularly for the detection of moderate to advanced visual field loss (Burgansky-Eliash et al., 2007; Hong et al., 2007). On the basis of these findings, despite the extensive literature, it is important to underline that the expected superiority of FDT to SAP remains unclear and FDT perimetry has not been yet substantiated as superior to the SAP gold standard (Liu et al., 2011; Lamparter et al., 2012; Redmond et al., 2013; McBride and Rowe, 2014).

1.10.5 Flicker Defined Form (FDF) technology

Another current technology used in visual field examination is the Flicker Defined Form (FDF) stimulus (Rogers-Ramachandran and Ramachandran, 1998), which stimulates the magnocellular pathway. The FDF stimulus creates an imaginary edge outline, which starts from a high temporal frequency driven imaginary stimulus based upon phase differences between the stimulus and the background (Flanagan et al., 1993; Rogers-Ramachandran and

Ramachandran, 1998). The commercially available Heidelberg Edge Perimeter (FDF, Heidelberg Engineering, Germany) utilises that stimulus. The test consists of flickering random dots on a background of 50cdm^{-2} of mean luminance. The diameter of the imaginary stimulus is 5° and is created by a phase reversal of the black and white dots that flicker in counter phase to the background dots at a temporal frequency of 15Hz.

The visual field indices, Mean Deviation and Pattern Standard Deviation, for the Edge perimeter exhibit only a modest correlation with those derived by SAP using the Humphrey Visual Field Analyzer (Perez et al., 2010a) for individuals with OAG (Perez et al., 2010b). The lack of agreement between the two types of perimetry may be explained by the presence of a considerable learning effect over three visits for the Edge stimulus (Lamparter et al., 2010). On this basis, SAP is still the gold standard for detecting early glaucoma defects.

1.10.6 Pulsar Perimetry

Pulsar perimetry is a technique implied to evaluate both the parvocellular and the magnocellular visual pathways (Gonzalez-Hernandez et al., 2000; González-Hernández et al., 2004). In this framework, the Pulsar perimeter evaluates the threshold of various visual functions, using high spatial and high temporal frequencies.

The Pulsar stimulus consists of two images, the phase and counterphase image that alternate with a frequency of 10 Hz over 500ms and merge with the background luminance of 32 cd/m^2 at the edges to avoid stimulating direction-selective ganglion cells.

The Pulsar examination method of the Octopus 600 (Haag-Streit, 2014) exclusively uses the Tendency Oriented Perimetry (TOP) fast-threshold strategy, delivers fast and reliable results in the Octopus Program GP (Glaucoma, 59 test locations, central 30°) that can be completed within 2–4 minutes.

TOP is an algorithm, which in Pulsar perimetry takes into account the correlation of the threshold values in neighbouring locations and reduces the examination time by nearly 80% to just over two minutes, compared to 6–8 minutes in Dynamic strategy or 10–12 minutes in Normal strategy (Gonzalez de la Rosa et al., 2007).

A number of studies demonstrated that Pulsar perimetry had greater sensitivity in the detection of early visual field loss in patients with OHT compared to SAP (Gonzalez-Hernandez et al., 2004). The between-examination variability was lower for Pulsar, compared to both standard automated perimetry (SAP) and FDT perimetry (Gonzalez de la Rosa et al., 2007; Gonzalez de la Rosa et al., 2011) and Pulsar perimetry seems able to detect more cases of clear progressive glaucomatous damage than either confocal scanning laser ophthalmoscopy or nerve fibre layer polarimetry (Gonzalez de la Rosa et al., 2009),

Although Pulsar perimetry demonstrates greater sensitivity than FDT and shows advantages in early diagnosis of glaucoma, it has not yet achieved extensive recognition among the clinicians.

1.10.7 Flicker perimetry

Flicker perimetry consists of three different techniques, but all of them stimulate M ganglion cell function. These are: the Temporal Modulation perimetry (TMP), Luminance Pedestal Flicker perimetry (LPF) and Critical Flicker Fusion perimetry (CFF).

TMP computes the contrast thresholds for a permanent temporal frequency, for instance the minimum luminance at which a flickering stimulus of a given temporal frequency is perceived to demonstrate flicker (Tyler et al., 1984). However, TMP is supposed to distinguish glaucomatous defects earlier than standard automated perimetry, but the hypothesis is ambiguous. At 25Hz, TMP did not show any increased sensitivity, compared with SAP, in the detection of field loss in glaucoma suspect individuals or in those with OAG exhibiting recognized field loss by SAP (Feghali et al., 1991). Nevertheless, Casson et al., (1992) recommended that TMP reveals considerably greater deformity in early glaucoma, at all temporal frequencies, and classified those cases of ocular hypertension that would develop glaucoma (Casson et al., 1993a; Yoshiyama and Johnson, 1997). Individuals with normal visual function appeared to show a greater age-associated reduction in sensitivity for high temporal frequencies compared to low and medium temporal frequencies (Casson et al., 1993b).

LPF perimetry demonstrates a flickering stimulus, superimposed on a base of a steady luminance, and specifies the temporal frequency required to separate the stimulus from the base (Anderson and Vingrys, 2000; 2002). The method is incorporated in the commercially available Medmont M600 perimeter (Medmont, Camberwell, Australia). Nonetheless, the clinical utility of LPF perimetry in patients with either OAG or OHT has not yet been investigated.

CFF perimetry determines the highest temporal frequency at which a flickering stimulus of constant luminance is originally perceived as a continuous (non-flickering) stimulus (Pieron, 1962; Midena, 1989). The literature is ambivalent as to whether the end point for CFF should be verified by increasing the temporal frequency until fusion is reported (Mahneke, 1957) or by reducing the temporal frequency until flicker is perceived (Knox, 1945).

From a clinical point of view, different methods of flicker perimetry have been reported to detect retinal (Phipps, Guymer and Vingrys, 1999; Vingrys, and Pesudovs, 1999; Stavrou and Wood, 2005) and macular abnormalities (Mayer et al., 1992a; Mayer et al., 1992b; Mayer et al., 1994; Phipps et al., 2004).

Numerous studies have also reported that this method is superior to SAP in the investigation of glaucomatous field loss, although it has not become prevalent among investigators (Lachenmayr et al., 1991a; Lachenmayr and Drance, 1992; Lachenmayr and Gleissner 1992; Lachenmayr, 1994; Matsumoto et al., 2006, Turpin et al, 2012).

1.10.8 Moorfields Motion Displacement test

A different current procedure, the motion detection threshold test (MDT) includes the presentation of a vertical bar of 85% Michelson contrast on a 10cdm^{-2} white background at each of 32 stimulus locations (Oleszczuk et al., 2012). Three fluctuations of 200 ms each alter the temporal location of each bar. Threshold is the detectable displacement perceived for 50% of the presentations.

Although MDT is a simple valuable test for the detection of glaucoma (Baez et al., 1995) and is relatively resistant to the effects of intra-ocular light scatter (Bergin et al., 2011; Oleszczuk et al., 2012), it still requires further comparative investigation.

1.11 Measuring structure and function

Visual field defects are associated with the loss of retinal ganglion cells (RGCs) in the inner retina and of their axons in the optic nerve head (ONH) (Werkmeister et al., 2013). For this reason, structural and functional events should be correlated to the loss of RGCs (Tate, 1985; Anderson and Knighton, 1988; Bartz-Schmidt and Weber, 1993). Several methods of quantifying the amount of RGC loss represented by the loss of axons or visual sensitivity have been proposed (Quigley, Dunkelberger and Green, 1989; Harwerth et al., 1999; 2002; 2004; 2007; Garway-Heath et al., 2000a; 2000b; Swanson et al., 2011; Harwerth and Quigley, 2006; Hood et al., 2007a; 2007b; Harwerth and Wheat, 2008; Harwerth et al., 2010; Medeiros et al., 2012a).

On the other hand, contemporary psychophysical tests do not detect glaucomatous damage until a significant minority of retinal ganglion cells has died. A combined structure-function model would have considerable clinical use for the diagnosis and evaluation of progression of glaucoma, or allow one test replacement by another when one of the trials is not possible.

Although standard automated perimetry (SAP) has been the most widely used method to assess glaucomatous progression, imaging of the ONH and RNFL also provides important measures by which anatomical changes associated with glaucoma can be measured (Bowd et al., 2001; Iester et al., 2008).

Existing structure-function maps have been formulated so as to create the anatomical association between visual field areas and regions of the ONH (Gardiner, Johnson and Cioffi, 2005; Strouthidis et al., 2006). A series of investigations and various studies have stated that there is a reasonable link between the appearance of the ONH, the retinal nerve fibre layer (RNFL), and visual field changes in glaucomatous patients (Lamparter et al., 2012).

Both scanning laser polarimetry (SLP) and optical coherence tomography (OCT) imaging techniques offer quantitative and objective measures of RNFL thickness (RNFLT). In numerous studies, rates of RNFLT change in glaucoma patients were not statistically different from control subjects for any modality. A significantly negative rate of MD change in patients suggests a genuine, continued deterioration in these patients not reflected by RNFLT changes. This indicates that most RNLF thickness changes in patients may have occurred in the earlier stages of the disease before taking into account the baseline differences in RNFL between patients and controls (O'Leary et al., 2012).

1.12 The structure-function relationship

The first report on experimental glaucoma (Harwerth et al., 1999) assumed the log-linear relationship between visual sensitivity and RGC density that had been applied in the studies of retinas from human patients (Quigley, Dunkelberger and Green, 1989; Kerrigan-Baumrind et al., 2000). The general relationship suggested that, when the RGC losses were less than about 50%, there were small reductions in visual sensitivity, although the functional losses were not relative to the structural losses. While both the typical structural and functional changes observed in the disease are eventually related to the pathological loss of retinal ganglion cell (RGC) somas and axons, the

measurements of structural and functional change are to some extent variable and have an inadequate relationship to one another, both for identifying the defects and for disease progression follow up (Leske et al., 2003; Miglior et al., 2005). Conversely, the correct nature of the 'structure–function' correlation in early glaucoma is still the topic of scientific uncertainty and the subject of systematic research (Quigley, Dunkelberger and Green, 1989; Harwerth et al., 1999; Spry et al., 2005; McKendrick and Turpin, 2005; Malik et al., 2012; Medeiros et al., 2012a; 2012b).

Standard automated perimetry (SAP) remains the standard technique for examining functional changes in the disease. On the other hand, patients possibly will present with structural alterations in the optic nerve or retinal nerve fibre layer (RNFL) before these changes are noticed with SAP (Medeiros et al., 2012a). In contrast, a number of patients show evidence of functional deterioration without considerable changes in currently existing structural tests (Kass et al., 2002; Miglior et al., 2005; Artes et al., 2005; Medeiros et al., 2012a).

In standard white on white perimetry, the 24-2 grid has visual field test points that are disproportionately distributed with respect to their optic disc sector correspondence and to the distribution of RGC density (Malik et al., 2012). On the other hand, the conventional Goldmann size III stimulus covers an irregular number of RGC receptive fields across the central 30 degrees. A better represented distribution of test locations of RGCs and a 'scaled' stimulus by RGC receptive field density approximations can be expected to yield stronger structure–function correlations. Clinical studies have also demonstrated that OCT and other imaging devices in fact perform disappointingly in differentiating

moderate from severe glaucoma. These comments about OCT performance and SAP routine without a doubt point towards the need for a combined approach to the identification and examination of glaucoma.

Despite the fact that the amount of RGC loss, related to early development of a field defect, will depend on the location and characteristics of the defect, normally one would first identify VF loss at a mean deviation of around -2 dB to -3 dB, corresponding to an RGC population of approximately 600,000 to 700,000 cells, according to a recent study (Medeiros, 2012a). Similar RGC populations correspond to just about 30 percent loss from the average RGC number in healthy eyes.

1.12.1 The combined structure-function Index (CSFI)

A few years ago, Medeiros and colleagues presented a combined structure and function index (CSFI), with the intention of merging the results of structural and functional tests into a single index that could be used for diagnosis, staging and detecting glaucomatous progression (Medeiros et al., 2012b). This combined index made use of estimates of RGC counts, acquired by previously derived empirical formulas and from two more sources, RNFL thickness estimation by optical coherence tomography (structural) and standard automated perimetry (functional). All these estimates were then merged using a weighted average to make available a single estimate of the RGC count for a particular eye. By combining structural and functional tests for each eye, into a single estimate of RGC loss, the index offered a very instinctive parameter to be used in clinical practice. Bizios and colleagues (2011), suggested that integrating parameters by including a priori relevant information through OCT

and SAP data fusion, may improve the glaucoma diagnosis accuracy compared to current available methods (Bizios et al., 2011).

Other studies have suggested combining structural and functional tests to identify glaucomatous progression, including the use of Bayesian algorithms to allow arrangement of different tests (Weinreb and Khaw, 2004). Additional studies are necessary to evaluate the best approach to clinical trials in glaucoma.

On the other hand, SAP remains the gold standard for the functional assessment of glaucoma. As more highly sophisticated tools have been developed to assess eyes for structural changes in glaucoma, the relationship and concordance of structural defects with functional insufficiency are becoming more obvious. Nevertheless, further study is necessary to confirm these results and to determine the clinical significance of all the findings (Lamparter et al., 2013).

1.13 Factors that possibly influence the perimetric examination outcome

Any visual field examination outcome in order to be successful must be a combination of the ability of the perimetrist, the understanding and the co-operation in the requirements of the visual field examination by the patient and the proficiency of the clinician in interpreting the statistical analysis. Any visual field test can be masked by one or more artefacts, which can either lead to the incorrect result of visual field loss or to the possible deterioration of existing loss.

1.13.1 Physical Factors

The anatomical structures of the face are significant causes of apparent deformity of the visual field (Cubbidge, 2005; Saigal, 2011). These artefacts can create defects that mimic inferior nasal steps or superior peripheral field defects. Reduced aperture trial lenses may also produce lens rim artefacts either due to thick rims or from incorrect placement. As a result, trial lenses should be used always in conformity with the instructions from the perimeter manufacturer (Weijland et al., 2004). Furthermore, time of day has a significant influence on the MD of measured sensitivity. According to recent studies, patients with early glaucoma performed significantly better in the early morning, compared with the rest of the day. Inter-seasonal differences also appeared to play a considerable role in visual field testing. Patients with early glaucoma appeared to have the highest sensitivity in the winter and patients with moderate/severe glaucoma in the spring (Montolio et al., 2012).

1.13.2 Age

The effect of age on the visual field outcome obtained by automated perimetry is another important factor. The visual fields of normal subjects undergoing SAP shows that the sensitivity decreases significantly with age (Brenton and Phelps, 1986; Haas et al., 1986). The sensitivity in blue-on-yellow perimetry also decreases with age in healthy subjects (Johnson et al., 1988) and even in Flicker perimetry contrast sensitivity decreases with age (Faubert and Bellavance, 2003; Bernardi et al, 2007

1.13.3 Defocus

The retinal image optical defocus decreases the visibility of the stimulus. Uncorrected or inappropriate refractive correction could cause the projected stimulus to be out of focus on the retina and therefore not only reduce

luminance but also increase the amount of blur (Henson and Morris, 1993; Saigal, 2011).

The effect appears to be more marked for smaller targets and less marked with increasing eccentricity (Atchison, 1987). On this basis, it is suggested that the visual field assessment should be undertaken with the trial lens fitted with distance refractive correction, together with any near correction, as required (Dul, 2013).

1.13.4 Media opacities

Many studies demonstrated the effect of cataract on visual field sensitivity, mainly by comparing visual function before and after cataract extraction and intraocular lens implantation (Bergin et al., 2011). One result of ageing in general, and cataract formation in particular, is an increase in intraocular straylight (IOS), arising from increased forward light scatter. Although IOS varies between individuals, even in the young healthy eye, IOS values associated with cataract are greater with a resulting reduction in the differential light sensitivity (Anderson, Shuey and Wall, 2009; Bergin et al., 2011).

On the other hand, any ocular media opacity, either a cataract or corneal cloudiness, will produce dullness, absorption and dispersion to a significant amount of light reaching the retina. From a clinical point of view, any opacity reduces the brightness of test stimuli and background equally, and therefore

has no effect other than overall depression of retinal sensitivity; this is reflected in changes to the total deviation plot and global indices, but no significant changes to the pattern deviation plot as this filters out the depression to identify focal losses (unless concurrent disease such as glaucoma is present).

Certainly, light scatter affects the differential light sensitivity more than light absorption (Bettelheim and Chylack, 1985). Cataract in general causes a diffuse loss of sensitivity (Guthauser and Flammer, 1988) and increasing age-related cataract could impair the interpretation of progressive glaucomatous visual field loss (Bengtsson, Olsson, and Heijl, 1997).

Clinical visual field testing may be unreliable when visual field locations have sensitivity below approximately 15 to 19 dB because of a reduction in the asymptotic maximum response probability. The outcome of visual field testing with standard automated perimetry in individuals with OAG or in otherwise normal individuals, illustrates no difference before and after cataract extraction by phacoemulsification and intra-ocular lens implantation (Kook et al., 2004; Siddiqui, Khairy and Azuara-Blanco, 2007). Patients with glaucoma and moderate to severe visual field loss may commonly have worsening sensitivity in these visual field locations (Gardiner et al., 2014).

1.13.5 Medications

Also, a significant number of systemic drugs, like chloroquine/ hydroxy-chloroquine, ethambutol and vigabatrin, give rise to visual field loss (Anderson Johnson and Werner, 2011). The progressive nature of the damage,

discussed despite the withdrawal of drug (Michaelides et al., 2011) and in relation to screening recommendations (Marmor et al., 2011). Studies of ethambutol toxicity suggest that visual field loss is reversible in 80% of eyes, one month after withdrawal of ethambutol (Menon et al., 2009) .

Nevertheless, the phenothiazines attach to melanin granules and can cause a severe phototoxic retinopathy but the associated visual field loss has not yet been documented.

The visual field loss occurring from the anti-epileptic drug vigabatrin is a bilateral concentric constriction, within the central field out to 30° of eccentricity, presented by static perimetry as a binasal annulus, which extends centripetally towards fixation (Krueger, 2013).

1.13.6 Pupil size

Pupil size and anomalies are also a significant factor. This is reflected in changes to the total deviation plot and global indices, but no significant changes to the pattern deviation plot as this filters out the depression to identify focal losses (unless concurrent disease such as glaucoma is present).

Pupil diameter can vary with factors such as ocular medication like miotics, neuroophthalmic disease, and age-related miosis. Pupil size can affect retinal illumination and influence visual field sensitivity; a constricted pupil dims both the intensity of the stimulus and that of the background. It may depress central and peripheral threshold sensitivities and increase the variability of threshold measures (Saigal, 2011).

1.14 Psychological Factors that possibly influence the perimetric examination outcome

1.14.1 Learning effect

One of the most important factors is the perimetric learning effect that is present in almost all types of perimetry. Differential light sensitivity can improve during the test examination of the first tested eye at the initial visit for perimetry (Lamparter et al., 2011; Lamparter et al., 2013).

To minimize learning effects, it is advisable to conduct a practice test procedure in “demonstration” mode where the patient can begin the examination, but data is not collected by the perimeter (Saigal, 2011). Therefore, the examiner must be present throughout the perimetry test and be responsive to providing an individualized test procedure (Johnson, 2013).

A number of possible factors are associated with the learning effect in a glaucoma patient, such as age, race, gender and previous experience (Castro, Kawase and Melo, 2008). Gardiner and his colleagues studied the learning effect over a period of six years, and concluded that is also present over the years and improving at each yearly visit (Gardiner, Demirel and Johnson, 2008). A more detailed analysis of the learning effect in perimetry follows in Chapter 2.

1.14.2 Fatigue effect

Another factor that influences stimulus visibility during the visual field examination is the fatigue effect that is present in all types of automated perimetry exhibiting a worsening of the differential light sensitivity during the

examination (Heijl, 1977; Heijl and Drance, 1983; Hudson, Wild and O'Neill, 1994).

Another source of fatigue is decreased patient vigilance. Signs of sleepiness were described as pupillary constriction and occasionally as “pupillary fatigue”, observed as oscillations in pupil size. A Pupillary Fatigue Index (PFI) was developed in order to describe changes in pupil size and unrest. Loss of vigilance was found to be associated with decreased sensitivity, which sequentially influences visual field variability (Henson and Emuh, 2010).

1.14.3 Test duration

Both learning effect and fatigue effect can influence visual field test results. Patients with prior visual field testing experience are usually more consistent and prepared for this evaluation, which produces better, more reliable results.

Alternatively, a longer test often produces a reduction in performance and results in less reliable test results. Some patients may have short attention spans and require multiple rest periods, need realignment of the head and eye being tested, etc.

1.15 Perimetrist and environmental factors

Perimetrist Instructions, prior to the visual field examination, may influence the threshold estimate by up to 2.04 dB in younger patients and up to 6.57 dB in older patients (Kutzko, Brito and Wall, 2000). If an educational video is shown

prior to the initial visual field examination, is likely to increase the number of outcomes considered to be ‘reliable’, mainly for the eye which is examined second (Sherafat et al., 2003).

For individuals with a low educational level or age greater than 70 years and previous visual field examination with a high number of incorrect responses to either the fixation loss or the false-positive catch trials, it may improve the reliability of the outcome of the visual field examination if prior to the test the patients are shown an educational video (Van Coevorden et al., 1999).

2 CHAPTER TWO - Review of the effect of Perimetric experience in measurement of visual fields

Perimetry is a subjective psychophysical test that requires patient co-operation and a high degree of his/her concentration during the test. After repeated attempts, patient performance may improve by learning and experience.

2.1 What is the learning effect

The Learning effect is an artefact of automated perimetry in visual field examination that masks the real defect and produces a confusing outcome. Subsequently, the development of an index that could discriminate between typically experienced and typically inexperienced visual field results in groups of normal, glaucomatous and ocular hypertensive individuals of various ages would be very much appreciated by clinicians trying to determine the perimetric outcome.

The fact is that the patient learns to respond consistently during the test. In clinical practice, learning may be observed within a single examination of a given eye, between eyes at the same visit, or between subsequent examinations. To minimize the learning effect, we either have to conduct a practice test procedure, as a demonstration for the patient without collecting data, or to calculate and establish a learning index of the specific patient.

In the late 80's, A. Heijl, colleagues and others stated: "a great number of individuals need perimetric experience before producing test results that can

be reliably interpreted" (Heijl et al., 1989; Oden, 1992). Accordingly, inexperienced subjects may often produce field tests that show abnormal results and there is the possibility of learning during the examination. In clinical settings, this is revealed with a dramatic improvement in the second or third field test result compared with the first; the magnitude of these improvements considerably decreases as the number of examinations increases.

2.2 What do we know about the learning effect

As discussed in chapter one, the learning effect in Standard automated perimetry has already been well documented (Wood et al., 1987; Werner, Adelson and Krupin, 1988; Heijl et al., 1989a;, Wild et al., 1989; Kulze, Stewart and Sutherland, 1990; Werner et al., 1990; Searle et al., 1991; Heijl and Bengtsson, 1996; Nordmann et al., 1998; Castro, Kawase and Melo, 2008).

A considerable learning effect between the first and second tests assumed to be present by normal and glaucomatous subjects for SAP (Heijl et al., 1989; Wild et al., 1989). SWAP also exhibits a learning effect that may be larger than for SAP (Gardiner et al., 2006; 2009) even among subjects experienced with prior testing (Wild et al., 2006). The reason for this is uncertain, although part of the dissimilarity may be due to the higher variability of SWAP (Blumenthal et al., 2000, Hutchings et al., 2001; Wild, 2001). Gardiner and associates (2006) suggest that the duration of the problem may have been underestimated, mostly for SWAP. It is likely that the actual mean sensitivities of some of these patients would have been declining due to disease progression (Gardiner et al., 2006).

A learning effect for FDT is also present in normal individuals (Iester et al., 2000; Horani et al., 2002; Joson et al., 2002; Fogagnolo et al., 2008), in patients with OHT (Centofanti et al., 2008) and in patients with OAG (Joson et al., 2002; Matsuo et al., 2002) and lasts until the third visit (Pierre-Filho et al., 2010). The learning effect for Critical Flicker Fusion perimetry occurs between the first and second visits in normal individuals (Bernardi et al., 2007). Flicker Defined Form perimetry shows evidence of a learning effect over the first three visits and a reduction in the variability associated with the threshold estimation technique (Lamparter et al., 2011).

2.3 Why is the learning effect important

Perimetry is an essential component of the examination of glaucoma. Actually, as it has been reported, up to one third of all cases of glaucoma may be missed if routine perimetry were ignored (Tielsch et al., 1991). Based on the above-mentioned studies the economic utility of perimetry is absolute. Up today, the distressing unanswered questions are how often do we need to order visual fields and in what extend is our current technology acceptable. Without doubt, any evidence of visual field progression deserves repeat testing, since recent studies show that 86% of the visual field abnormalities in OHT individuals are reverted to normalcy on repeat testing (Keltner et al., 2000). Conversely, repeating SAP and confirming a change in the visual field is less expensive than a lifetime of potentially unnecessary treatment (Kammer, 2011).

2.4 What should be done to address the outstanding issue

In view of the fact that clinically it can take up to 3 or 4 visits for examiners to decide whether a patient's visual field presents real or masked defective visual field locations, Olsson and colleagues decided in the late 90's to implement an index, initially named Learner's Index (Olsson et al., 1997).

The underlying principle of this index was that a visual field obtained from a normal individual with satisfactory perimetric experience should produce an index value around 0. Index values bigger than 0, either positive or negative indicate that this individual has the possibility to learn and may produce a second examination with better performance and improved test results.

Olsson and associates (1997), in order to detect concentric peripheral depressions, divided the central 30 degrees of the visual field into 5 concentric zones, and then calculated, the average deviation from the age-corrected normal threshold in each zone. After that first attempt by Olsson and colleagues to establish a learning index (LI) for the visual field results, very little was done to improve or recalculate this index, and there are no specific studies, although clinicians still come up against this artefact with every inexperienced patient. Furthermore, the detailed LI calculation is going to be reviewed in Chapters 3 and 4.

2.5 Aims and Objectives

2.5.1 Previous work

This work is a continuation of the development of the “Learner’s Index” (L.I.) that Olsson first introduced in 1997 and an investigation of the learning effect under the same testing protocol. Olsson and colleagues used only normal individuals for their study and utilized two groups of test results, one trained (obtained at the third test session) and one untrained (obtained at the first test session) group of field tests (Olsson et al., 1997).

By the time of this thesis submission no other effort or different method to establish such an index has come to the author’s knowledge. In the research described in the present thesis was used a large group of individuals, healthy, glaucomatous and hypertensive, of various ages, with and without perimetric experience.

2.5.2 Overall and specific aims of the study

The overall aim of this work was to examine new methods for the estimation of the learning index with the intention by the establishment of such an index to assist the clinician in detecting possible masked or overestimated visual field defects or progression of glaucoma damage. The specific aims are twofold.

Firstly, to develop particular software to calculate the index and subsequently to investigate the relationship with the perimetric global indices and the rest of functional aspects of automated perimetry.

Secondly, to investigate the behaviour and influence of novel filters on denoising the perimetric results. An ideal filter that could be quite effective is a

filter that itself adjusts its transfer function according to an optimising algorithm. Because of the complexity of the algorithms, most adaptive filters become accustomed to the performance based on the input signal.

More specific aims of this thesis were initially to determine the extent of the learning index among the perimetric strategies SITA Standard, SITA Fast and Short Wave Automated Perimetry (SWAP) and finally to determine any between-algorithm differences and between-individual variations regarding the magnitude of the learning index.

2.6 Author's background

The author is an optician-optometrist, registered since 1981, with the Commission of Ministry of Health and Welfare Specialities in Greece. Since 1989 he is a senior lecturer at the Department of Optics and Optometry at the Technological Institution of Athens, Greece. In January 2009, the author enrolled for a full-time research degree at the Cardiff School of Optometry and Vision Sciences. The period of full-time study was covered by absence of leave of the Greek Ministry of Education. The research was conducted under the academic supervision of Professor John M. Wild.

At the end of the first year of research, the author was required to undergo a presentation of his results in front of the research group of the School. At second year he presented a poster about the "Learning index in automated perimetry" and he presented his results of filtering VF outcome, in front of the research group of the School. At the third year the author continued his research for the degree of PhD from Cardiff University.

Since the sabbatical of the author was limited to three years, then he had to write up this thesis back in his home Institution. This produced some difficulties and drawbacks to the completion of the thesis. First of all was the communication problem between the author and his supervisor. He initially scheduled bimonthly visits to the School to collaborate with his supervisor, although the cost of this endeavor was prohibitive and the leave from author's working place was restricted.

Later on, this problem was tided over using modern communication means like Skype conference meetings with the supervisor under high-speed Internet connection. This remote collaboration took part at least once per week and worked out quite well until the submission of this thesis.

Another complexity was the different computer software platforms used by author' s Institution, where he had to repeat or update some results of the study. Loading to the computer new versions of the software has easily transcended this drawback. In addition during this period was decided to repeat the calculation of the learning index results in a more accurate way, so the author had to deal with Mathematicians and Statistics specialists. This problem produced much delay in thesis completion.

Nevertheless, although all these above-mentioned shortcomings the time spent to this thesis satisfied both the professional and the personal level of the author.

SECTION B: EXPERIMENTAL WORK

3 CHAPTER THREE - General methods of the Learning Index

3.1 Cohort

The sample included 79 individuals from optometric practices in Landquart, Switzerland who met the inclusion criteria for taking part in the study and who, during the enrolment phase, had volunteered to take part in the study. According Castelberg (2010), all individuals were provided with verbal and written information concerning the nature of the study, and had given written consent, in agreement with the requirements, and approval, of the National Commission of Swiss Graubünden Kantons, and in accordance with the tenets of the Declaration of Helsinki.

Distribution of patients according to gender and age				
Group	Age group (years)	Gender		Total
		Female n	Male n	
1 NRM	40 to 76	16	13	29
2 OAG	46 to 76	17	8	25
3 OHT	46 to 78	14	11	25
	Total	47	32	79
n= number of patients				

Table 3.1. Age distribution within each of the three sample groups.

The cohort comprised three groups of individuals (Table 3.1). One group consisted of 29 normal individuals (16 females and 13 males) who were enlisted from the optometric practice of Dr. Castelberg in Landquart, Switzerland. The group had a mean age of 54.8 years (SD 9.7; range 40-76 years). Each of the

remaining two groups contained 25 individuals. One group involved individuals with OAG and consisted of 17 females and 8 males. The mean age of this group was 63 years (SD 8.3; range 46-73 years). The third group included individuals with OHT and consisted of 14 females and 11 males. This group mean age was 60.0 years (SD 7.9; range 48-76 years).

Twenty-two of the 25 individuals with OAG and 22 of the 25 individuals with OHT were drawn from the ophthalmological practice of PD Dr.med. Zulauf, in Chur, Switzerland. The remaining 6 individuals were drawn from the practices of three ophthalmologists within Landquart, Switzerland.

Normal individuals (Castelberg, 2010) were naïve to any type of perimetry so all the group could be assumed that possibly will learn at the first, second and third test session. On the other hand, the OAG group and OHT group in line to Castelberg thesis were much experienced of Standard Automated Perimetry (SAP) as they had 5-6 previous tests. The individuals of these two groups were expected to learn only in SITA SWAP where the used pathway is different from the SAP.

3.1.1 Inclusion criteria

Each of the studies required five visits each separated by one week and an initial visit to determine suitability for inclusion into the given study. Based upon a range of differences in the visual field index MD of +/- 3.0dB (range 6.0), the SD of the differences was estimated to be approximately 1.5dB (4SD being

95% of the distribution). As a result a sample of 26 patients provided 90% power of detecting a 1.0dB difference between visits and/ or between algorithms (Wild et al 1999a,b; 2006).

Each individual was required to exhibit in each eye a visual acuity of 6/9 or better; a distance refractive error of ≤+/-7.0 dioptres mean sphere and ≤+/-3.0 dioptres cylinder; a normal anterior segment, and lenticular changes not greater than NC2.0, NO2.0, C1.0, or P1.0 by the Lens Opacities Classification System III (LOCS III) (Castelberg, 2010).

In addition, no individual was receiving systemic medication, or manifested any systemic disease, known to affect the visual field; all had a negative family history of ocular disease or any systemic disease with potential ocular involvement.

Normal individuals were categorized on the basis of normal findings from the clinical examination and exhibited an upper limit for the IOP of ≤20mmHg.

Individuals with OAG were categorized on the basis of an optic nerve head, viewed by stereo-observation. Moreover, by the basic characteristic of the disease including generalized or focal thinning of the neuro-retinal rim, disc asymmetry, changes in the lamina cribrosa, pallor, vessel changes or disc margin haemorrhage. For the 25 individuals with OAG inclusion criteria were also the Heidelberg Retina Tomograph (HRT) reflectance images for the optic nerve heads and the values of the parameters for Disc Area, Cup Shape Measure, Height Variation Contour and the Linear Cup Disc (Castelberg, 2010).

For the individuals with OAG, the severity of the visual field loss was graded, post hoc, on the appearance of the eye with the more severe loss recorded with the SITA Standard algorithm at the last visit of the study protocol. The staging system was that of Hodapp and associates (1993), modified by Litwak (2001) for the SITA algorithms, which classifies field loss in terms of the number and severity of the Pattern Deviation probability levels at each location and in terms of the defect depth at the four central locations adjacent to fixation. In general, 5 of the 25 individuals exhibited a normal visual field, 15 exhibited mild loss, 4 moderate losses and one severe loss.

Individuals with OHT were categorized on the basis of a central corneal thickness-corrected IOP of ≥22mmHg in both eyes on at least two occasions separated by at least one month, or a pre-treatment IOP ≥22 mmHg under similar circumstances, in the presence of a normal disc by stereo observation and a normal visual field, considered post hoc, on the basis of the results from the study. A normal appearance of the field was defined after Morgan and colleagues (2005), exhibiting complete normality by Pattern Deviation probability analysis.

Four of the 25 individuals with OHT were each receiving a single topical agent in each eye for IOP control (two were receiving a non selective β-adrenergic receptor blocker, one an α-adrenergic agonist and one a carbonic anhydrase inhibitor). A fifth individual was being treated with a combination therapy of a carbonic anhydrase inhibitor and a β-adrenergic receptor blocker. All five had

been treated with the given regimen for at least two months prior to entry into the study and remained on the same regimen throughout the five-week period.

The level of risk of the OHT in the worst eye was classified, post hoc, using the STAR II system (Scoring Tool for Assessing Risk, Pfizer Inc.) (Gordon et al 2007) which determines the level of risk on the basis of the following: the magnitude of the corneal thickness-corrected IOP; the more asymmetric disc; a thin corneal thickness; and the mean of the PSD index obtained at the two most recent visual field examinations.

The OHT group comprised with 4 individuals at low risk (mean 3.8%; SD=0.6), 16 individuals designated at medium risk (mean 9.7%; SD 2.6) and 5 at high risk (mean 28.4%; SD=10.6). Nineteen of the 25 individuals with OHT had previous experience of standard automated perimetry (SAP). The mean number of previous examination sessions for these 19 individuals was 4.7 (SD=3.2; range 1-12 sessions).

Four of the 29 normal individuals, two of the 25 individuals with OHT and 5 of the 25 individuals with OAG were receiving artificial tears because of minor dry eye problems.

3.1.2 Exclusion criteria

Each of the studies required a number of inclusion criteria for all the individuals at the five consequent visits each separated by one week and also at the initial visit in order to establish suitability for inclusion into the specified study.

Many patients did not meet the strict inclusion criteria for each of the studies. General health problems, such as stroke or diabetes or, cataract often reduced the number of potential individuals.

Therefore, individuals that did not meet the criteria of normality in MD differences and visual acuity were excluded of the normal cohort was used at the studies. Individuals that did not meet the criteria of basic disease characteristics, the state of optic nerve head and the severity of visual field loss were excluded of the OAG cohort. Also individuals that did not meet the criteria of central corneal thickness and glaucoma risk level were excluded of the OHT cohort used to all studies.

3.1.3 Strengths and weaknesses of the cohort

The normal individuals (according to Castelberg, 2010) were naïve to any type of perimetry so all groups could possibly learn at the first, second and third test session. On the other hand, the OAG group and OHT group as stated in the Castelberg thesis, were very experienced in Standard Automated Perimetry (SAP) as they had 5-6 previous tests. The individuals of these two groups were expected to learn only in SITA SWAP where the pathway being tested is different from that tested with SAP.

Therefore, in this study the untrained group consisted of normal individuals at the first test session and the same individuals became a trained group at the fifth test session, as they had already done 5 tests to both eyes.

For this experimental design the strongly controlled conditions, the random sampling, and the use of statistical probabilities suggest the strength of the characteristics of the given population.

The main strength of the cohort used is that the normal population is naïve to perimetry and followed a specific procedure of test instructions. Through a process of elimination using carefully selected tests led to very similar results as they had the same characteristics in disease or normality.

More strength for the present method of LI calculation, provided by the findings that can be generalised as the selection process was well designed and the sample was representative (normal, glaucomatous and ocular hypertensive cohorts all at a similar range of age). Even if findings cannot be generalised to a larger population, however, they can be transferable to another setting of individuals.

Nevertheless, the perimetric experience of OHT and OAG groups in SAP was not well documented, as there was no information provided about any specific criteria involved for what constitutes a naïve observer and what is an experienced observer. As a consequence, the definition of experienced and naïve individuals might be weak.

As there was no record of the frequency and the type of perimetry used in prior visual field tests in the thesis of Castelberg, this may be a potential weakness of the cohort and explains why there were no more criteria for this.

3.2 Examination protocol

According to Castelberg (2010), who collected all the data for his thesis purpose, each individual attended for five visits. Each of these five visits was separated by one week and was divided into two sessions. At the first session, each eye was examined with Program 24-2 of the Humphrey Field Analyzer 745i (HFA; Carl Zeiss Meditech Inc., Dublin, CA) using the SITA Standard algorithm. At the second session, each eye was tested with Program 24-2 and the SITA SWAP and SITA Fast algorithms using the same perimeter.

The order of the sessions varied over of the five visits. On the other hand the order of the algorithms within the sessions were randomised within individuals. The visual field of the right eye was always examined before that.

With a view to ensure adequate saturation of the MWS and LWS pathways, each eye underwent an adaptation time more than three minutes to the bowl luminance of the perimeter prior to examination with the SITA SWAP algorithm. For the SITA Standard and SITA Fast algorithms the corresponding adaptation time was roughly one minute.

To facilitate the fatigue effect influence, a rest period of approximately one minute-halfway provided through the examination of each eye and a five-minute rest period between the examinations of each eye, within a given session. During the rest periods the individual stayed adapted to the perimeter bowl between sessions. A rest period of approximately 30 minutes was offered. At

each visit and throughout each examination, the same instructions received by every patient.

The value of left eye data initially was considered not to be of high importance, as it was often affected by fatigue due to the duration of the perimetric test and because always-left eye was tested second.

On the other hand, the left eye could be used as a second test before the next session, offering more perimetric experience to the individual. Therefore, concentrating to the behaviour of LI it was interesting to compare the change of LI magnitude first to right and then to left eye, having of course in mind the possible fatigue effect.

3.3 Methods for the calculation of the Learning Index (LI)

3.3.1 Olsson's method

The model population used by Olsson and colleagues (1997) for the construction of LI consisted of 72 normal individuals subjected to three bilateral visual field tests on three, different occasions, all within 7 months in both eyes.

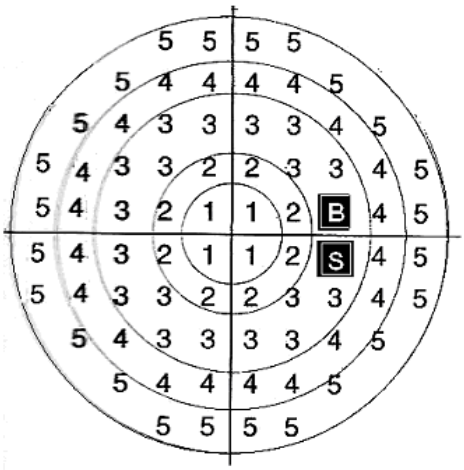

Figure 3.1 The five concentric annuli used for the calculation of the Learning Index (LI). The locations B and S are excluded as they fall within the Blind Spot (after Olsson et al., 1997)

All participants were randomly selected and their median age was 55 years (range 21-79 years): All were normal on clinical examination and careful history could not reveal any diseases that might impair the visual field (Heijl et al.1987a).

Olsson and associates calculated a symmetric 5 by 5 inverse covariance matrix, Σ^{-1}, for average deviations in zones 1 through 5 in the trained group of visual fields (Fig. 3.1). To make LI stronger, they fitted the inverse covariance matrix to each of several mathematical models. The average inexperienced visual field result for learners was represented by the average deviations found in each of the 5 zones, μ (containing one element for each zone, μ_1-μ_5) for the untrained group of 7-field test. In a measured visual field the zone-by-zone average deviations from age-corrected normal thresholds are represented by x (containing one element for each zone x_1-x_5). LI is then, calculated as the linear discriminant function,

$$LI = \mu^T \Sigma^{-1} x / K,$$

where $K = \mu^T \Sigma^{-1} \mu$ provides a numerical normalization of LI resulting in the value of 1 for an average subject in the untrained group. Olsson and his colleagues used two groups of test results, one trained (obtained at the third test session) and one untrained (obtained at the first test session) group of field tests.

All visual field tests that were obtained by Olsson team used the Humphrey 30-2 Full Threshold program and all the sample population were 72 normal individuals. According to Olsson the index was intended to identify patterns of differential light sensitivity values typical of initial field tests in perimetric learners that probably need additional perimetric experience. An essential minority of inexperienced subjects fail to respond adequately in the mid-peripheral field. Such learners usually improve noticeably after two or three test sessions and thereafter show marginal or no improvement. Non-learners, on the other hand, show stable results from the very first test (Heijl et al. 1989).

Therefore, a high LI at a first field test should increase the suspicion that any apparent defects may be due to the need of experience rather than proper disease. However, a high LI may happen also in visual fields with true defects. Nevertheless, these defects will be reproducible and LI will remain high upon follow-up testing.

The above illustrated method, for an average subject in the untrained group LI results in the value of 1. But if LI changes from significant to normal and the field result does the same, then the subject may be classified as normal.

Accordingly in a normal and experienced population LI has an expected value of 0 (Olsson et al., 1997).

3.3.2 The method of LI calculation in the present study

The present study, as a continuation of Olsson and associates method follows a similar design. They used only normal individuals for their study and utilized two groups of test results, one trained (obtained at the third test session) and one untrained (obtained at the first test session) group of field tests The cohort in the present study comprises 79 individuals. These individuals were categorised in 29 normal individuals, 25 glaucomatous patients and the rest 25 ocular hypertensive individuals. The trained group acquired at the fifth test session and the untrained one obtained at the first test session group of field tests.

All tests were performed using the Humphrey 24-2 program and SITA Standard, SITA Fast and SITA SWAP algorithms in five subsequent test sessions. Dr Carlo Knupp, Senior Lecturer at Cardiff School of Optometry and Vision Sciences undertook the coding for the LI calculation (Fig.3.2).

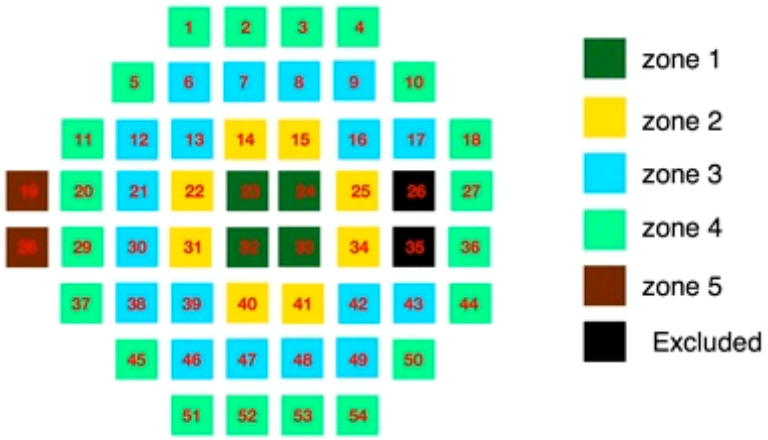

Figure 3.2 The coding of the stimulus locations in the 5 zones used in the MatLab® subroutine to calculate the Learning Index.

The Learning Index (LI) was calculated with custom software written in MatLab® (MatLab 7® version 2006b, Natick, MA, U.S.A.) and in Microsoft Windows Excel® version 2003 (Redmond, WA, U.S.A.).

The learning index calculation follows a method comparable to Olsson's and incorporates the calculation of the averages of deviations from the age-corrected normal threshold values clustered in concentric zones and in relation with the total and pattern deviation.

As illustrated in Fig.3.2, zones 1 and 2 incorporate the same locations as the 1st and 2nd concentric annuli used by Olsson (Fig.3.1). Zones 3 and 4 include the same number of locations as the 3rd and 4th annuli in Olsson's design but with a different arrangement of locations. Zone 5 includes only 2 locations in comparison to the 5th concentric annulus, as a result of the different program of data collection. These two locations in Zone 5 are very important to include because they are very representative of glaucoma, in the typical glaucomatous visual field feature known as the nasal or Ronnie's step.

Both methods exclude the Blind Spot locations as these represent the Optic Nerve Head, where due to the anatomical structure there is no light perception.

3.3.3 Comparison of the two methods.

In order to investigate the similarities and differences between the Olsson's method and the MatLab method used in the study, firstly the data of the Olsson's publication was used to calculate the LI with the new MatLab method. The results were very similar to the Olsson's calculation (Fig. 3.3)

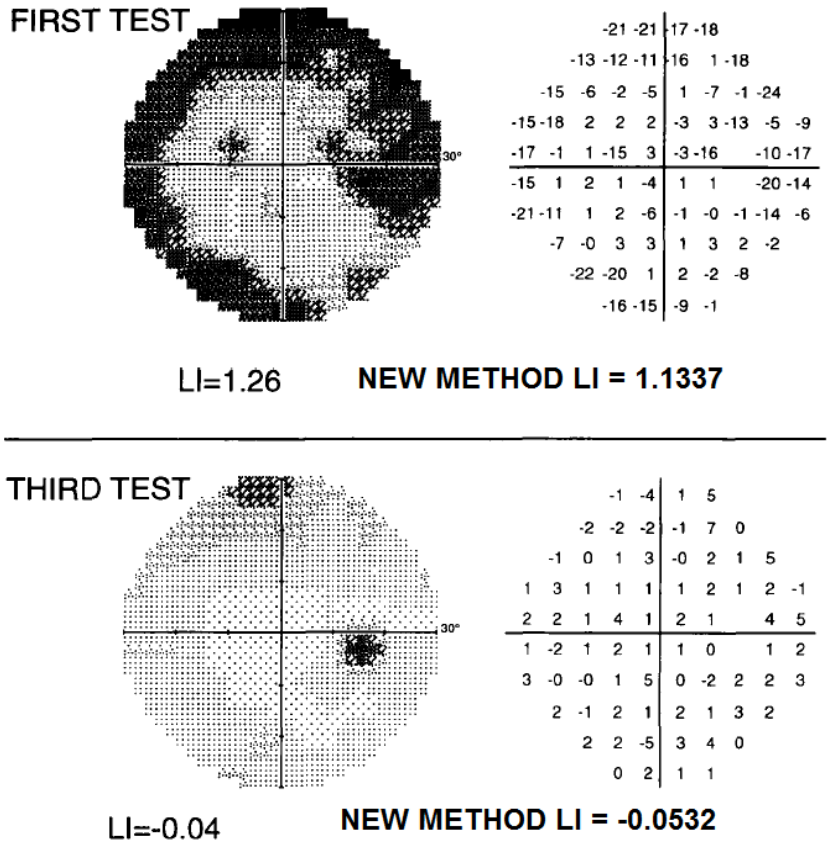

Figure 3.3. the results of LI calculation for Olsson's method (LI) and the results of the same data by the present study (NEW METHOD LI) (modified after Olsson et al., 1997)

Secondly, the data of this study were used to calculate LI by both methods for the first and third visit, for SITA standard and the right eye of normal cohort. The ANOVA one-sample T-Test results present statistically significant difference between the two methods in first visit ($p = 0.015$) and for third visit ($p= 0.010$). This difference is probably because the MatLab design instead of the third test, uses the fifth test data for the LI calculation. It is expected that in

the fifth visit, the individuals would present more perimetric experience than at the third visit, giving a total final LI higher than using third visit results.

On the other hand, the MatLab method uses SITA Standard instead of Full Threshold that used by Olsson and the 24-2 program, where a few peripheral locations used by 30-2 program are omitted. All these limitations probably produce higher numbers of LI and consequently the 1 for Learners and 0 for the individuals that cannot learn anymore could not be applied in the present study. Instead, for this MatLab study the Learner could be expected to produce a value of LI > 1 and the non-learning a LI around 0.

3.3.4 Results

The following pages illustrate the results of Learning Index calculation at first, third and fifth visit for both eyes, for normal, OAG and OHT individuals with all algorithms. Figures 3.4 to 3.16 include representative cases plots of the Total Deviation and Pattern Deviation, numerical and probability plots of all algorithms, for right and left eye respectively, at first, third and fifth visit, for 5 normal, 5 OAG and 3 OHT.

In advance of testing hypotheses, it was necessary to determine whether parametric or non-parametric statistical tests were most apprpriate. Therefore, the distribution of the data in question was inspected from histograms.

The plots show that the data were normally distributed. As a result, the most appropriate parametric descriptive statistics and tests could be used for these data.

S1F4 visit 1

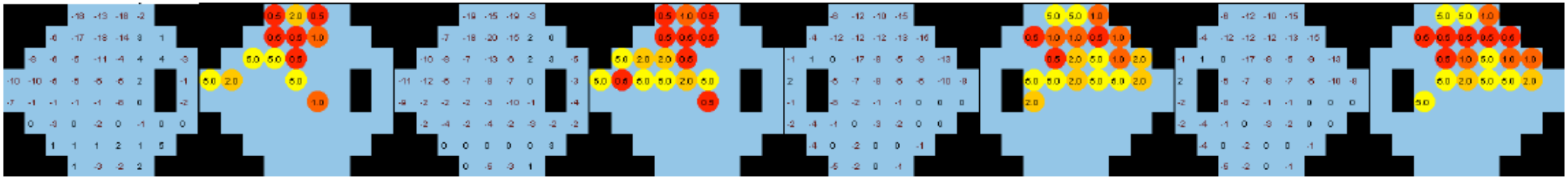

SW FL=0/12 FP=2 FN=5 LI=0.48 FL=0/11 FP=0 FN=6 LI=2.34

S1F4 visit 3

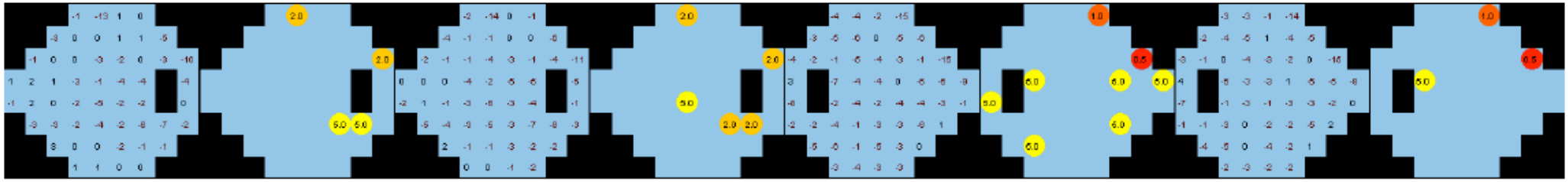

SW FL=0/11 FP=2 FN=1 LI=0.77 FL=0/12 FP=1 FN=3 LI=1.78

S1F4 visit 5

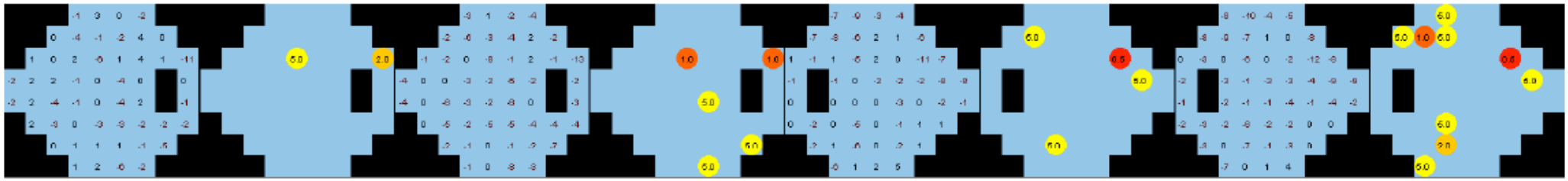

SW FL=0/12 FP=5 FN=3 LI=-0.21 FL=0/11 FP=0 FN=4 LI=-0.23

Figure 3.4. The Total Deviation and Pattern Deviation numerical and probability plots of SITA SWAP algorithm, for right and left eye respectively, at 1st (top), 3rd (middle) and 5th visit (bottom), for normal female individual aged 53, naïve to perimetry. The outcome of Learning index is likely to be influenced by the lack of experience and the specific difficulty of blue on yellow strategy.

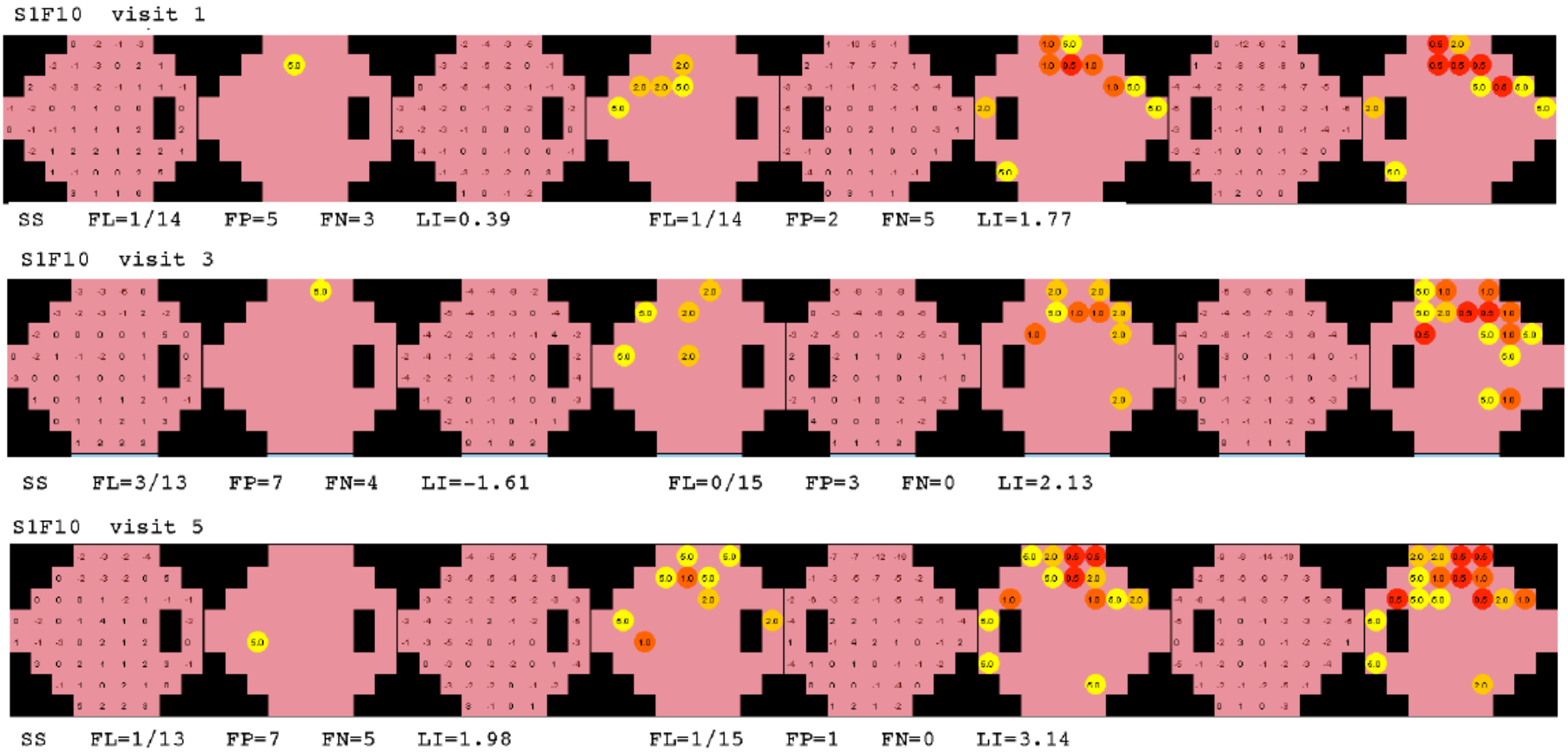

Figure 3.5. The Total Deviation and Pattern Deviation numerical and probability plots of SITA Standard algorithm, for right and left eye respectively, at 1st (top), 3rd (middle) and 5th visit (bottom), for normal female individual aged 59, naïve to perimetry. The outcome of high Learning index in left eye is likely to be influenced by the fatigue of the previous tests of the right eye or defective areas that cannot learn by repeated tests.

S1F20 visit 1

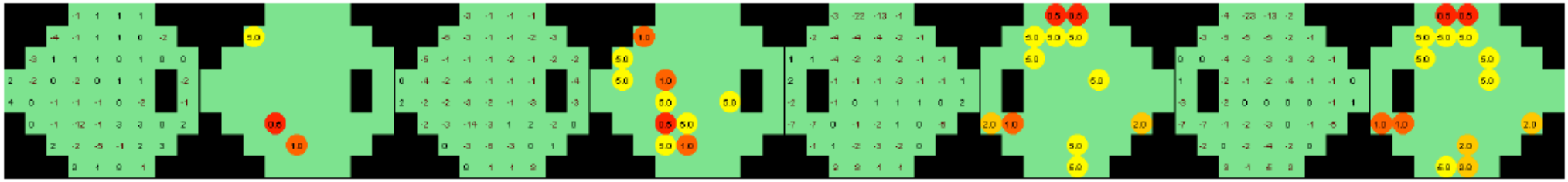

SF FL=2/10 FP=19 FN=10 LI=1.3 FL=0/11 FP=4 FN=12 LI=2.49

S1F20 visit 3

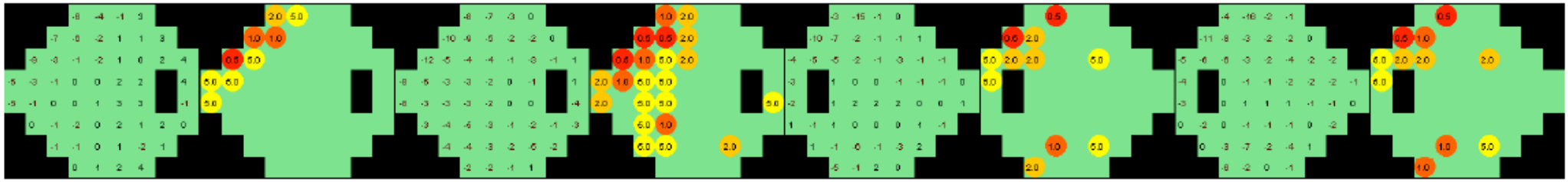

SF FL=0/10 FP=5 FN=2 LI=2.02 FL=1/10 FP=5 FN=7 LI=1.98

S1F20 visit 5

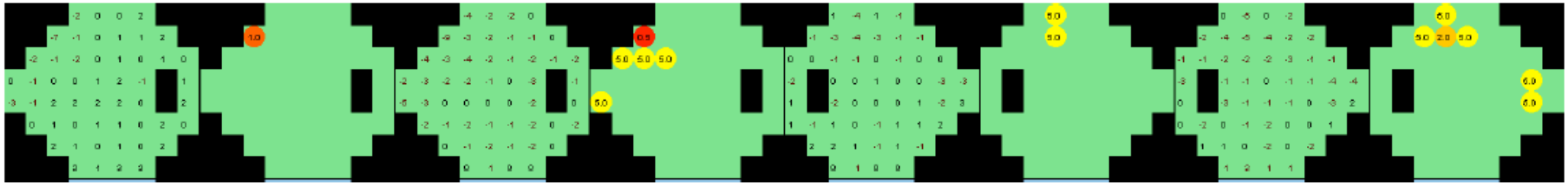

SF FL=0/10 FP=0 FN=0 LI=2.2 FL=0/11 FP=0 FN=0 LI=1.15

Figure 3.6. The Total Deviation and Pattern Deviation numerical and probability plots of SITA Fast algorithm, for right and left eye respectively, at 1st (top), 3rd (middle) and 5th visit (bottom), for normal female individual aged 48, naïve to perimetry. The outcome of high Learning index at 3rd and 5th visit, in right eye, is likely to be due to the quick algorithm that does not permit the eye to develop enough performance, but only after the 5th visit.

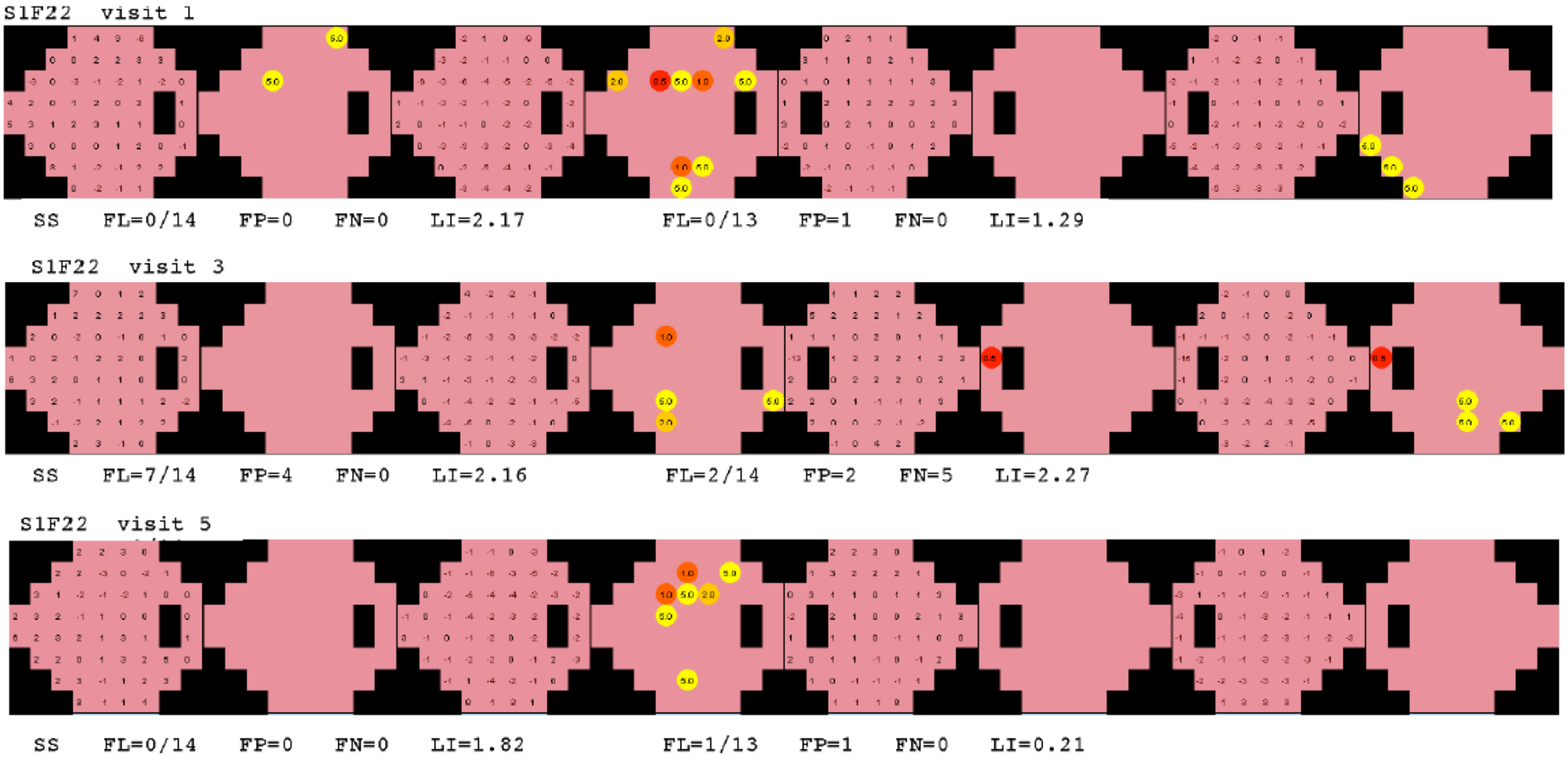

Figure 3.7 The Total Deviation and Pattern Deviation numerical and probability plots of SITA Standard algorithm, for right and left eye respectively, at 1st (top), 3rd (middle) and 5th visit (bottom), for normal female individual aged 69, naïve to perimetry. The outcome of high Learning index in both eyes at 3rd visit is likely to influenced by the inconsistency of the individual during the test (many false positives and negatives indicating poor test reliability).

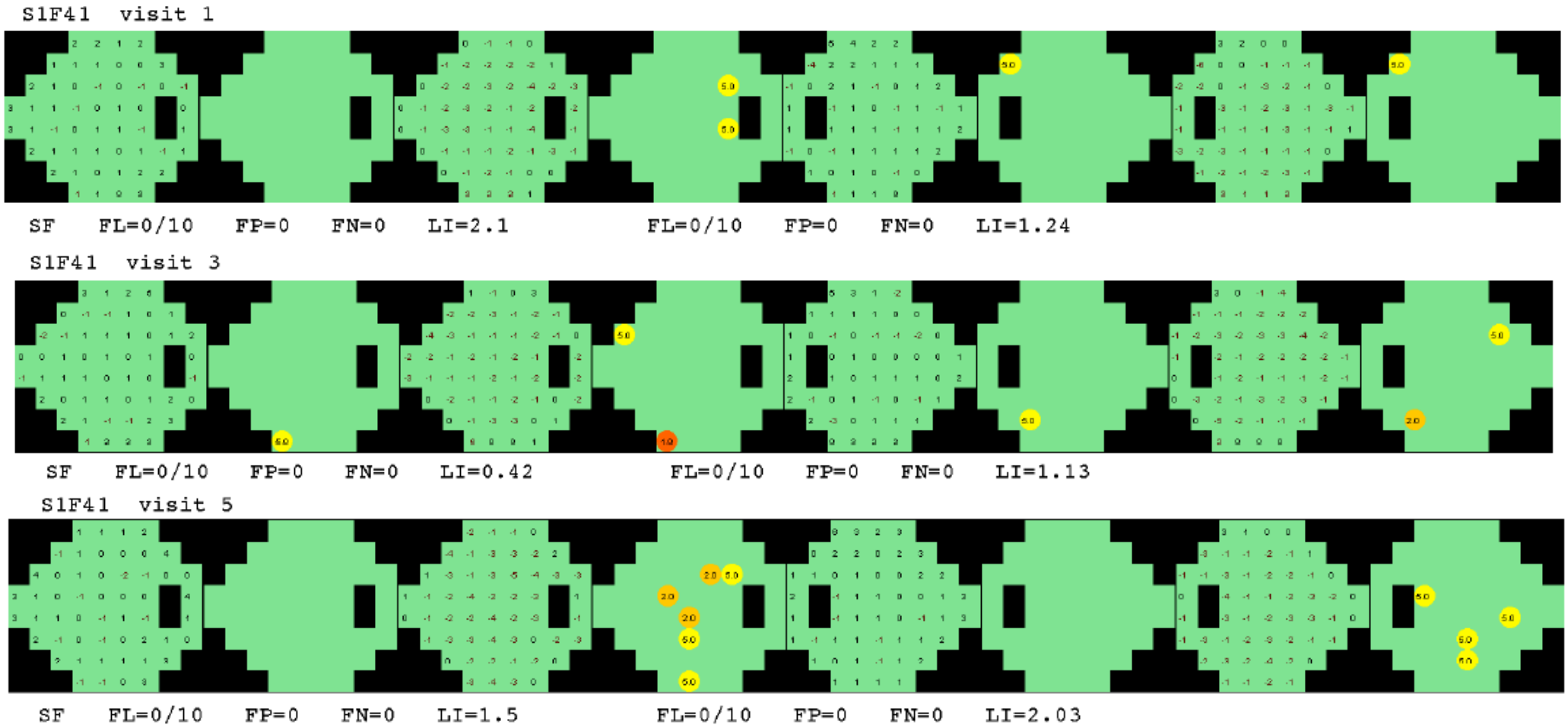

Figure 3.8. The Total Deviation and Pattern Deviation numerical and probability plots of SITA Fast algorithm, for right and left eye respectively, at 1st (top), 3rd (middle) and 5th visit (bottom), for normal female individual aged 49, naïve to perimetry. The outcome of high Learning index in both eyes at 5th visit is likely to influenced by the fatigue of previous tests.

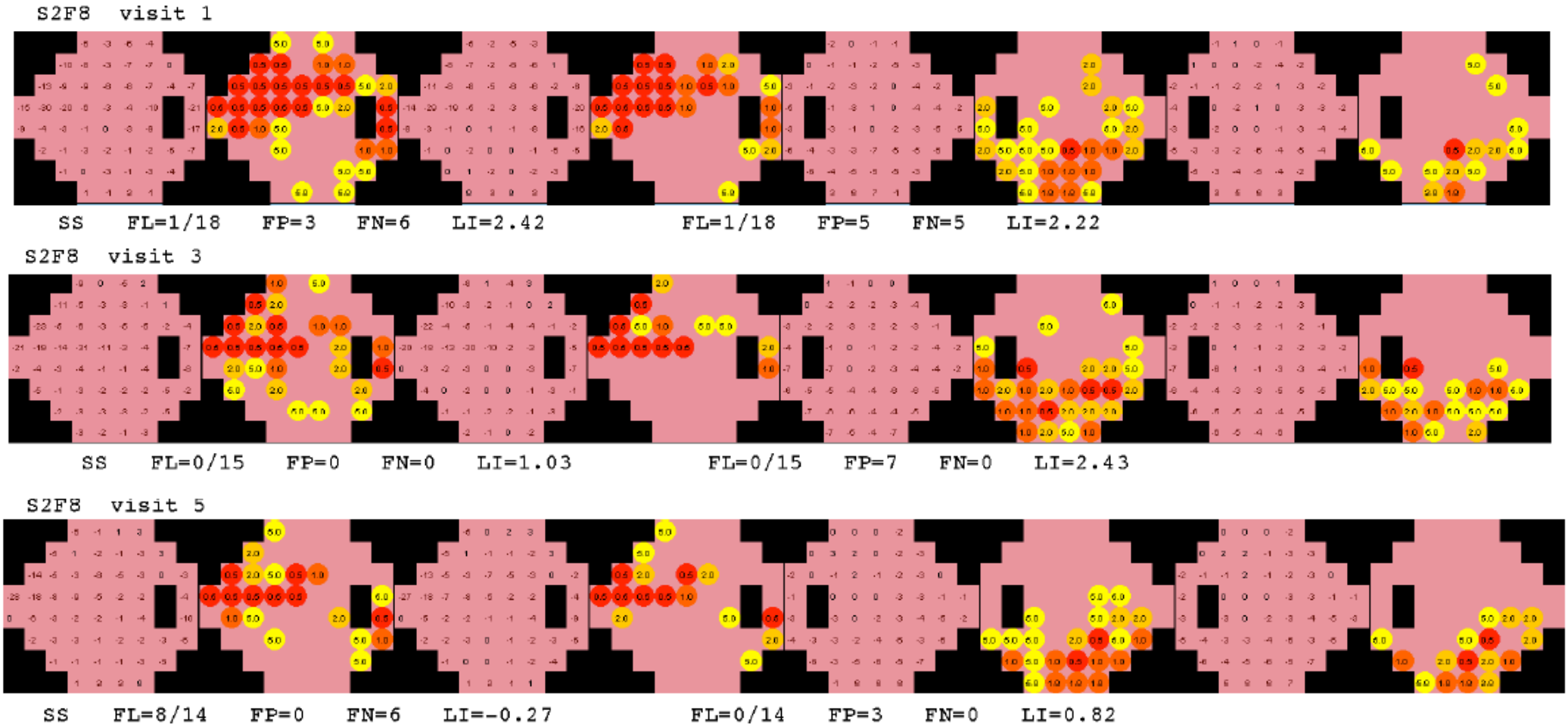

Figure 3.9 The Total Deviation and Pattern Deviation numerical and probability plots of SITA Standard algorithm, for right and left eye respectively, at 1st (top), 3rd (middle) and 5th visit (bottom), for OAG female patient aged 49. The reliability indices during the test are not acceptable and the outcome of high Learning index in both eyes at 1st and 3rd visits is likely to be due to many false positives and negatives indicating poor test reliability.

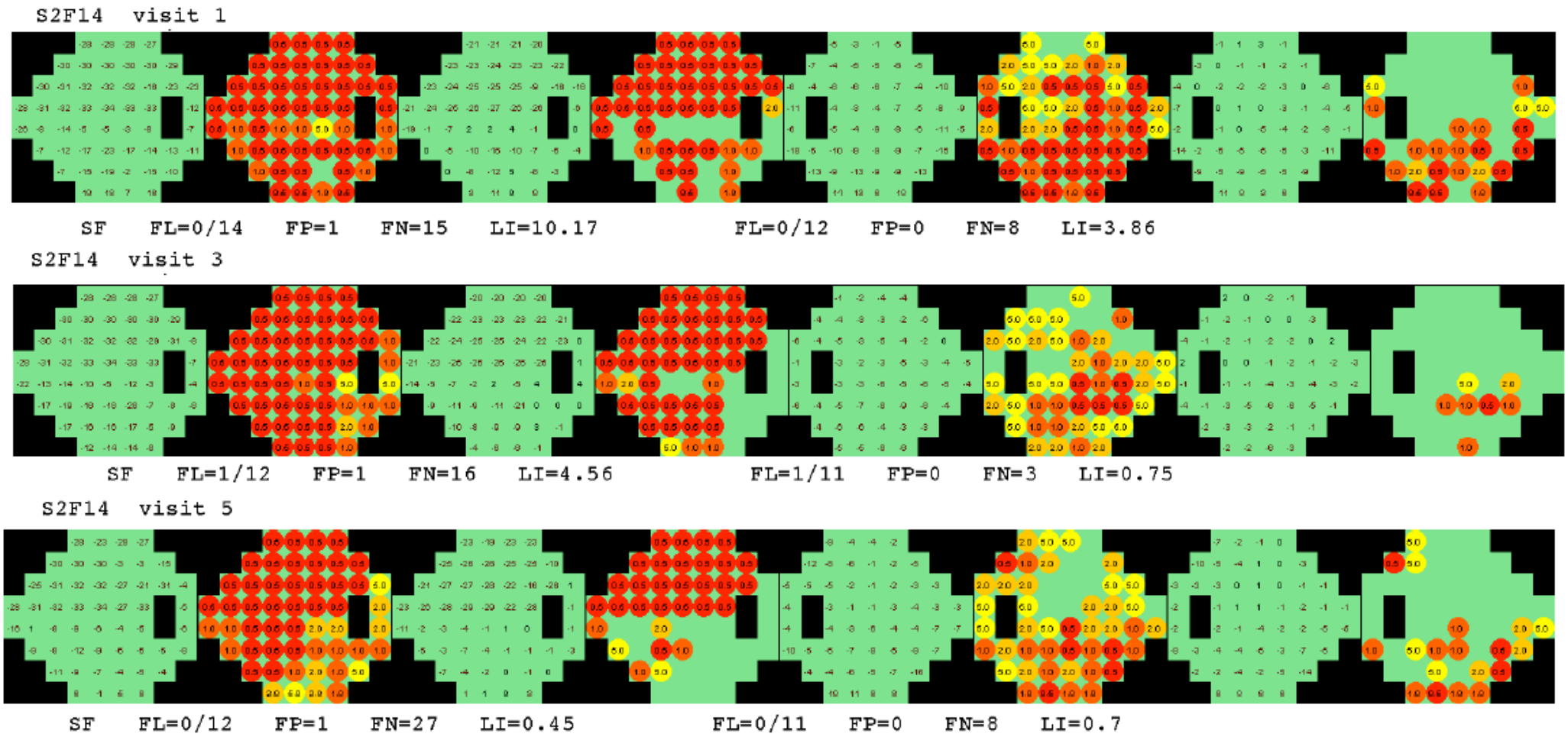

Figure 3.10 The Total Deviation and Pattern Deviation numerical and probability plots of SITA Fast algorithm, for right and left eye respectively, at 1st (top), 3rd (middle) and 5th visit (bottom), for OAG female patient aged 76.

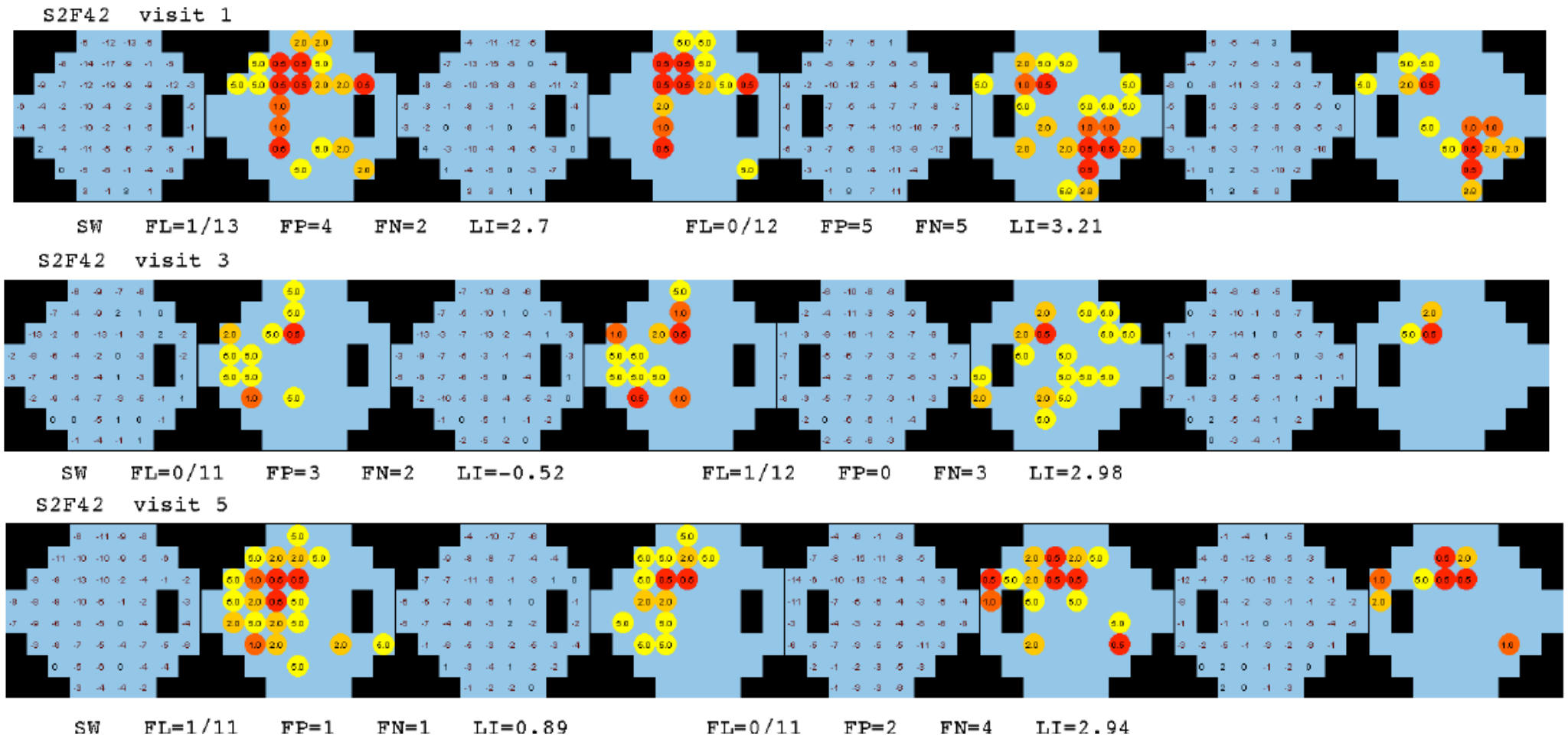

Figure 3.11 The Total Deviation and Pattern Deviation numerical and probability plots of SITA SWAP algorithm, for right and left eye respectively, at 1st (top), 3rd (middle) and 5th visit (bottom), for OAG female patient aged 69. The reliability indices during the test show poor performance, and the high Learning Index for the left eye is likely to be due to fatigue because of the difficulty of blue on yellow strategy.

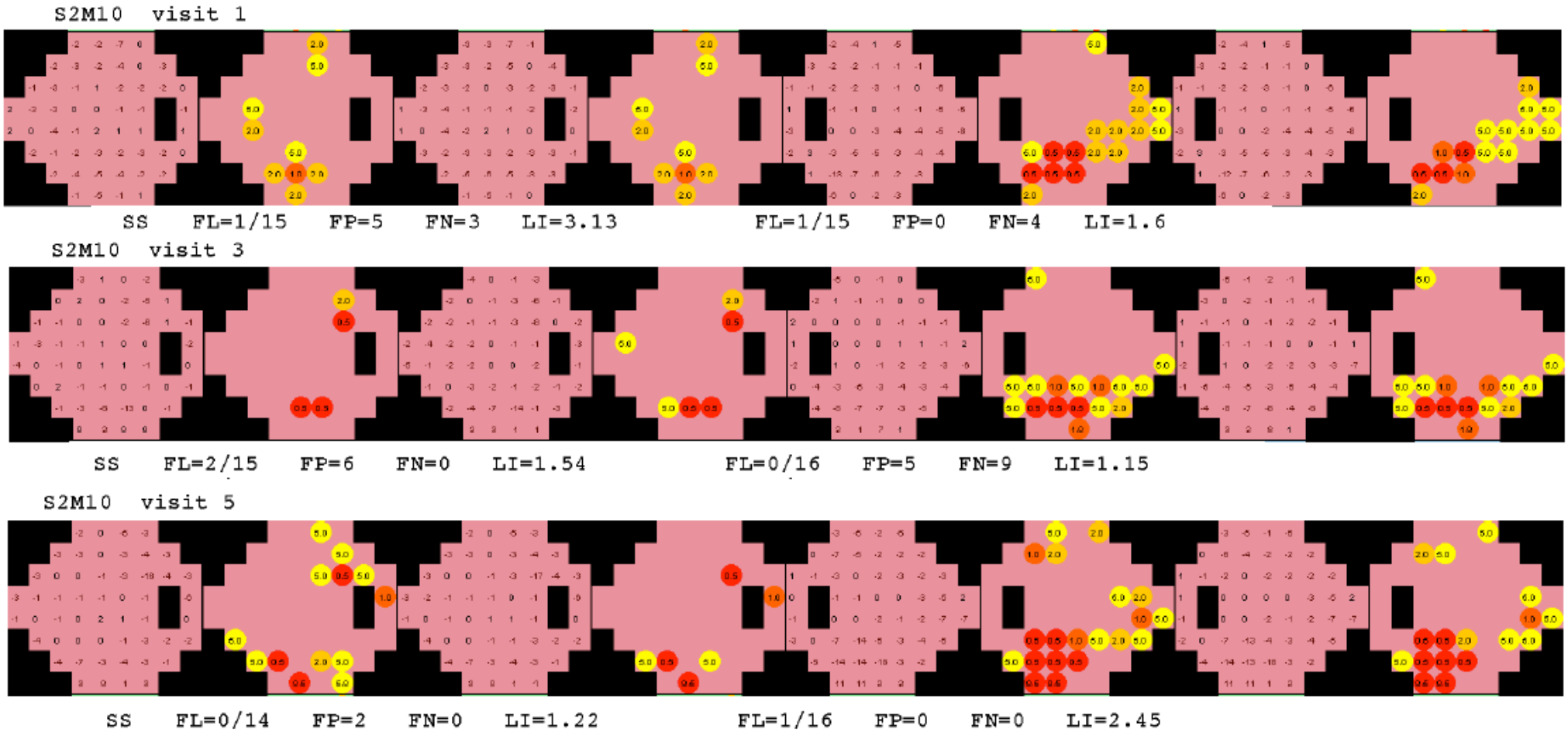

Figure 3.12 The Total Deviation and Pattern Deviation numerical and probability plots of SITA Standard algorithm, for right and left eye respectively, at 1st (top), 3rd (middle) and 5th visit (bottom), for OAG male patient aged 70. The reliability indices during the test show poor performance, and the high Learning Index is likely to be due to the defective areas that could not learn more.

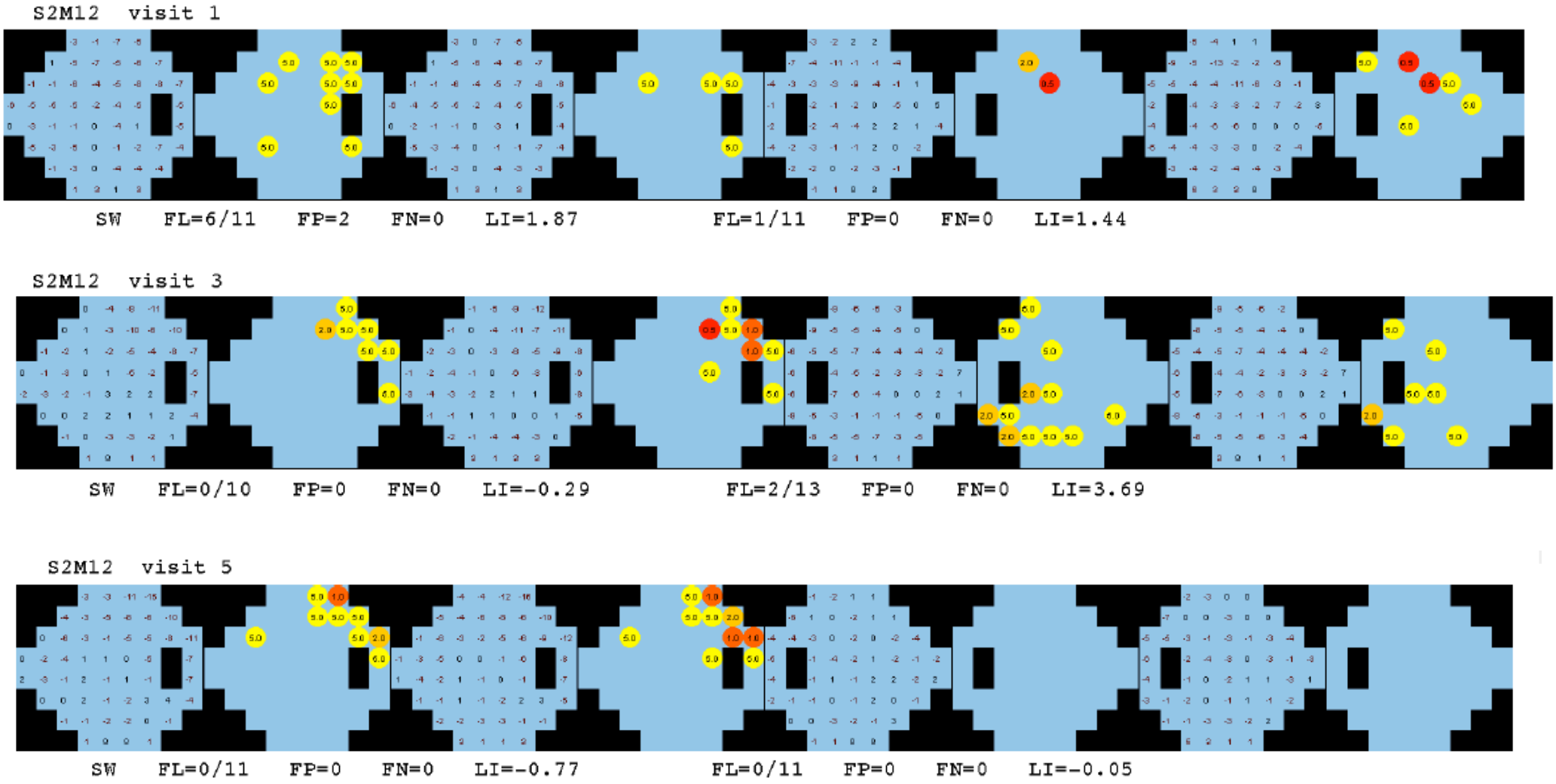

Figure 3.13 The Total Deviation and Patterns Deviation numerical and probability plots of SITA SWAP algorithm, for right and left eye respectively, at 1st (top), 3rd (middle) and 5th visit (bottom), for OAG male patient aged 52. The reliability indices during the test show very good patient performance, and the variability Learning Index is likely to be due to the difficulty of blue on yellow strategy.

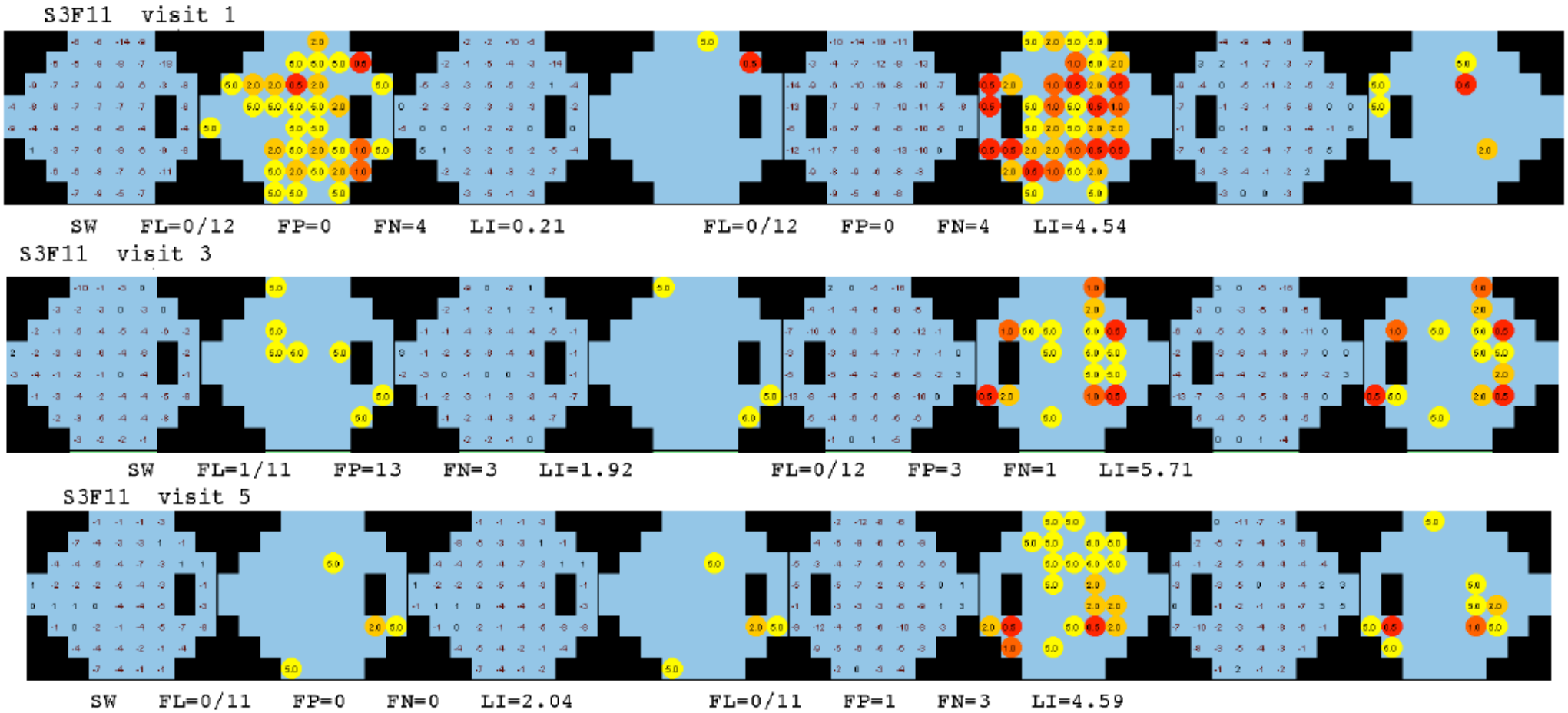

Figure 3.14 The Total Deviation and Patterns Deviation numerical and probability plots of SITA SWAP algorithm, for right and left eye respectively, at 1st (top), 3rd (middle) and 5th visit (bottom), for OHT female individual aged 71. The reliability indices during the test show poor test performance, and the high Learning Index is likely to be due to the difficulty of blue on yellow strategy and the fatigue effect that masks the learning effect.

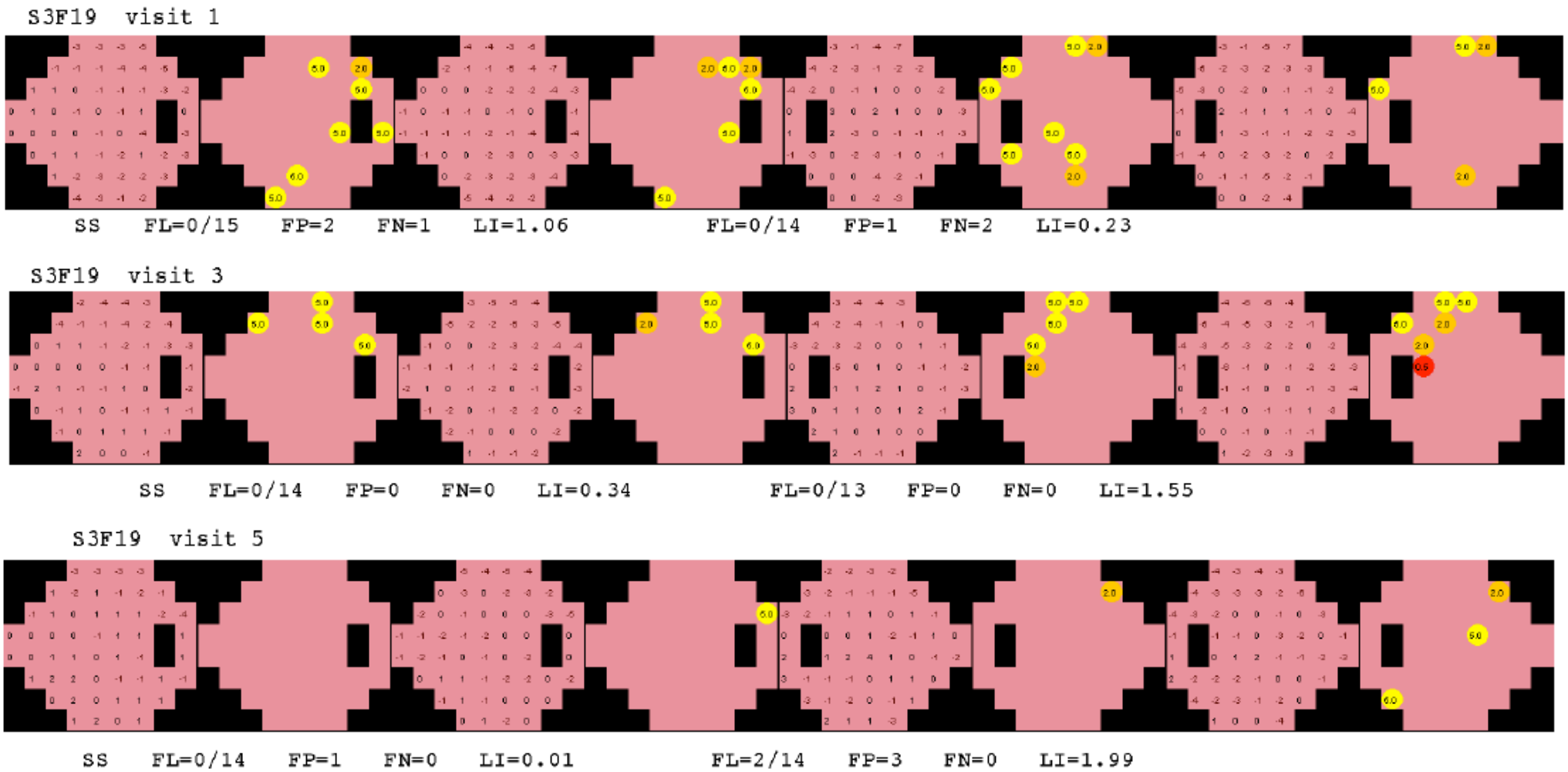

Figure 3.15 The Total Deviation and Pattern Deviation numerical and probability plots of SITA Standard algorithm, for right and left eye respectively, at 1st (top), 3rd (middle) and 5th visit (bottom), for OHT female individual aged 53. The reliability indices during the test are in general acceptable. Although at visit 1 there appears a learning transfer from the right to the left eye, next visit illustrate high index to the left eye probably due to the fatigue from previous tests.

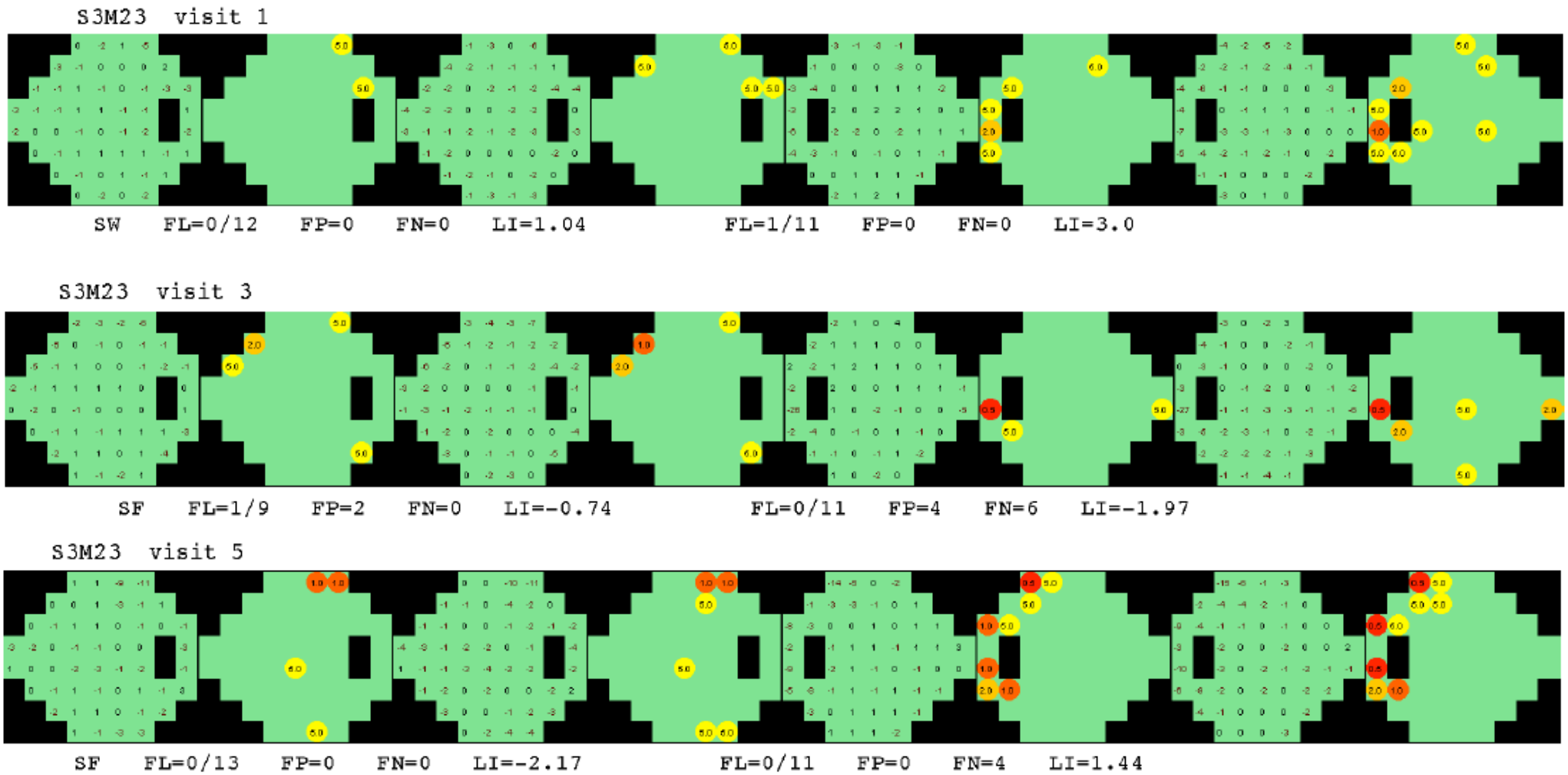

Figure 3.16 The Total Deviation and Pattern Deviation numerical and probability plots of SITA Fast algorithm, for right and left eye respectively, at 1st (top), 3rd (middle) and 5th visit (bottom), for OHT male individual aged 50. The reliability indices during the test are in general acceptable but the various Learning Index in both eyes is most likely due to the fatigue from previous tests.

Figure 3.17 illustrates the descriptive statistics and the Box and Whisker plots for the Learning Index for normal individuals, across the five visits, for the right eye, within algorithm for SITA Standard, SITA Fast and SITA SWAP

Figures 3.18 and 3.19 illustrate the descriptive statistics and the Box and Whisker plots for the Learning Index for the glaucomatous and the hypertensive individuals, respectively, across the five visits, for the right eye, within algorithm for SITA Standard, SITA Fast and SITA SWAP.

Figures 3.20, 3.21 and 3.22 illustrates the descriptive statistics and the Box and Whisker plots for the Learning Index for all cohorts, across the five visits, within algorithm for SITA Standard, SITA Fast and SITA SWAP, for the left eye.

Normal Cohort
Algorithm

SITA STANDARD

Eye Right

Visit	1	2	3	4	5
Mean	0.89	0.78	0.83	1.07	1.11
SD	1.04	0.97	1.03	0.68	1.06
Median	0.68	0.57	1.12	1.12	1.23
Min	-1.08	-0.93	-1.61	-0.42	-1.32
Max	3.09	3.12	2.53	2.53	3.08
1st quartile	0.31	0.23	-0.02	0.63	0.52
3rd quartile	1.71	1.19	1.68	1.43	1.87

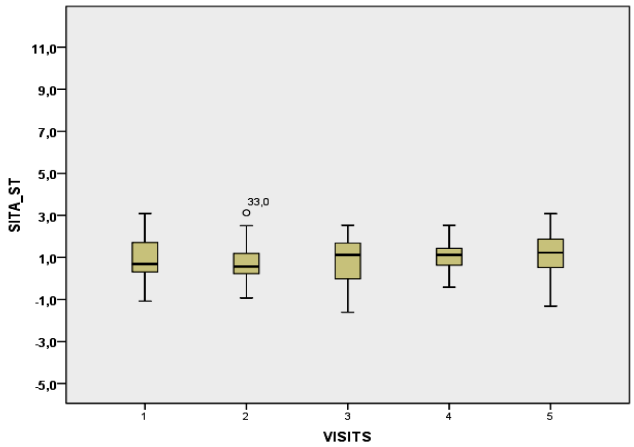

Normal Cohort
Algorithm

SITA FAST

Eye Right

Visit	1	2	3	4	5
Mean	0.96	1.01	1.07	0.79	0.90
SD	1.40	0.79	0.70	1.16	1.04
Median	1.17	1.02	1.11	1.05	1.04
Min	-1.28	-0.55	-0.47	-2.34	-1.05
Max	4.09	2.76	2.45	2.25	2.57
1st quartile	0.05	0.56	0.50	0.04	0.32
3rd quartile	1.80	1.47	1.57	1.74	1.50

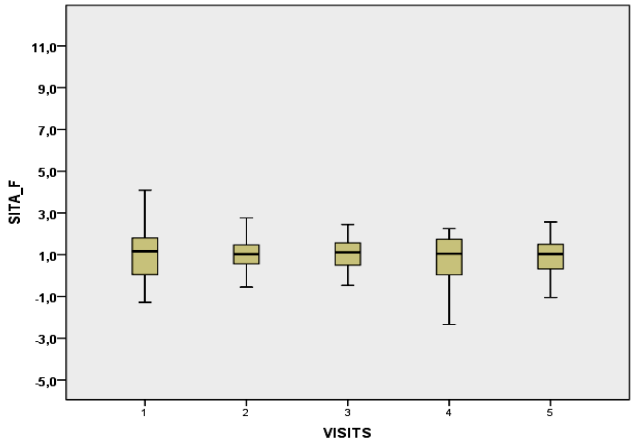

Normal Cohort
Algorithm

SITA SWAP

Eye Right

Visit	1	2	3	4	5
Mean	0.77	0.80	0.83	0.85	0.65
SD	0.86	1.17	1.17	1.61	1.24
Median	0.58	0.62	1.05	1.01	0.62
Min	-0.87	-1.65	-2.14	-1.93	-2.27
Max	2.64	3.49	2.68	5.50	3.26
1st quartile	0.38	0.20	0.11	-0.51	-0.02
3rd quartile	1.31	1.41	1.67	1.68	1.41

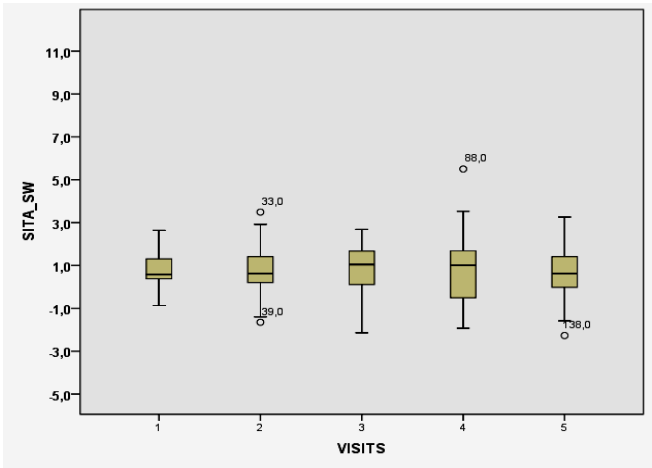

Figure 3.17 The descriptive statistics (left panel), for the Learning Index for normal individuals (right eye), across the five visits, for each of the three algorithms. Box and Whisker plots (right panel), of the Learning Index distribution for the normal individuals (right eye), across the five visits, within algorithm for SITA Standard (top), SITA Fast (middle) and SWAP (bottom).

Glaucoma Cohort
Algorithm

SITA STANDARD

Eye	Right				
Visit	1	2	3	4	5
Mean	1.33	1.42	1.34	1.07	0.99
SD	1.26	1.13	0.87	1.24	1.24
Median	1.14	1.42	1.53	1.01	0.89
Min	-1.07	-0.44	-0.30	-1.22	-1.87
Max	4.54	4.12	3.54	3.34	3.31
1st quartile	0.74	0.60	0.74	0.14	0.28
3rd quartile	1.88	2.12	1.85	1.84	1.46

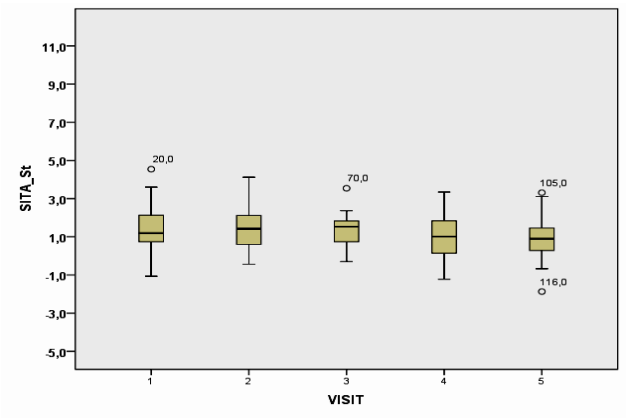

Glaucoma Cohort
Algorithm

SITA FAST

Eye	Right				
Visit	1	2	3	4	5
Mean	1.40	1.26	1.19	1.47	1.17
SD	2.26	1.80	1.27	1.83	1.02
Median	1.24	1.08	1.11	0.99	1.16
Min	-3.35	-0.85	-0.89	-0.67	-1.13
Max	10.17	8.59	4.56	8.49	2.67
1st quartile	0.38	0.26	0.56	0.64	0.44
3rd quartile	2.38	1.83	1.55	1.82	2.16

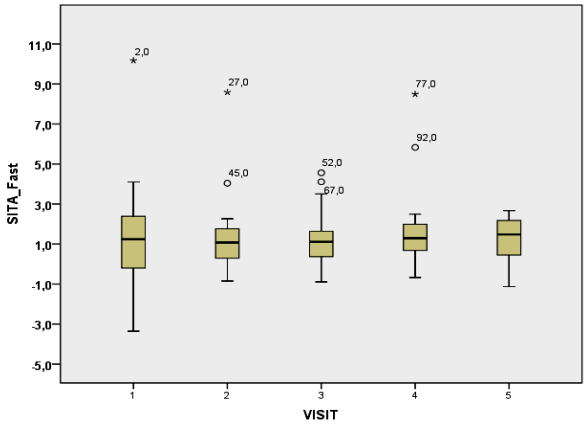

Glaucoma Cohort
Algorithm

SITA SWAP

Eye	Right				
Visit	1	2	3	4	5
Mean	1.20	1.46	1.38	1.33	1.32
SD	1.38	1.97	2.23	2.27	2.11
Median	0.95	0.92	0.90	0.86	1.22
Min	-0.50	-0.97	-3.14	-2.54	-3.78
Max	5.90	7.11	8.73	10.30	7.91
1st quartile	0.20	-0.04	-0.07	-0.01	0.09
3rd quartile	1.90	2.87	2.59	2.19	2.11

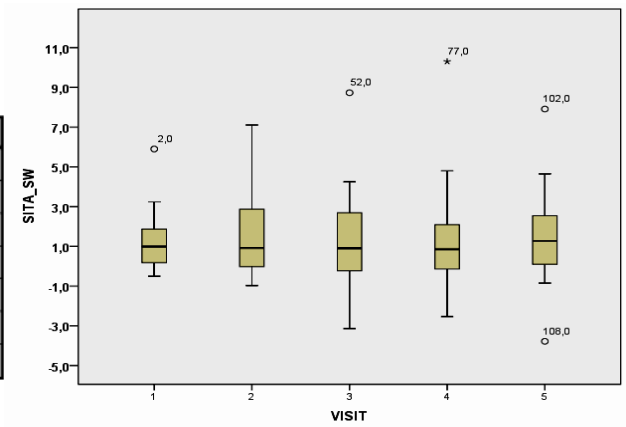

Figure 3.18. The descriptive statistics (left panel), for the Learning Index for OAG individuals (right eye), across the five visits, for each of the three algorithms. Box and Whisker plots (right panel), of the Learning Index distribution for the OAG individuals (right eye), across the five visits, within algorithm for SITA Standard (top), SITA Fast (middle) and SWAP (bottom).

OHT Cohort
Algorithm

SITA STANDARD

Eye Right

Visit	1	2	3	4	5
mean	0.82	1.31	1.03	0.99	0.99
SD	1.18	0.80	1.10	1.09	1.05
median	0.88	1.20	1.12	1.10	0.77
min	-1.89	-0.11	-0.89	-1.79	-1.41
max	3.49	7.75	2.78	2.98	3.14
1st quartile	0.21	0.19	0.34	0.32	0.28
3rd quartile	1.75	2.81	2.16	1.51	1.81

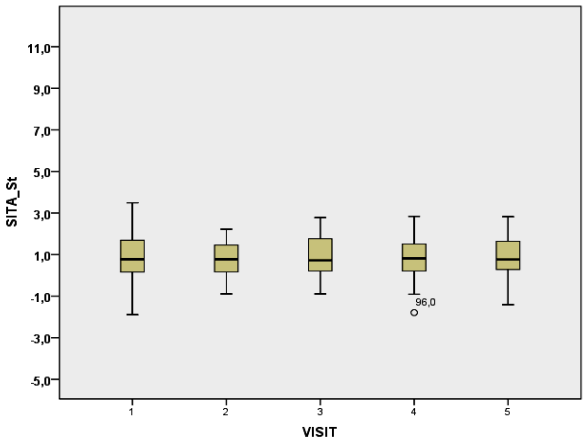

OHT Cohort
Algorithm

SITA FAST

Eye Right

Visit	1	2	3	4	5
mean	0.70	0.74	0.75	0.67	0.93
SD	1.08	1.06	0.70	1.05	1.13
median	0.85	0.62	0.89	0.68	1.15
min	-1.67	-2.33	0.00	-1.92	-2.17
max	2.49	2.21	6.27	2.29	2.92
1st quartile	0.22	0.29	0.17	0.18	0.35
3rd quartile	1.26	1.57	2.17	1.21	1.67

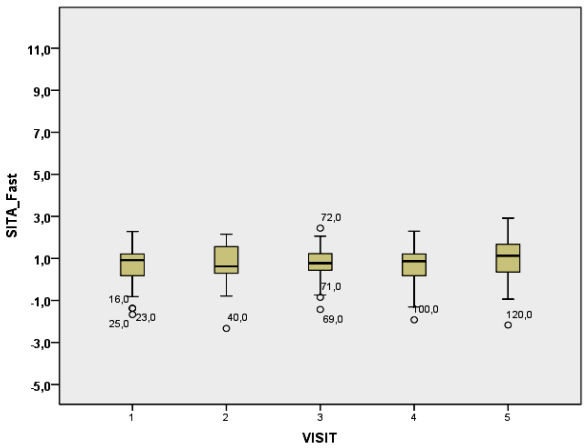

OHT Cohort
Algorithm

SITA SWAP

Eye Right

Visit	1	2	3	4	5
mean	1.05	0.70	0.69	0.85	1.05
SD	1.12	1.56	1.28	1.61	1.30
median	0.85	0.52	0.46	1.01	1.11
min	-1.37	-1.97	0.00	-1.93	-1.30
max	2.90	3.95	8.90	5.50	3.34
1st quartile	0.20	-0.41	-0.10	-0.51	0.09
3rd quartile	1.94	2.01	2.93	1.68	1.93

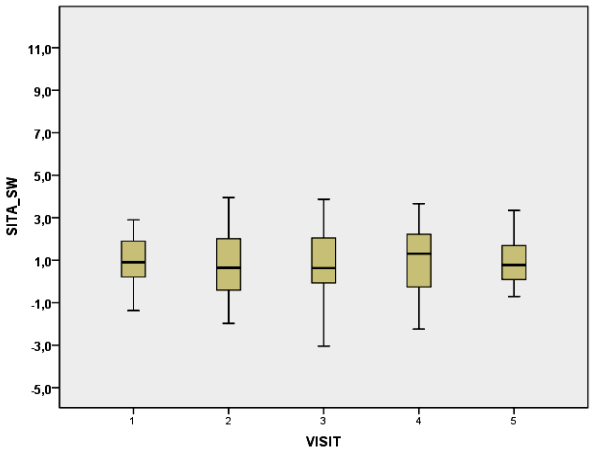

Figure 3.19. The descriptive statistics (left panel), for the Learning Index for OHT individuals (right eye), across the five visits, for each of the three algorithms. Box and Whisker plots (right panel), of the Learning Index distribution for the OHT individuals (right eye), across the five visits, within algorithm for SITA Standard (top), SITA Fast (middle) and SWAP (bottom).

Normal Cohort
Algorithm

SITA STANDARD

Eye Left

Visit	1	2	3	4	5
Mean	0.99	0.98	0.95	1.06	1.10
SD	0.86	1.00	0.85	0.97	1.33
Median	1.29	0.80	0.99	1.06	1.05
Min	-0.78	-1.12	-0.39	-0.85	-2.44
Max	2.99	3.03	2.90	2.98	4.17
1st quartile	0.17	0.30	0.46	0.48	0.27
3rd quartile	1.54	1.70	1.31	1.55	1.65

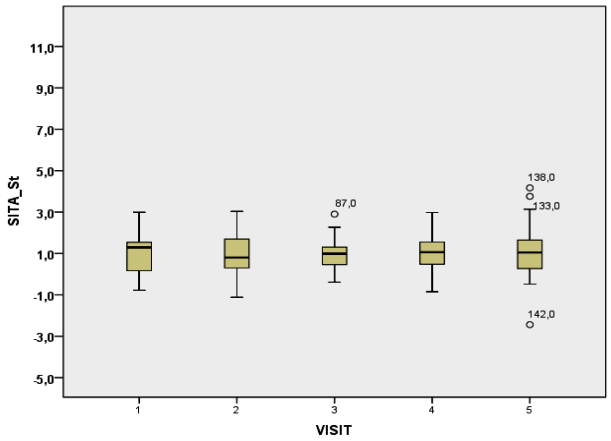

Normal Cohort
Algorithm

SITA FAST

Eye Left

Visit	1	2	3	4	5
Mean	0.89	1.12	0.98	0.91	0.90
SD	1.03	0.89	0.85	0.91	0.89
Median	0.78	1.08	0.93	1.01	0.92
Min	-0.47	-0.81	-0.77	-1.62	-1.50
Max	3.09	2.41	2.55	2.21	2.66
1st quartile	0.08	0.47	0.48	0.27	0.17
3rd quartile	1.53	2.02	1.62	1.58	1.62

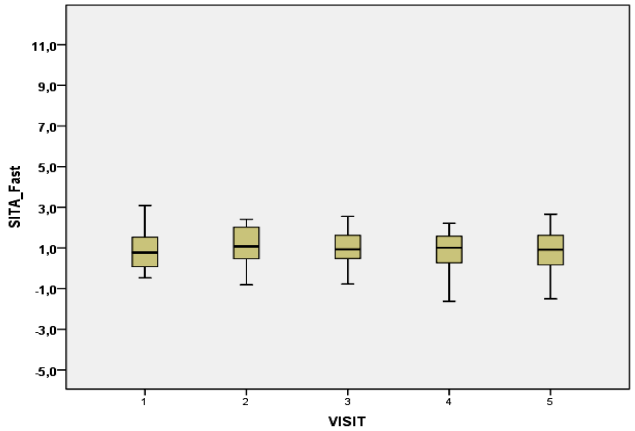

Normal Cohort
Algorithm

SITA SWAP

Eye Left

Visit	1	2	3	4	5
Mean	0.99	0.91	1.09	1.01	0.75
SD	1.15	1.41	1.79	1.22	1.26
Median	0.89	1.24	1.34	0.97	0.90
Min	-1.27	-2.54	-2.41	-1.10	-1.73
Max	2.84	3.05	4.15	3.55	3.34
1st quartile	0.29	0.19	-0.14	0.08	0.12
3rd quartile	1.84	1.78	2.49	2.15	1.56

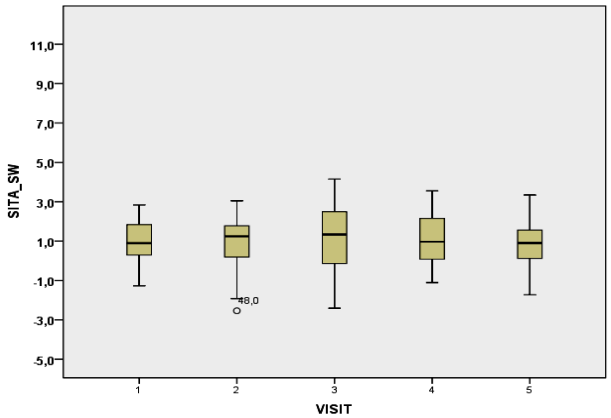

Figure 3.20 The descriptive statistics (left panel), for the Learning Index for normal individuals (left eye), across the five visits, for each of the three algorithms. Box and Whisker plots (right panel), of the Learning Index distribution for the normal individuals (left eye), across the five visits, within algorithm for SITA Standard (top), SITA Fast (middle) and SWAP (bottom).

Glaucoma Cohort
Algorithm

SITA STANDARD

Eye Left

Visit	1	2	3	4	5
Mean	1.31	1.36	1.03	1.10	1.05
SD	1.37	1.49	1.23	1.32	0.87
Median	1.00	1.29	1.15	1.21	1.22
Min	-0.95	-1.57	-1.17	-2.25	-0.56
Max	4.81	5.30	3.00	4.05	2.45
1st quartile	0.29	0.29	0.05	0.06	0.47
3rd quartile	2.00	2.29	1.83	1.92	1.72

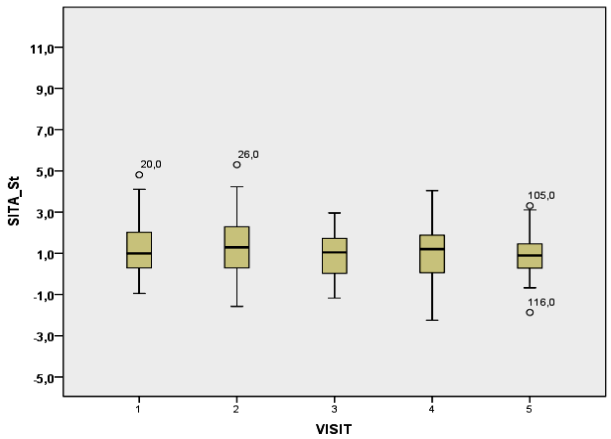

Glaucoma Cohort
Algorithm

SITA FAST

Eye Left

Visit	1	2	3	4	5
Mean	1.30	1.15	1.07	1.13	1.09
SD	1.40	0.83	1.04	1.26	1.09
Median	1.26	1.23	1.14	1.08	1.30
Min	-1.76	-1.35	-2.20	-2.61	-2.59
Max	3.86	2.43	2.55	2.98	2.57
1st quartile	0.67	0.97	0.59	0.51	0.70
3rd quartile	2.46	1.53	1.82	2.24	1.76

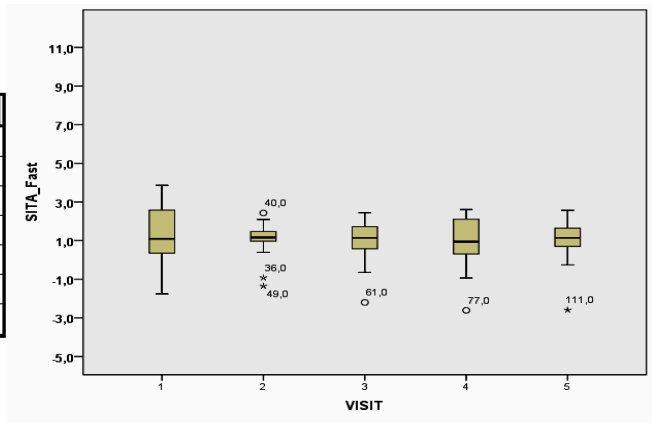

Glaucoma Cohort
Algorithm

SITA SWAP

Eye Left

Visit	1	2	3	4	5
Mean	1.43	1.36	1.48	1.32	1.39
SD	1.71	1.69	1.85	1.84	1.57
Median	1.06	1.15	1.55	1.19	1.34
Min	-1.29	-2.34	-2.00	-1.54	-1.22
Max	6.40	5.49	5.71	6.81	4.59
1st quartile	0.27	0.34	0.29	0.43	0.23
3rd quartile	2.24	2.19	2.53	2.25	2.13

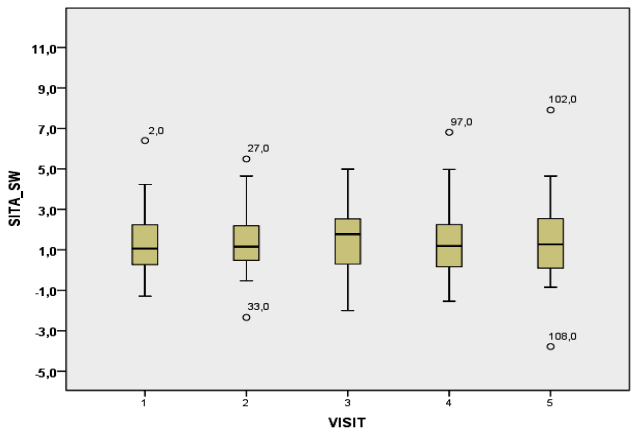

Figure 3.21 The descriptive statistics (left panel), for the Learning Index for OAG individuals (left eye), across the five visits, for each of the three algorithms. Box and Whisker plots (right panel), of the Learning Index distribution for the OAG individuals (left eye), across the five visits, within algorithm for SITA Standard (top), SITA Fast (middle) and SWAP (bottom).

OHT Cohort
Algorithm

SITA STANDARD

Eye Left

Visit	1	2	3	4	5
mean	0.79	0.72	1.19	1.03	1.01
SD	1.14	0.90	0.93	1.31	0.96
median	0.76	0.66	1.27	1.32	1.05
min	-1.93	-0.88	-0.61	-1.79	-0.93
max	2.59	2.43	3.21	3.46	2.44
1st quartile	0.02	-0.03	0.49	-0.14	0.39
3rd quartile	1.77	1.34	1.91	1.91	1.74

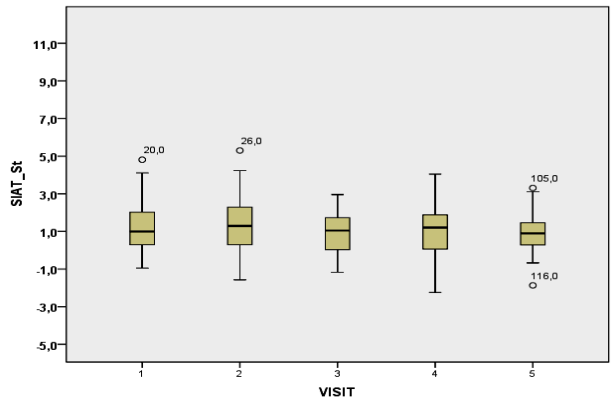

OHT Cohort
Algorithm:

SITA FAST

Eye Left

Visit	1	2	3	4	5
mean	0.97	0.79	1.23	0.62	1.07
SD	1.09	1.21	1.33	0.77	1.26
median	1.15	1.20	1.20	0.72	1.39
min	-0.94	-2.15	-1.97	-0.03	-1.62
max	3.49	2.37	5.50	7.22	3.16
1st quartile	0.09	0.11	0.61	0.10	0.79
3rd quartile	1.47	1.70	1.82	1.85	2.04

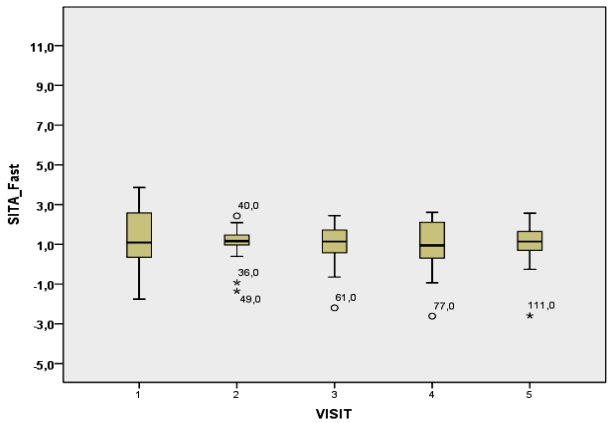

OHT Cohort
Algorithm:

SITA SWAP

Eye Left

Visit	1	2	3	4	5
mean	0.72	0.85	0.44	1.11	1.13
SD	1.40	1.56	1.84	1.53	1.34
median	0.18	0.44	0.51	1.03	1.08
min	-1.20	-1.14	-4.86	-0.24	-1.01
max	4.54	4.81	5.71	10.29	4.59
1st quartile	-0.27	-0.21	-0.52	0.20	0.23
3rd quartile	1.24	1.82	1.30	2.85	1.86

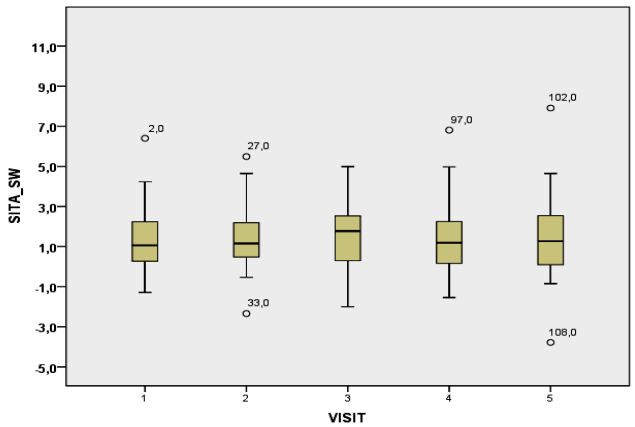

Figure 3.22. The descriptive statistics (left panel), for the Learning Index for OHT individuals (left eye), across the five visits, for each of the three algorithms. Box and Whisker plots (right panel), of the Learning Index distribution for the OHT individuals (left eye), across the five visits, within algorithm for SITA Standard (top), SITA Fast (middle) and SWAP (bottom).

3.3.5 Discussion

Fulfilling the purpose of this study, a learning index was developed in a similar way to Olsson's Learner's Index (Olsson et al., 1997). Then a set of case series of visual fields of three different groups was considered in terms of reliability indices, TD and PSD compared to the Learning Index for each of the first, third and fifth consecutive sessions.

3.3.5.1 Typical Results from Individual Subjects

Considering results from normal individuals for the SITA Standard algorithm observed an expected decrease of LI between 1st and 3rd or 5th visit in some subjects. This LI reduction after 2 or 3 perimetric tests probably is owing to the performance of naïve in perimetry normal individuals that was expected to improve and as a result the LI expected to be closer to zero (0). In contrast, the left eye either demonstrated fatigue or inconsistency of the examined individual (for example Fig.3.5 and 3.7).

The SITA Fast algorithm often showed a higher LI than for the SITA Standard algorithm (for example Fig. 3.6 and 3.8) because probably the quick algorithm does not permit the eye to develop enough performance or because the results were influenced by expected fatigue of previous tests, although these subjects had completed SITA Standard tests 5 times for each eye before and were expected to exhibit more perimetric experience due to the learning transfer from the previous algorithm. Also, the lack of previous experience in the case of SITA SWAP (for example Fig. 3.4) combined with the difficulty of the blue on yellow algorithm influenced the LI results.

In glaucomatous patients for the SITA Standard algorithm, observed very high LI at 1st visit, and slightly lower values at 3rd and 5th visit (for example Fig.3.9 and 3.11), probably due to defective areas that could not learn or due to the inconsistency of the individual, although these subjects were more experienced in perimetry. For SITA Fast algorithm, exhibited poor performance (for example Fig. 3.10) as the quick algorithm combined with the defective areas most likely produced ambiguous LI results. For SITA SWAP although the good performance of the patient (for example Fig. 3.13), the great difficulty of blue on yellow perimetry combined with the glaucoma defects and the fatigue on left eye (for example Fig. 3.11), provided higher LI results.

The ocular hypertensive individuals for SITA Standard presented higher LI for the left eye (for example Fig. 3.15) most likely due to some fatigue transferred from the right eye, as the right was always tested before the left eye at every session. For SITA Fast exhibited high LI for both eyes (Fig. 3.15) most likely due to fatigue transferred from previous tests and for SITA SWAP high LI probably due to the difficulty of Blue on Yellow algorithm.

3.3.5.2 Summary descriptive statistics for each group

For a more general analysis of the behaviour of the different examined groups towards the LI development, the descriptive statistics in Figures 3.17, 3.18 and 3.19 may be evaluated for the right eyes and for the left eyes in Figures 3.20, 3.21 and 3.22.

3.3.5.3 Statistical analysis of any change in mean LI over five visits.

One-way repeated measures ANOVA analysis was carried out to test the hypothesis that the LI did not change significantly across visits for any of the tests and in any of the participant groups. The test analysis showed that in the normal cohort with the SITA Standard algorithm, within-subject effects p-values were p=0.566 for the right eye and p=0.953 for the left eye, for SITA Fast algorithm, were p=0.823 for the right eye and p=0.849 for the left eye and for SITA SWAP algorithm, p-values were p=0.942 for the right eye and p=0.660 for the left eye. These findings indicate that there was no statistically significant variation in LI across visits.

In the glaucoma cohort and with the SITA Standard algorithm, within-subject effects p-values were p=0.472 for the right eye and p=0.270 for the left eye, with the SITA Fast algorithm, p-values were p=0.657 for the right eye and p=0.888 for the left eye and with the SITA SWAP algorithm, p-values were p=0.923 for the right eye and p=0.920 for the left eye. These findings indicate that there was not statistically significant variation in LI across visits.

In the OHT cohort and with the SITA Standard algorithm, within-subjects effects p-values were p=0.980 for the right eye and p=0.200 for the left eye, with SITA Fast algorithm, p-values were p=0.889 for the right eye and p=0.776 for the left eye and with the SITA SWAP algorithm, p-values were p=0.873 for the right eye and p=0.263 for the left eye. These findings indicate that there was no statistically significant variation in LI across visits.

The group mean MD and the mean LI for each eye of each of the 3 groups of patients at each of the 5 visits is shown in Table 3.2 for the right eye and Table 3.3 for the left one. Subsequent figures (3.23 to 3.25) show the how mean LI is associated (or otherwise) with mean MD, for all visits and with each of the threshlding algorithms.

The group mean MD was better for the right (first examined) eye than for the left eye across the 5 visits for the 3 cohorts; however, this difference varied between groups ($p<0.001$) and was most negative (worst) with SITA SWAP, being present for the group with OAG and for the group with OHT, although experienced in perimetry. The magnitudes of the MD also was not dependent on the extent of the previous perimetric experience of groups ($p=0.567$) as the groups with OAG and with OHT were more experienced in perimetry, and of the order of the three algorithms within the examination ($p=0.509$).

The magnitude of the association between mean LI and mean MD is, in general, small, as denoted by the modest linear regression slopes, however, it should be borne in mind that because mean values are regressed, these slopes represent the average association. In some individuals, the association will likely be greater, while for others, it will likely be smaller. The strength of the relationship, as denoted by the R^2 values, is reasonably strong in most cases. A stronger association can be observed in normal individuals than in the OAG and OHT cohorts.

Algorithm	Visit 1		Visit 2		Visit 3		Visit 4		Visit 5	
	MD	LI	MD	LI	MD	LI	MD	LI	MD	LI
SITA Standard	0.88 (0.99)	0.89 (1.04	0.63 (0.96)	0.78 (0.97)	0.63 (0.99)	0.83 (1.03)	0.88 (0.99)	1.07 (0.68)	0.72 (1.13)	1.11 (1.06)
SITA Fast	0.02 (1.03)	0.96 (1.40)	0.29 (0.74)	1.01 (0.79)	0.49 (0.85)	1.07 (0.70)	0.36 (1.00)	0.79 (1.16)	0.59 (0.73)	0.90 (1.04)
SITA SWAP	-1.78 (2.94)	0.77 (0.86)	-1.02 (2.78)	0.80 (1.17)	-0.84 (2.63)	0.83 (1.17)	-0.93 (2.70)	0.85 (1.61)	-0.43 (2.54)	0.65 (1.24)
SITA Standard	-1.42 (4.90)	1.33 (1.26)	-1.03 (4.16)	1.42 (1.13)	-0.90 (4.29)	1.34 (0.87)	-0.75 (3.99)	1.07 (1.24)	-0.18 (4.01)	0.99 (1.24)
SITA Fast	-1.41 (4.21)	1.40 (2.26)	-1.22 (4.24)	1.26 (1.80)	-1.06 (4.47)	1.19 (1.27)	-0.97 (4.01)	1.47 (1.83)	-0.53 (3.61)	1.17 (1.02)
SITA SWAP	-3.15 (4.80)	1.20 (1.38)	-2.48 (4.59)	1.46 (1.97)	-1.97 (4.33)	1.38 (2.23)	-1.40 (4.44)	1.33 (2.27)	-1.58 (4.37)	1.32 (2.11)
SITA Standard	0.42 (1.06)	0.82 (1.18)	0.85 (1.16)	1.31 (0.80)	1.00 (1.56)	1.03 (1.10)	1.01 (1.11)	0.99 (1.09)	1.06 (1.10)	0.99 (1.05)
SITA Fast	0.28 (1.02)	0.70 (1.08)	0.55 (1.02)	0.74 (1.06)	0.48 (1.14)	0.75 (1.06)	0.71 (1.14)	0.67 (1.05)	0.71 (1.30)	0.93 (1.13)
SITA SWAP	-1.90 (3.21)	1.05 (1.12)	-0.53 (2.64)	0.70 (1.56)	-0.25 (0.55)	0.69 (1.28)	-0.32 (1.99)	0.85 (1.61)	-0.21 (2.31)	1.05 (1.30)

Table 3.2. The group mean deviation (MD) and the group mean learning index (LI), at each of the five visits for the right eye, as a function of the algorithm, for normal individuals (no-shading), OAG patients (light shading) and OHT individuals (dark shading).

Algorithm	Visit 1		Visit 2		Visit 3		Visit 4		Visit 5	
	MD	LI	MD	LI	MD	LI	MD	LI	MD	LI
SITA Standard	0.08 (1.07)	0.99 (1.86)	0.11 (1.29)	0.98 (1.00)	0.11 (1.06)	0.95 (0.85)	0.42 (0.97)	1.06 (0.97)	0.43 (1.33)	1.10 (1.33)
SITA Fast	-0.19 (1.13)	0.89 (1.03)	0.16 (0.93)	1.12 (0.89)	0.14 (1.07)	0.98 (0.85)	0.28 (1.05)	0.91 (0.91)	0.27 (0.94)	0.90 (0.89)
SITA SWAP	-1.61 (2.79)	0.99 (1.15)	-1.31 (2.99)	0.91 (1.41)	-1.13 (2.91)	1.09 (1.79)	-1.27 (2.89)	1.01 (1.22)	-0.85 (2.55)	0.75 (1.26)
SITA Standard	-1.20 (2.33)	1.31 (1.37)	-0.95 (1.67)	1.36 (1.49)	-0.56 (1.88)	1.03 (1.23)	-0.53 (1.74)	1.10 (1.32)	-0.60 (1.70)	1.05 (0.87)
SITA Fast	-1.27 (2.04)	1.30 (1.40)	-0.96 (1.85)	1.15 (0.83)	-0.66 (1.69)	1.07 (1.04)	-0.59 (1.64)	1.13 (1.26)	-0.65 (1.53)	1.09 (1.09)
SITA SWAP	-2.92 (3.94)	1.43 (1.71)	-2.16 (3.02)	1.36 (1.69)	-1.63 (2.93)	1.48 (1.85)	-1.22 (2.93)	1.32 (1.84)	-1.27 (2.75)	1.39 (1.57)
SITA Standard	0.32 (1.17)	0.79 (1.14)	0.57 (1.00)	0.72 (0.90)	0.55 (1.00)	1.19 (0.93)	0.59 (1.30)	1.03 (1.31)	0.64 (1.00)	1.01 (0.96)
SITA Fast	0.07 (1.16)	0.97 (1.09)	0.39 (1.24)	0.79 (1.21)	0.52 (1.00)	1.23 (1.33)	0.45 (1.01)	0.62 (0.77)	0.37 (1.29)	1.07 (1.26)
SITA SWAP	-1.03 (2.91)	0.72 (1.40)	-0.45 (2.79)	0.85 (1.56)	-0.01 (2.52)	0.44 (1.84)	-0.36 (2.34)	1.11 (1.53)	-0.32 (2.39)	1.13 (1.34)

Table 3.3.The group mean deviation (MD) and the group mean learning index (LI), at each of the five visits for the left eye, as a function of the algorithm, for the normal individuals (no-shading), OAG patients (light shading) and OHT individuals (dark shading).

Right Eye

Left Eye

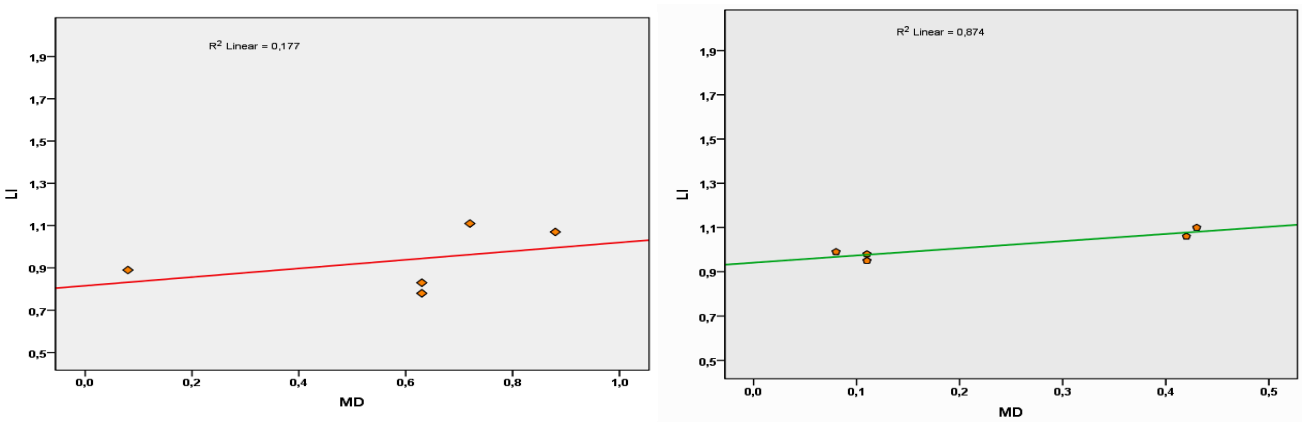

SITA Standard

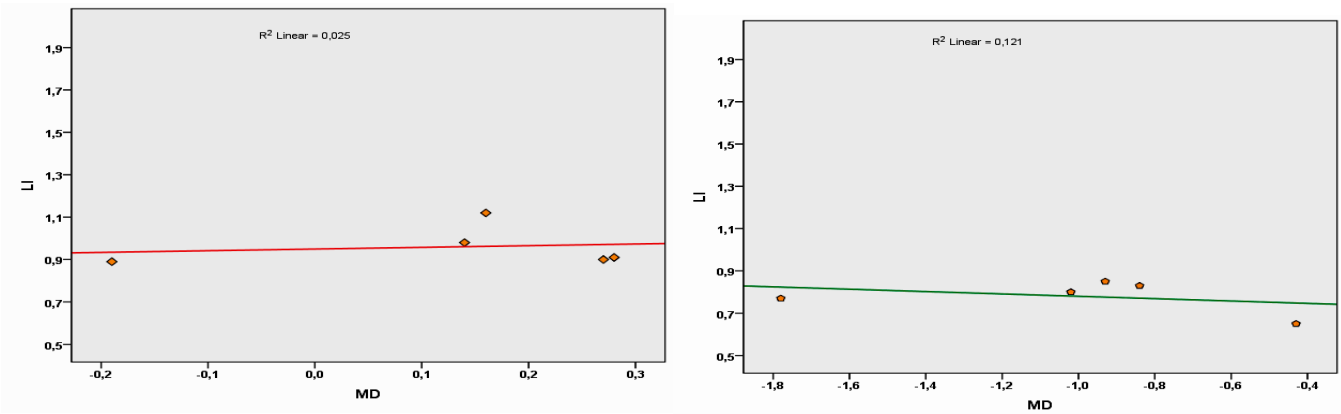

SITA Fast

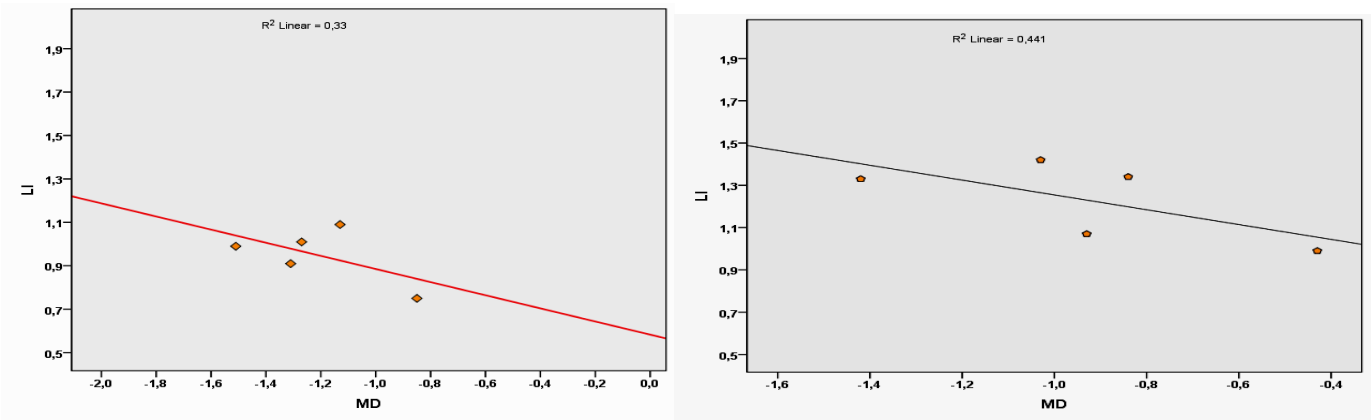

SITA SWAP

Figure 3.23 Linear regression for mean LI against mean MD, as a function of algorithm, for right eye (left panel) and for left eye (right panel), at every visit for normal individuals.

Right Eye

Left Eye

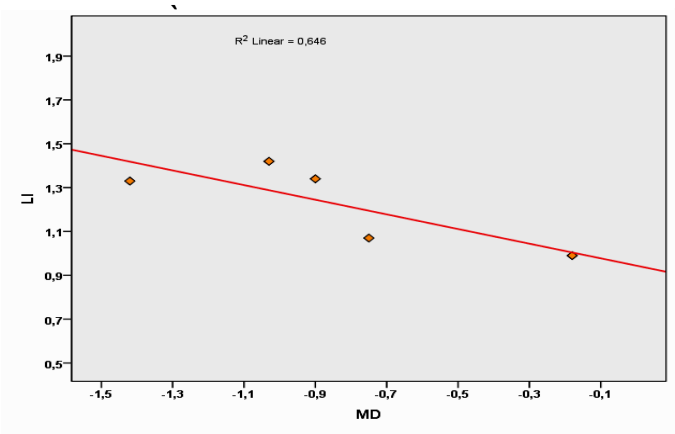

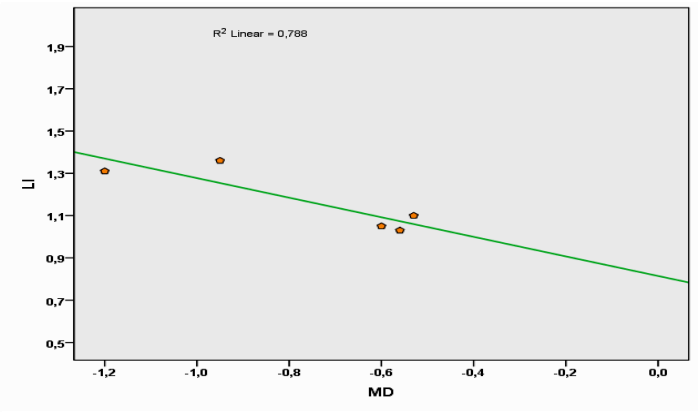

SITA Standard

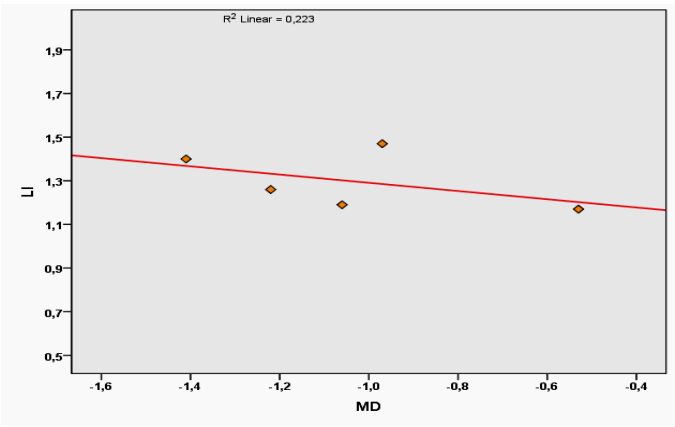

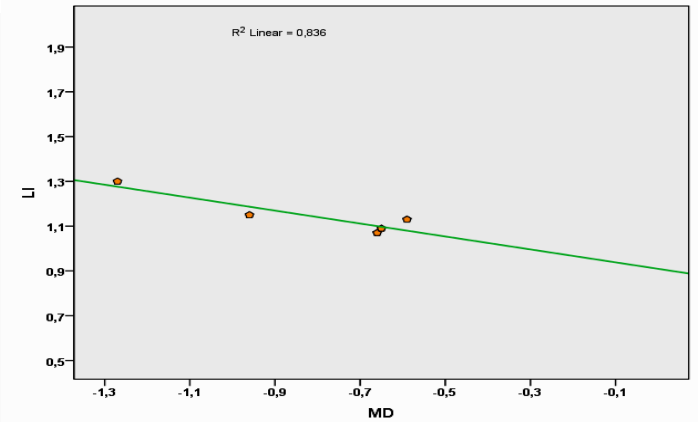

SITA Fast

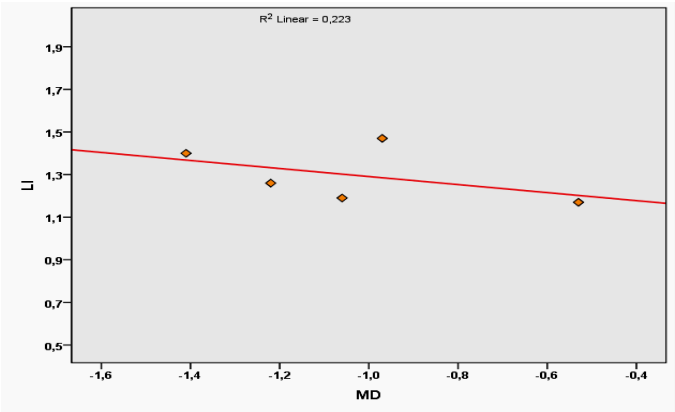

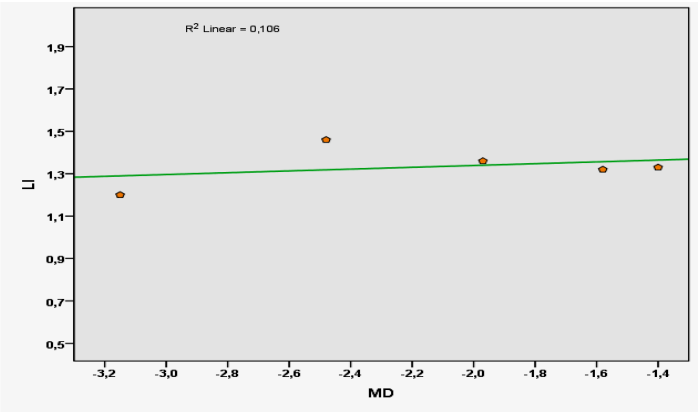

SITA SWAP

Figure 3.24 Linear regression for mean LI against mean MD, as a function of algorithm, for right eye (left panel) and for left eye (right panel), at every visit for glaucoma patients.

Right Eye

Left Eye

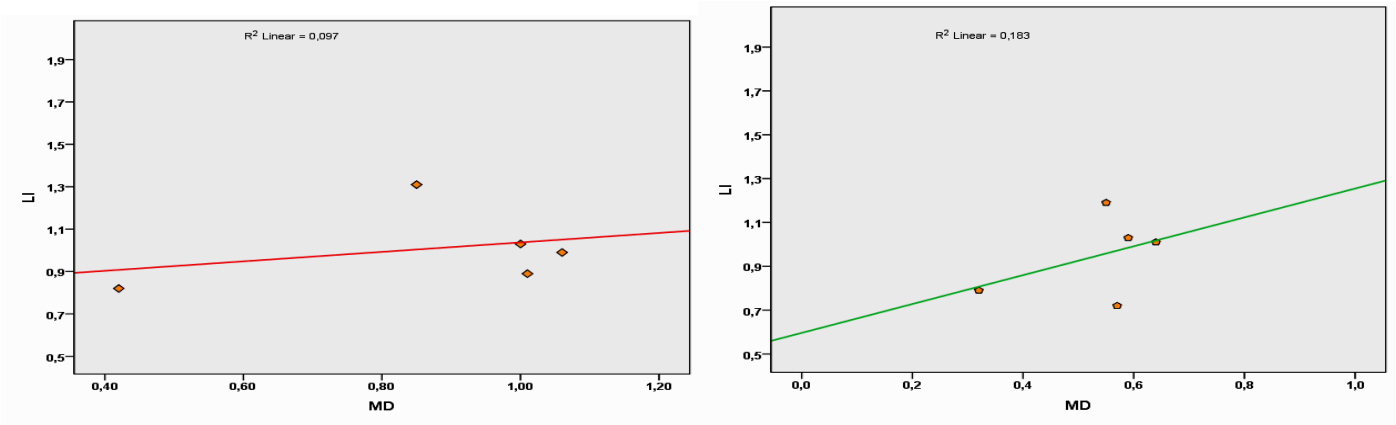

SITA Standard

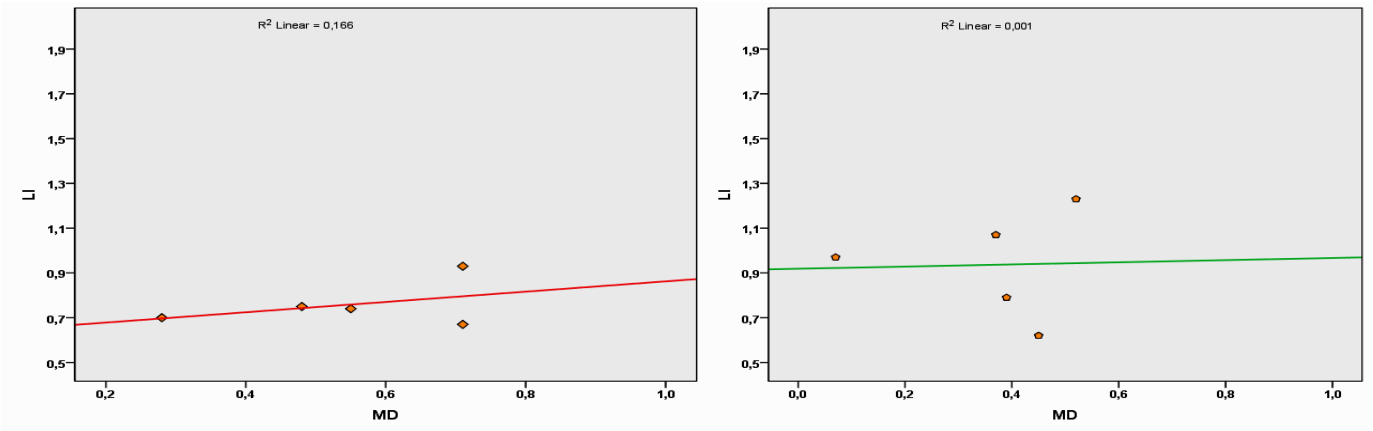

SITA Fast

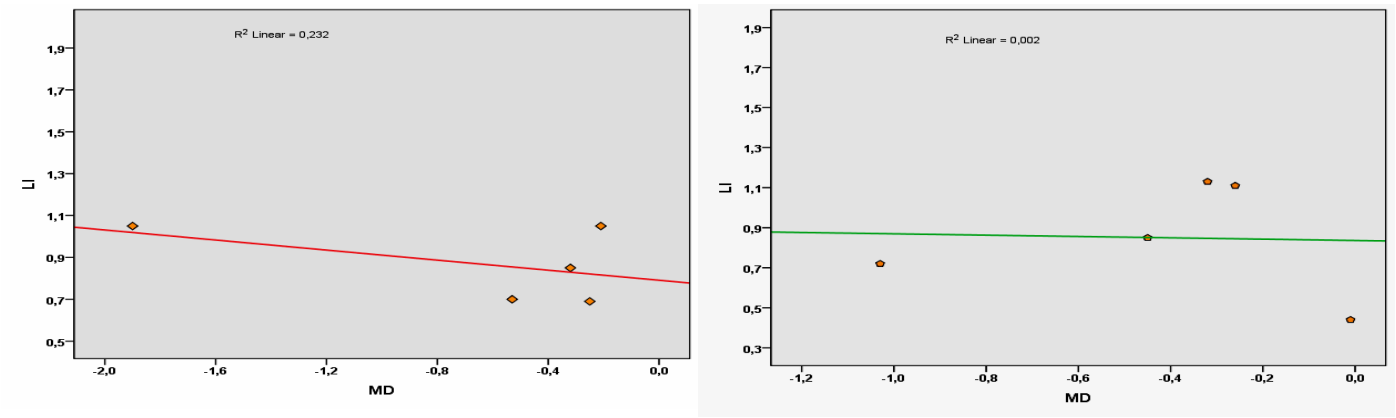

SITA SWAP

Figure 3.25 Linear regression for mean LI against mean MD, as a function of algorithm, for right eye (left panel) and for left eye (right panel), at every visit for OHT individuals.

The group mean PSD and the mean LI for each eye of each of the 3 groups of patients at each of the 5 visits is shown in Table 3.4 for the right eye and Table 3.5 for the left. Next figures 3.26 to 3.28 illustrate the linear regression for the mean LI against the mean PSD, for all visits as a function of the algorithm.

The group mean PSD in the right (first examined) eye was better (less positive) than that of the left eye across the 5 visits for the 3 cohorts and the magnitude of this difference varied between groups ($p<0.001$) and was largest (worst) for SITA SWAP.

The group mean PSD exhibited a slight improvement over the 5 visits across the 3 cohorts.

The magnitude of the association is weak in some cases, but stronger in others. according the regression analysis and present a stronger association for normal individuals but weaker for OAG and OHT individuals.

The magnitude of the association between mean LI and mean PSD is, as denoted by the regression slopes, is great in some conditions, while weak in other conditions. Moreover, there does not appear to be a consistent trend across all conditions; the association is positive in some conditions and negative in others, without any obvious rationale. Again, it should be borne in mind that because mean values are regressed, these slopes represent the average association. In some individuals, the association will likely be greater, while for others, it will likely be smaller. The strength of the relationship, as denoted by the R^2 values, is reasonably strong in many conditions, but weak in others. There also appears to be considerable variation in

association even between right and left eyes. Again, it is difficult to make firm conclusions about these data, given the lack of consistency in the association between eyes and large variation in slope across conditions.

Algorithm	Visit 1		Visit 2		Visit 3		Visit 4		Visit 5	
	PSD	LI	PSD	LI	PSD	LI	PSD	LI	PSD	LI
SITA Standard	1.58 (0.46)	0.89 (1.04)	1.48 (0.56)	0.78 (0.97)	1.48 (0.32)	0.83 (1.03)	1.39 (0.30)	1.07 (0.68)	1.50 (0.58)	1.11 (1.06)
SITA Fast	1.51 (0.51)	0.96 (1.40)	1.30 (0.21)	1.01 (0.79)	1.35 (0.35)	1.07 (0.70)	1.38 (0.30)	0.79 (1.16)	1.34 (0.33)	0.90 (1.04)
SITA SWAP	2.88 (0.89)	0.77 (0.86)	2.47 (0.49)	0.80 (1.17)	2.40 (0.52)	0.83 (1.17)	2.42 (0.46)	0.85 (1.61)	2.31 (0.43)	0.65 (1.24)
SITA Standard	2.33 (1.95)	1.33 (1.26)	2.41 (2.20)	1.42 (1.13)	2.52 (2.56)	1.34 (0.87)	2.34 (2.14)	1.07 (1.24)	2.24 (2.19)	0.99 (1.24)
SITA Fast	2.17 (2.28)	1.40 (2.26)	2.25 (2.14)	1.26 (1.80)	2.21 (2.22)	1.19 (1.27)	2.22 (2.42)	1.47 (1.83)	2.00 (2.26)	1.17 (1.02)
SITA SWAP	3.50 (1.34)	1.20 (1.38)	3.22 (1.38)	1.46 (1.97)	3.17 (1.33)	1.38 (2.23)	3.09 (1.47)	1.33 (2.27)	3.04 (1.39)	1.32 (2.11)
SITA Standard	1.58 (0.36)	0.82 (1.18)	1.60 (0.56)	1.31 (0.80)	1.66 (0.38)	1.03 (1.10)	1.46 (0.23)	0.99 (1.09)	1.57 (0.24)	0.99 (1.05)
SITA Fast	1.40 (0.24)	0.70 (1.08)	1.36 (0.19)	0.78 (0.97)	1.48 (0.32)	0.75 (1.06)	1.35 (0.22)	0.67 (1.05)	1.40 (0.34)	0.93 (1.13)
SITA SWAP	3.00 (0.80)	1.05 (1.12)	2.55 (2.64)	1.01 (0.79)	2.59 (0.55)	0.69 (1.28)	2.55 (0.46)	0.85 (1.61)	2.48 (0.61)	1.05 (1.30)

Table 3.4. The cohort mean pattern standard deviation (PSD) and the cohort mean learning index (LI), at each of the five visits for the right eye, as a function of the algorithm, for normal individuals (no-shading), OAG patients (light shading) and OHT individuals (dark shading).

Algorithm	Visit 1		Visit 2		Visit 3		Visit 4		Visit 5	
	PSD	LI	PSD	LI	PSD	LI	PSD	LI	PSD	LI
SITA Standard	1.54 (0.49)	0.99 (1.86)	1.58 (0.30)	0.98 (1.00)	1.58 (0.45)	0.95 (0.85)	1.42 (0.45)	1.06 (0.97)	1.55 (0.80)	1.10 (1.33)
SITA Fast	1.42 (0.48)	0.89 (1.03)	1.43 (0.46)	1.12 (0.89)	1.40 (0.42)	0.98 (0.85)	1.41 (0.46)	0.91 (0.91)	1.37 (0.30)	0.90 (0.89)
SITA SWAP	2.75 (0.84)	0.99 (1.15)	2.60 (0.52)	0.91 (1.41)	2.46 (0.63)	1.09 (1.79)	2.54 (0.66)	1.01 (1.22)	2.38 (0.52)	0.75 (1.26)
SITA Standard	2.48 (1.73)	1.31 (1.37)	2.18 (1.37)	1.36 (1.49)	2.01 (1.05)	1.03 (1.23)	1.93 (0.88)	1.10 (1.32)	1.95 (1.07)	1.05 (0.87)
SITA Fast	2.07 (1.52)	1.30 (1.40)	1.99 (1.44)	1.15 (0.83)	1.99 (1.26)	1.07 (1.04)	1.68 (0.65)	1.13 (1.26)	1.96 (0.85)	1.09 (1.09)
SITA SWAP	3.54 (1.79)	1.43 (1.71)	3.23 (1.23)	1.36 (1.69)	3.16 (1.12)	1.48 (1.85)	2.81 (0.62)	1.32 (1.84)	2.94 (1.09)	1.39 (1.57)
SITA Standard	1.80 (0.76)	0.79 (1.14)	1.82 (0.85)	0.72 (0.90)	1.70 (0.69)	1.19 (0.93)	1.70 (1.74)	1.03 (1.31)	1.64 (0.69)	1.01 (0.96)
SITA Fast	1.69 (0.79)	0.97 (1.09)	1.55 (0.56)	0.79 (1.21)	1.64 (0.77)	1.23 (1.33)	1.50 (0.83)	0.62 (0.77)	1.76 (1.29)	1.07 (1.26)
SITA SWAP	2.89 (1.03)	0.72 (1.40)	2.89 (0.72)	0.85 (1.56)	2.64 (0.98)	0.44 (1.84)	2.55 (0.63)	1.11 (1.53)	2.56 (0.64)	1.13 (1.34)

Table 3.5. The cohort mean pattern standard deviation (PSD) and the cohort mean learning index (LI), at each of the five visits for the left eye, as a function of the algorithm, for normal individuals (no-shading), OAG patients (light shading) and OHT individuals (dark shading).

Right Eye

Left Eye

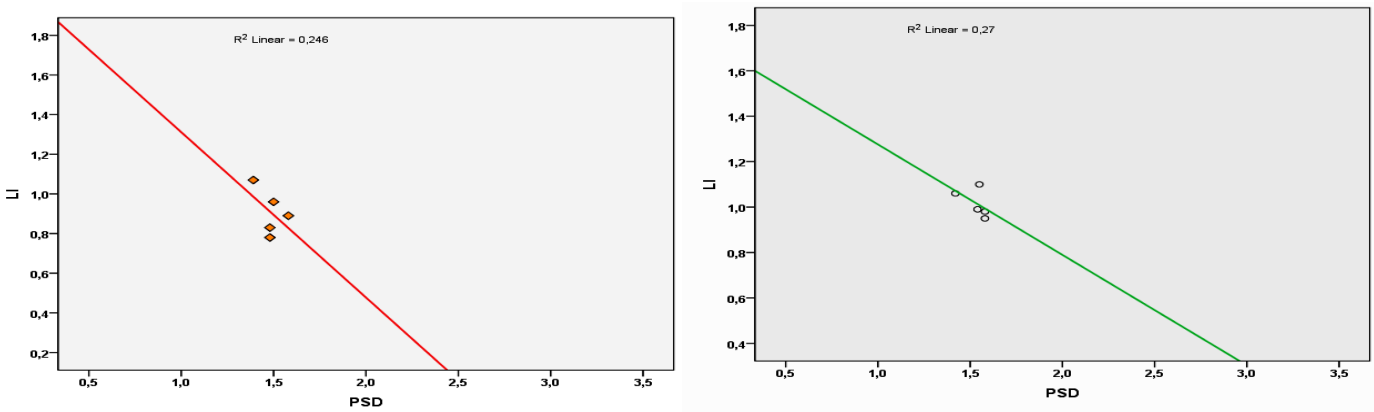

SITA Standard

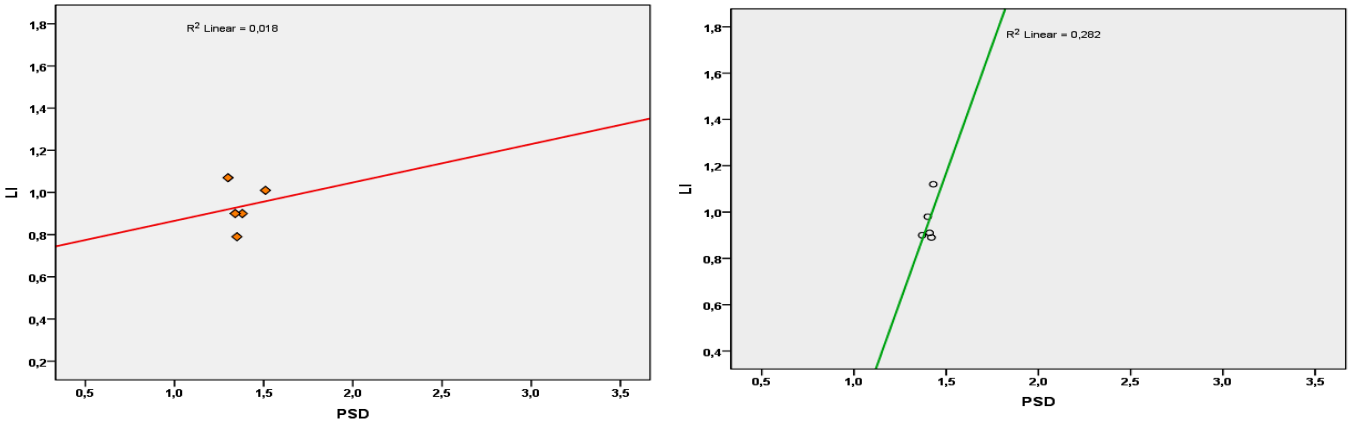

SITA Fast

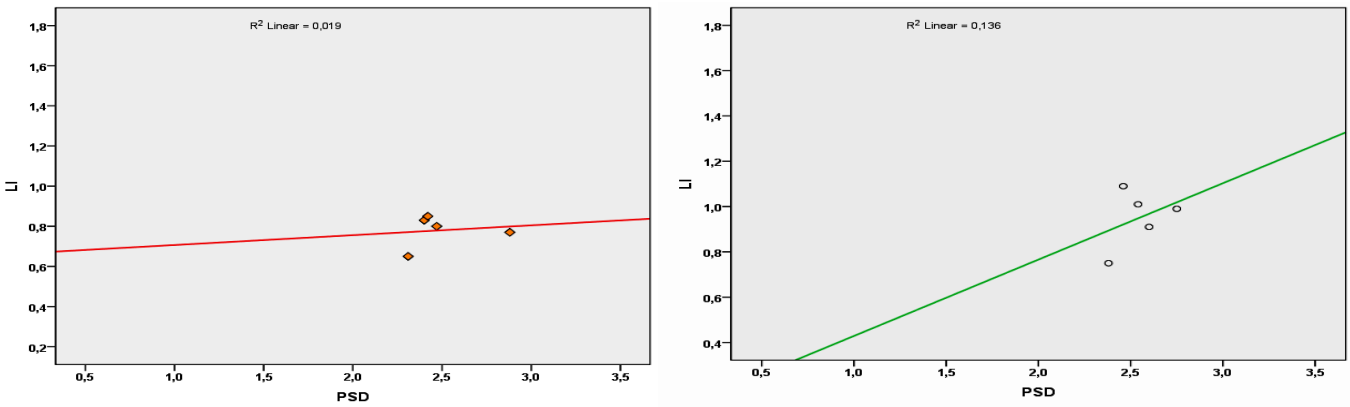

SITA SWAP

Figure 3.26 Linear regression for mean LI against mean PSD, as a function of algorithm, for right eye (left panel) and for left eye (right panel), at every visit for normal individuals.

Right Eye

Left Eye

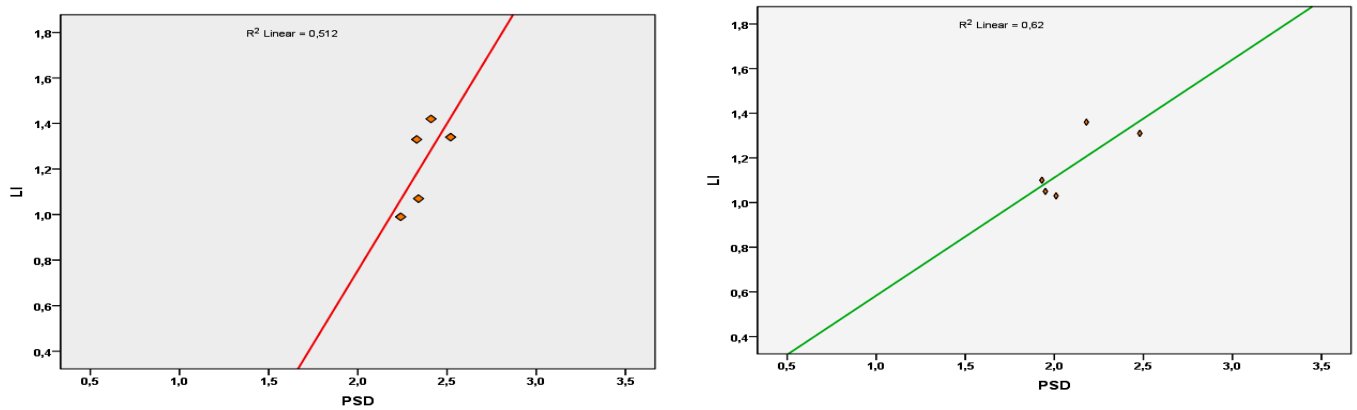

SITA Standard

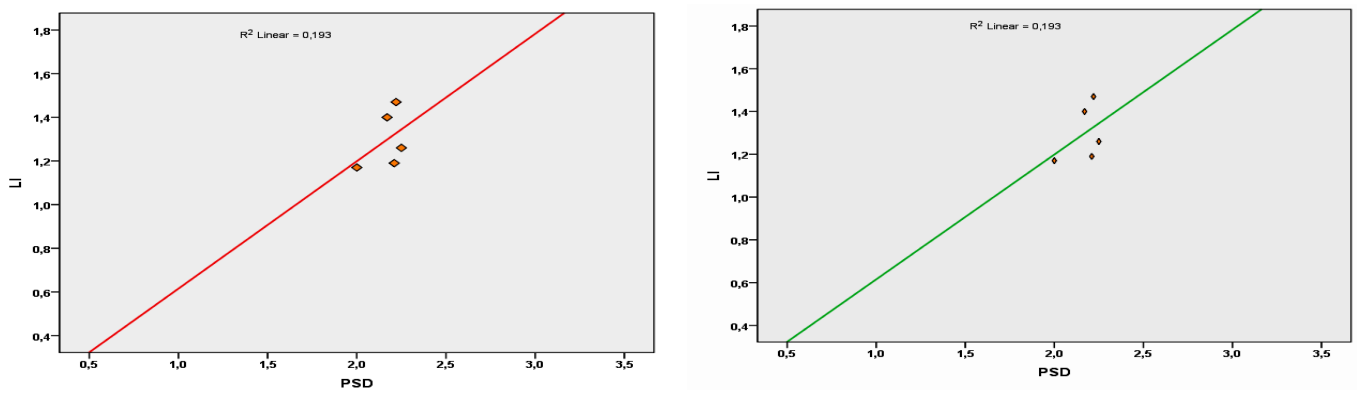

SITA Fast

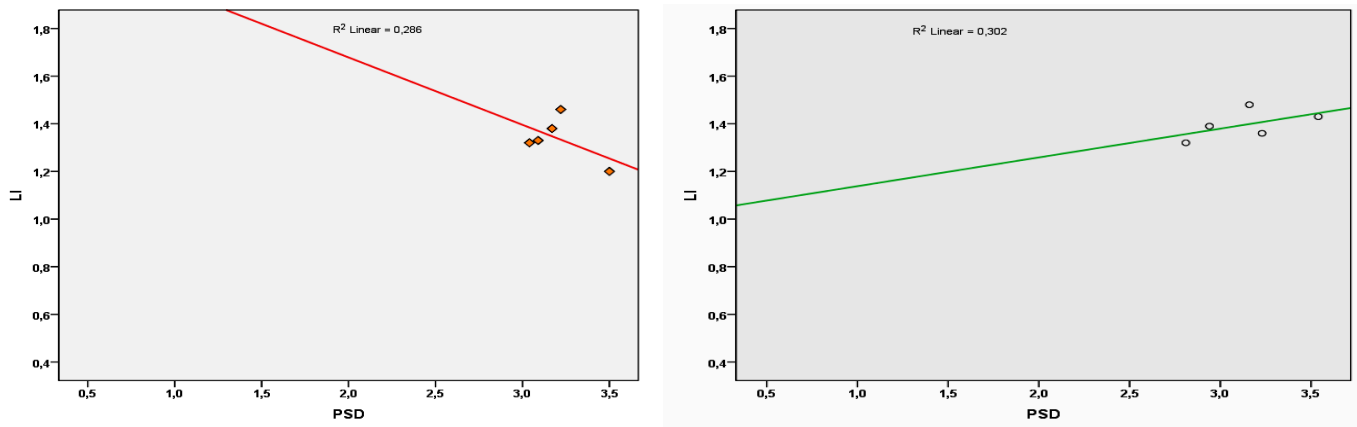

SITA SWAP

Figure 3.27. Linear regression for mean LI against mean PSD, as a function of algorithm, for right eye (left panel) and for left eye (right panel), at every visit for glaucoma patients.

Right Eye

Left Eye

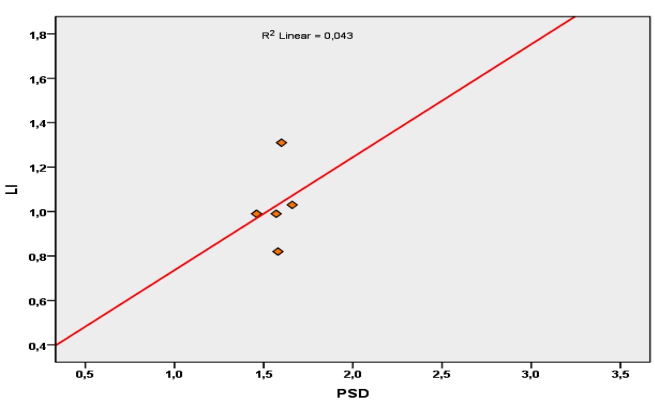

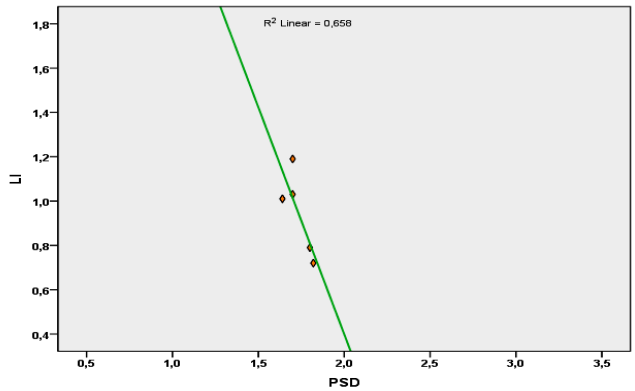

SITA Standard

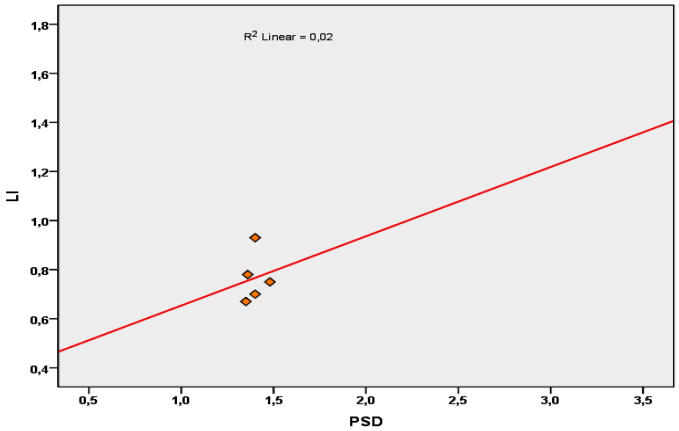

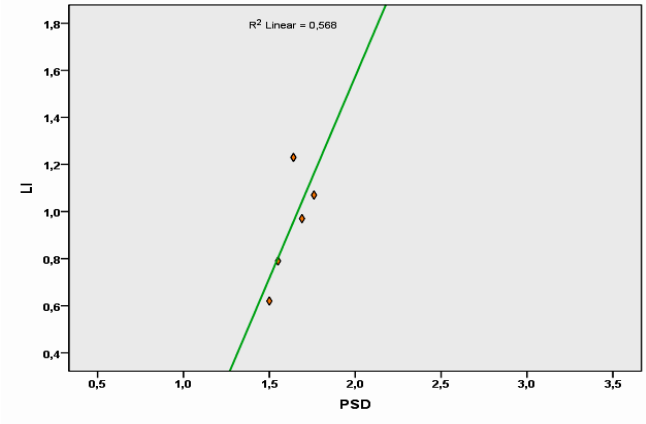

SITA Fast

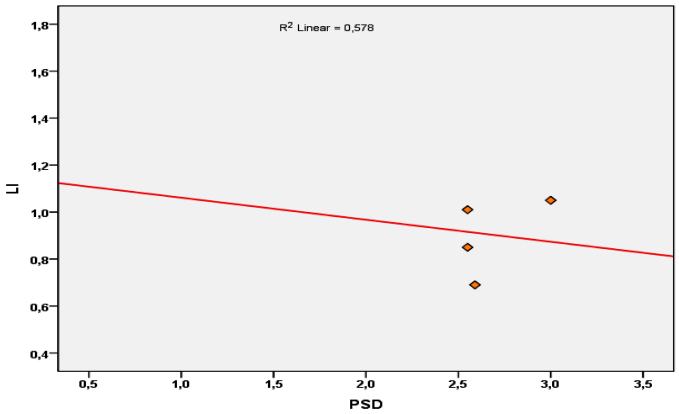

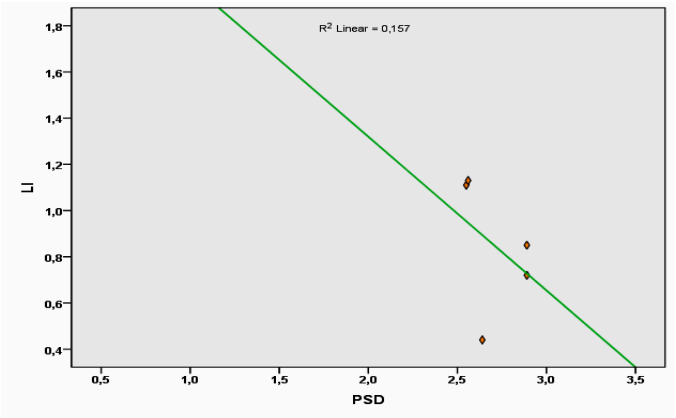

SITA SWAP

Figure 3.28. Linear regression for mean LI against mean MD, as a function of algorithm, for right eye (left panel) and for left eye (right panel), at every visit for OHT individuals.

3.4 Chapter Discussion

The present study produced a Learning Index, in a manner similar to the Learner's index that Olsson and colleagues attempted to develop 20 years ago. The characteristics of the established LI were thoroughly investigated in terms of different groups of those experienced in and naïve to perimetry, both healthy and glaucomatous and different algorithms.

The equation used for the LI calculation by Olsson's colleagues is the same used in the new study and the normalisation factor K was exactly the same. The only difference between the two methods was that Olsson used Full Threshold 30-2 program output data and in the new study all the output data came from 24-2 program and SITA Standard, SITA Fast and SITA SWAP algorithms. Therefore, the Olsson's study used more locations' data for the calculation of Learning Index, but these locations were in periphery and on the other hand the new study used data was drawn from 5 repeated test sessions instead of 3 test sessions used by Olsson.

The cohort of the study included healthy normal individuals with no previous perimetric experience, glaucoma patients likely experienced in SAP and ocular hypertensive individuals naïve in SITA SWAP. The normal individuals (according to Castelberg , 2010) were naïve to any type of perimetry so all the group could be assumed that possibly will learn at the first, second and third test session. On the other hand, the OAG group and OHT group in line to Castelberg thesis, were much experienced of Standard Automated Perimetry (SAP) as they had 5-6 previous tests. The individuals of these two groups were expected to learn only in SITA SWAP where the used pathway is different from the SAP.

The untrained group consisted of normal individuals who were naïve to perimetry, but by the fifth test session, they were no longer regarded as naïve observers.

Amid the first conclusions was the certainty that learning effect is not only transferred between visits and from one eye to the other, but also that demonstrate an inverse relation with the inconsistency and the concentration of the subject during the examination. The results of many psychophysical tests improve as the subject gains more experience performing the test. Accordingly, the variability of test results may decrease significantly with experience. A proper interpretation of perimetric results first requires an adequate evaluation of patient reliability that emerges as an important limiting factor in testing. High frequency of false positive, false negative or fixation losses is an indicator of patient's lack of concentration or visual fatigue. Conversely, high reproducibility of test measurements is often considered an indication of high reliability of test results.

Whenever possible, a patient who is new to perimetry should undergo several test sessions, to establish adequate experience. The magnitude of learning effect will be reduced, as the experience of the individual will increase. Moreover, the age, the general health state of individuals and the various therapies they follow or even uncomfortable chairs, could contribute to fatigue that may produce inconsistent responses.

In contrary, this study concluded that the more inexperienced in perimetry is the individual, the more the application of the index. Patients who were naïve to

perimetry, however, may demonstrate a dramatic improvement in the second test compared with the first, producing a high LI. A number of them continue to improve over the three, four or five visual fields and produce gradually lower LI. Of course, definitely the power of the LI is influenced by the performance of the subject during the test.

As expected the application of the LI in ocular hypertensive individuals is ambiguous and using the SITA SWAP algorithm, the results are disappointing, as the algorithm is very difficult for inexperienced subjects and the LI becomes probably useless for this group.

A negative association between mean LI and mean MD is evident (i.e. as MD becomes worse, LI increases). However it is difficult to draw firm conclusions from these data, as there may be consideratble variance around the mean slope in individual participants. In addition, although it is assumed that no true deterioration has taken place between visits, test-retest variability increases with depth of defect (Artes et al., 2002, Wall et al., 2009). A difficulty in intepreting the LI in cohorts with glaucoma is that test-retest variability could be conflated with a real learning effect. For this reason, the data from the normal cohort may be more informative when considering the utility of the LI, but with the caveat that the range of MD over which an association can be determined is very narrow in normal controls.

4 CHAPTER FOUR – Alternative methods of Learning Index Calculation

4.1 The Learning Index calculation following GHT pattern.

The Glaucoma Hemifield Test (GHT) is based on the characteristic of glaucoma, which damages the superior and inferior fields asymmetrically. The GHT was described in details in the Introduction, section 1.5.6.

The GHT evaluates mirror-image clusters of points in the upper and lower fields, in order to alert the clinician when significant differences of sensitivity exist between the two hemifields. GHT is comparing these differences by the magnitude of the Pattern Deviation probability level at each of five zones on either side of the midline (Fig.4.1). Every zone comprises of 3 up to 6 stimulus locations (Asman and Heijl, 1992a). These 5 mirror zones were used in calculation of the Learning Index, instead of the 5 concentric annuli used in Chapter 3. The mean value for each of the 5 mirror zones was calculated and combined in a single vector.

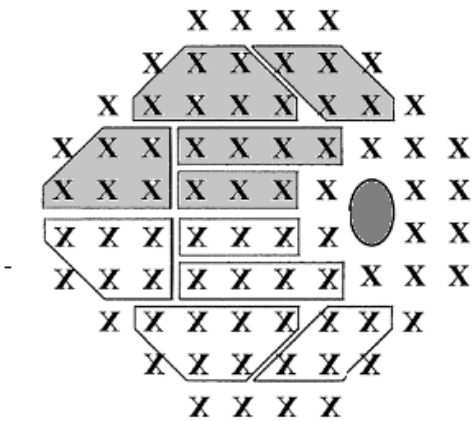

Figure 4.1 Graphic illustration of the five zones analysed in the glaucoma hemifield test for the right eye (shaded zones = superior hemifield, no-shaded zones = mirrored inferior hemifield).

4.1.1 Aim of the study

In this study the Learning Index was calculated following the pattern of GHT. The GHT uses empirically determined limits of normality for up-down differences in the probability maps of the Humphrey Field Analyzer to detect localized visual field loss. It is also constructed to detect field loss that is symmetric around the horizontal meridian (Asman and Heijl, 1992a; Boland and Quigley, 2011).

The aim of the study was to evaluate the calculated LI results of asymmetrically mirrored locations between the superior and inferior hemifield in the magnitude of the Pattern Deviation probability level at either side of midline and to compare the results with the method of LI calculations in the same manner to that of Olsson et al (1997).

4.1.2 Methods

4.1.2.1 The cohort

The cohort comprised three different groups of individuals as described previously in Chapter 3. The right eye was always examined first at each of the five visits.

4.1.2.2 Method of LI calculation following GHT pattern.

The LI calculations following the GHT pattern arose by a design in a manner identical to that of Olsson et al (1997). Dr Carlo Knupp, Senior Research Fellow in Cardiff University undertook the coding for the calculation of LI following the GHT pattern (Fig.4.2).

Analysis was done in five corresponding pairs of sectors that are based on the normal anatomy of the retinal nerve fiber layer. Deviations from the age-corrected normal threshold in the most sensitive portions of the visual field are used to detect general reductions of sensitivity or abnormally high sensitivities

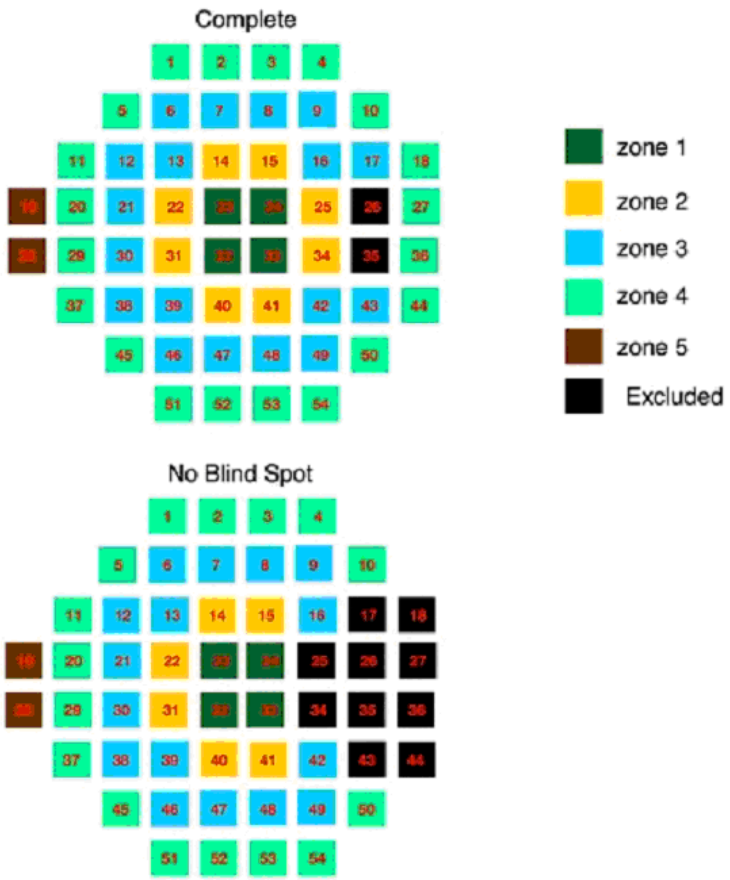

Figure 4.2 Distribution of data in five zones used for Olsson's (Olsson, Asman and Heijl, 1997) complete method of LI calculation (top) and distribution of GHT pattern data in 5 sets (green, blue and yellow shaded location areas, plus the nasal locations 19 and 27, and central locations 23, 24, 33 and 34) in visual field output of 54 locations in program 24-2 (bottom). Locations 26 and 35, situated with in the Blind Spot, plus 8 more locations around the Blind Spot, were also excluded.

4.1.3 Results

The results of the above method are presented as descriptive statistics for Learning Index calculation (left panel) and Box and Whisker plots of the Learning Index distribution (right panels) for normal individuals, for glaucoma patients and for ocular hypertensive individuals, for SITA Standard, SITA Fast and SITA SWAP algorithms, for the right and left eye, respectively.

Figures 4.3 to 4.8 illustrate descriptive statistics results of the study (left panel), which present no major changes of LI results compared to the complete pattern method (Fig 3.17 to 3.22). A good overview of the data distribution of LI results calculated with GHT pattern, are the box and whisker plots in figures 4.3 to 4.8.

For SITA Standard algorithm and for normal individuals (Fig.4.3, top) there is a minor decrease of LI values, for right eye and noticeable high values for the left eye (Fig. 4.6), probably due to fatigue, as it is known that the right eye is always tested first. For glaucoma patients (Fig.4.4 and 4.7, top), as expected due to the existence of defective locations resulting from glaucoma, that could not learn in any case, LI values show more variability. Finally for ocular hypertensive individuals (Fig 4.5 and 4.8, top), lower LI values were observed, as OHT individuals had undergone at least 5 previous tests and were most likely experienced.

For the SITA Fast algorithm, the normal individuals show a reduced amount of variability in the LI values (Fig.4.3, middle), as the median maintains a value just under 1,0 after 2nd visit, and likely indicate some fatigue in the left eye data (Fig.4.6, middle). On the other hand, glaucoma patients (Fig 4.4 and 4.7, middle) show higher

LI variability for the right eye and lower variability for the left eye), and the OHT cohort (Fig 4.5 and 4.8, middle) demonstrates lower LI variability, in general. It is possible that the reduced variability in the OHT cohort was because they were more familiar with perimetry from undertaking previous tests with the SITA Standard algorithm.

At last, for SITA SWAP algorithm and for normal cohort (Fig 4.3 and 4.6, bottom) more variability for right eye results is noticeable in all visits (most likely due to the greater difficulty with the SWAP task than with that for SAP. The glaucoma patients continued to present increased LI variability between visits (Fig 4.4 and 4.7, bottom). Rather low mean values (mostly for the left eye) and considerable inconsistency in results were observed in the OHT cohort, most likely due to the algorithm.

Next figures 4.9 to 4.17 illustrate the Bland and Altman Plots of Learning Index (LI) calculation results of both methods, complete and GHT pattern, as a simple way to estimate an agreement interval, within which 95% of the differences of the second method, compared to the first one fall.

For SITA Standard and normal individuals, the one-sample T-Test of the difference (GHT pattern minus complete pattern) does not demonstrate any statistically significant difference as for the right eye and for left eye ($p > 0.05$). The linear regression demonstrates less variability at the left eye but the R^2 values reveal a rather weak association between the two methods, for both eyes. For SITA Fast and normal individuals, the one-sample T-Test of the difference reveals $p>0.05$ for the right eye, and $p>0.05$ for the left eye, that denotes no statistically significant

difference between the two methods. Similar results are found for SITA SWAP in normal individuals with one sample T-Test the p value for right eye was >0.05 and for the left eye > 0.1 that indicates no significant difference between the two methods.

For SITA Standard and OAG individuals, the one sample T-Test of the difference (GHT pattern minus complete pattern) demonstrates no significant difference for both eyes (p>0.05). The linear regression demonstrates less variability at the left eye and a rather weak association between the two methods, for both eyes. For SITA Fast and OAG individuals, the one sample T-Test of the difference for both eyes (p>0.35), indicates no statistically significant difference between the two methods. Comparable is the performance of the results for SITA SWAP and OAG individuals where the one sample T-Test (p>0.05) for both eyes, signify no essential difference.

The one-sample T-Test of the difference (GHT pattern minus complete pattern) for SITA Standard algorithm and ocular hypertensive individuals, demonstrate no statistically significant difference and the linear regression demonstrates less variability at the left eye but a rather weak association between the two methods, in both eyes. For SITA Fast and OHT individuals, the one-sample T-Test of the difference indicates no statistically significant difference between the two methods, and the results for SITA SWAP and OHT individuals the T-Test demonstrates no significant difference between the two methods.

Normal Cohort
Algorithm SITA STANDARD
Eye Right

	N	Min.	Max.	Mean	Std. Dev.
VIS_1	29	-1.06	3.19	1.0438	1.07094
VIS_2	29	-.50	3.18	.9059	.98566
VIS_3	29	-1.39	2.81	.8962	1.06352
VIS_4	29	-.62	2.55	1.1831	.74698
VIS_5	29	-1.06	2.67	1.1652	1.02060

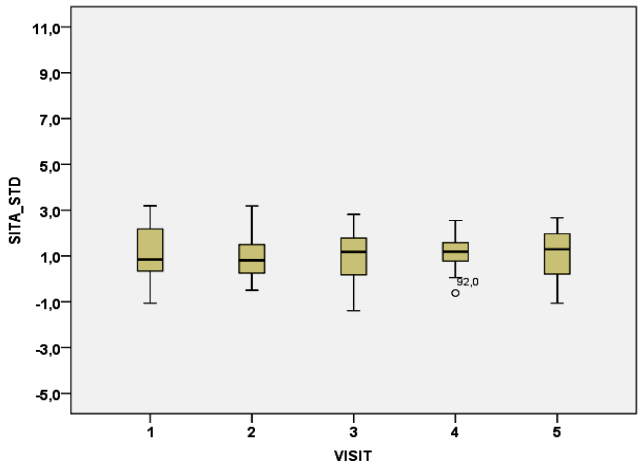

Normal Cohort
Algorithm SITA FAST
Eye Right

	N	Min.	Max.	Mean	Std. Dev.
VIS_1	29	-1.11	2.61	.8290	.93500
VIS_2	29	-2.56	4.15	.8086	1.37092
VIS_3	29	-2.58	2.75	.7776	1.29266
VIS_4	29	-2.44	5.57	.9814	1.67630
VIS_5	29	-2.56	2.84	.7390	1.20518

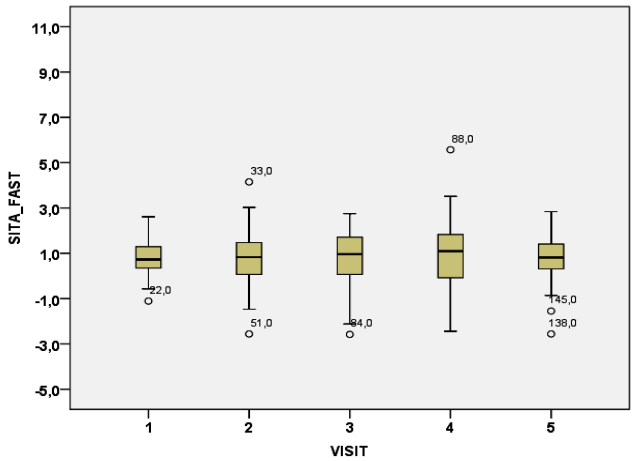

Normal Cohort
Algorithm SITA SWAP
Eye Right

	N	Min.	Max.	Mean	Std. Dev.
VIS_1	29	-1.30	5.46	1.0841	1.57697
VIS_2	29	-.47	2.52	1.0407	.81612
VIS_3	29	-.93	2.34	1.0300	.77804
VIS_4	29	-2.05	2.54	.8093	1.20998
VIS_5	29	-1.01	2.62	1.0183	.94449

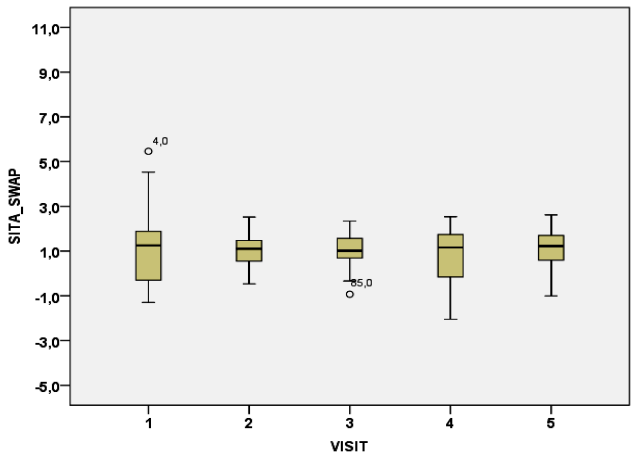

Figure 4.3. The descriptive statistics (left panel), for the Learning Index for normal individuals (right eye), across the five visits, for each of the three algorithms, calculated with GHT pattern. Box and Whisker plots (right panel), of the Learning Index distribution for the normal individuals (right eye), across the five visits, within algorithm for SITA Standard (top), SITA Fast (middle) and SWAP (bottom).

Glaucoma Cohort
Algorithm SITA STANDARD
Eye Right

	N	Min.	Max.	Mean	Std. Dev.
VIS_1	25	-1.03	5.74	1.2788	1.39356
VIS_2	25	-.12	6.50	1.5156	1.48466
VIS_3	25	.04	3.61	1.4048	.87165
VIS_4	25	-1.20	2.58	.9592	1.13424
VIS_5	25	-1.14	3.24	1.0468	1.20773

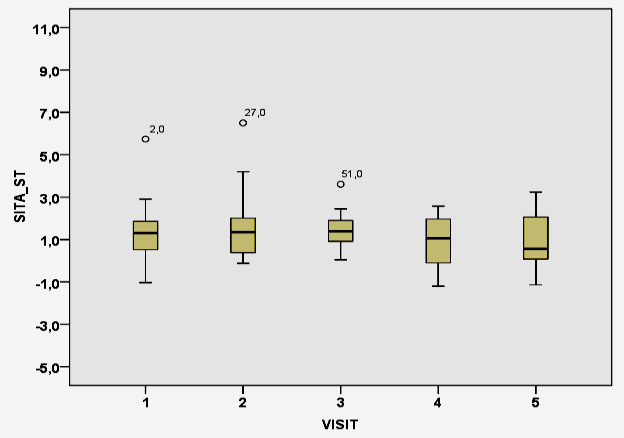

Glaucoma Cohort
Algorithm SITA FAST
Eye Right

	N	Min.	Max.	Mean	Std. Dev.
VIS_1	25	-1.16	8.96	1.4724	1.89711
VIS_2	25	-.20	7.20	1.2764	1.44556
VIS_3	25	-.55	5.99	1.3608	1.44098
VIS_4	25	-.27	7.72	1.5744	1.92769
VIS_5	25	-1.31	3.57	1.2048	1.07703

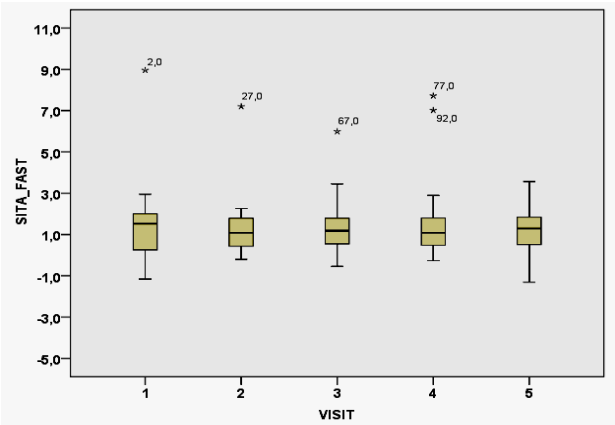

Glaucoma Cohort
Algorithm SITA SWAP
Eye Right

	N	Min.	Max.	Mean	Std. Dev.
VIS_1	25	-.57	4.94	1.1552	1.30290
VIS_2	25	-1.18	6.45	1.4444	1.89692
VIS_3	25	-2.01	7.28	1.2496	2.08254
VIS_4	25	-3.37	9.88	1.3872	2.48768
VIS_5	25	-4.34	7.53	1.4748	2.20944

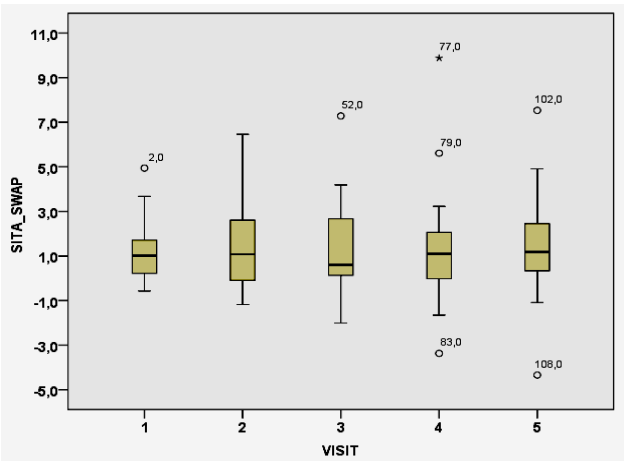

Figure 4.4. The descriptive statistics (left panel), for the Learning Index for OAG individuals (right eye), across the five visits, for each of the three algorithms, calculated with GHT pattern. Box and Whisker plots (right panel), of the Learning Index distribution for the OAG individuals (right eye), across the five visits, within algorithm for SITA Standard (top), SITA Fast (middle) and SWAP (bottom).

OHT Cohort
Algorithm SITA STANDARD
Eye Right

	N	Min.	Max.	Mean	Std. Dev.
VIS_1	25	-2.13	2.96	.7700	1.10956
VIS_2	25	-.93	4.03	.9972	.96036
VIS_3	25	-.24	2.81	1.0428	1.01203
VIS_4	25	-1.50	2.52	.8720	1.07571
VIS_5	25	-.98	2.69	.9044	.93364

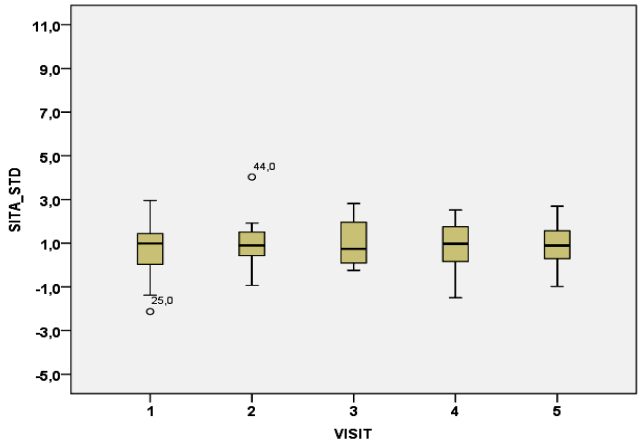

OHT Cohort
Algorithm SITA FAST
Eye Right

	N	Min.	Max.	Mean	Std. Dev.
VIS_1	25	-1.02	1.82	.4900	.80842
VIS_2	25	-1.88	2.24	.6584	.93832
VIS_3	25	-1.33	2.81	.7096	.98760
VIS_4	25	-1.16	2.63	.6916	.93691
VIS_5	25	-1.99	3.26	.8904	1.12144

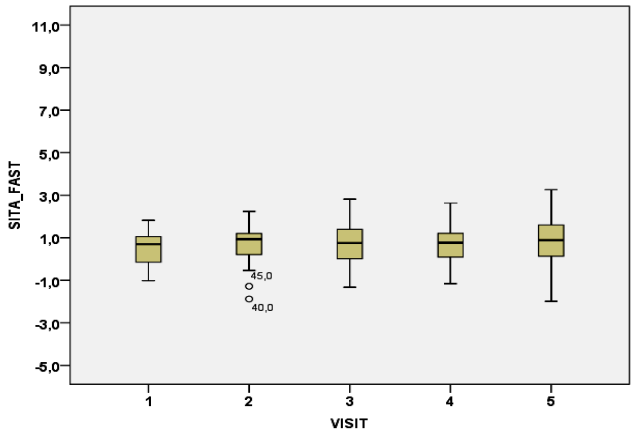

OHT Cohort
Algorithm SITA SWAP
Eye Right

	N	Min.	Max.	Mean	Std. Dev.
VIS_1	25	-1.14	3.08	1.0520	1.02951
VIS_2	25	-2.76	3.65	.8464	1.64523
VIS_3	25	-2.68	4.21	.9312	1.87826
VIS_4	25	-2.25	3.46	.8928	1.50427
VIS_5	25	-.66	3.32	.9132	1.13408

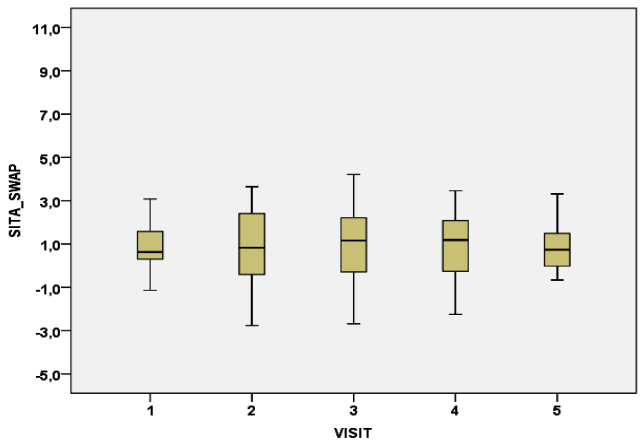

Figure 4.5. The descriptive statistics (left panel), for the Learning Index for OHT individuals (right eye), across the five visits, for each of the three algorithms, calculated with GHT pattern. Box and Whisker plots (right panel), of the Learning Index distribution for the OHT individuals (right eye), across the five visits, within algorithm for SITA Standard (top), SITA Fast (middle) and SWAP (bottom).

Normal Cohort
Algorithm SITA STANDARD
Eye Left

	N	Min.	Max.	Mean	Std. Dev.
VIS_1	29	-.78	3.05	1.0238	.87857
VIS_2	29	-1.20	3.35	1.0259	1.02240
VIS_3	29	-.61	3.04	1.0562	.89100
VIS_4	29	-.41	3.16	1.1693	.96086
VIS_5	29	-2.71	4.29	1.1048	1.35982

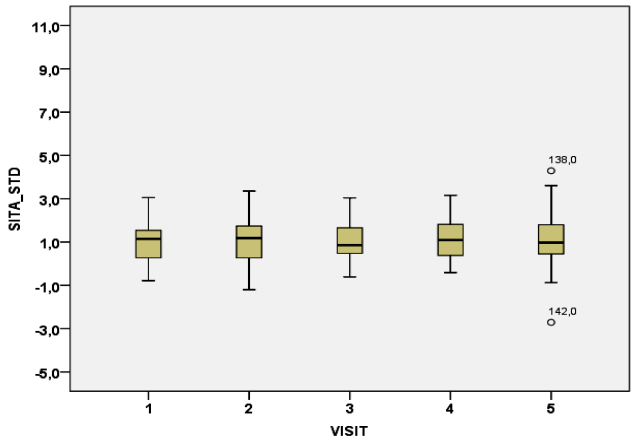

Normal Cohort
Algorithm SITA FAST
Eye Left

	N	Min.	Max.	Mean	Std. Dev.
VIS_1	29	-.71	3.32	1.0203	.88270
VIS_2	29	-.52	2.45	1.1645	.84980
VIS_3	29	-.73	2.62	.9824	.84333
VIS_4	29	-1.73	2.90	.9683	1.10332
VIS_5	29	-1.33	2.44	.8848	.93340

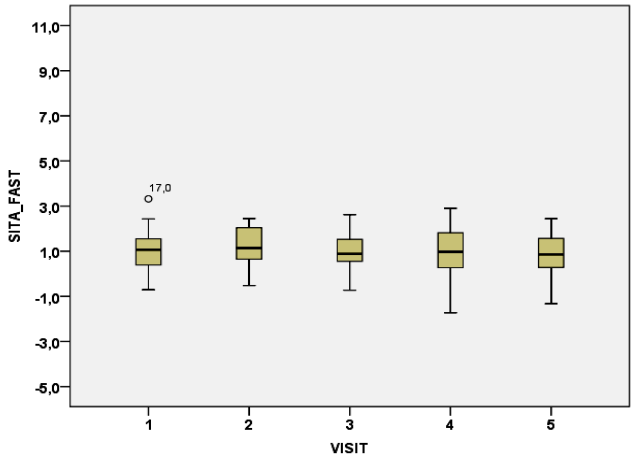

Normal Cohort
Algorithm SITA SWAP
Eye Left

	N	Min.	Max.	Mean	Std. Dev.
VIS_1	29	-1.28	3.19	1.0069	1.15738
VIS_2	29	-2.43	2.74	.9634	1.41032
VIS_3	29	-2.82	4.14	1.0979	1.82894
VIS_4	29	-1.25	3.86	1.1214	1.19262
VIS_5	29	-1.44	3.24	.6772	1.21110

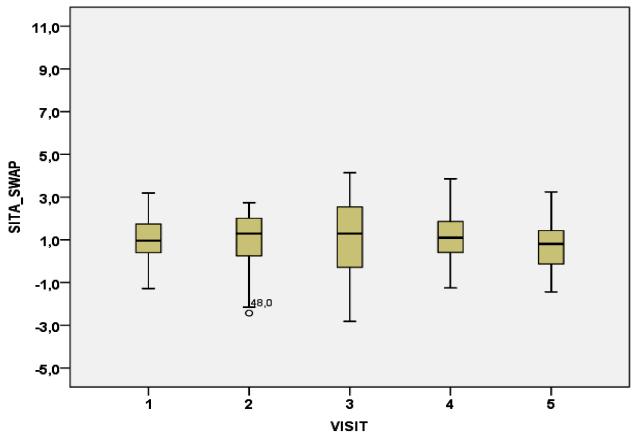

Figure 4.6. The descriptive statistics (left panel), for the Learning Index for normal individuals (left eye), across the five visits, for each of the three algorithms, calculated with GHT pattern. Box and Whisker plots (right panel), of the Learning Index distribution for the normal individuals (left eye), across the five visits, within algorithm for SITA Standard (top), SITA Fast (middle) and SWAP (bottom).

Glaucoma Cohort
Algorithm SITA STANDARD
Eye Left

	N	Min.	Max.	Mean	Std. Dev.
VIS_1	25	-.86	4.25	1.4220	1.44111
VIS_2	25	-1.40	6.04	1.4484	1.54739
VIS_3	25	-1.27	4.11	.8936	1.39005
VIS_4	25	-2.63	2.33	1.0168	1.16480
VIS_5	25	-.41	2.76	1.0168	.92182

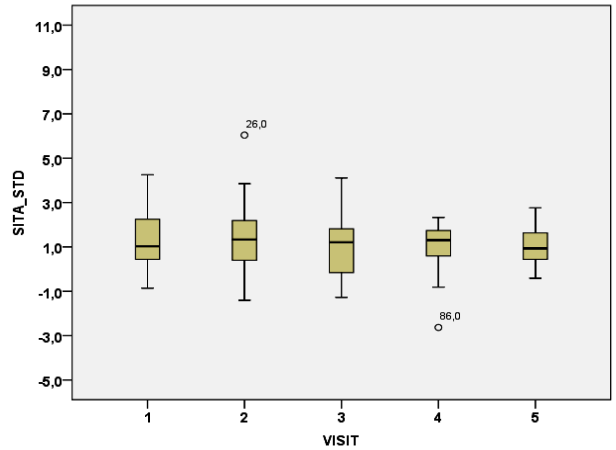

Glaucoma Cohort
Algorithm SITA FAST
Eye Left

	N	Min.	Max.	Mean	Std. Dev.
VIS_1	25	-2.15	4.96	1.1472	1.49304
VIS_2	25	-1.16	2.72	1.0156	.87757
VIS_3	25	-2.45	2.47	.9988	1.02723
VIS_4	25	-1.53	3.54	1.0752	1.19057
VIS_5	25	-2.65	3.06	1.1008	1.22282

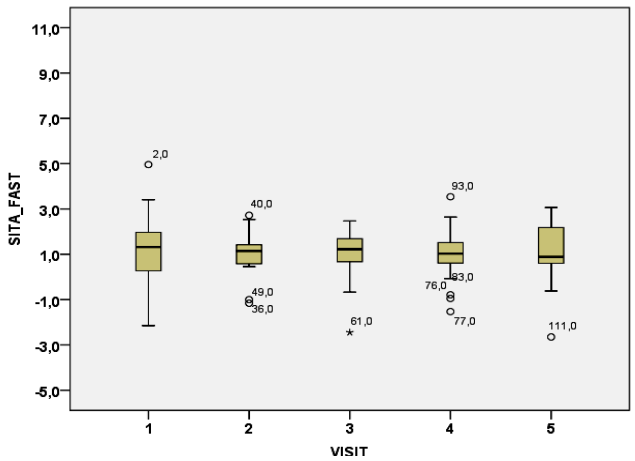

Glaucoma Cohort
Algorithm SITA SWAP
Eye Left

	N	Min.	Max.	Mean	Std. Dev.
VIS_1	25	-1.38	6.78	1.4708	1.73896
VIS_2	25	-3.13	5.91	1.3820	1.78017
VIS_3	25	-2.53	6.16	1.7088	2.06545
VIS_4	25	-2.50	8.18	1.2996	2.24512
VIS_5	25	-1.43	5.17	1.3140	1.72175

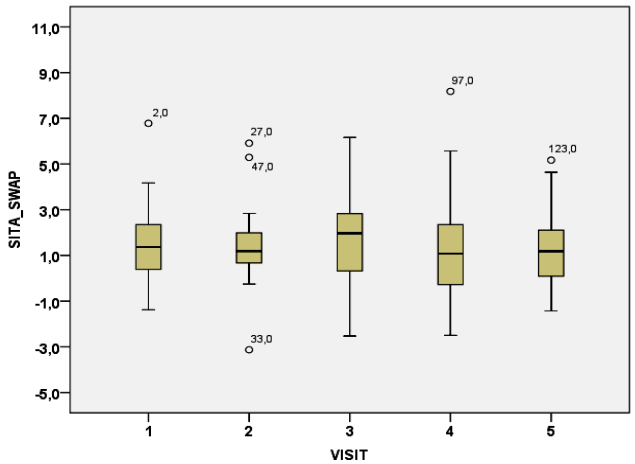

Figure 4.7. The descriptive statistics (left panel), for the Learning Index for OAG individuals (left eye), across the five visits, for each of the three algorithms, calculated with GHT pattern. Box and Whisker plots (right panel), of the Learning Index distribution for the OAG individuals (left eye), across the five visits, within algorithm for SITA Standard (top), SITA Fast (middle) and SWAP (bottom).

OHT Cohort
Algorithm SITA STANDARD
Eye Left

	N	Min.	Max.	Mean	Std. Dev.
VIS_1	25	-2.06	2.48	.6832	1.13805
VIS_2	25	-.73	2.38	.6836	.85068
VIS_3	25	-.56	3.35	1.1384	.93547
VIS_4	25	-1.26	3.23	.8920	1.29623
VIS_5	25	-.92	2.22	.9772	.93843

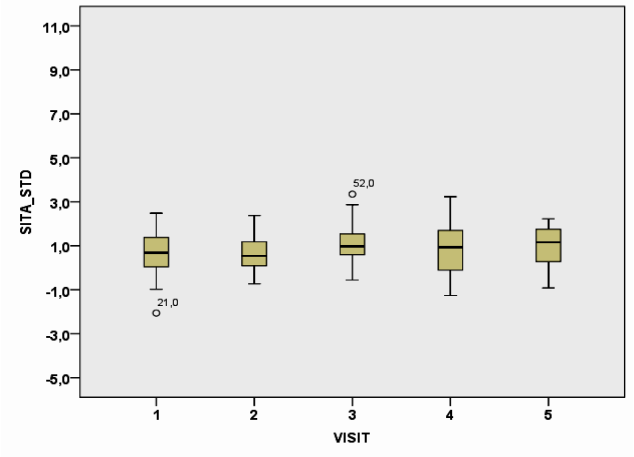

OHT Cohort
Algorithm SITA FAST
Eye Left

	N	Min.	Max.	Mean	Std. Dev.
VIS_1	25	-1.42	3.16	.8388	1.19594
VIS_2	25	-2.05	2.74	.8116	1.15375
VIS_3	25	-1.38	2.57	1.0724	.93639
VIS_4	25	-2.59	2.93	1.1180	1.39575
VIS_5	25	-1.42	3.61	1.1236	1.18372

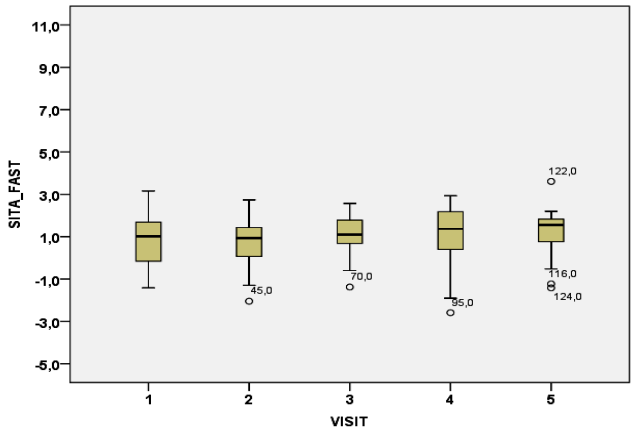

OHT Cohort
Algorithm SITA SWAP
Eye Left

	N	Min.	Max.	Mean	Std. Dev.
VIS_1	25	-1.15	4.59	.5820	1.32140
VIS_2	25	-1.12	4.74	.7096	1.61047
VIS_3	25	-6.14	5.41	.3428	2.09541
VIS_4	25	-2.20	3.06	.6144	1.42933
VIS_5	25	-.96	4.97	1.1088	1.44786

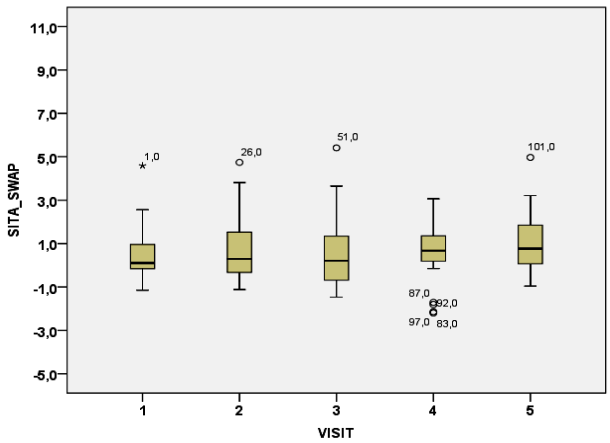

Figure 4.8. The descriptive statistics (left panel), for the Learning Index for OHT individuals (left eye), across the five visits, for each of the three algorithms, calculated with GHT pattern. Box and Whisker plots (right panel), of the Learning Index distribution for the OHT individuals (leftt eye), across the five visits, within algorithm for SITA Standard (top), SITA Fast (middle) and SWAP (bottom).

Normal Cohort
Algorithm SITA STANDARD
Visit 1 3 5

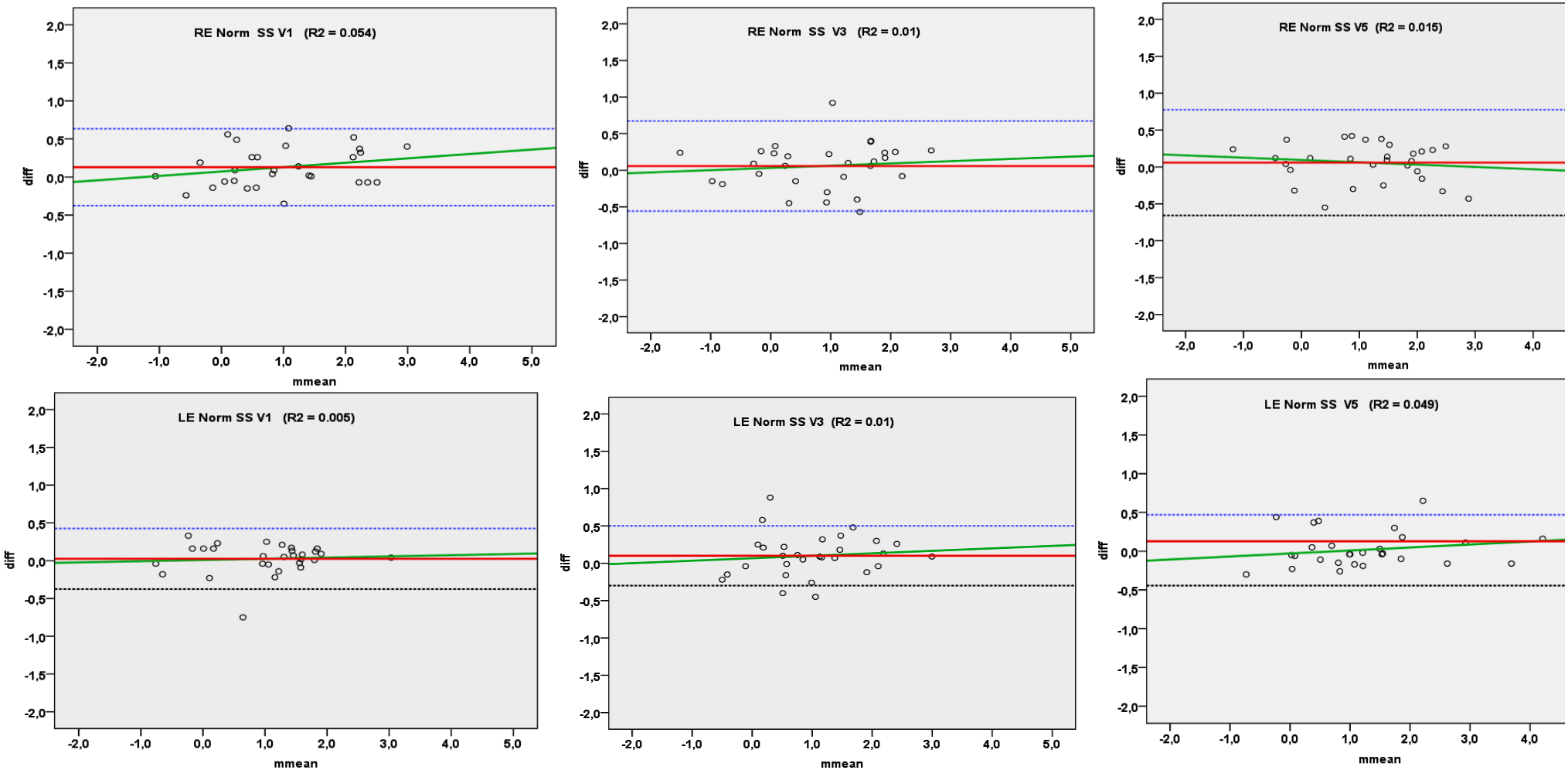

Figure 4.9 Bland and Altman plot of the difference between complete and GHT pattern method LI results (y axis) against the mean of bot methods (x axis), for right eye (top) and left eye (bottom), for SITA Standard algorithm and normal individuals at visit 1 (left panel), visit 3 (middle panel) and visit 5 (right panel). The reference line for mean difference is the red line, the blue dot lines illustrate the 95% confiden lines (+/- 1.96xSD) and the green line is the linear regression line for the referenced R^2 value.

Normal Cohort
Algorithm SITA FAST
Visit 1 3 5

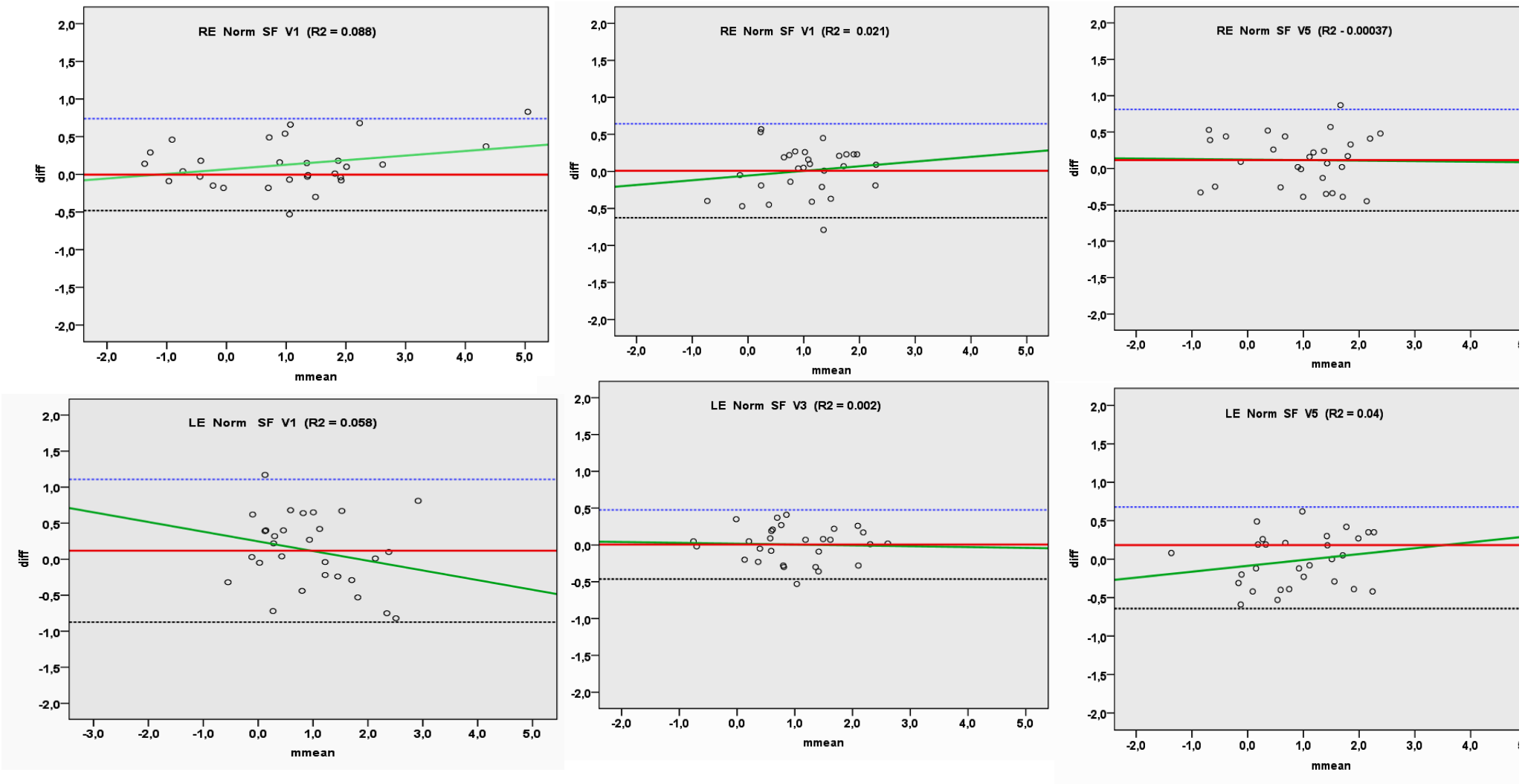

Figure 4.10 Bland and Altman plot of the difference between complete and GHT pattern method LI results (y axis) against the mean of bo methods (x axis), for right eye (top) and left eye (bottom), for SITA Fast algorithm and normal individuals at visit 1 (left panel), visit 3 (mido panel) and visit 5 (right panel). The reference line for mean difference is the red line, the blue dot lines illustrate the 95% confidence lines 1.96xSD) and the green line is the linear regression line for the referenced R^2 value.

Normal Cohort
Algorithm SITA SWAP
Visit 1 3 5

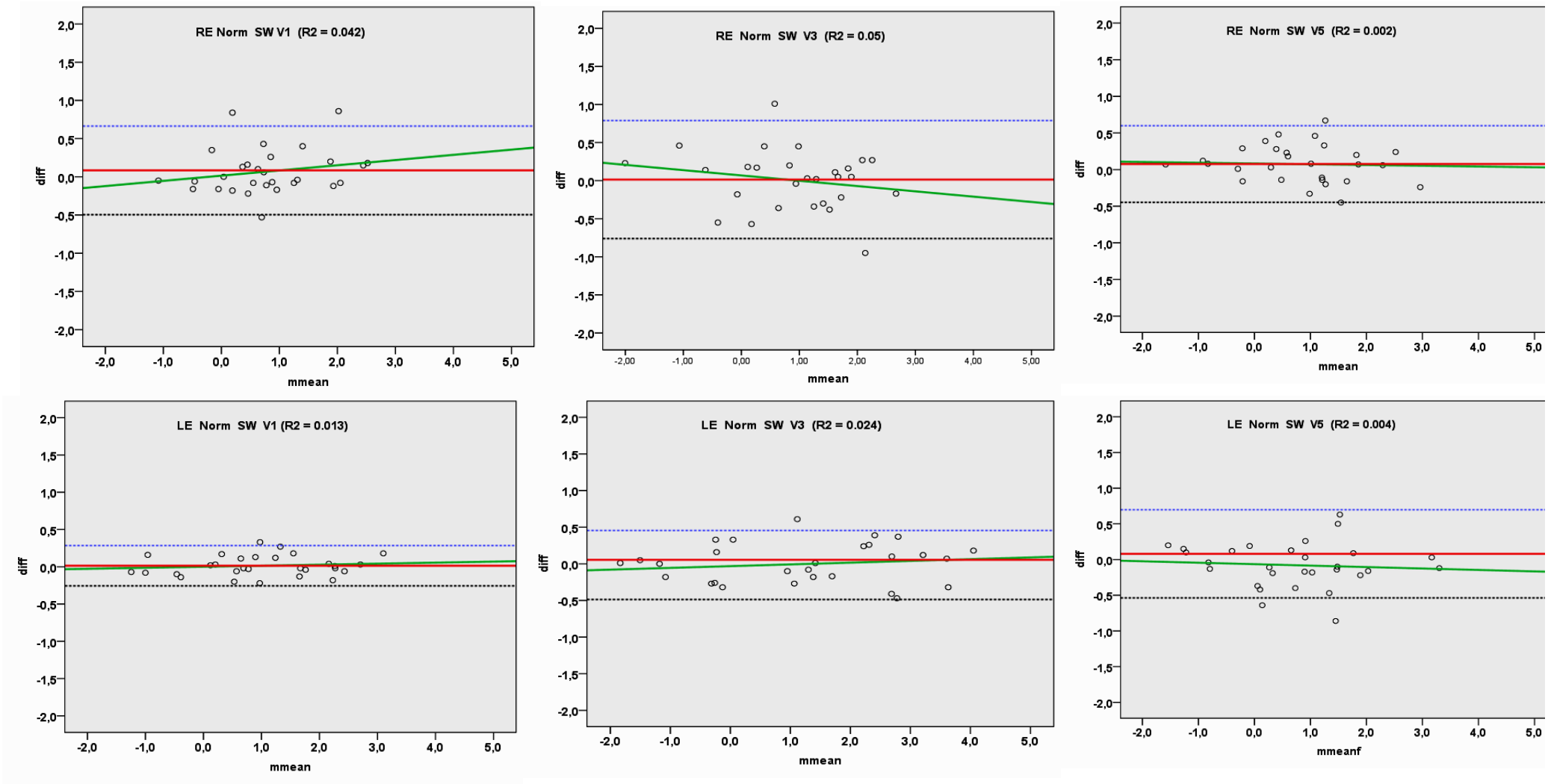

Figure 4.11 Bland and Altman plot of the difference between complete and GHT pattern method LI results (y axis) against the mean of bo methods (x axis), for right eye (top) and left eye (bottom), for SITA SWAP algorithm and normal individuals at visit 1 (left panel), visit 3 (middle panel) and visit 5 (right panel). The reference line for mean difference is the red line, the blue dot lines illustrate the 95% confidenc lines (+/- 1.96xSD) and the green line is the linear regression line for the referenced R^2 value.

OAG Cohort
Algorithm SITA STANDARD
Visit 1 3 5

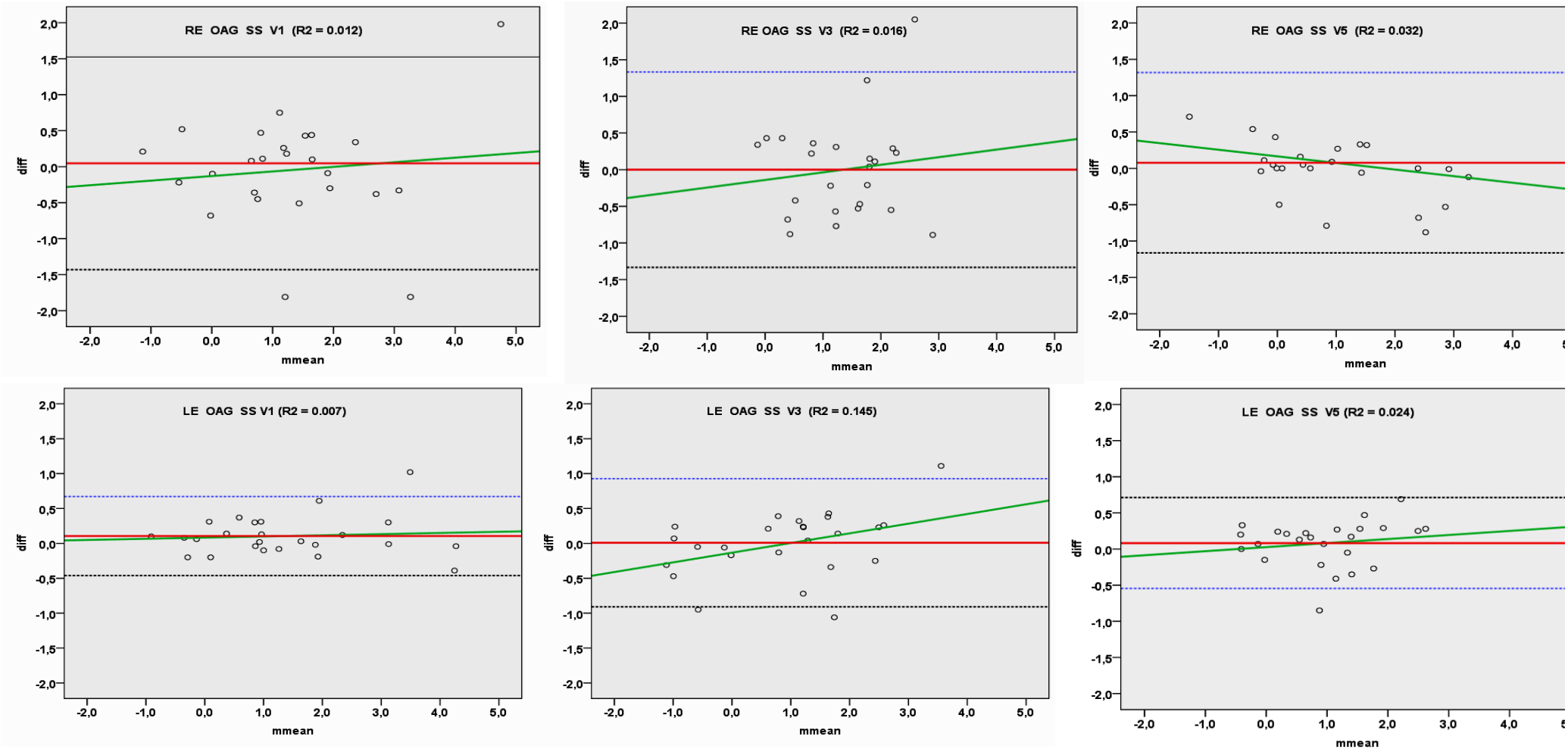

Figure 4.12 Bland and Altman plot of the difference between complete and GHT pattern method LI results (y axis) against the mean of bo methods (x axis), for right eye (top) and left eye (bottom), for SITA Standard algorithm and OAG individuals at visit 1 (left panel), visit 3 (middle panel) and visit 5 (right panel). The reference line for mean difference is the red line, the blue dot lines illustrate the 95% confidenc lines (+/- 1.96xSD) and the green line is the linear regression line for the referenced R^2 value.

OAG Cohort
Algorithm SITA FAST
Visit 1 3 5

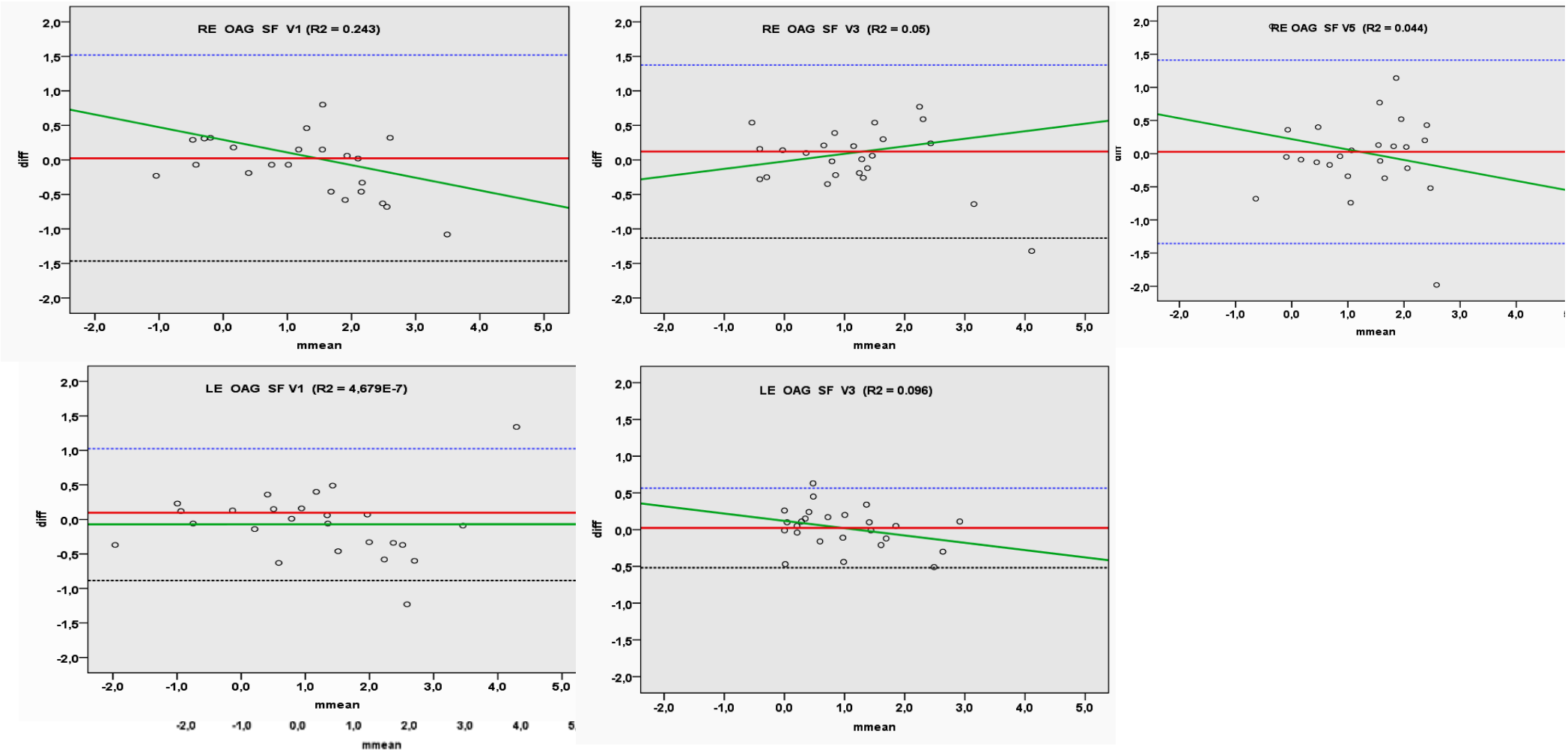

Figure 4.13 Bland and Altman plot of the difference between complete and GHT pattern method LI results (y axis) against the mean of bo methods (x axis), for right eye (top) and left eye (bottom), for SITA Fast algorithm and OAG individuals at visit 1 (left panel), visit 3 (middle panel) and visit 5 (right panel). The reference line for mean difference is the red line, the blue dot lines illustrate the 95% confidence lines (1.96xSD) and the green line is the linear regression line for the referenced R^2 value.

OAG Cohort
Algorithm SITA SWAP
Visit 1 3 5

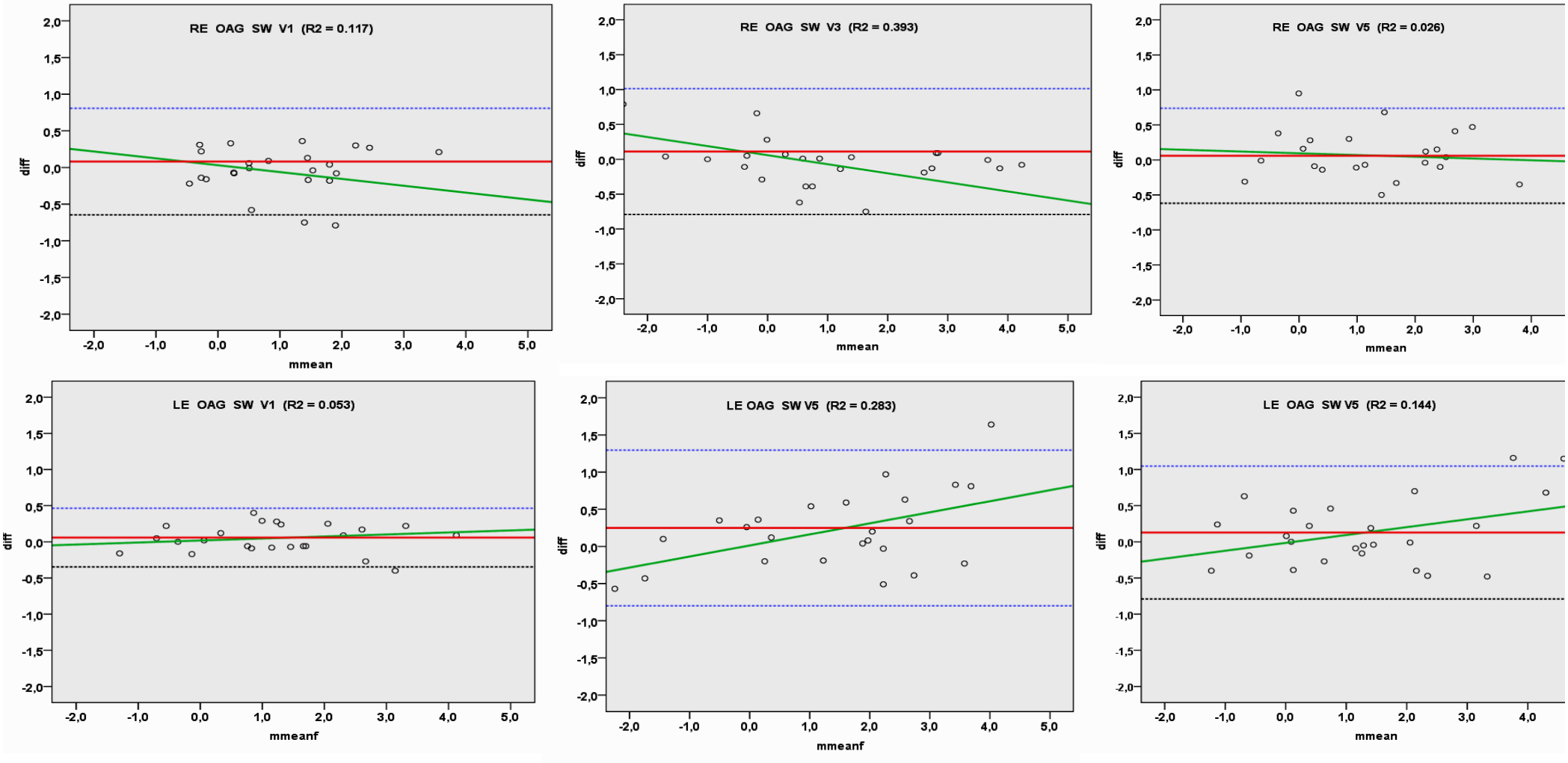

Figure 4.14 Bland and Altman plot of the difference between complete and GHT pattern method LI results (y axis) against the mean of bo methods (x axis), for right eye (top) and left eye (bottom), for SITA SWAP algorithm and OAG individuals at visit 1 (left panel), visit 3 (mid panel) and visit 5 (right panel). The reference line for mean difference is the red line, the blue dot lines illustrate the 95% confidence lines (1.96xSD) and the green line is the linear regression line for the referenced R^2 value.

OHT Cohort
Algorithm SITA STANDARD
Visit 1 3 5

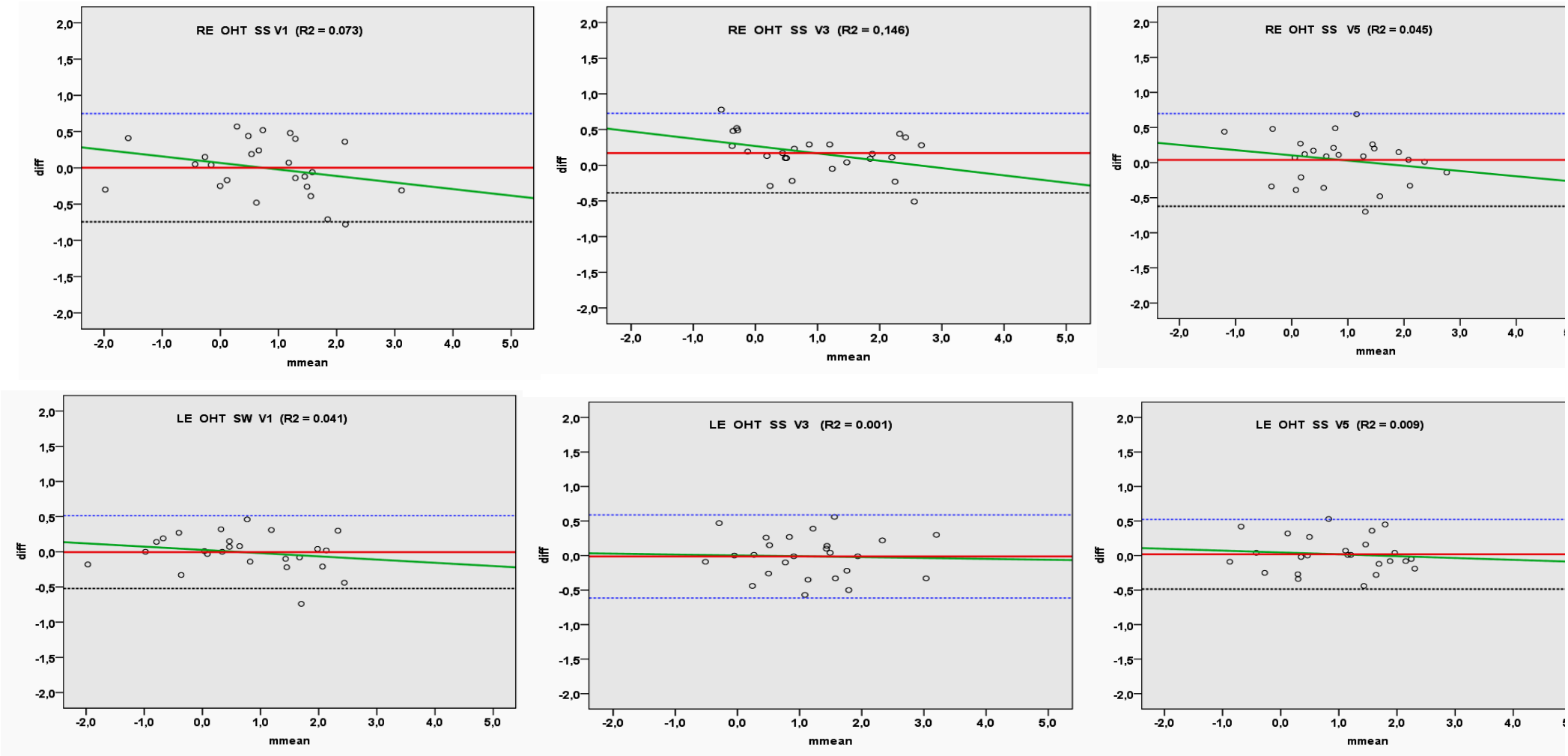

Figure 4.15 Bland and Altman plot of the difference between complete and GHT pattern method LI results (y axis) against the mean of bo methods (x axis), for right eye (top) and left eye (bottom), for SITA Standard algorithm and OHT individuals at visit 1 (left panel), visit 3 (middle panel) and visit 5 (right panel). The reference line for mean difference is the red line, the blue dot lines illustrate the 95% confidenc lines (+/- 1.96xSD) and the green line is the linear regression line for the referenced R^2 value.

OHT Cohort
Algorithm SITA FAST
Visit 1 3 5

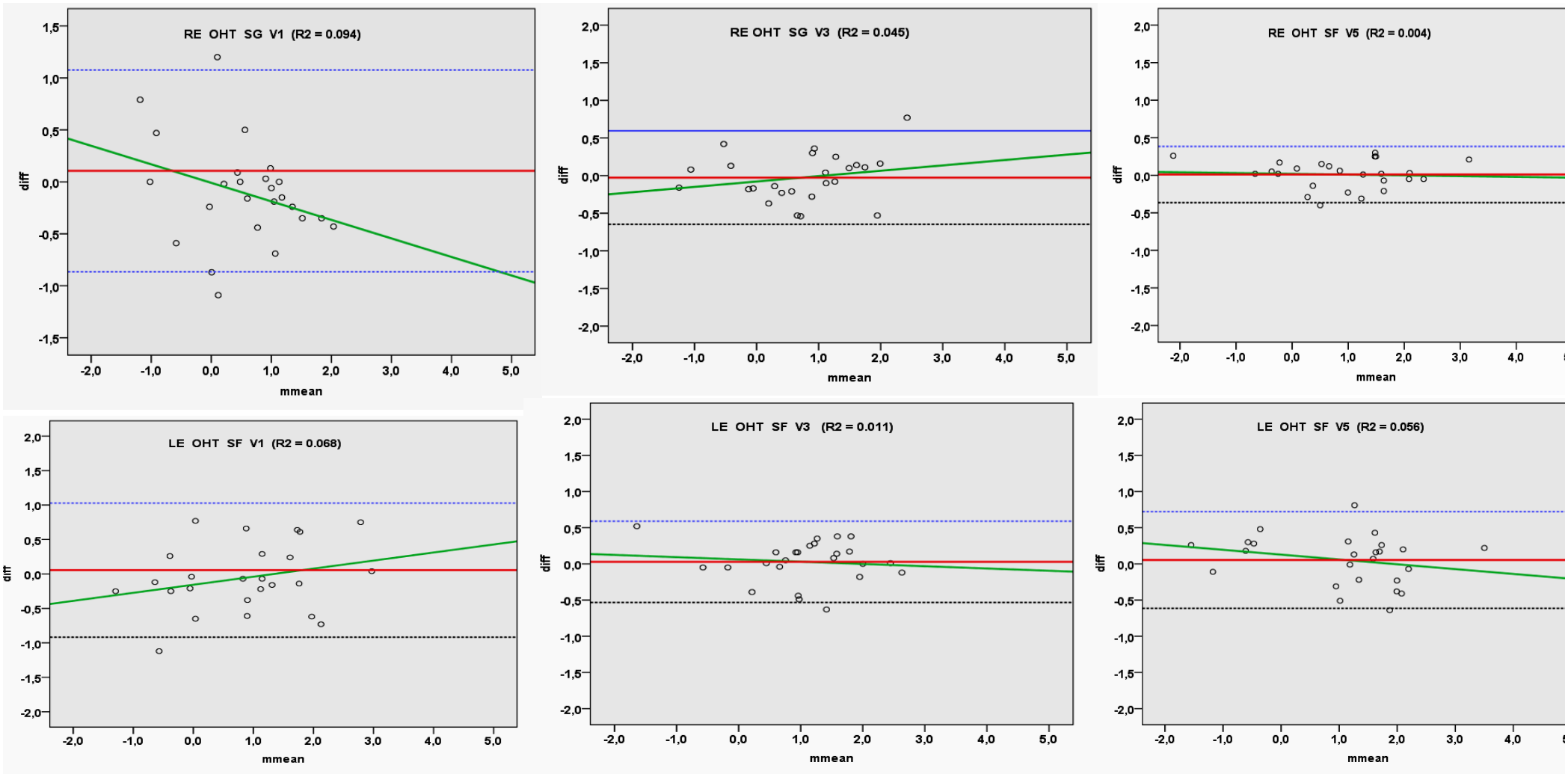

Figure 4.16 Bland and Altman plot of the difference between complete and GHT pattern method LI results (y axis) against the mean of both methods (x axis), for right eye (top) and left eye (bottom), for SITA Fast algorithm and OHT individuals at visit 1 (left panel), visit 3 (middle panel) and visit 5 (right panel). The reference line for mean difference is the red line, the blue dot lines illustrate the 95% confidenc lines (+/- 1.96xSD) and the green line is the linear regression line for the referenced R^2 value.

OHT Cohort
Algorithm SITA SWAP
Visit 1 3 5

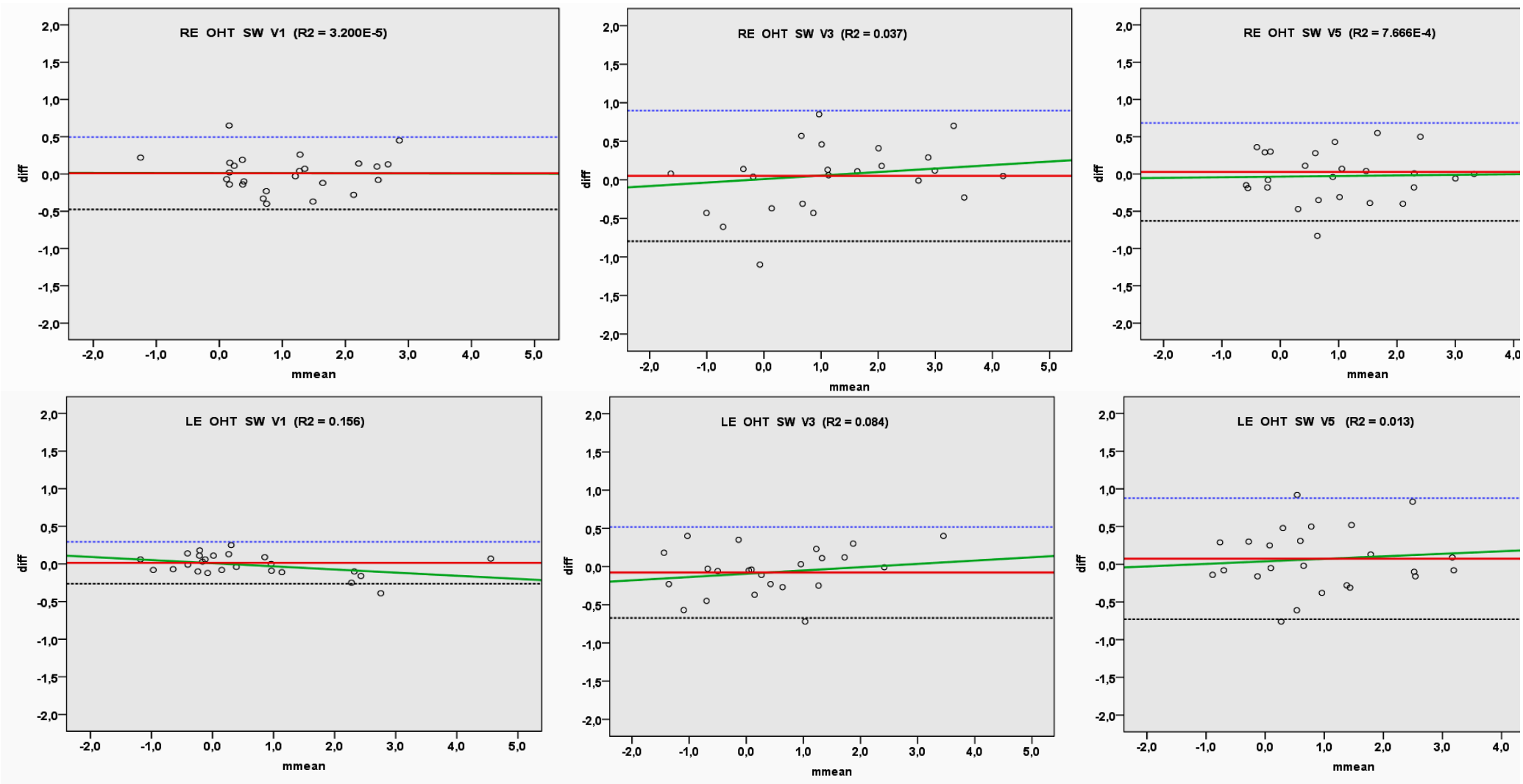

Figure 4.17 Bland and Altman plot of the difference between complete and GHT pattern method LI results (y axis) against the mean of bo methods (x axis), for right eye (top) and left eye (bottom), for SITA SWAP algorithm and OHT individuals at visit 1 (left panel), visit 3 (mid panel) and visit 5 (right panel). The reference line for mean difference is the red line, the blue dot lines illustrate the 95% confidence lines 1.96xSD) and the green line is the linear regression line for the referenced R^2 value.

4.1.4 Discussion

The current study describes an effort to examine whether this design that followed the GHT pattern will yield better results of LI calculations than the previous method with the complete pattern, as described in Chapter 3.

The results of applying GHT pattern method for LI calculation, for healthy normal individuals, lacking perimetric experience, for the SITA Standard algorithm demonstrate a minor decrease of LI values for the 3rd test session and a slight increase for the 5th session, for both eyes. With SITA Fast algorithm the LI results demonstrate a reduced amount of variability that is more evident in right eye. This is most likely due to the fact that a considerable number of these individuals undergone before some sessions with SITA Standard. As a result, the first session of SITA Fast for these individuals may stand for the third or higher test session for the right eye. With SITA SWAP algorithm the LI results exhibit rather high variability, for both eyes, mostly between the first and fifth visit. Wild and his colleagues found similar variation in results of MD, between visit 1 and 5 for inexperienced individuals with SITA SWAP (Wild et al., 2006).

For glaucoma patients and SITA Standard algorithm, although more experienced in SAP, the results reveal a great discrepancy of LI values. This poor performance of glaucoma patients is most likely due to the fact that defected locations cannot learn but because of the defects the LI maintains a high value, over repeated test sessions. This is falling in line with the Kulze and associates conclusion that learning is positively correlated to defect depth (Kulze, Stewart and Sutherland, 1990). For ghd SITA Fast algorithm and glaucomatous individuals, the results of LI calculation demonstrate higher LI values for the right eye and less for left eye.

Higher values were probably expected as the algorithm is very quick for glaucoma patients and consequently these individuals show reduced performance. After all, for SITA SWAP the LI values exhibit increased variability between visits. According Wild and colleagues, apparent deeper or wider field loss in the initial examinations with SWAP compared with that exhibited by SAP in OAG also may arise from inexperience in SWAP (Wild et al., 2006).

Although ocular hypertensive individuals are quite experienced in SAP they carry on the lack of perimetric experience in SITA SWAP. It is unclear why the calculated LI values for SITA Standard for both eyes exhibit great discrepancy. For SITA Fast algorithm and for both eyes the situation is similar and the results of LI calculation exhibit also quite large variation. After all, for SITA SWAP algorithm demonstrate a slight reduction of LI values for the 3rd test session and a minor raise for the 5th session, for both eyes. In previous study about learning effect in OHT patients, Rossetti and colleagues concluded that a significant learning effect was apparent at full threshold SWAP algorithm (Rossetti et al., 2006). A few years later, Fogagnolo and associates studying the behaviour of SITA SWAP 24-2 program in OHT individuals, concluded that SITA SWAP is affected by a rather small learning effect interfering only the first test, contrary to the result of Rosseti's full threshold SWAP algorithm used earlier (Fogagnolo et al., 2010).

4.1.5 Conclusions

The present study intended to consider the possibility of incorporation of GHT pattern LI calculation to previous complete pattern method. Normal individuals

demonstrated a minor decrease of LI values for SITA Standard algorithm, mainly in the right eye. With the SITA Fast algorithm, demonstrate a reduced amount of variability of LI results, and with SITA SWAP, the LI results exhibit rather high inconsistency, for both eyes, mostly between the first and fifth visit. However, none of these findings were statistically significant.

For glaucoma patients, although more experienced in SAP, the results for all algorithms reveal a great discrepancy of LI values. This poor performance of glaucoma patients for SITA Standard is most likely due to the fact that damaged locations cannot learn, for SITA Fast probably due to the speed of algorithm and for SITA SWAP, probably owed to the difficulty of the blue on yellow algorithm.

Ocular hypertensive individuals exhibit great discrepancy of LI values for all algorithms for both eyes, although the performance for SITA SWAP observed slightly better although the difficulty of the blue on yellow algorithm.

A visual judgement of the Bland-Altman plots reveals that the points are scattered fairly randomly, above and below zero, which in turn suggests that there is no consistent bias of one approach versus the other. The one-sample T-Test results do not reveal any statistically significant difference between the two methods, and as a result the GHT pattern method is therefor not of any important clinical interest.

4.2 The Learning Index calculation excluding eyelid effect.

Ptosis (or Blepharoptosis) is a downward displacement of the upper eyelid margin and can restrict and even block normal vision (fig.4.18). The lid may droop only slightly, or it may cover the pupil entirely. It may be noticed that even when the lid margin is about a millimeter above the pupil rim some obstruction of the field may occur (Fisher, 1967).

Ptosis takes place when the muscles that raise the eyelid (levator and superior tarsal muscles) are not strong enough to do so properly and produce partial obstruction of vision during visual field assessment commonly in elderly individuals. In general, ptosis may affect one or both eyelids, be inherited, be present at birth or occur later in life. Usually, the condition of drooping upper eyelids occurs as a result of a number of distinct diagnoses, which are treated by different operative procedures (Cahill et al, 2011)

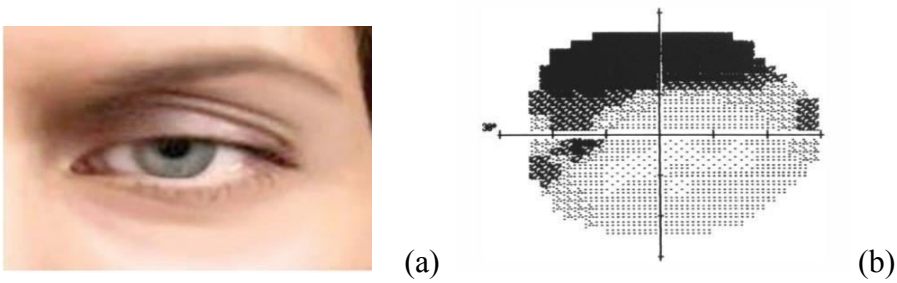

Figure 4.18 Ptosis (drooping eye) of left eye of a normal individual (a) and the greyscale printout showing similar damage to glaucoma damage affecting the superior visual field (b).

4.2.1 Aim of the study

Perimetry is the most common method to find functional visual field loss in glaucomatous patients. Typically these patients are of old age and they very often suffer from ptosis. In particular, the upper row locations' values may

be omitted during calculation, as these locations of visual field may be obstructed just by the lid and not by a potential glaucoma disease.

Then the results of lid effect calculations could be compared with complete visual field (no-lid) results and evaluated in order to check the likelihood of using this method of calculation to produce a learning index.

4.2.2 Methods

4.2.2.1 The cohort

The cohort is the same that used in previous studies and comprised of three different groups of normal individuals, glaucoma patients and ocular hypertensive individuals.

4.2.2.2 Methods for no-lid L I calculation.

In this study, the method of learning index calculation takes in account the eyelid effect (droopy eye or ptosis). The LI calculations following the No-Lid pattern arose by a design in a manner identical to that of Olsson et al (1997), except that the upper first row of sensitivity values was omitted.

Dr Carlo Knupp, Senior Research Fellow in Cardiff University, undertook the coding for the calculation following the pattern of “No Eyelid” as illustrated in figure 4.19 on the next page.

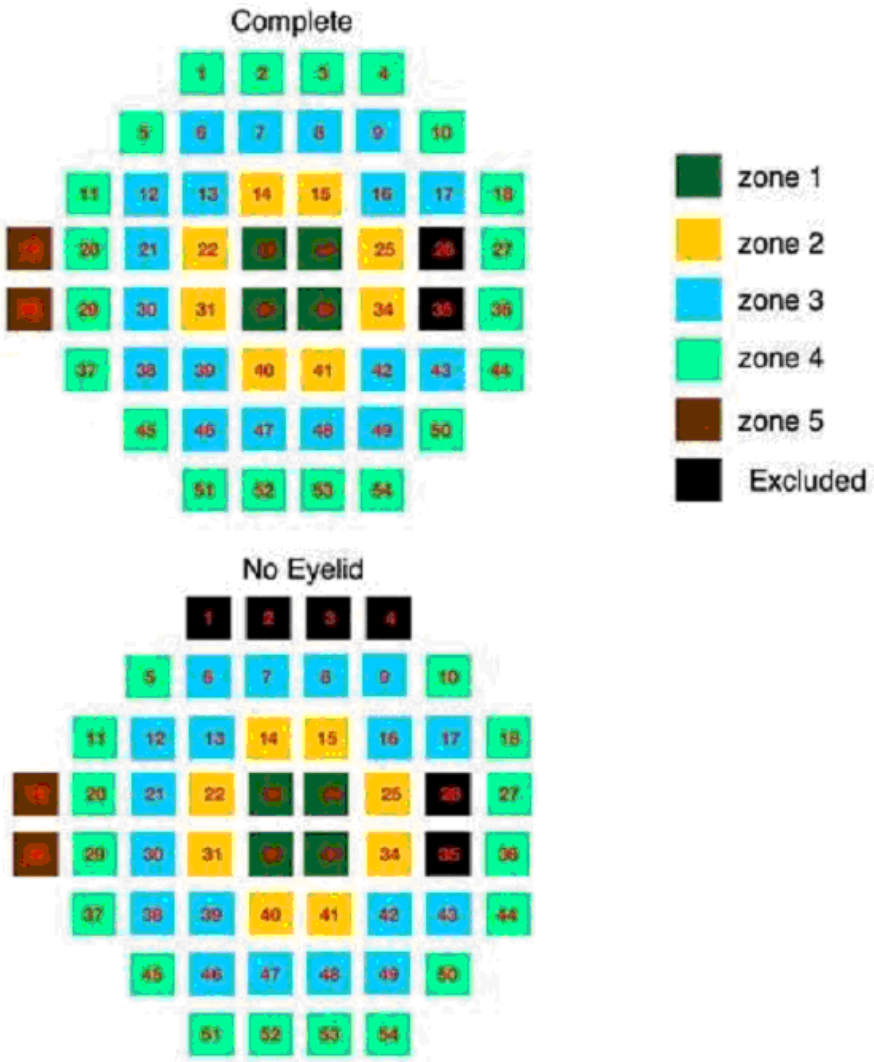

Figure 4.19 Distribution of data in five zones as Olsson's (Olsson, Asman and Heijl., 1997) complete method of LI calculation (top) and distribution of No Eyelid pattern data (bottom) in 5 zones (green, blue, yellow and grey shaded location areas, plus the nasal locations 19 and 27). Locations 1 to 4 (top row), were excluded.

4.2.3 Results

The results of the above method are presented as descriptive statistics for Learning Index calculation (left panel) and Box and Whisker plots of the Learning Index distribution (right panels) for normal individuals, for glaucoma patients and for ocular hypertensive individuals, for SITA Standard, SITA Fast and SITA SWAP algorithms, for the right and left eye, respectively.

Figures 4.20 to 4.22 illustrate the descriptive statistics tables (left panel) and Box and Whisker plots of the learning index distribution (right panel) for right eye, for all algorithms at all five visits for normal (top), glaucoma (middle) and hypertensive cohort (bottom). Figures 4.23 to 4.25 illustrate analogous results for left eye.

For SITA Standard algorithm and for normal individuals (Fig.4.20, top) for right eye and (Fig. 4.23, top) for the left eye, demonstrate high values of LI, probably an indication that individuals did not learn due to their inexperience in perimetry.

For glaucoma patients (Fig.4.21 and 4.24, top), the LI values for right eye exhibit slight decrease mainly at fifth test and for left eye the LI results show more variability and high values, probably due to increased fatigue. Finally for ocular hypertensive individuals (Fig.4.22 and 4.25, top), the LI results exhibit a great discrepancy of values.

For the SITA Fast algorithm, the normal individuals show a slight inconsistency of the LI values for the right eye (Fig.4.20, middle), and a rather minor reduction

for the third test session for the left eye (Fig.4.23, middle). Glaucoma patients (Fig 4.21 and 4.24, middle for the right and the left eye, respectively) exhibit a great variability of the LI results,. The OHT cohort (Fig 4.22 and 4.25, middle for the right and left eye, respectively) demonstrate quite high variability of the LI results. Finally, for SITA SWAP algorithm and for normal cohort (Fig 4.20 and 4.23, bottom) show a reduced amount of the LI values at the fifth test session, for both eyes, most likely due to the greater difficulty with the SWAP task than with that for SAP. The glaucoma patients continued to present increased LI variability between visits (Fig 4.21 and 4.24, bottom). Rather low LI values at third test session (for both eyes) and considerable inconsistency in results were observed in the OHT cohort, most likely due to the algorithm.

Next Figures 4.26 to 4.34 include the Bland and Altman Plots of Learning Index (LI) calculation results of both methods, complete and No-Eyelid pattern, as a simple way to estimate an agreement interval, within which 95% of the differences of the second method, compared to the first one fall.

Normal Cohort
Algorithm SITA STANDARD
Eye Right

	N	Min.	Max.	Mean	Std. Dev.
VIS_1	29	-1.08	2.90	.9021	1.02621
VIS_2	29	-.86	3.08	.7914	.97382
VIS_3	29	-1.54	2.56	.8376	1.01672
VIS_4	29	-.34	2.56	1.0428	.66281
VIS_5	29	-1.29	3.11	1.1052	1.05562

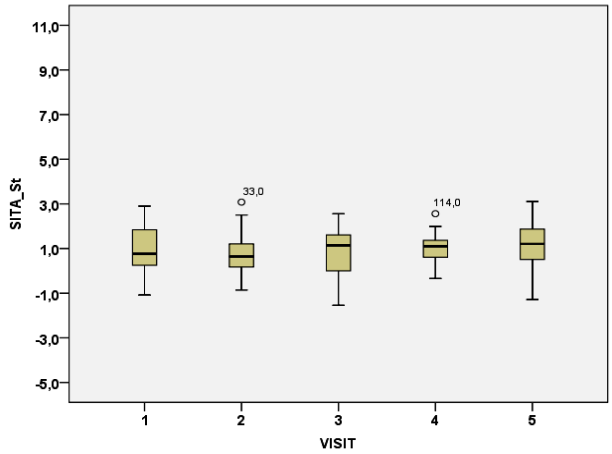

Normal Cohort
Algorithm SITA FAST
Eye Right

	N	Min.	Max.	Mean	Std. Devi.
VIS_1	29	-1.47	4.77	.8859	1.45277
VIS_2	29	-.64	2.79	.8610	.80990
VIS_3	29	-.37	2.34	.9959	.69943
VIS_4	29	-2.21	2.42	.7334	1.16004
VIS_5	29	-1.13	2.35	.8138	.95778

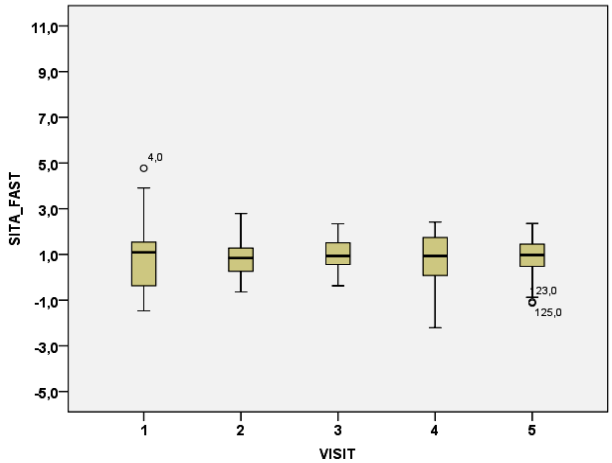

Normal Cohort
Algorithm SITA SWAP
Eye Right

	N	Min.	Max.	Mean	Std. Dev..
VIS_1	29	-.75	2.66	.7810	.82221
VIS_2	29	-.75	2.66	.7810	.82221
VIS_3	29	-1.83	2.69	.8493	1.18772
VIS_4	29	-1.76	5.27	.9462	1.52662
VIS_5	29	-1.90	3.32	.6259	1.19608

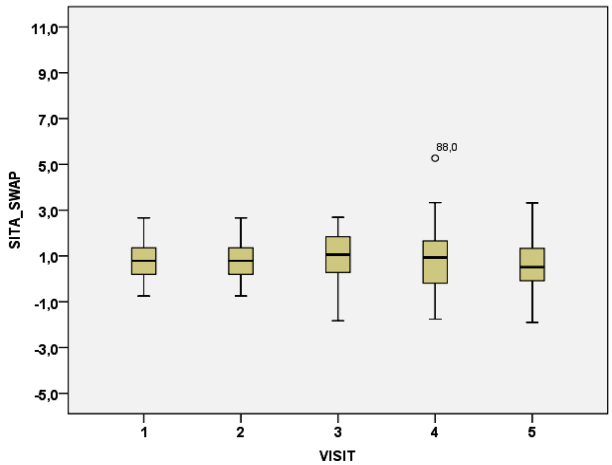

Figure 4.20. The descriptive statistics (left panel), for the Learning Index for normal individuals (right eye), across the five visits, for each of the three algorithms, calculated with No-Eyelid pattern. Box and Whisker plots (right panel), of the Learning Index distribution for the normal individuals (right eye), across the five visits, within algorithm for SITA Standard (top), SITA Fast (middle) and SWAP (bottom).

Glaucoma Cohort
Algorithm SITA STANDARD
Eye Right

	N	Min.	Max.	Mean	Std. Dev.
VIS_1	25	-1.07	4.39	1.3932	1.33017
VIS_2	25	-.38	3.90	1.4368	1.14645
VIS_3	25	-.28	3.91	1.3064	.90427
VIS_4	25	-1.16	3.22	1.0372	1.25027
VIS_5	25	-1.89	3.29	.9916	1.30832

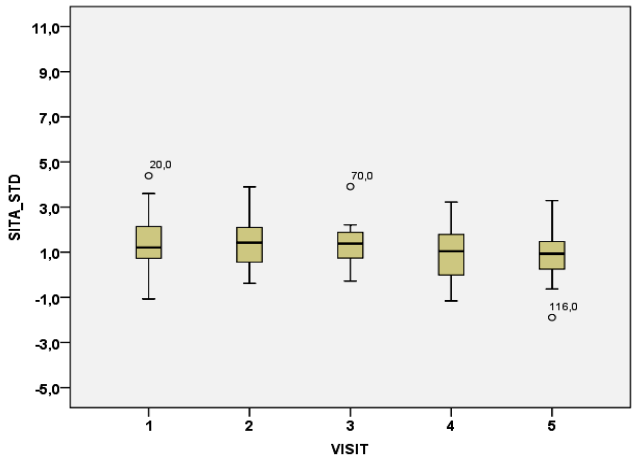

Glaucoma Cohort
Algorithm SITA FAST
Eye Right

	N	Min.	Max.	Mean	Std. Dev.
VIS_1	25	-4.51	11.98	1.4460	2.82495
VIS_2	25	-1.31	11.30	1.3940	2.45214
VIS_3	25	-.88	6.76	1.2464	1.62003
VIS_4	25	-.73	9.92	1.6416	2.17910
VIS_5	25	-1.04	3.15	1.2484	1.00312

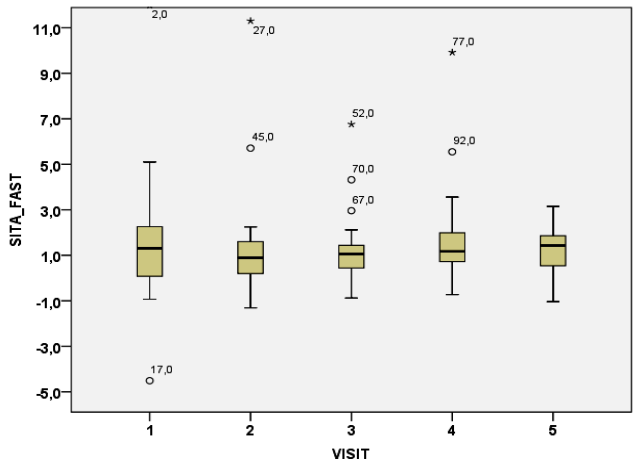

Glaucoma Cohort
Algorithm SITA SWAP
Eye Right

	N	Min.	Max.	Mean	Std. Dev.
VIS_1	25	-.45	6.25	1.2264	1.51986
VIS_2	25	-.45	6.25	1.2264	1.51986
VIS_3	25	-4.14	9.57	1.4240	2.58916
VIS_4	25	-3.33	11.47	1.3152	2.63938
VIS_5	25	-4.39	8.64	1.5028	2.35550

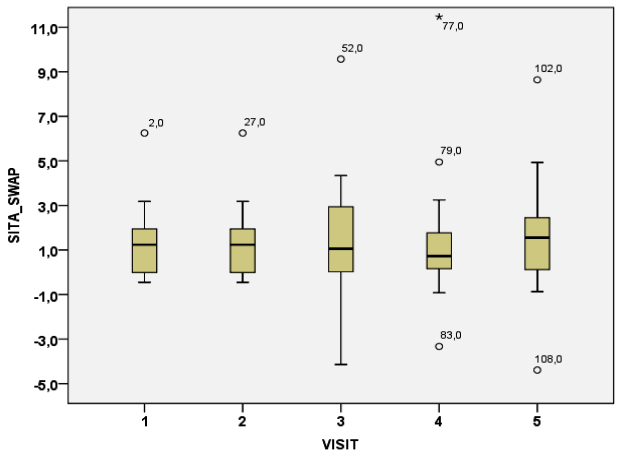

Figure 4.21. The descriptive statistics (left panel), for the Learning Index for OAG individuals (right eye), across the five visits, for each of the three algorithms, calculated with No-Eyelid pattern. Box and Whisker plots (right panel), of the Learning Index distribution for the OAG individuals (right eye), across the five visits, within algorithm for SITA Standard (top), SITA Fast (middle) and SWAP (bottom).

OHT Cohort
Algorithm SITA STANDARD
Eye Right

	N	Min.	Max.	Mean	Std. Dev.
VIS_1	25	-1.84	3.64	.6976	1.21130
VIS_2	25	-.60	2.09	.7912	.77614
VIS_3	25	-.80	2.51	.9088	1.04593
VIS_4	25	-1.69	2.82	.8792	1.07931
VIS_5	25	-1.39	2.81	.8760	.99572

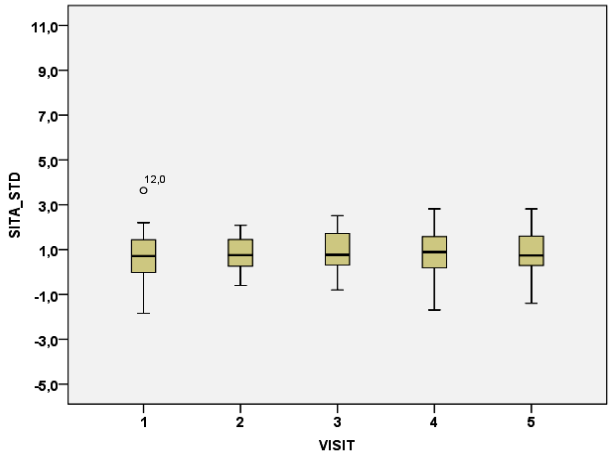

OHT Cohort
Algorithm SITA FAST
Eye Right

	N	Min.	Max.	Mean	Std. Dev.
VIS_1	25	-1.96	2.41	.6260	1.18729
VIS_2	25	-2.40	2.55	.6512	1.14154
VIS_3	25	-1.57	2.47	.6972	.86766
VIS_4	25	-2.11	2.03	.6564	1.05022
VIS_5	25	-1.54	2.63	.8924	1.05131

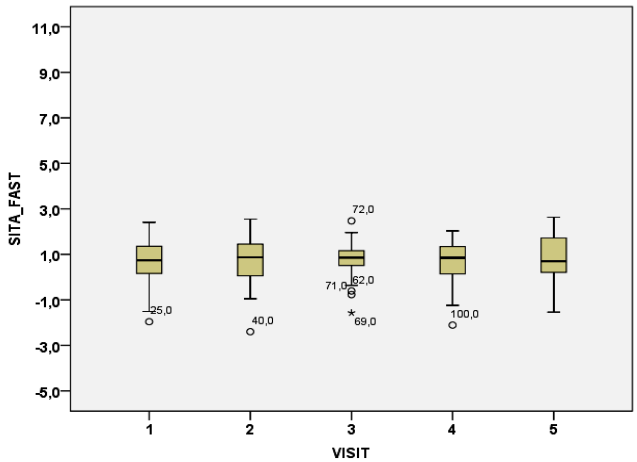

OHT Cohort
Algorithm SITA SWAP
Eye Right

	N	Min.	Max.	Mean	Std. Dev.
VIS_1	25	-1.23	3.51	1.0920	1.12315
VIS_2	25	-1.86	3.96	.8084	1.52145
VIS_3	25	-2.90	3.59	.7924	1.60266
VIS_4	25	-2.35	3.62	.8104	1.61694
VIS_5	25	-1.07	3.27	.9336	1.19256

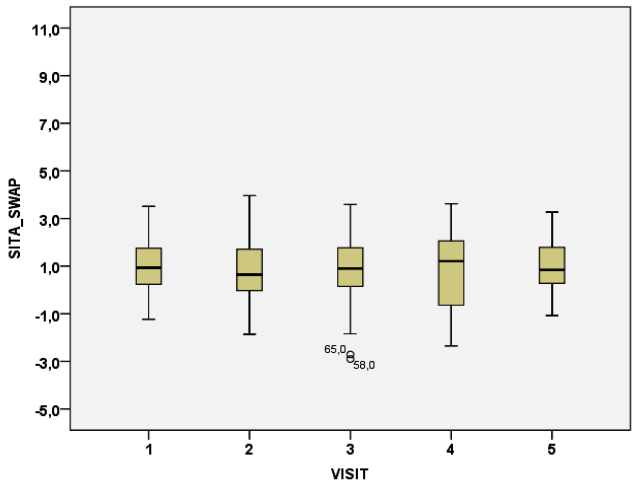

Figure 4.22. The descriptive statistics (left panel), for the Learning Index for OHT individuals (right eye), across the five visits, for each of the three algorithms, calculated with No-Eyelid pattern. Box and Whisker plots (right panel), of the Learning Index distribution for the OHT individuals (right eye), across the five visits, within algorithm for SITA Standard (top), SITA Fast (middle) and SWAP (bottom).

Normal Cohort
Algorithm SITA STANDARD
Eye Left

	N	Min.	Max.	Mean	Std. Dev.
VIS_1	29	-.82	2.96	.9762	.88204
VIS_2	29	-.89	3.04	.9797	.98515
VIS_3	29	-.41	2.85	.9500	.87622
VIS_4	29	-.82	3.04	1.0552	.96700
VIS_5	29	-2.53	4.11	1.0886	1.35150

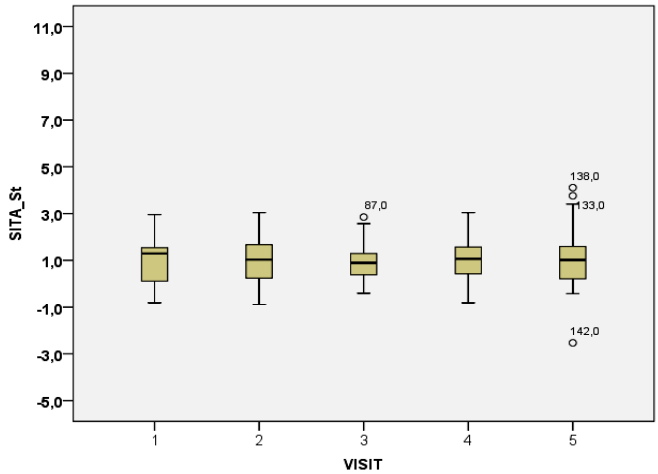

Normal Cohort
Algorithm SITA FAST
Eye Left

	N	Min.	Max.	Mean	Std. Dev.
VIS_1	25	-1.76	3.77	1.2348	1.48611
VIS_2	25	-1.37	2.45	1.0788	.81926
VIS_3	25	-2.21	2.40	.9300	1.03824
VIS_4	25	-2.69	2.58	.9972	1.25073
VIS_5	25	-2.60	2.56	1.0472	1.07554

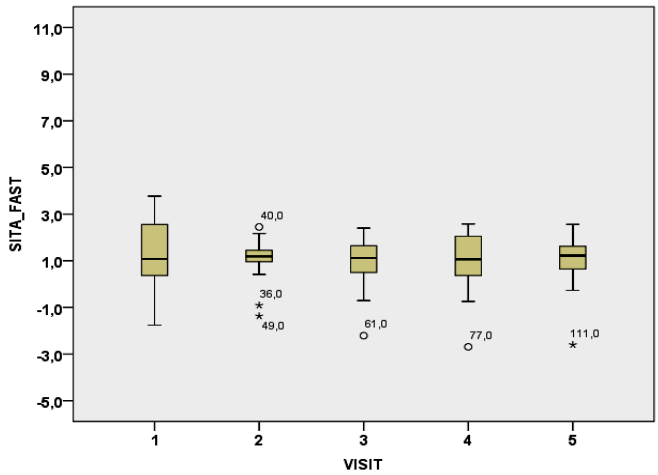

Normal Cohort
Algorithm SITA SWAP
Eye Left

	N	Min.	Max.	Mean	Std. Dev.
VIS_1	29	-1.20	3.04	.9993	1.15016
VIS_2	29	-2.63	3.05	.9321	1.44058
VIS_3	29	-2.49	4.46	1.1100	1.88964
VIS_4	29	-1.06	3.60	1.0214	1.21430
VIS_5	29	-1.67	3.44	.7531	1.25299

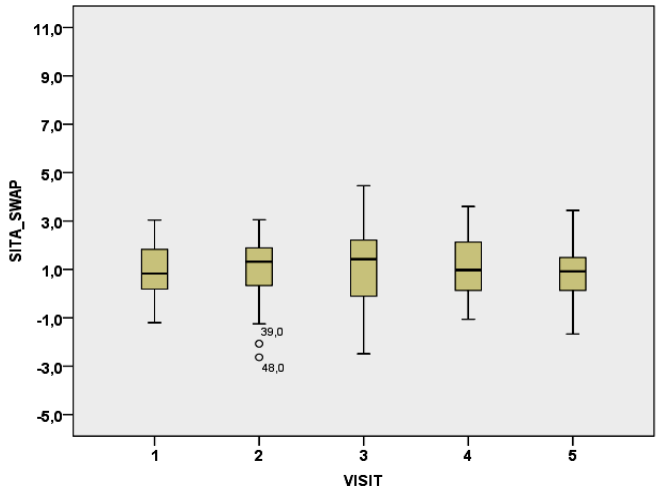

Figure 4.23. The descriptive statistics (left panel), for the Learning Index for normal individuals (left eye), across the five visits, for each of the three algorithms, calculated with No-Eyelid pattern. Box and Whisker plots (right panel), of the Learning Index distribution for the normal individuals (left eye), across the five visits, within algorithm for SITA Standard (top), SITA Fast (middle) and SWAP (bottom).

Glaucoma Cohort
Algorithm SITA STANDARD
Eye Left

	N	Min.	Max.	Mean	Std. Dev.
VIS_1	25	-,86	4,25	1,4220	1,44111
VIS_2	25	-1,40	6,04	1,4484	1,54739
VIS_3	25	-1,27	4,11	,8936	1,39005
VIS_4	25	-2,63	2,33	1,0168	1,16480
VIS_5	25	-,41	2,76	1,0168	,92182

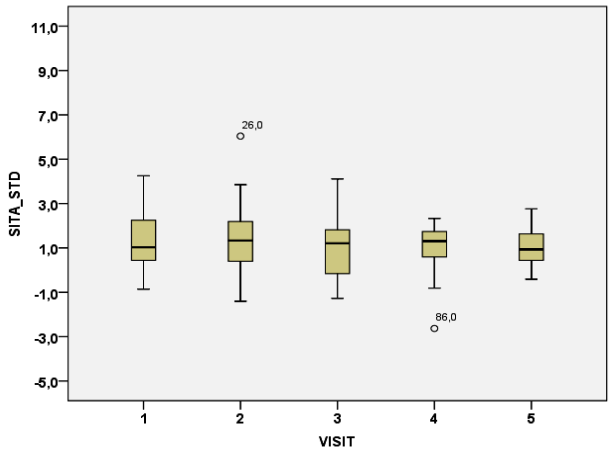

Glaucoma Cohort
Algorithm SITA FAST
Eye Left

	N	Min.	Max.	Mean	Std. Dev.
VIS_1	25	-2,15	4,96	1,1472	1,49304
VIS_2	25	-1,16	2,72	1,0156	,87757
VIS_3	25	-2,45	2,47	,9988	1,02723
VIS_4	25	-1,53	3,54	1,0752	1,19057
VIS_5	25	-2,65	3,06	1,1008	1,22282

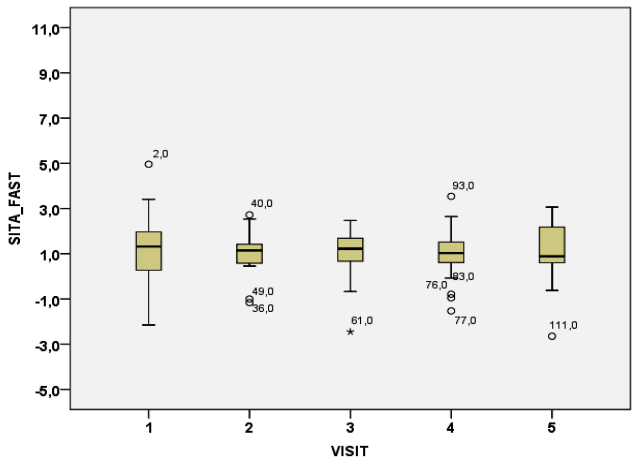

Glaucoma Cohort
Algorithm SITA SWAP
Eye Left

	N	Min.	Max.	Mean	Std. Dev.
VIS_1	25	-1.24	6.23	1.4004	1.68650
VIS_2	25	-2.33	5.82	1.3984	1.64680
VIS_3	25	-1.89	5.20	1.5376	1.83545
VIS_4	25	-1.52	6.69	1.2684	1.92242
VIS_5	25	-1.24	4.02	1.2396	1.54818

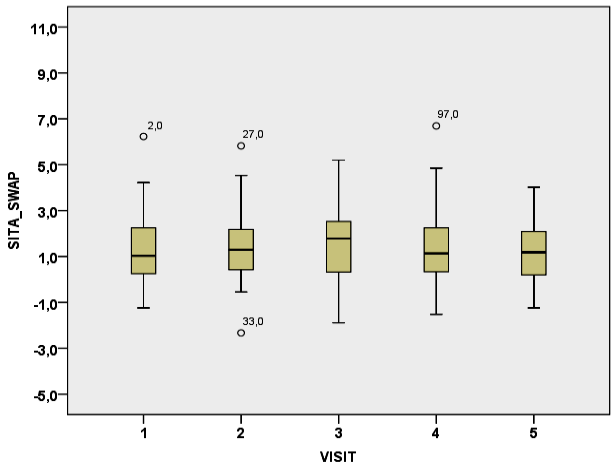

Figure 4.24. The descriptive statistics (left panel), for the Learning Index for OAG individuals (left eye), across the five visits, for each of the three algorithms, calculated with No-Eyelid pattern. Box and Whisker plots (right panel), of the Learning Index distribution for the OAG individuals (left eye), across the five visits, within algorithm for SITA Standard (top), SITA Fast (middle) and SWAP (bottom).

OHT Cohort
Algorithm SITA STANDARD
Eye Left

	N	Min	Max	Mean	Std Dev
VIS_1	25	-1.93	2.47	.6828	1.14796
VIS_2	25	-1.00	2.30	.6236	.89988
VIS_3	25	-.60	3.18	1.2204	.94531
VIS_4	25	-1.11	3.50	.9300	1.31925
VIS_5	25	-.87	2.59	.9948	.93728

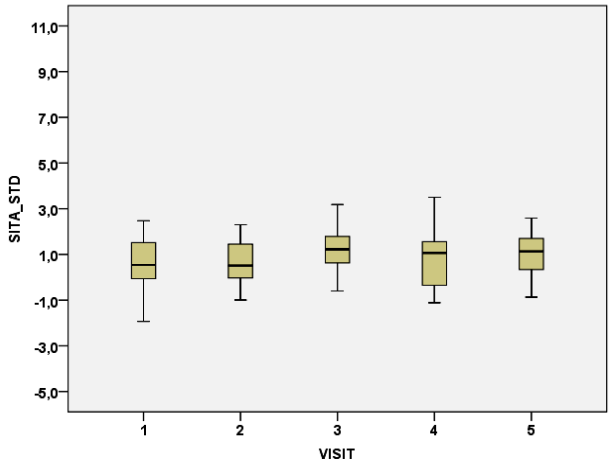

OHT Cohort
Algorithm SITA FAST
Eye Left

	N	Min.	Max.	Mean	Std. Dev.
VIS_1	25	-.98	2.82	.8732	1.04390
VIS_2	25	-2.08	2.35	.7848	1.21032
VIS_3	25	-2.04	2.67	1.0888	1.02159
VIS_4	25	-2.43	3.26	1.1368	1.29084
VIS_5	25	-1.60	3.14	1.0800	1.26371

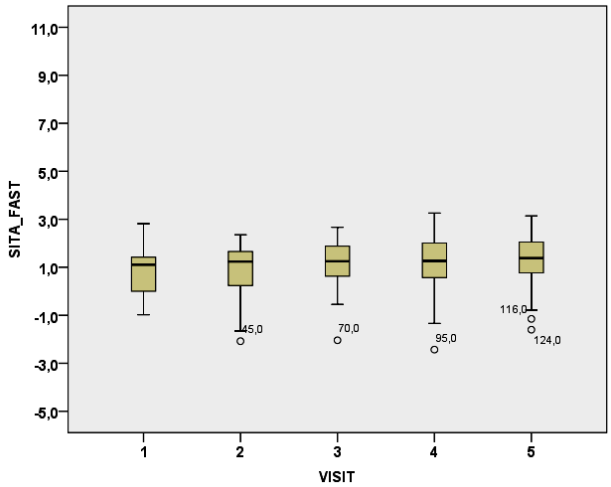

OHT Cohort
Algorithm SITA SWAP
Eye Left

	N	Min.	Max.	Mean	Std. Dev.
VIS_1	25	-1.20	4.56	.6040	1.37988
VIS_2	25	-1.24	4.69	.7436	1.60769
VIS_3	25	-4.75	5.55	.4296	1.86213
VIS_4	25	-2.19	2.62	.6992	1.37152
VIS_5	25	-1.11	4.63	1.0440	1.43307

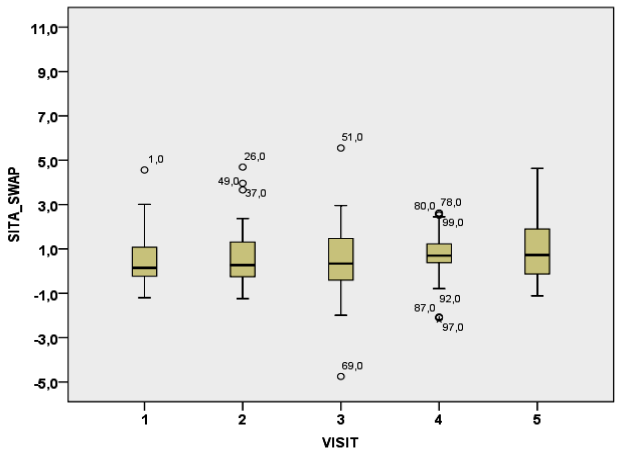

Figure 4.25. The descriptive statistics (left panel), for the Learning Index for OHT individuals (left eye), across the five visits, for each of the three algorithms, calculated with No-Eyelid pattern. Box and Whisker plots (right panel), of the Learning Index distribution for the OHT individuals (leftt eye), across the five visits, within algorithm for SITA Standard (top), SITA Fast (middle) and SWAP (bottom).

Normal Cohort
Algorithm SITA STANDARD
Visit **1** **3** **5**

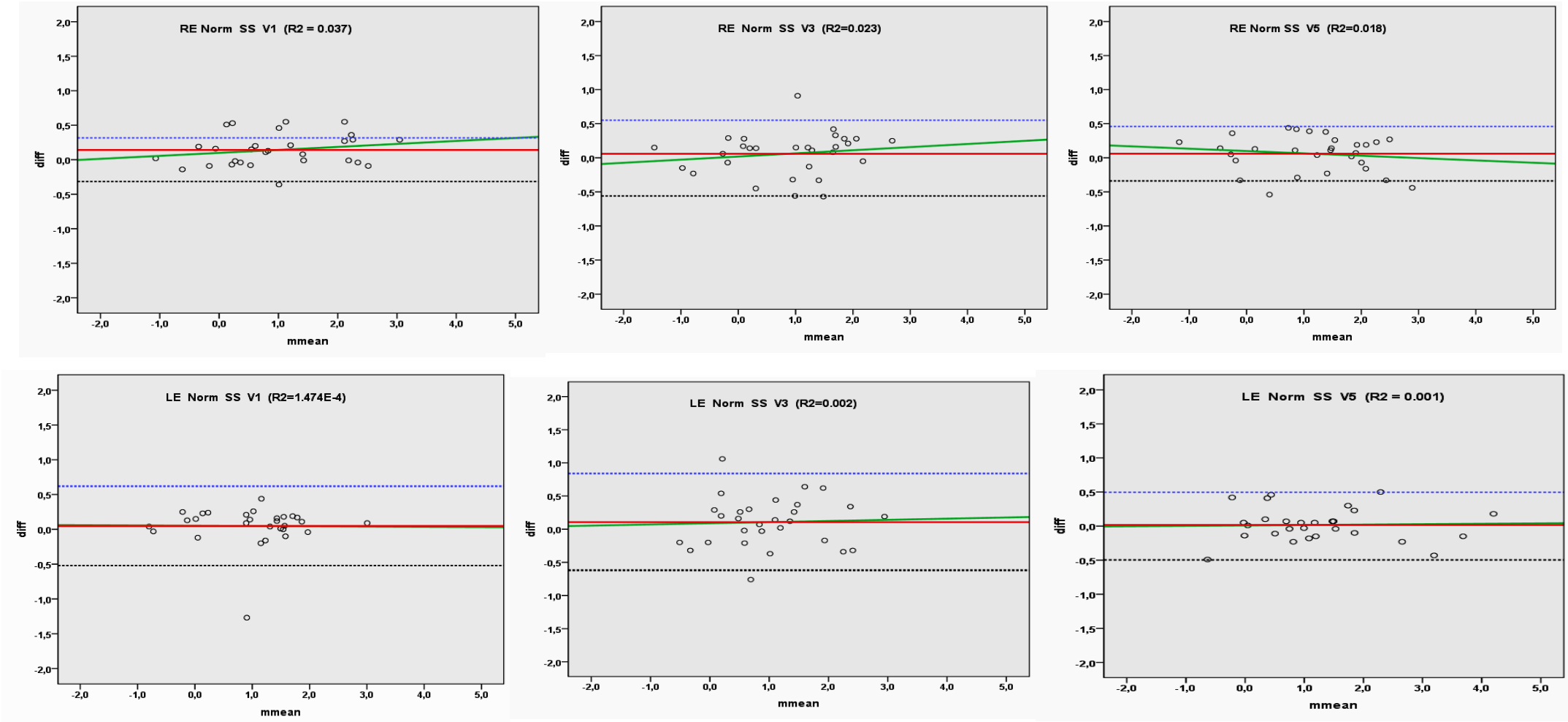

Figure 4.26. Bland and Altman plot of the difference between complete and No-Eyelid pattern method LI results (y axis) against the mean of both methods (x axis), for right eye (top) and left eye (bottom), for SITA Standard algorithm and normal individuals at visit 1 (left panel), visit 3 (middle panel) and visit 5 (right panel). The reference line for mean difference is the red line, the blue dot lines illustrate the 95% confidence lines (+/- 1.96xSD) and the green line is the linear regression line for the referenced R^2 value.

Normal Cohort
Algorithm SITA FAST
Visit 1 3 5

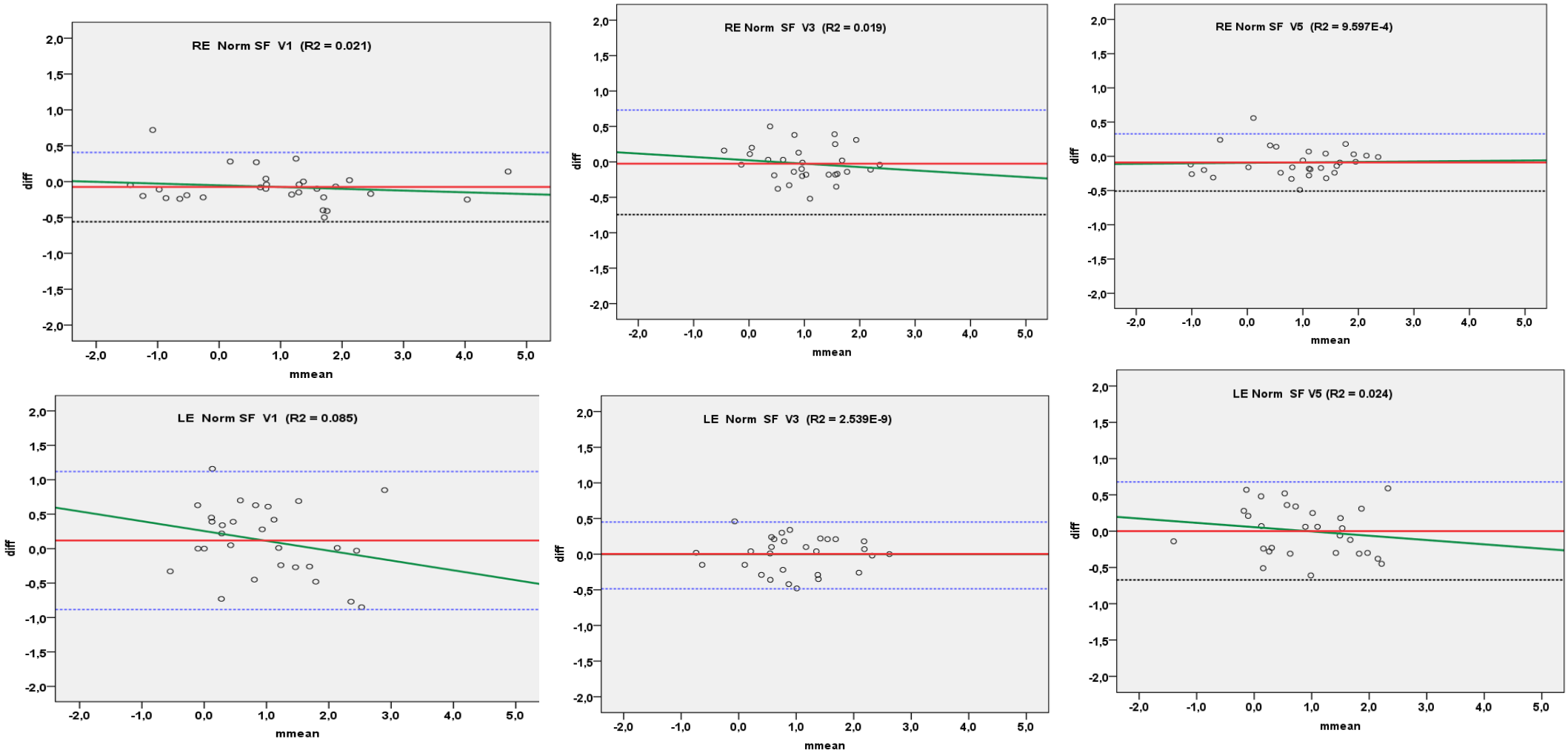

Figure 4.27. Bland and Altman plot of the difference between complete and N0-Eyelid pattern method LI results (y axis) against the mean of both methods (x axis), for right eye (top) and left eye (bottom), for SITA Fast algorithm and normal individuals at visit 1 (left panel), visit 3 (middle panel) and visit 5 (right panel). The reference line for mean difference is the red line, the blue dot lines illustrate the 95% confidence lines (+/- 1.96xSD) and the green line is the linear regression line for the referenced R^2 value.

Normal Cohort
Algorithm SITA SWAP
Visit 1 3 5

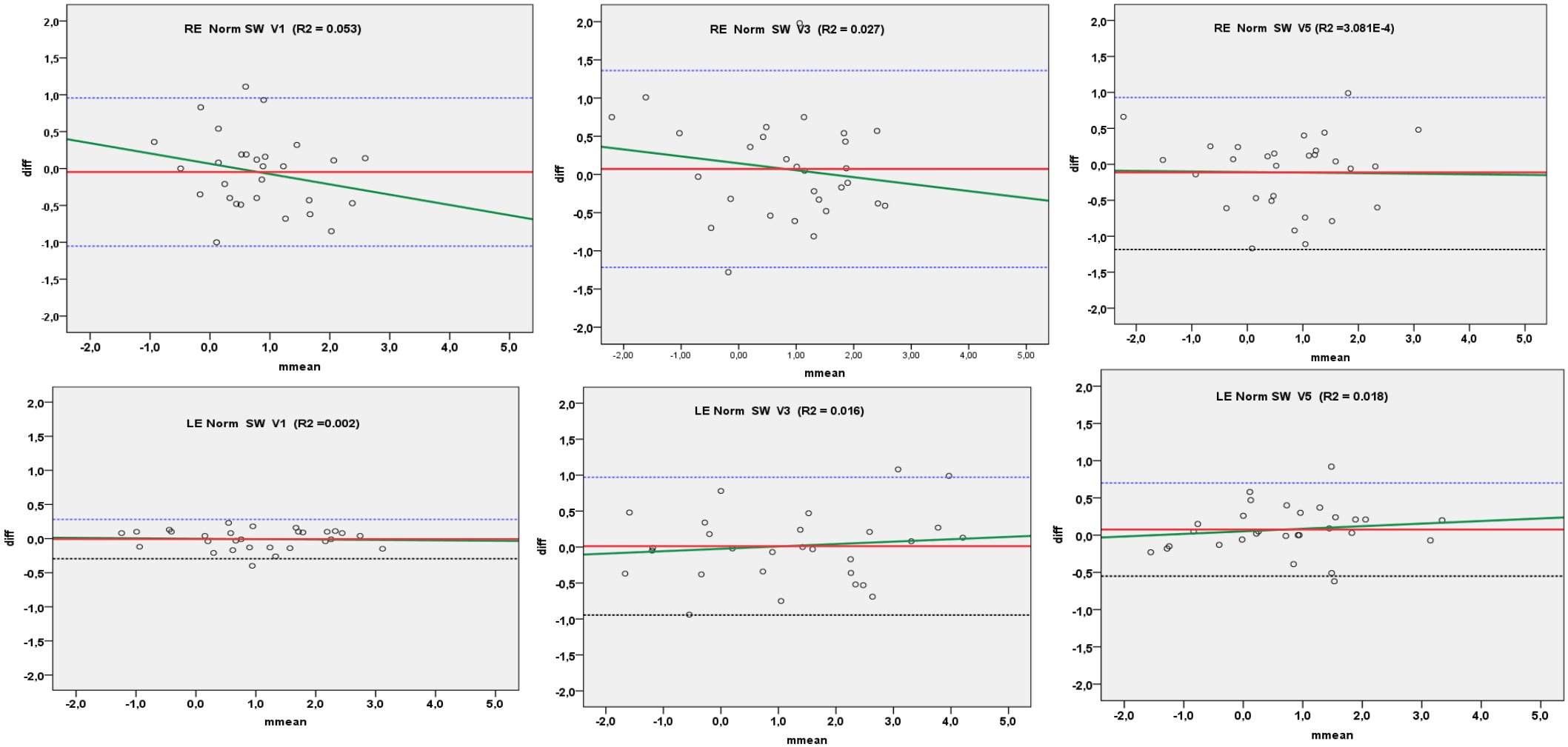

Figure 4.28. Bland and Altman plot of the difference between complete and No-Eyelid pattern method LI results (y axis) against the mean of both methods (x axis), for right eye (top) and left eye (bottom), for SITA SWAP algorithm and normal individuals at visit 1 (left panel), visit 3 (middle panel) and visit 5 (right panel). The reference line for mean difference is the red line, the blue dot lines illustrate the 95% confidence lines (+/- 1.96xSD) and the green line is the linear regression line for the referenced R^2 value.

OAG Cohort
Algorithm SITA STANDARD
Visit 1 3 5

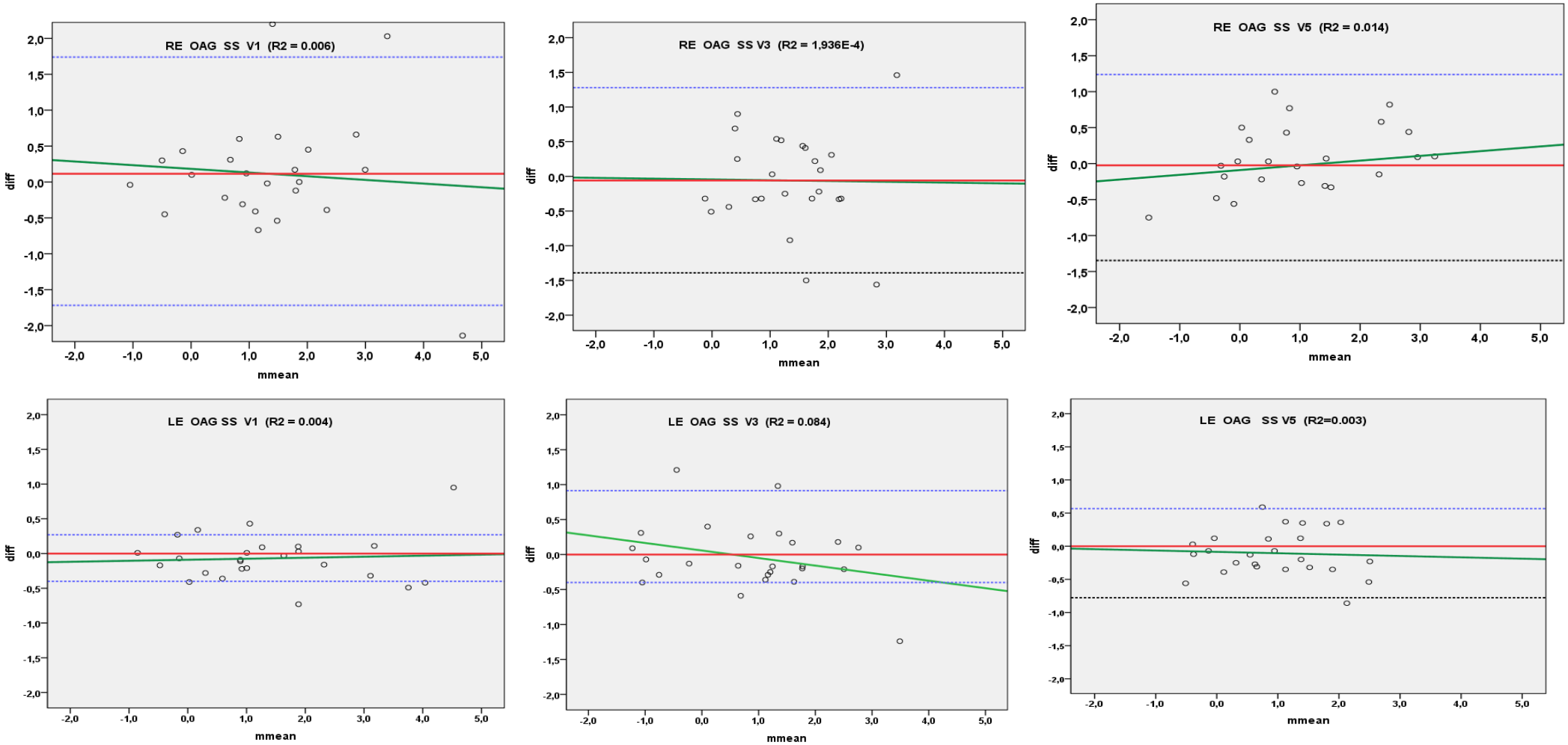

Figure 4.29. Bland and Altman plot of the difference between complete and No-Eyelid pattern method LI results (y axis) against the mean of both methods (x axis), for right eye (top) and left eye (bottom), for SITA Standard algorithm and OAG individuals at visit 1 (left panel), visit 3 (middle panel) and visit 5 (right panel). The reference line for mean difference is the red line, the blue dot lines illustrate the 95% confidence lines (+/- 1.96xSD) and the green line is the linear regression line for the referenced R^2 value.

OAG Cohort
Algorithm SITA FAST
Visit 1 3 5

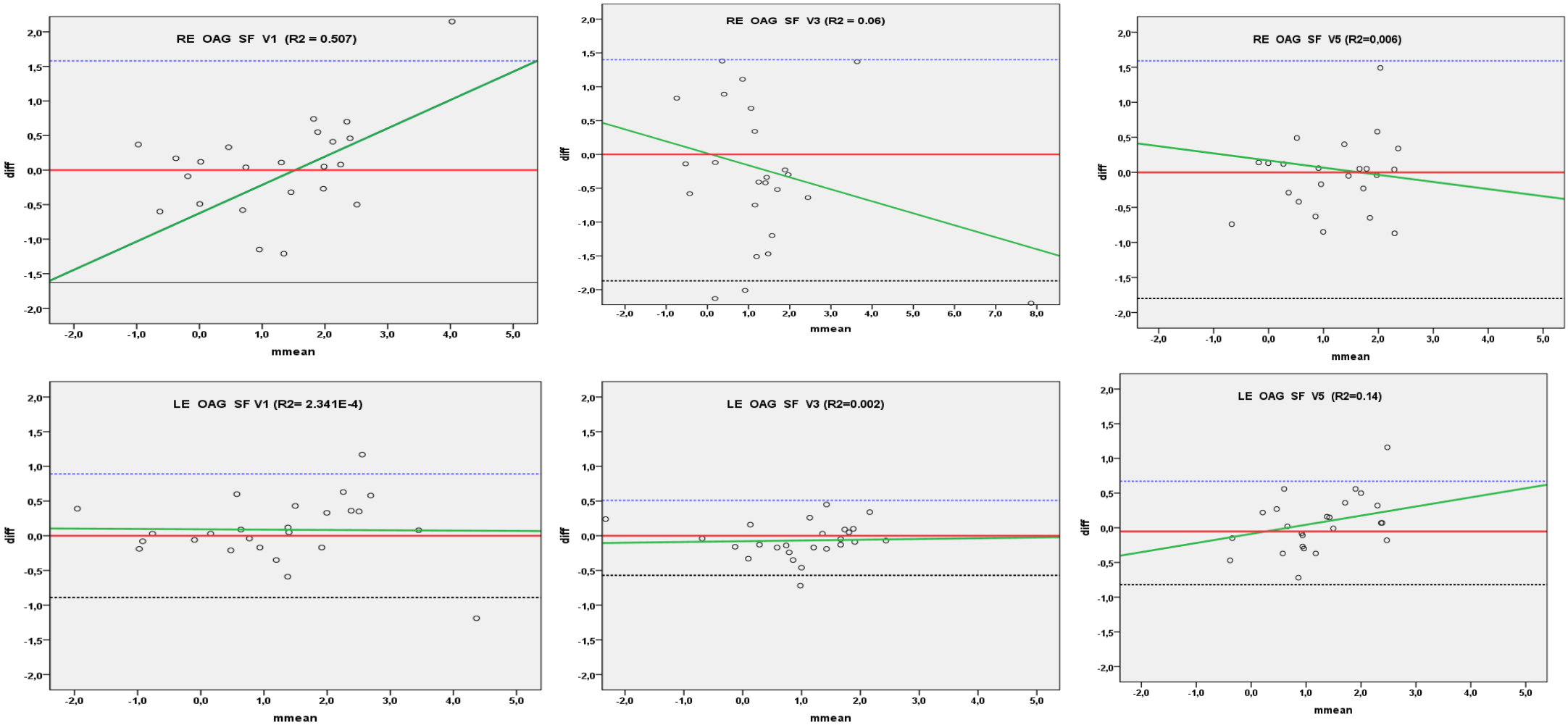

Figure 4.30. Bland and Altman plot of the difference between complete and No-Eyelid pattern method LI results (y axis) against the mean of both methods (x axis), for right eye (top) and left eye (bottom), for SITA Fast algorithm and OAG individuals at visit 1 (left panel), visit 3 (middle panel) and visit 5 (right panel). The reference line for mean difference is the red line, the blue dot lines illustrate the 95% confidence lines (+/- 1.96xSD) and the green line is the linear regression line for the referenced R^2 value.

OAG Cohort
Algorithm SITA SWAP
Visit 1 3 5

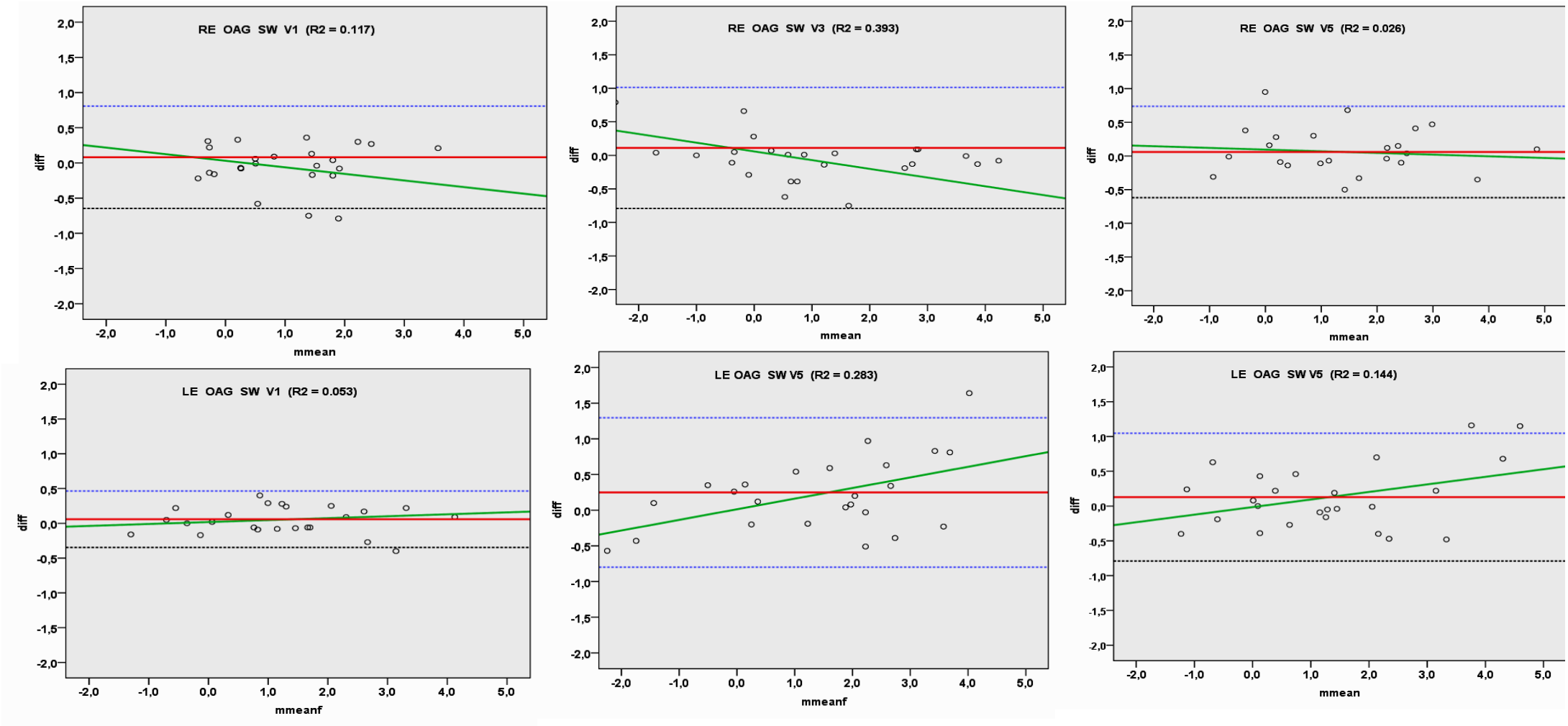

Figure 4.31. Bland and Altman plot of the difference between complete and No-Eyelid pattern method LI results (y axis) against the mean of both methods (x axis), for right eye (top) and left eye (bottom), for SITA SWAP algorithm and OAG individuals at visit 1 (left panel), visit 3 (middle panel) and visit 5 (right panel). The reference line for mean difference is the red line, the blue dot lines illustrate the 95% confidence lines (+/- 1.96xSD) and the green line is the linear regression line for the referenced R^2 value.

OHT Cohort
Algorithm SITA STANDARD
Visit **1** **3** **5**

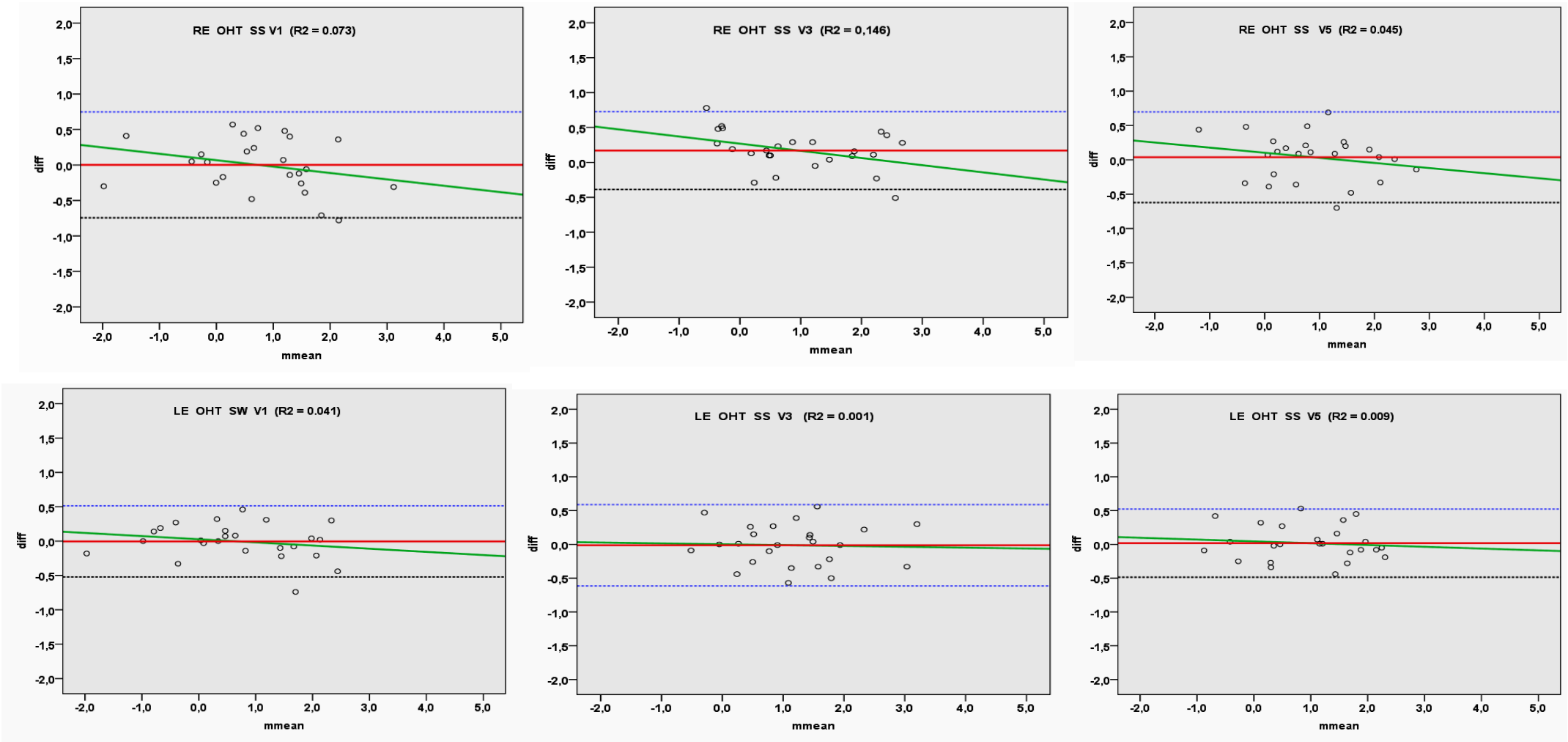

Figure 4.32. Bland and Altman plot of the difference between complete and No-Eyelid pattern method LI results (y axis) against the mean of both methods (x axis), for right eye (top) and left eye (bottom), for SITA Standardt algorithm and OHT individuals at visit 1 (left panel), visit 3 (middle panel) and visit 5 (right panel). The reference line for mean difference is the red line, the blue dot lines illustrate the 95% confidence lines (+/- 1.96xSD) and the green line is the linear regression line for the referenced R^2 value.

OHT Cohort
Algorithm SITA FAST
Visit 1 3 5

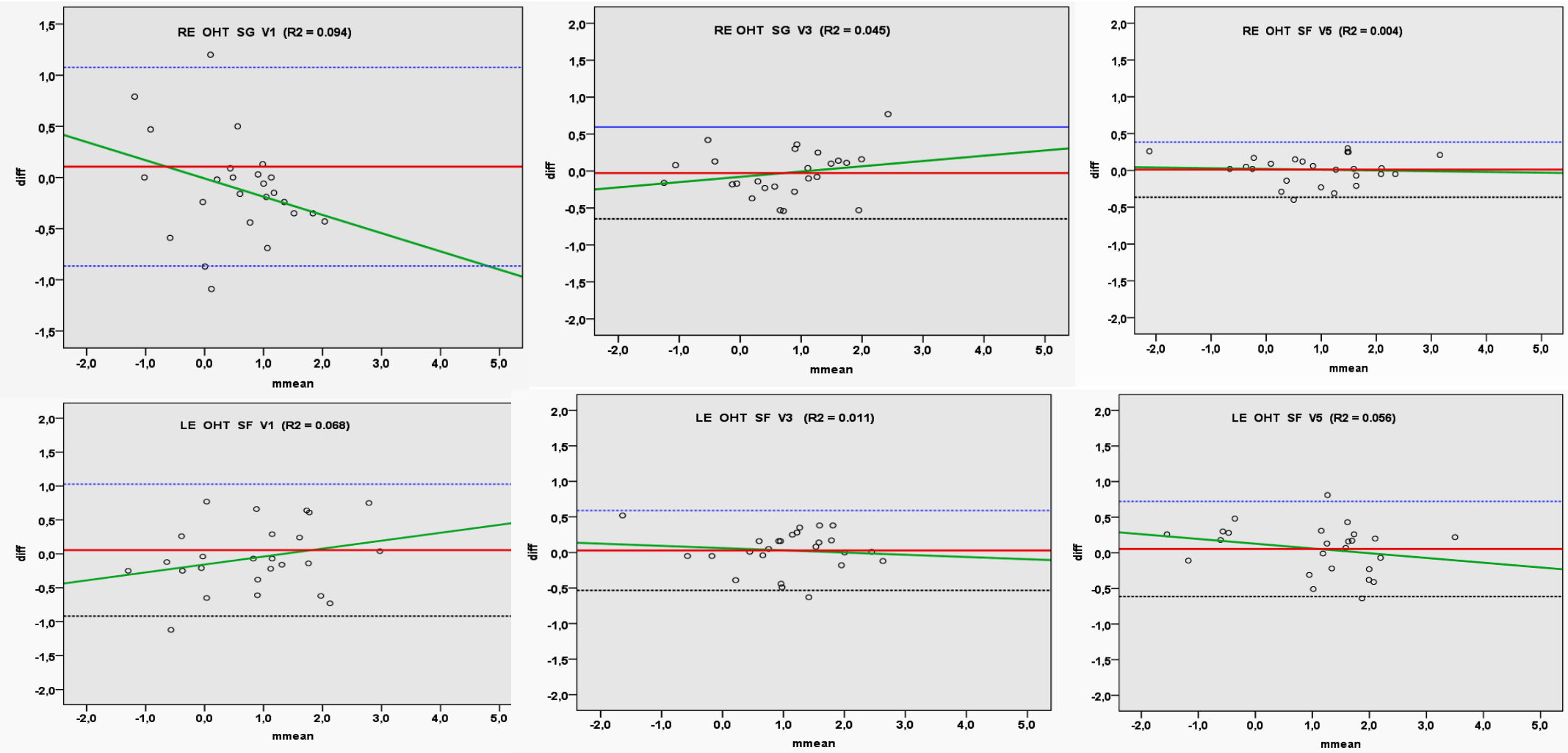

Figure 4.33. Bland and Altman plot of the difference between complete and No-Eyelid pattern method LI results (y axis) against the mean of both methods (x axis), for right eye (top) and left eye (bottom), for SITA Fast algorithm and OHT individuals at visit 1 (left panel), visit 3 (middle panel) and visit 5 (right panel). The reference line for mean difference is the red line, the blue dot lines illustrate the 95% confidence lines (+/- 1.96xSD) and the green line is the linear regression line for the referenced R^2 value.

OHT Cohort
Algorithm SITA SWAP
Visit 1 3 5

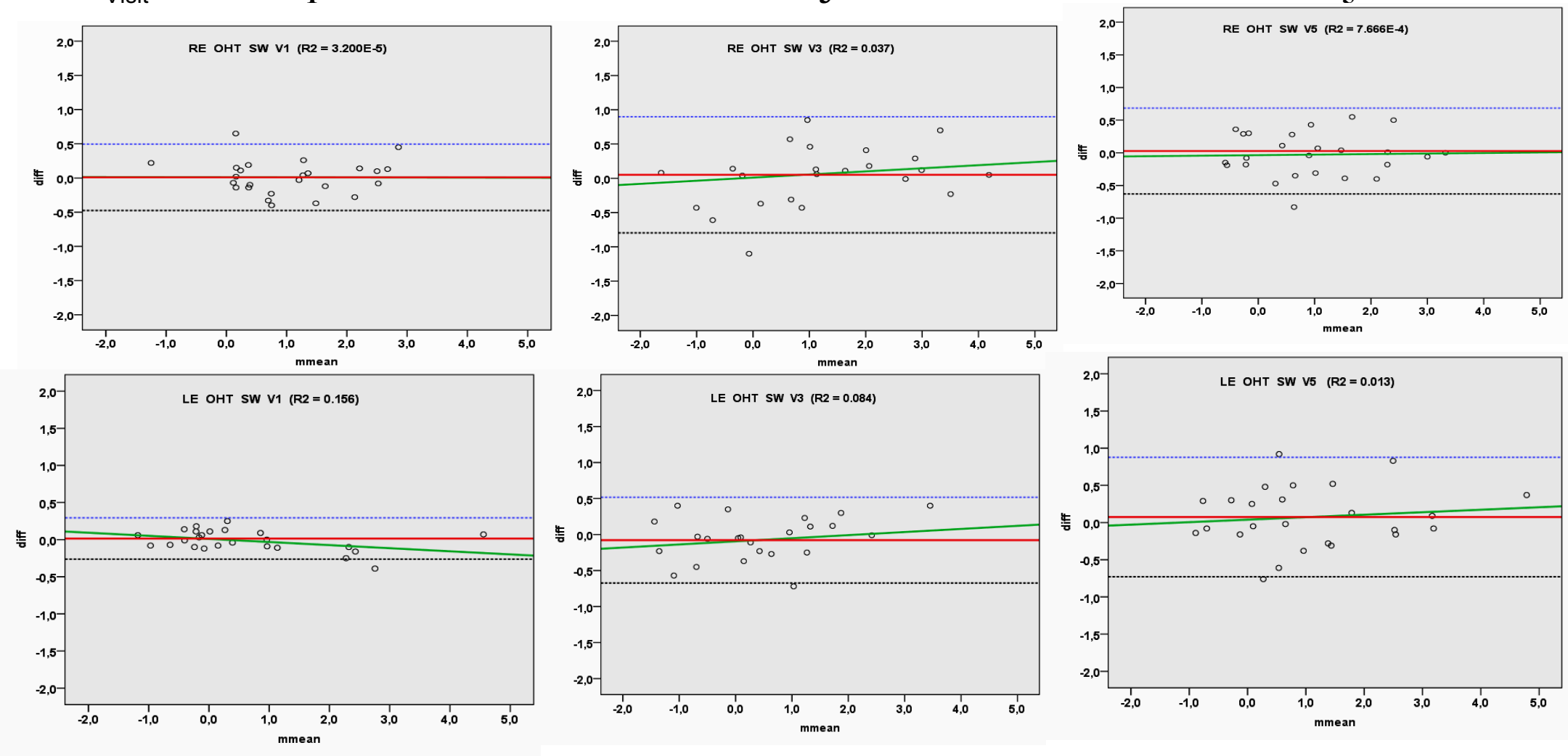

Figure 4.34. Bland and Altman plot of the difference between complete and No-Eyelid pattern method LI results (y axis) against the mean of both methods (x axis), for right eye (top) and left eye (bottom), for SITA SWAP algorithm and OHT individuals at visit 1 (left panel), visit 3 (middle panel) and visit 5 (right panel). The reference line for mean difference is the red line, the blue dot lines illustrate the 95% confidence lines (+/- 1.96xSD) and the green line is the linear regression line for the referenced R^2 value.

4.2.4 Discussion

In order to compare the No Eyelid pattern method with the original complete pattern method, the Bland and Altman plots were implemented. These plots show that the majority of the points are scattered all over the place, above and below zero, which suggests that there is no consistent bias of one approach versus the other (of course, there could be hidden biases that this plot does not show up). The presentation of the 95% limits of agreement does not provide power to the judgement that the two methods of measurement agree, as the range between these two limits is quite large. From a clinical point of view, the No Eyelid method do not propose any new or innovate aspect in the learning index development.

4.3 The Learning near the defective areas in the visual field of glaucoma patients.

4.3.1 Aim of the study

This study investigates the learning at border locations near the defective areas of visual field in glaucoma patients in order to evaluate whether these locations demonstrate any improvement of sensitivity after repeated visits and compare this to possible improvement of learning index.

4.3.1.1 Cohort

The open angle glaucoma group who took part in this study consisted of 25 individuals (17 females and 8 males) with primary open angle glaucoma with a mean age of 63 years (SD 8.3; range 46-73 years). Two male glaucoma patients were selected to serve as examples and the locations were selected to be in the inner border area of the defective locations and arranged in a concentric manner.

4.3.2 Methodology

For the evaluation of the possible improvement in sensitivity values at the inner border locations to the defective areas, the chosen algorithm was SITA SWAP. Although it is an algorithm that normally is difficult for the patient in comparison to SITA Standard and SITA Fast, however, numerous researchers suggest SITA SWAP as a more sensitive algorithm to locate early changes of glaucoma defects. Having in mind that these patients were not naive to perimetry they faced the least difficulty due to the algorithm, compared to other individuals who had perimetry for the first time.

Furthermore, the right eye was selected as it was always first tested at all visits. This has the advantage of involving least risk of fatigue compared to left eye results. Thinking also that many investigators suggest that the periphery learns more than the central visual field locations the selected locations were, where possible, in an inner ring-shaped line close to the defect in the periphery.

In other words, locations that exist near a defective area (in Fig. 4.35 and 4.36 illustrated full visual field printout) were evaluated for visit 1, visit 3 and visit 5, respectively. The defective areas of these visual fields were likely not to show any improvement, as damaged locations cannot see and consequently cannot learn.

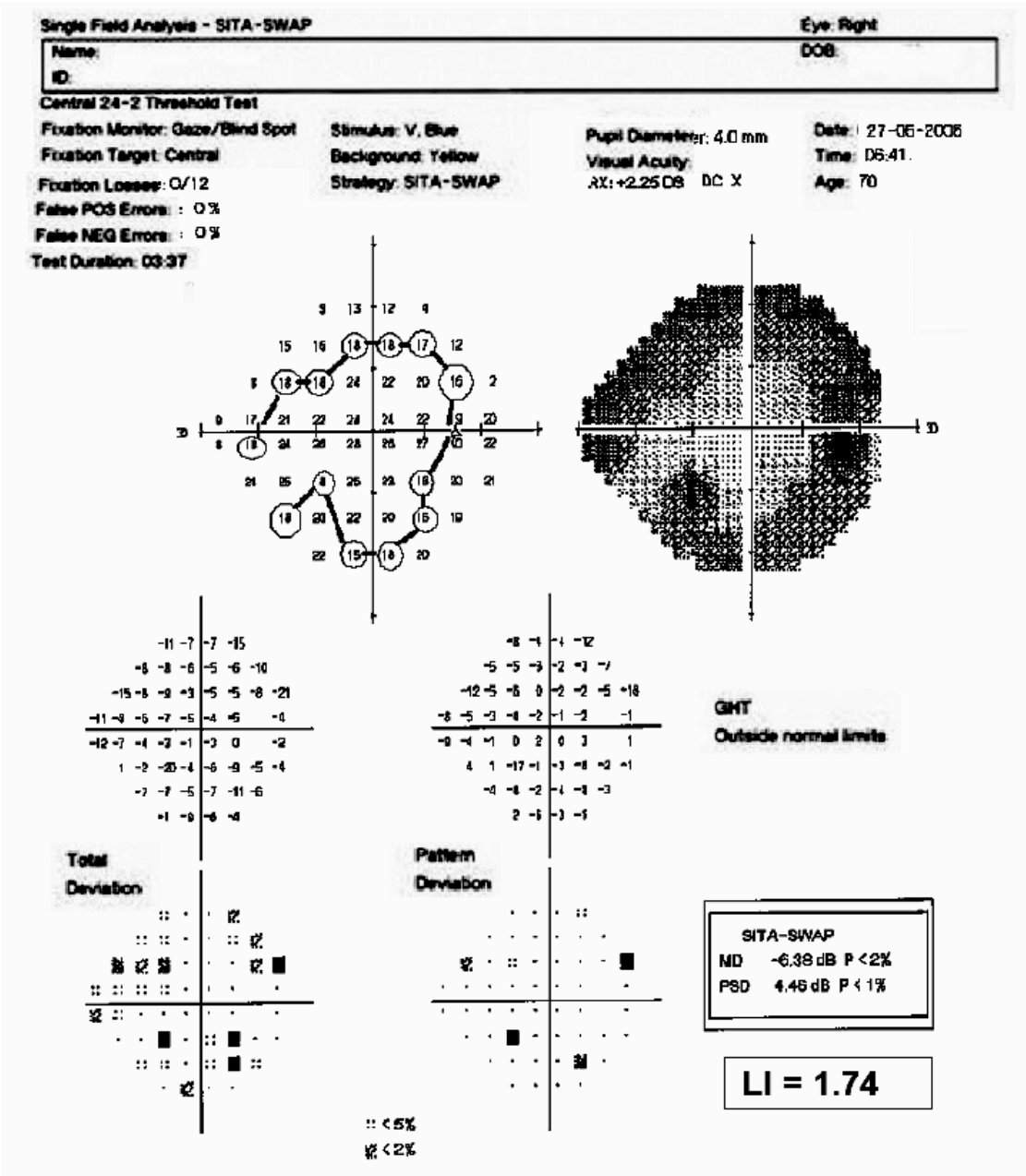

Figure 4.35. Visual Field printouts of visit 1 and selection of near defect locations to compare (example subject 1).

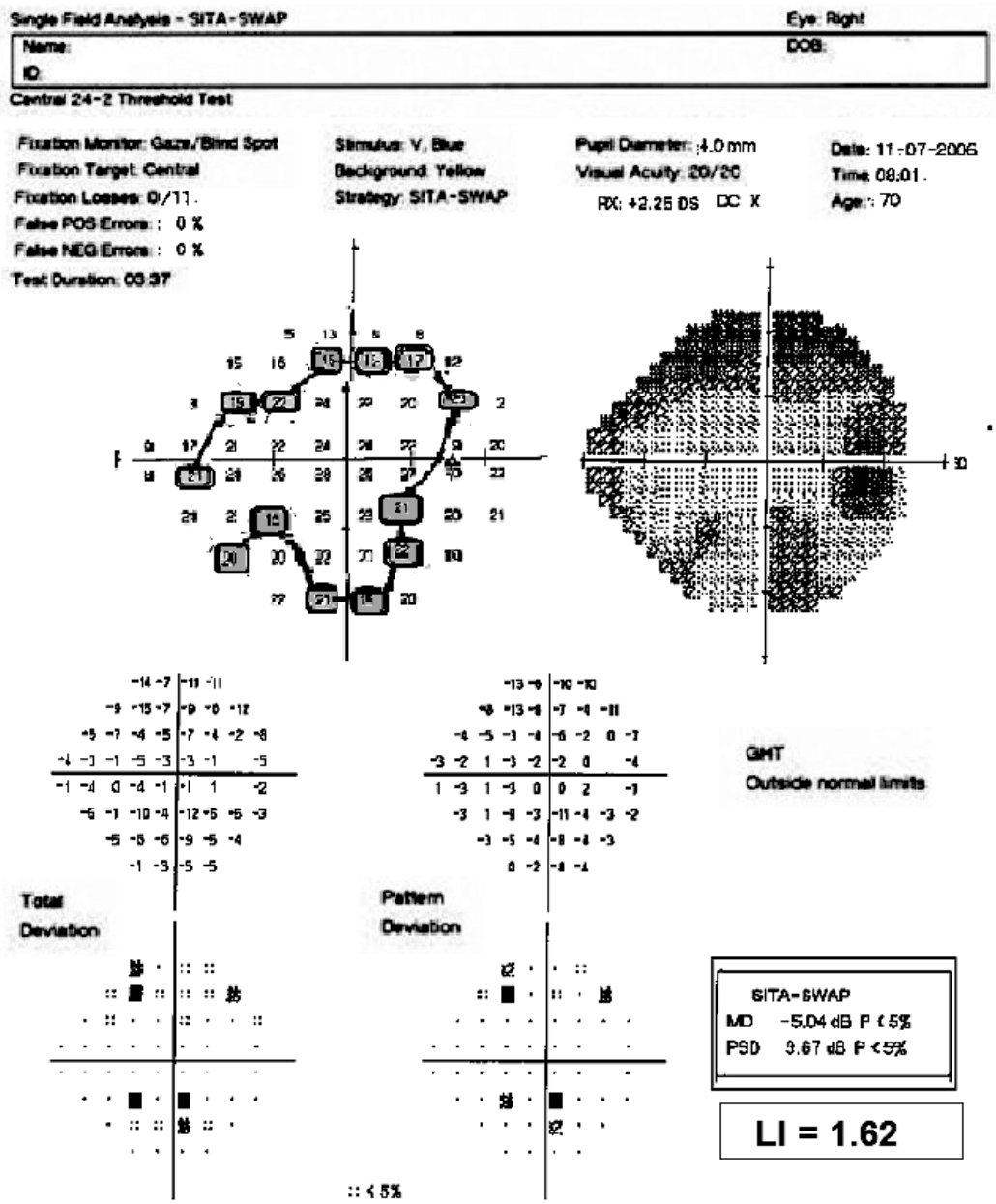

Figure 4.36. Visual Field printouts of visit 3 and selection of near defect locations to compare (example subject 1).

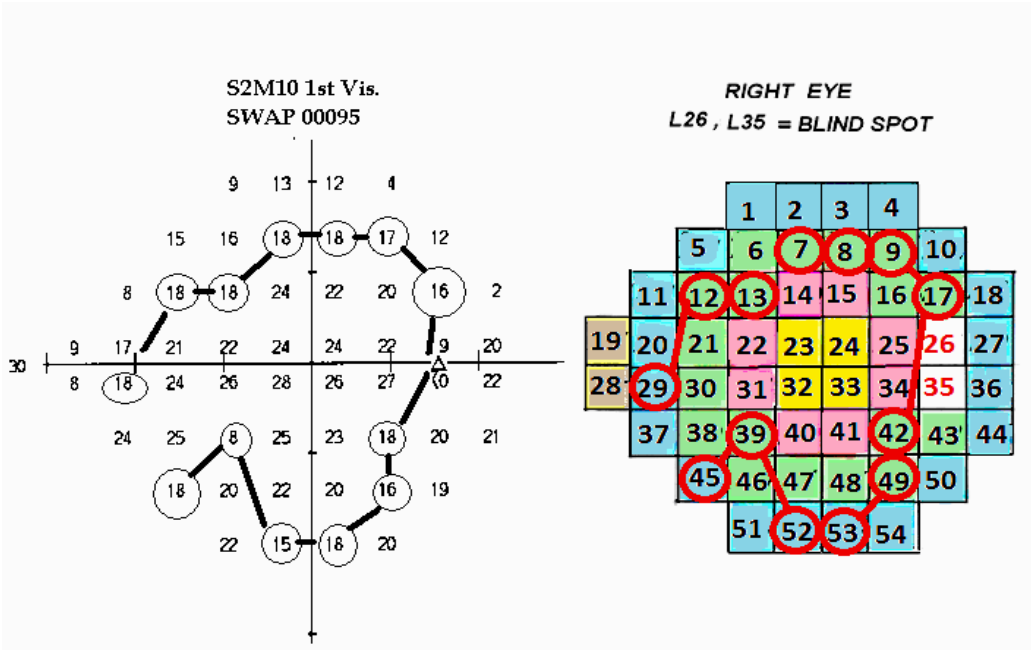

Figure 4.37. The near defective areas stimulus locations to compare for a glaucoma individual's visual field output at visit 1 (left) and the corresponding designation (right) for the coding of the LI calculation method (example subject 1).

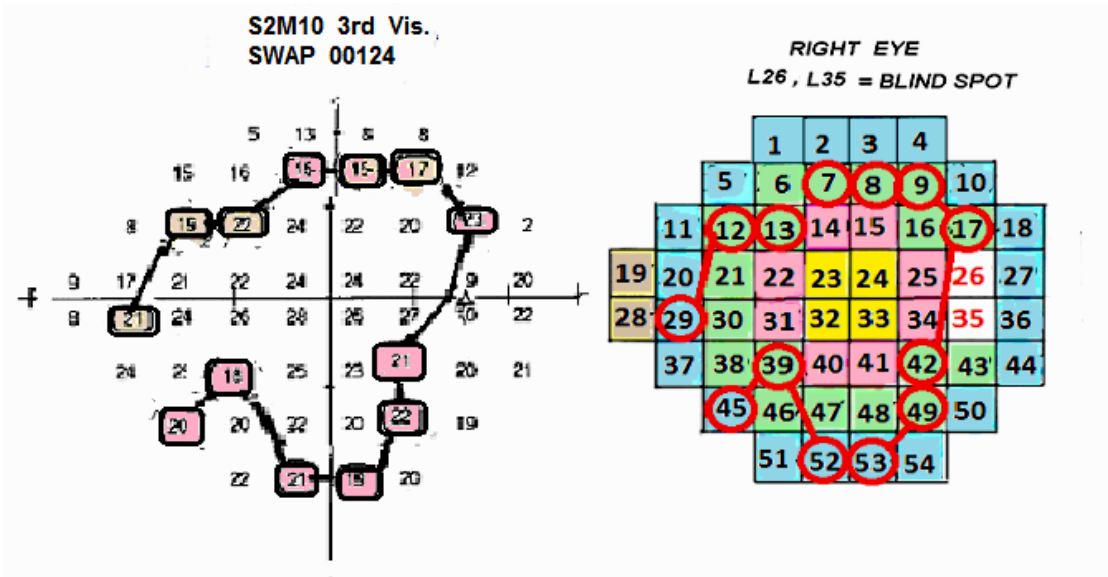

Figure 4.38. The near defective areas stimulus locations to compare for a glaucoma individual's visual field output at visit 3 (left) and the corresponding designation (right) for the coding of the LI calculation method (example subject 1).

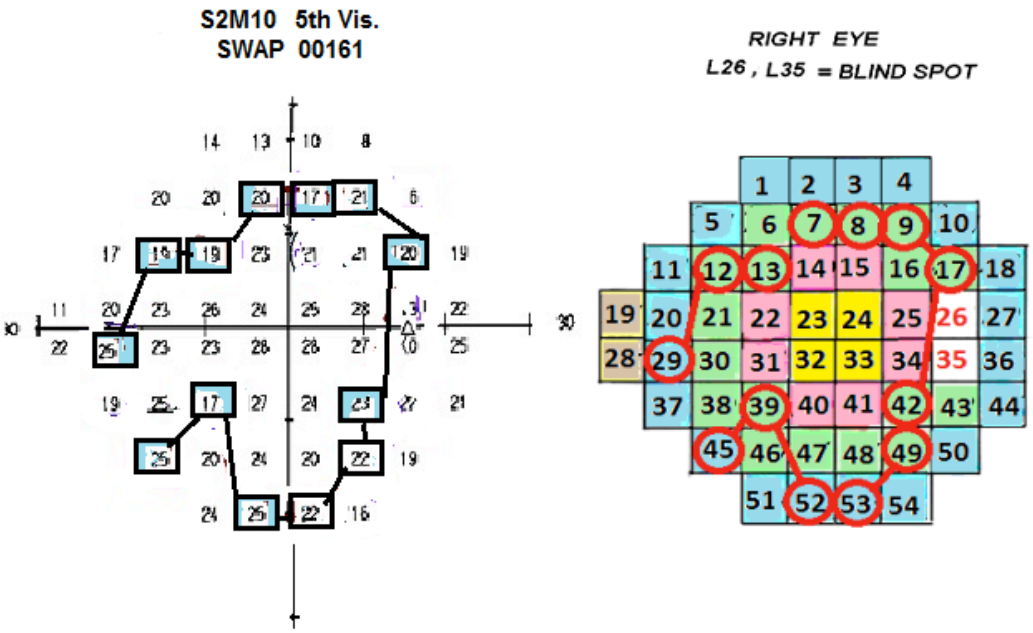

Figure 4.39.The near defective areas stimulus locations to compare for a glaucoma individual's visual field output at visit 5 (left) and the corresponding designation (right) for the coding of the LI calculation method (example subject 1).

Locations	Visit 1	visit 3	Visit 5	(v3-v1)%	(v5-v1)%
L29	18	21	25	16.7	38.9
L12	18	19	19	5.6	5.6
L13	18	22	19	22.2	5.6
L7	18	16	20	-11.1	11.1
L8	18	15	17	-16.7	-5.6
L9	17	17	21	0.0	23.5
L17	16	23	20	43.8	25.0
L42	18	21	23	16.7	27.8
L49	16	22	22	37.5	37.5
L53	18	19	22	5.6	22.2
L52	15	21	26	40.0	73.3
L39	8	18	17	125.0	112.5
L45	18	20	25	11.1	38.9
Mean	16.6	19.5	21.2	22.8	32.0
St.Dev	2.7	2.4	2.8	34.5	30.1
Median	18.0	19.5	21.0	16.7	27.8
L.I.	1.74	1.62	1.22		

Table 4.1. The near defective areas locations sensitivity of the right eye visual field of a glaucoma patient at visit 1, visit 3 and visit 5 and the corresponding proportional (%) improvement of sensitivity between visits (example subject 1).

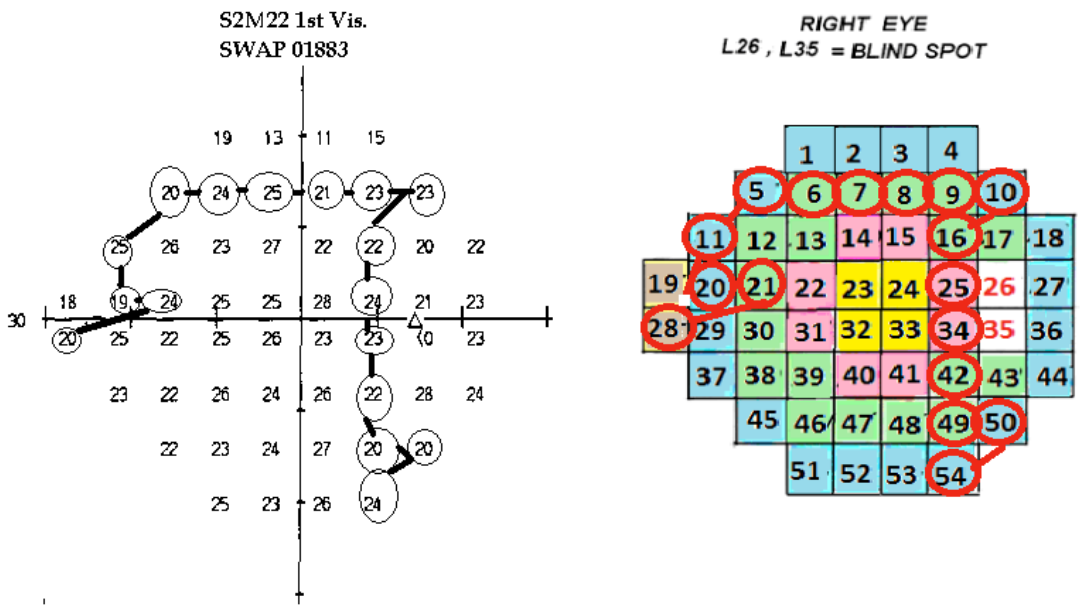

Figure 4.40. The near defective areas stimulus locations to compare for a glaucoma individual's visual field output at visit 1 (left) and the corresponding designation (right) for the coding of the LI calculation method (example subject 2).

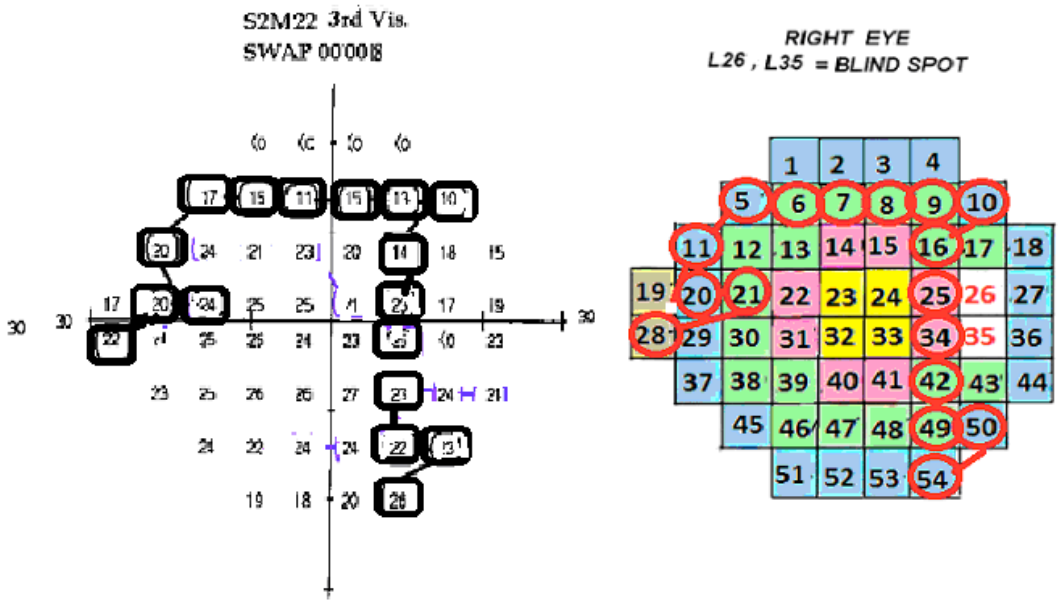

Figure 4.41. The near defective areas stimulus locations to compare for a glaucoma individual's visual field output at visit 3 (left) and the corresponding designation (right) for the coding of the LI calculation method (example subject 2).

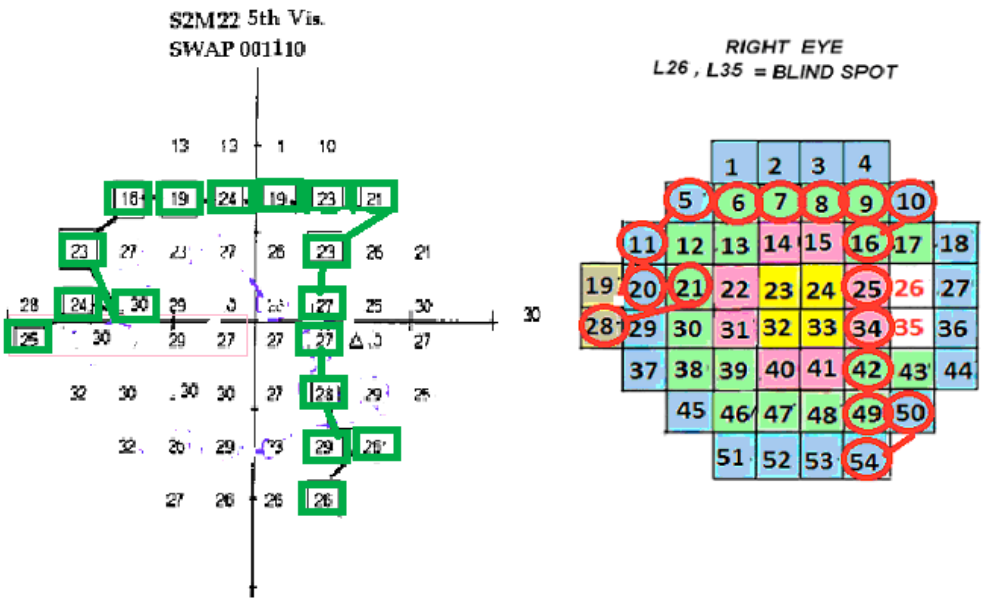

Figure 4.42. The near defective areas stimulus locations to compare for a glaucoma individual's visual field output at visit 3 (left) and the corresponding designation (right) for the coding of the LI calculation method (example subject 2).

Locations	Visit 1	visit 3	Visit 5	(v3-v1)%	(v5-v1)%
L28	20	22	25	10.0	25.0
L21	24	24	30	0.0	25.0
L20	19	20	24	5.3	26.3
L11	25	20	23	-20.0	-8.0
L5	20	17	18	-15.0	-10.0
L6	24	15	19	-37.5	-20.8
L7	25	11	24	-56.0	-4.0
L8	21	15	19	-28.6	-9.5
L9	23	13	23	-43.5	0.0
L10	23	10	21	-56.5	-8.7
L16	22	14	23	-36.4	4.5
L25	24	23	27	-4.2	12.5
L34	23	25	27	8.7	17.4
L42	22	23	28	4.5	27.3
L49	20	22	29	10.0	45.0
L50	20	23	26	15.0	30.0
L54	24	26	26	8.3	8.3
Mean	22.3	18.8	24.2	-13 .9	9.4
St. Dev	1.9	4.8	3.5	23.0	15.2
Median	22.3	19.4	24.0	-19.0	4.5
L.I.	0.99	3.15	2.10		

Table 4.2. The near defective areas locations sensitivity of the right eye visual field of a glaucoma patient at visit 1, visit 3 and visit 5 and the corresponding proportional (%) improvement of sensitivity between visits (example subject 2).

4.3.3 Discussion

The study describes an attempt to consider if the near defect locations area enhance or diminish the end result of learning index of the entire visual field. Figures 4.35 and 4.36 demonstrate single visual field printouts of visit 1 and visit 3 respectively, where in the numerical chart is illustrated the selection of ring-shaped area bordered to defective locations. These locations are taken as

defective because data do not show a significant improvement on subsequent visits.

In figure 4.37, the study identifies and associates the corresponding locations for a glaucoma individual's visual field output at visit 1 (left) with the designation of the coding calculation diagram (right) of the learning index as described in Chapter 3.

In figure 4.38, the study relates the corresponding locations for a glaucoma individual's visual field output at visit 3 (left) with the coding designation (right) and figure 4.39 at visit 5, respectively.

Next page table 4.1 illustrates a concise descriptive table of the sensitivity values of all selected locations at visits 1, 3 and 5 and the percentage proportion of change between visit 1and 3 and visit 3 and 5, respectively. And the mean, median and standard deviation of this ring-shaped selected area compared with the entire learning index at visits 1, 3 and 5. This comparison show clearly that the increase of mean sensitivity at visits 3 and 5 coresponds to a decline of learning index at the respective visits which is an indication that these areas do not produce any negative effect at learning index calculation, but the index is reduced as these locations begin to learn.

In figure 4.40, the study relates the corresponding locations for a second glaucoma individual's visual field output at visit 1 (left) with the coding designation (right) and figures 4.41 and 4.42, at visit 3 and 5, respectively.

Next page table 4.2, similar to table 4.1, demonstrates a concise descriptive table of the sensitivity values of all selected locations at visits 1,3 and 5 and the percentage proportion of change between visit 1 and 3 and visit 1 and 5, respectively.

The mean, median and standard deviation of this ring-shaped selected area were compared with the entire learning index at visits 1, 3 and 5. This comparison showed that at visit 3, where the mean sensitivity of selected locations declined, the learning index increased, as an indication that these areas may not learn and decreased again at visit 5, when the mean sensitivity has a positive change, which is an indication that these areas do not produce any negative effect at learning index calculation, but the index reduces as these locations learn.

These two examples are indicative of the fact that learning effect often is related to other factors apart from learning, which mask the learning effect, like fatigue or concentration loss of the examined individual.

4.3.4 Conclusions

The present study aimed to match up the contribution of a selected set of locations in the border of defective areas to the configuration of the learning index of the entire visual field of glaucoma patients

Glaucoma patients, exhibit increased variability in sensitivity for SITA SWAP algorithm, usually due to the difficulty of the specific test. On the other hand is

believed to be the most sensitive algorithm for early glaucoma detect. In the present study two glaucoma patients were selected from the glaucoma cohort. The criteria to select these 2 example subjects were at first the severity of defects. The severe glaucoma patients and the very early glaucoma individuals were excluded, either because the severe cases could produce much difficulty to identify the learning, or in early glaucoma cases where the defective areas may be difficult to be spotted in a concentric manner. From the rest moderate glaucoma individuals were selected two that demonstrated quite concentric defective areas in similar manner as the concentric model of learning index calculation. Only the visual field output of their right eye was assessed, as was the one that was measured always first at all visits, in order to eliminate the fatigue effect transfer between eyes.

The comparison included the 1st visit that by and large exhibits the maximum sensitivity variability and a high learning index, the 3rd visit as it is the visit by which regularity of learning seems to be completed and the 5th visit where the learning in any case is over (Wild et al., 2006).

The SITA SWAP algorithm was selected the difficulty of the used pathway, mainly because clinicians considered that SWAP could reveal glaucomatous field loss earlier than SAP (Jampel et al., 2011).

In practical terms, however, it is difficult to consider how the LI may be useful when used in this way. Such an approach is highly subjective and time-

consuming, given that visual field defects must be identified, quantified, and input manually in order to calculate the learning index.

5 CHAPTER FIVE - A novel approach assessing learning in visual field output

In this advanced method to assess a learning index, different types of filters have been applied to the first visit printout in order to simulate it as to be the third or fifth visit printout by filtering the noise, which probably as the first test mostly includes the learning effect.

5.1 Introduction to filters

A signal can be defined as the physical carrier of information (Astola and Kuosmanen, 1997). By and large, a signal is an official description of an observable fact that evolves time or space (Ruelle, 1987. By signal processing any manual or “mechanical” operation could be designated, which may modify, analyse or otherwise manipulate the information contained in a signal (Baraniuk, 2003).

A signal can be mathematically represented in many ways. A natural representation of a signal is a function f(x), where x denotes a variable. The representation of light waves carrying information from a scene to the eye is quite complicated but the final image is simply represented as a function of two variables f (x,y). For example, in a black and white image the (x,y) is the spatial location of the point in the image and f(x,y) is the brightness value of that point. A colour image is represented as a vector valued function [R(x,y), G(x,y) and B(x,y)], where R, G and B are the intensities of red, green and blue colours, respectively (Astola and Kuosmanen, 1997).

A crude division of signal problems may include three phases. The first is the removal of interference, the second may be the signal transformation to another form and finally the analysis and extraction of some characteristics (Oppenheim and Verghese, 2010)

Noise in the majority of signal systems is a product of both internal and external sources to the system. All measurements in the real world are bothered by noise. In fact, a noisy signal consists of electronic noise, but can also incorporate external procedures that affect the considered phenomenon — wind, vibrations, differences of temperature, deviation of humidity, etc., and depend on the measured matter and on the sensitivity of the device of measurement.

Signal-to-noise ratio is a determination used in science to compute how much a signal has been distorted by noise. It is the relation between signal strength and the noise influence, which distorts the signal. It is recognized as the power ratio between the significant information (signal) and the useless signal (noise): In practice, if the transmitted signal falls below the level of the noise in the system, data can no longer be decoded or evaluated by the receiver. More often than not, it is possible to decrease the noise if you control the environment or the source event. Mainly this could be done using different types of filters.

The objective of any type of filter is to extract the noise that has distorted the signal. Generally it is based on a statistical approach. However, the design of some filters takes a different approach. One filter design makes it possible to

have data of the properties of both the initial signal and the noise, and another one may look for the output that would come as close to the unique signal as possible.

5.2 Common types of filters

Mean filtering is a simple, spontaneous and easy to implement method of smoothing results, i.e. reducing the amount of intensity variation between one value and the next. Often it is based around a 3×3 square kernel (fig.5.1), which represents the shape and size of the neighbourhood to be sampled when calculating the mean. The Mean filter replaces each pixel value in a system with the mean or the average value of its neighbours, including itself. This has the effect of eliminating values that are unrepresentative of their surroundings.

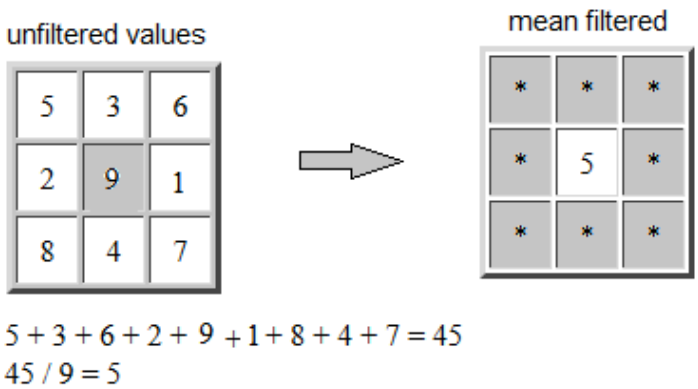

Figure 5.1 Schematic representation of mean filtering in a 3X3 kernel, where after the summation of the values of the neighbourhood, they are divided by the total number of pixels and the result value replaces the original one.

Two main problems are evident with mean filtering. Firstly that a single location with a very misleading value, can significantly affect the mean value of all the other locations in its neighbourhood, and secondly, when the filter

neighbourhood overlaps an edge, the filter will interpolate new values for locations on the edge, as we require sharp edges in the output and so the filter will blur that edge and the overall appearance may look fuzzy or blurry.

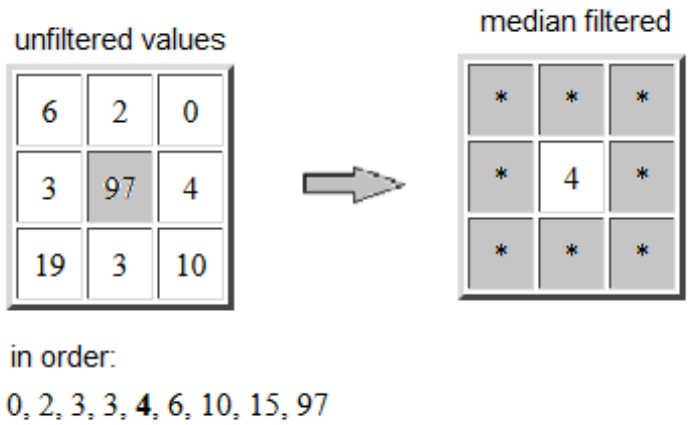

Figure 5.2 Schematic representation of median filtering in a 3X3 kernel where after setting the values of the neighbourhood in ascending array the median of these values is selected to replace the original one.

One more common non-linear filtering technique, used to remove noise, employs the median filter. Median filtering is extensively applied in digital processing as it maintains edges while getting rid of noise. This technique calculates the median of the surrounding locations to determine the new value of the location. A window of size 3*3 is taken (fig.5.2). The nine elements in this window are stored in an array and then these elements are sorted in ascending order of their pixel values. The median is calculated from these sorted pixels and then the centre element of the 3*3 kernel is replaced by this median value.

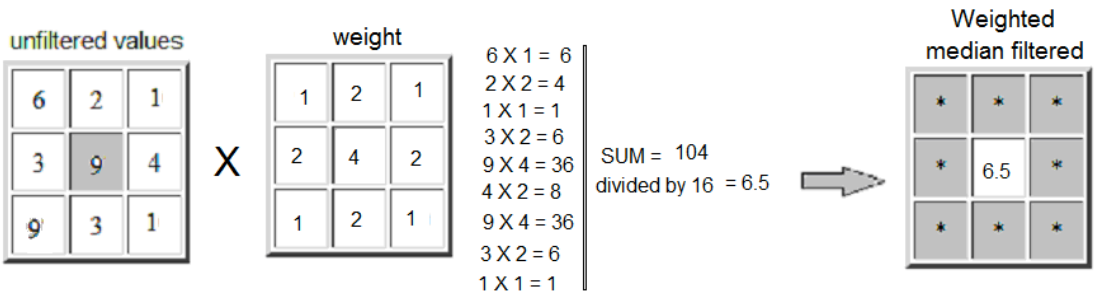

Figure 5.3 Schematic representation of weighted median filtering in a 3X3 kernel, after multiplying the neighbourhood values with the corresponding weights the summation is divided by the overall weight and the resulting value replaces the original one.

Weighted Median (WM) filters are another type of filters, which have the robustness and edge preserving capability of the classical median filter and are similar to linear filters in certain properties. In WM filtering a window of a 3X3 kernel is used (fig.5.3) in the example shown. All nine value of the neighbourhood are multiplied by the nine corresponding values of the weight. The summation of these nine products divided by the total weight gives the filtered value to replace the respective initial pixel value. Weighted Median filters belong to the broad class of non-linear filters and enable noise attenuation capability, where intensity values are examined and depending on the range of intensity, particular weights are multiplied.

5.3 Filtering the perimetric results

Automated perimetry is widely used for the detection and follow up of glaucomatous field loss. The most important component of perimetric

estimation is the assessment of the pointwise sensitivity or threshold variation in visual field data. Especially the early glaucomatous field loss is characterised by this variability and fluctuation (Crabb et al. 1995; Fitzke et al., 1995; Gardiner et al., 2004; Nevalainen et al, 2009; Kirwan et al., 2014).

The Humphrey Field Analyser (HFA) is typical of advanced perimeters in providing the clinician with a series of mechanisms to quantify and interpret this pointwise sensitivity variation and threshold fluctuation. The Single Field Analysis printout illustrates a numeric sensitivity chart, on the left of the grayscale graph, for the central 30 degrees of the eye field (fig. 5.4). A signal is a sequence of functions of integers (f: z = R). So, the data i.e: 21, 22, 21, 19, 21, 23, 21, 24, 21, 19, 21, 20, ….if it is a sequence of real values, could be a signal. In the visual field numeric printout there are many sequences of different values.

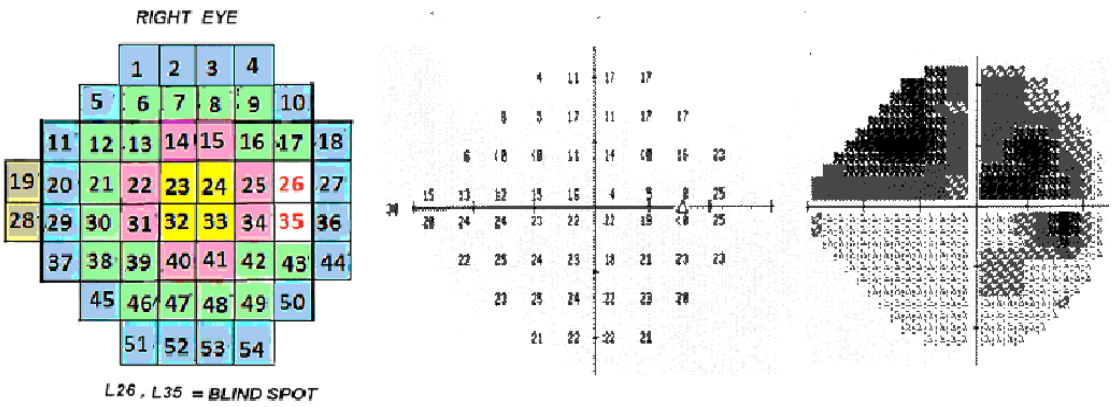

Figure 5.4 The numeric chart of the HFA visual field output (middle) and the grayscale graph (right) and the corresponding table of sensitivity values of the visual field numeric chart to the data locations (left), for the right eye of a glaucoma patient.

This numeric chart if deployed as a series of values, following the location map as in figure 5.4, it could be a signal, which may well be processed with any common filter to remove the unnecessary noise as in the block diagram in fig. 5.5.

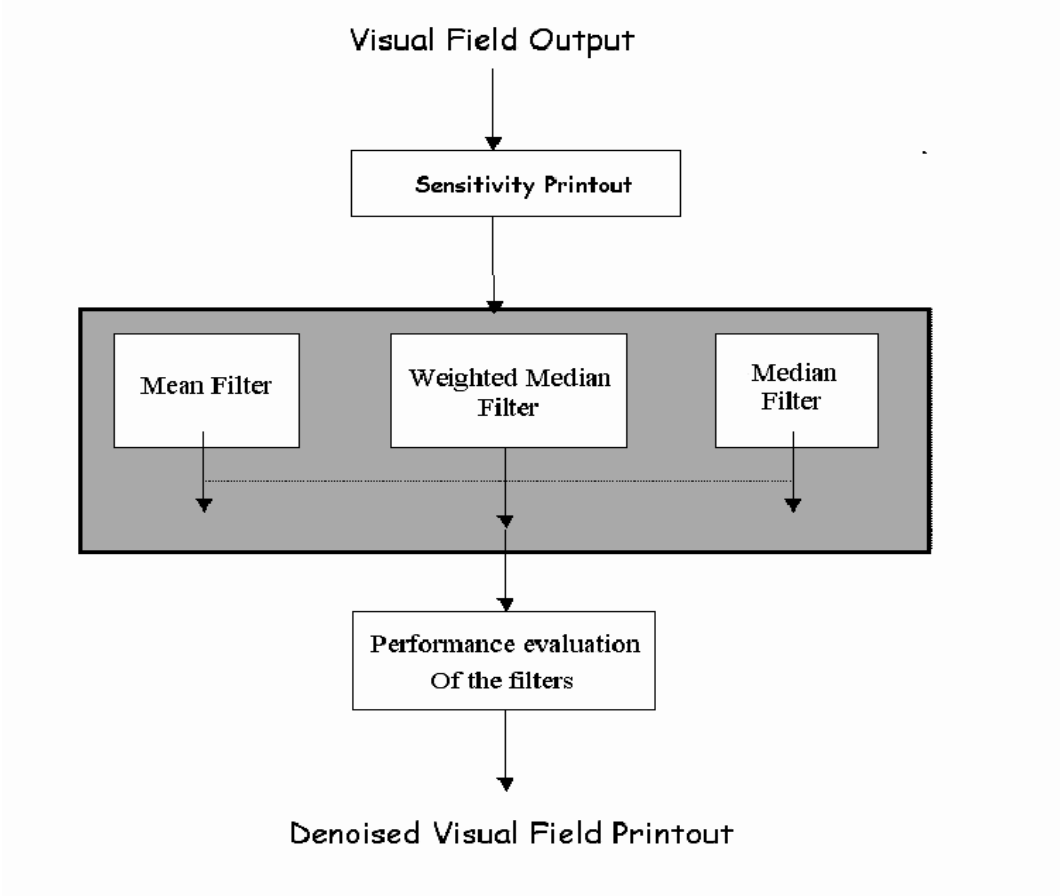

Figure 5.5 Block diagram illustrates the phases of denoising visual field printout.

5.4 Previous studies of Visual Field filtering

Initially, Fitze et al, (1995) introduced a method of improving the repeatability of visual field data by applying techniques used in image processing. Crabb and colleagues (1995) demonstrated a new framework for evaluating pointwise

sensitivity variation in computerised visual field. Furthermore, Crabb and associates (1997) show how the predictive performance of a method for determining glaucomatous progression in a series of visual fields can be improved by first subjecting the data to a spatial filtering technique (Fitze et al., 1995; Crabb et al., 1995; 1997).

They also concluded that the spatial filter decreases the number of false-positives when detecting progression by reducing the level of noise present. In addition, the filter increased the likelihood of detecting true deteriorating locations of the visual field and reduced the probability of flagging not viable defects (Crabb et al., 2003).

In this method, the raw sensitivity value is replaced by one derived from a linear combination of the sensitivities at the nine points in a 3X3 square centered on the point of interest. This is repeated for each point in the field in turn, each time looking at the points in a square surrounding the point of interest.

Strouthidis and colleagues (2007) concluded that application of the spatial filter resulted in similar specificity but with a higher rate of detected progression. This filter may therefore be useful in the monitoring of glaucomatous progression as it may reduce the dependence on confirmatory testing, although it has yet to be applied to longitudinal SITA data (Strouthidis et al., 2007).

Gardiner and associates (2004) tested a physiologically accurate spatial filter to be applied to the data after patient examination, by impeding the quantity of

noise present in the readings (Gardiner et al., 2004). A Virtual Eye computer simulation was used to test the filter.

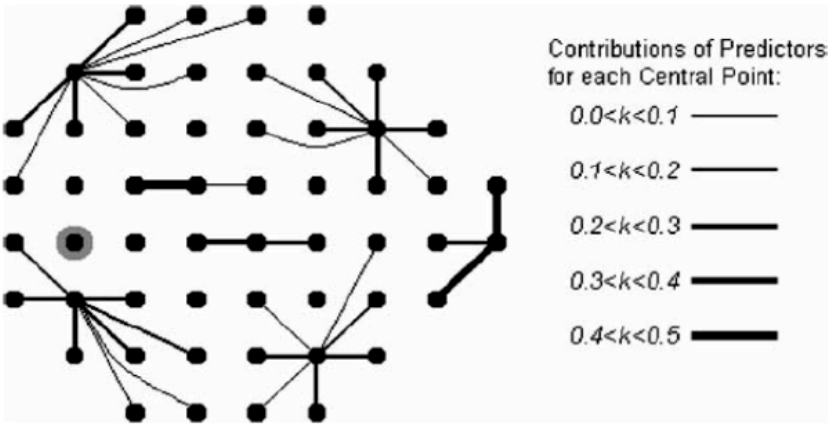

Figure 5.6 Gardiner's proposed Predictor filter with the group of points connected with lines of different thickness, named as k-factor (right table) for the applied filter (after Gardiner et al., 2004).

The filter obeys the rules of the accepted physiological shape of the retinal nerve fibre layer. Fig.5 6 illustrates a few of the Central Points that are employed to the filter. If a point is connected to the Central Point by a line, it indicates that this point is a predictor for the Central Point. As noted in the table at the right of the graph, the thicker the line, the larger the effect it has on the prediction. The remaining contribution to the filtered value comes from the Central Point itself. It is seen that predictors are not necessarily neighbours of the Central Point (as they would be if the Gaussian filter was being considered), but they follow the expected arcs (Gardiner et al., 2004).

Additionally, the performance of Gardiner's filter, according to the study, was much better than the Gaussian filter. By the way, it was common for defects to

be blurred out by the Gaussian filter. To this point, this is really difficult given the inaccuracy of threshold perimetry (in terms of the high inter-test and intra-test variability) and the various components of variability (or noise) associated with the perimetric process (Flammer, Drance and Zulauf, 1984; Wild et al., 1991; Spry and Johnson, 2002).

5.5 Aim of the study

The design of this study involved performance evaluation of different filters on visual field output. The critical arrangement was to develop a code to combine statistics with a workable diagnostic system that is capable of detecting deterioration of visual field in the early stages of glaucoma. Moreover, to develop a system that could predict improvement or deterioration of the tested visual field of a glaucoma suspect, most likely after the first or second visit and not to expect to conclude after the completion of the fifth visit assessment.

In other words, the plan was to apply a set of different filters in order to select the most efficient one that could remove the most of the noise of the test printout, of which probably the greater part of this removed noise could be the component of the learning effect, as it was expected to be at the first or second session. The common mean and median filters were initially used and later on an adapted or Hybrid filter was designed in a similar philosophy to Gardiner's Predictor filter. In case of real visual field deterioration, as in most of the OAG patients' printouts, the filter expected not to denoise much learning, as the defected locations could not learn any more. At the same time, a comparison with the learning index, as calculated in chapter 3, throughout the five sessions,

could give an indication of the index power and the relationship with the field progression in order to be used as a prognostic index of learning from a clinical point of view.

5.6 Methods

5.6.1 Cohort

The design of the study included normal individuals that were naïve to any type of perimetry and could be expected to improve over the five sessions for all types of perimetry and OAG patients that would improve over the five visits for the SITA algorithms, except SITA Standard given their previous experience. These two groups were described in Chapter 3.

The OHT individuals were not used in the study mainly because these individuals were quite experienced in SITA Standard and SITA Fast algorithms and were not expecting to learn any more for these algorithms. Also, these individuals in LI calculation studies (chapter 3) demonstrated erratic results for SITA SWAP algorithm.

5.7 Results

Initially, Dr. Frank Rakenbrant, Mathematician, designed and modified two filters by integrating the well known mean and median filters in MatLab© (Version 7.5, 2007) environment that was used in previous similar studies (Crabb et al, 1995; 1997), by coding the modules files for the appropriate applying method.

Afterwards, taking into account the details of the study data, an Adaptive or Hybrid filter was designed following the deployment of the optic nerve fibre layers of the retina (fig.5.7 at the right-top) and selecting different weights (fig.5.7, right column) depending on the locations of posible glaucoma defects, in proportion to the Garway-Heath and associates study (Garway-Heath et al., 2000; Gardiner et al., 2004).

Bundle Name	Group of Points	Weight
Superior bundle	sup=([1:5,9,10,17]);	(+/-3.01)
Upper bundle	upper=([6:8,11:16,]);	(+/-2.37)
Temporal bundle	temp=([18,27,36,44]);	(+/-1.60)
Central bundle	centre=([23:25,32:34]);	(+/-1.60)
Inferior bundle	inf=([37,43,45,46,49:54]);	(+/-2.27)
Lower bundle	lower=([28:31,38:42,47,48]);	(+/-2.37)
Nasal bundle	nasal=([19:22]);	(+/-2.37)

Locations 26 and 35 = Blind Spot

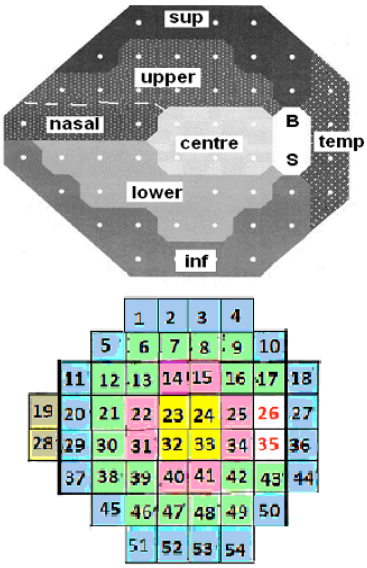

Figure 5.7 Graphic illustration of the design of a Hybrid filter according to the deployment of the optic nerve bundles. The numbers of group points (middle column) all over the field follow the bundles of the retinal nerve fiber layers (after Garway-Heath et al., 2000) at the top-right of the illustration and the weight (right column) that was calculated from the sensitivity variation of the particular group of points in the retinal bundles.

Therefore, Figure 5.8 illustrates the result of applying the mean (SENS1mean3s.mat) and the median (SENS1median3s.mat) types of filters, respectively, to the sensitivity printout of a normal individual right eye, to the visual field printout at all visits, for SITA Standard algorithm.

Figure 5.9 illustrates the difference of applying the mean (SENS1mean3s.mat) and the median (SENS1median3s.mat) types of filters, respectively; The learning index (LI) in both figures 5.9 and 5.9, at every visit is the index as calculated previously by the method described in chapter 3.

Figure 5.10 illustrates the graphical representation of filtering results, for the right eye of a normal subject visual field, for all visits and SITA Standard algorithm. The first column on the left illustrates the Total Deviation probability values. The second column from the left demonstrates the raw sensitivity values printout for every visit. The third column from the left demonstrates the sensitivity values after applying the adaptive/hybrid (SENSNovels.mat) filter. Subsequently, the 1st visit filtered outcome can be compared with the 3rd visit raw sensitivity chart.

Figure 5.11 represents the filtering results, for the same subject and algorithm, as in fig. 5.10 but the 1st visit filtrated outcome can be compared with the 5th visit raw sensitivity chart.

Figure 5.12 illustrates the filtering results, for the right eye of a mild glaucoma patient's visual field, for all visits and SITA Standard algorithm. The 1st visit filtered outcome can be compared with the raw sensitivity values of 3rd visit and with the raw sensitivity of 5th visit and the matching locations of the visual field is coloured yellow. Next figure 5.13 demonstrates the same glaucoma patient, as in fig. 5.12 for all 5 visits but at this time for SITA SWAP algorithm.

The Graphical representation of 1st visit raw sensitivity filtered outcome for the right eye of a normal subject's visual field after applying the adaptive hybrid (SENSNovels.mat) filter to the Total Deviation probability values, with purpose to compare with the 3rd visit raw sensitivity chart, where the matching area of the visual field is coloured yellow. The right eye was selected as the always first measured and consequently having the least fatigue that may mask the learning effect.

On the other hand, figures 5.14 and 5.15 illustrate the discrepancy of sensitivity elevation of raw data versus the data after the use of the adaptive filter, for the right eye of normal subjects and OAG patients respectively, for SITA Standard (Top) and SITA Fast (bottom) strategies, at all five visits and the median learning index at every visit for an effortless comparison with the sensitivity change

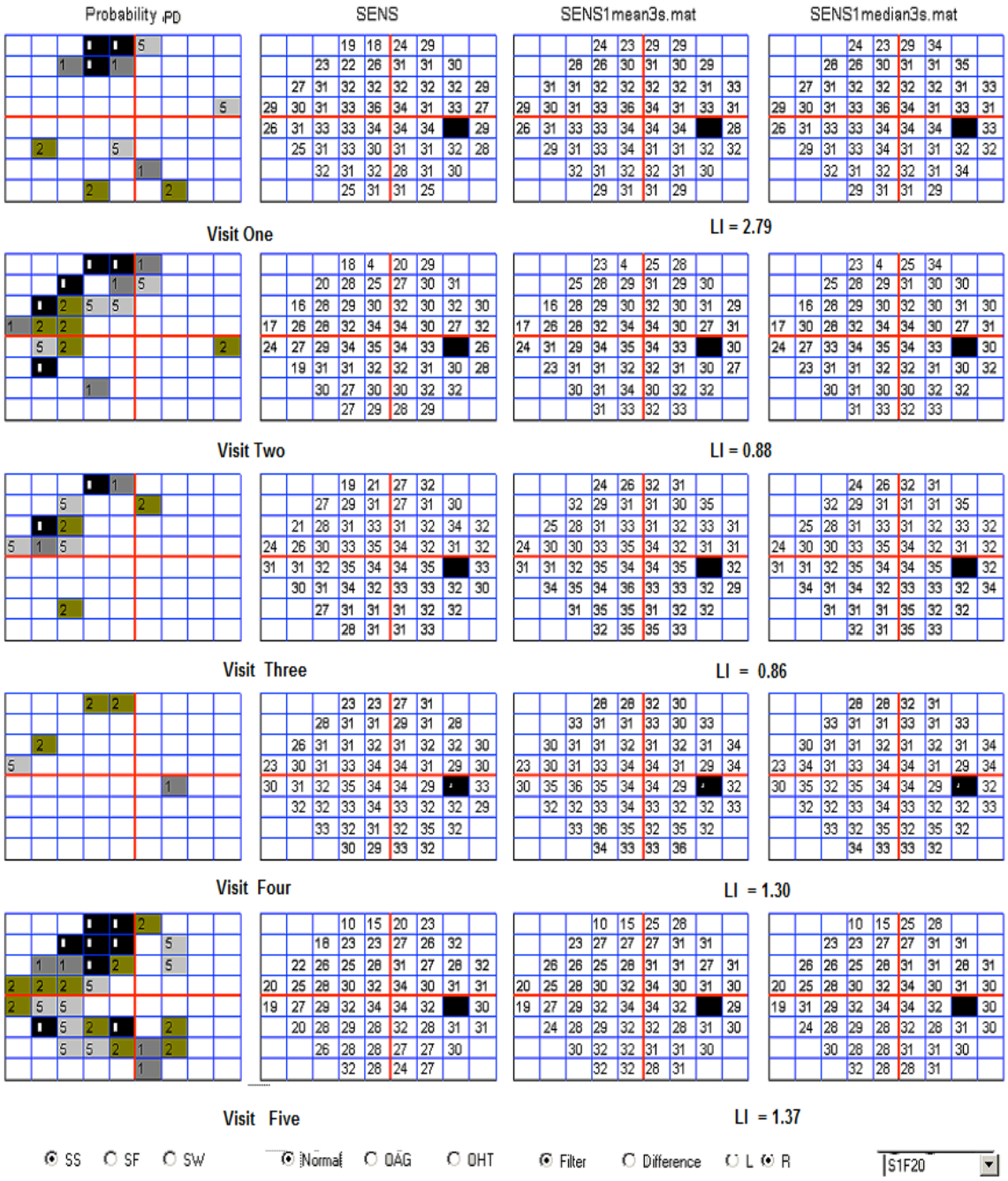

Figure 5.8 Graphical representation of filtering results for the right eye of a normal subject's visual field, for all visits and SITA Standard algorithm. The first from the left column illustrates the Pattern Deviation probability values, the second column the raw sensitivity values and the third and fourth column the sensitivity values after applying the mean (SENS1mean3s.mat) and the median (SENS1median3s.mat) filter, respectively. The learning index (LI) is the index as calculated previously by the method described in chapter 3.

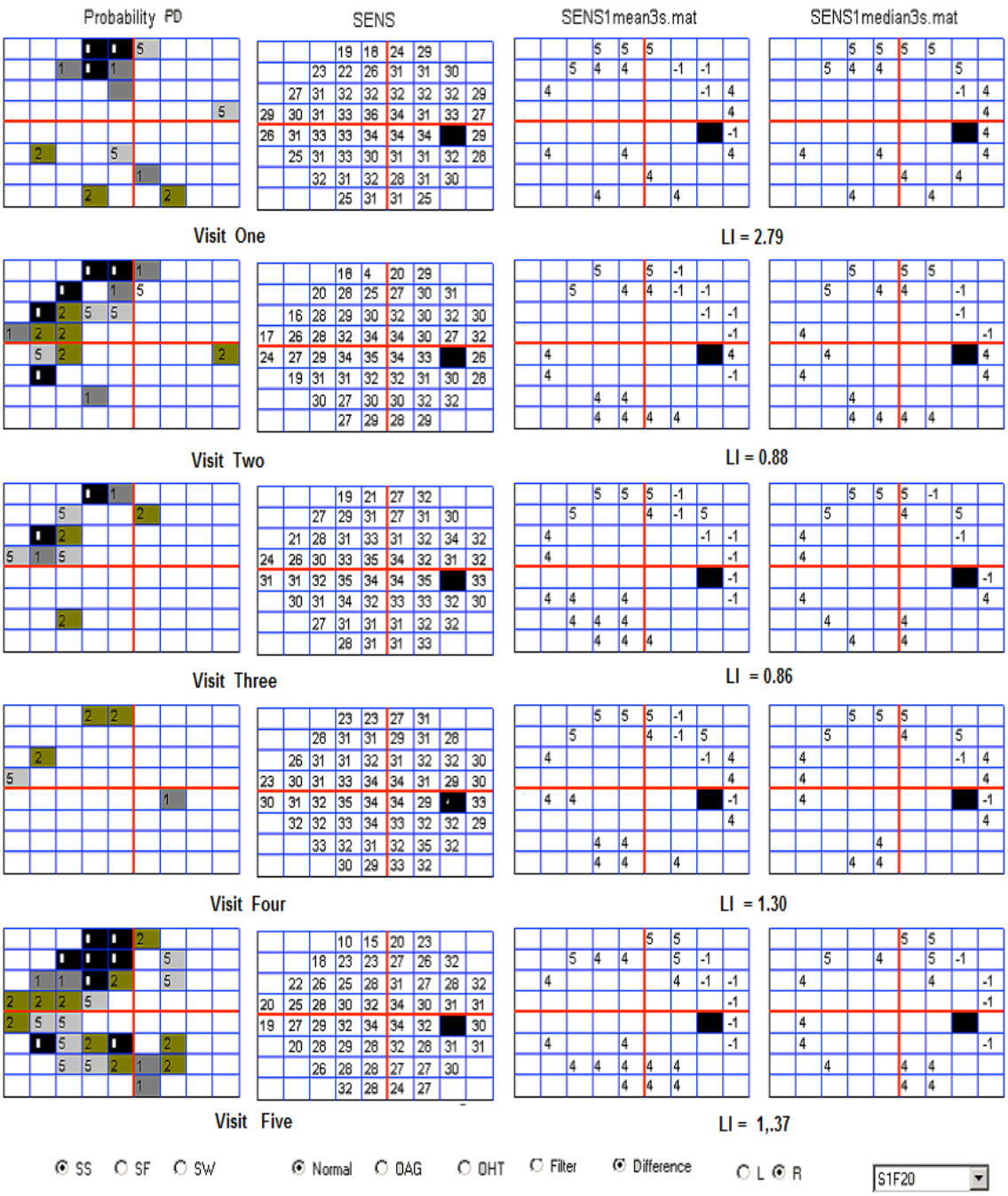

Figure 5.9 Graphical representation of filtering results difference from raw sensitivity values, for the right eye of a normal subject's visual field, for all visits and SITA Standard algorithm. The first from the left column illustrates the Pattern Deviation probability values, the second column the raw sensitivity values and the third and fourth column the mean (SENS1mean3s.mat) and median (SENS1median3s.mat) filter difference from raw data after applying the filter, respectively. The learning index (LI) is the index as calculated previously by the method described in chapter 3.

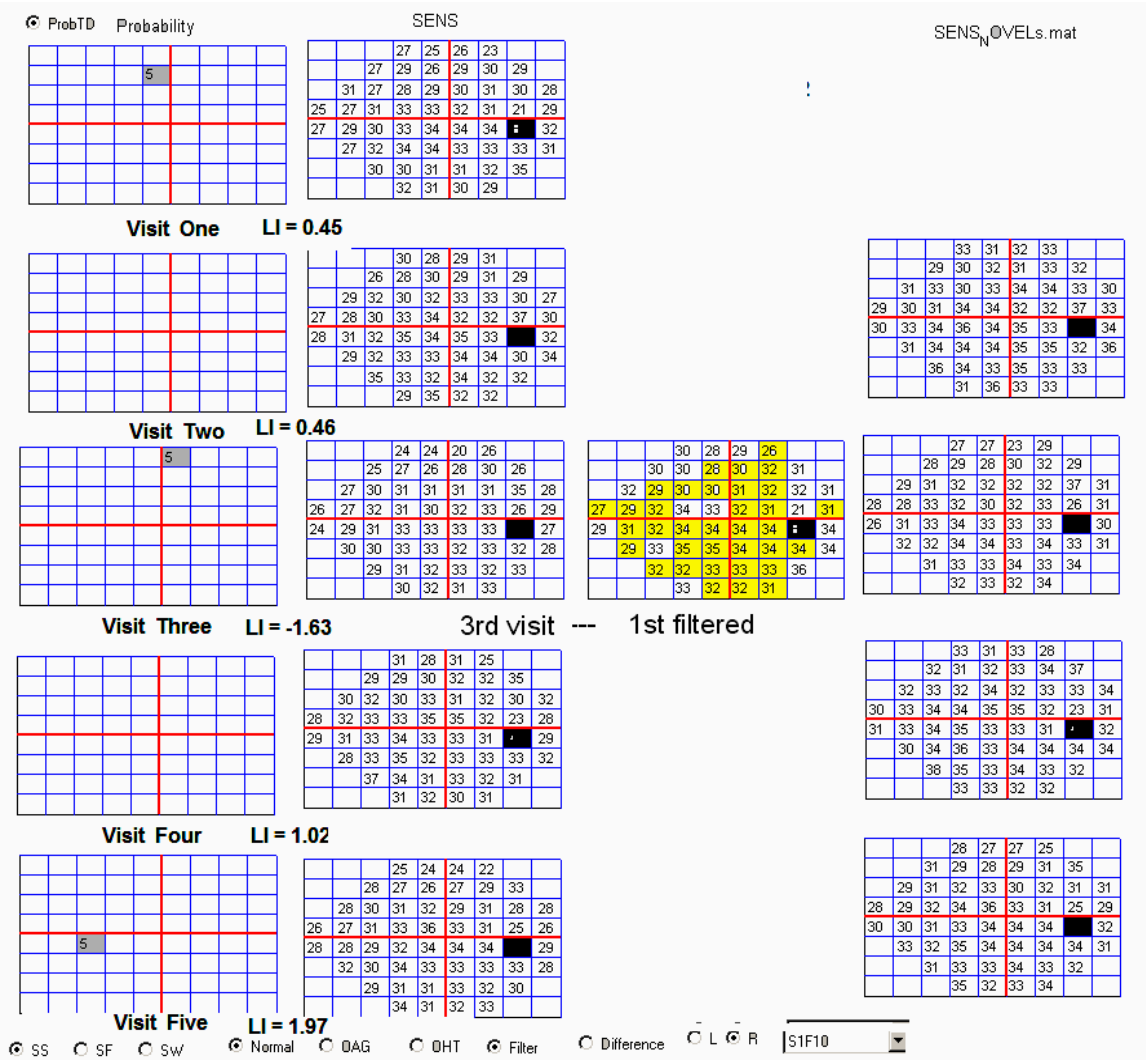

Figure 5.10 Graphical representation of filtering results, for the right eye of a normal subject's visual field, for all visits and the SITA Standard algorithm. The first from the left column illustrates the Total Deviation probability values, the second column the raw sensitivity values and the third column the sensitivity values after applying the adaptive hybrid (SENSNovels.mat) filter. The 1st visit filtered outcome can be compared with the 3rd visit raw sensitivity chart, where the matching locations of the visual field are shaded yellow.

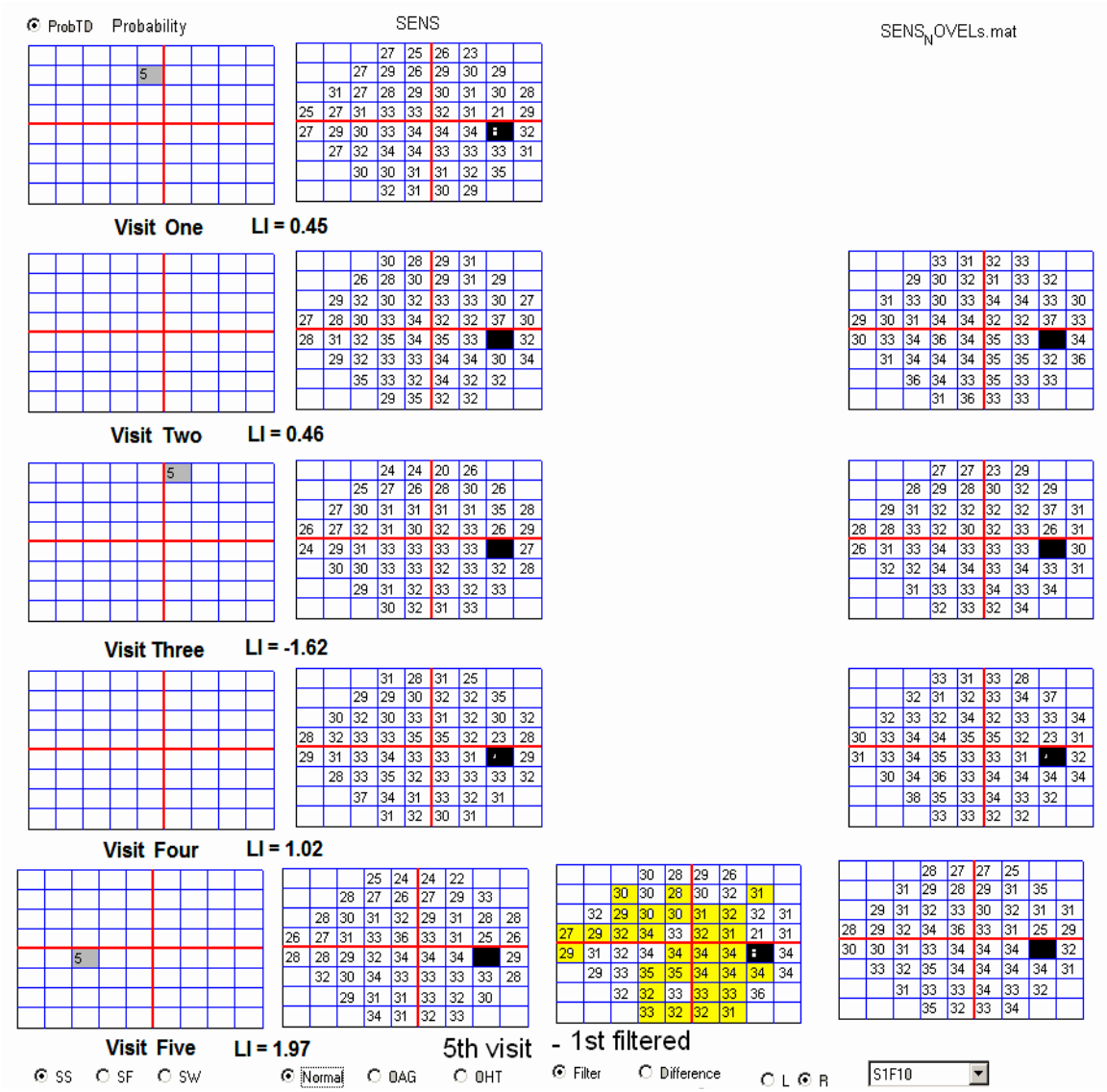

Figure 5.11 Graphical representation of filtering results, for the right eye of a normal subject's visual field, for all visits and the SITA Standard algorithm. The first from the left column illustrates the Total Deviation probability values, the second column the raw sensitivity values and the third column the sensitivity values after applying the adaptive hybrid (SENSNovels.mat) filter. The 1st visit filtered outcome can be compared with the 5th visit raw sensitivity chart, where the matching locations of the visual field are shaded yellow.

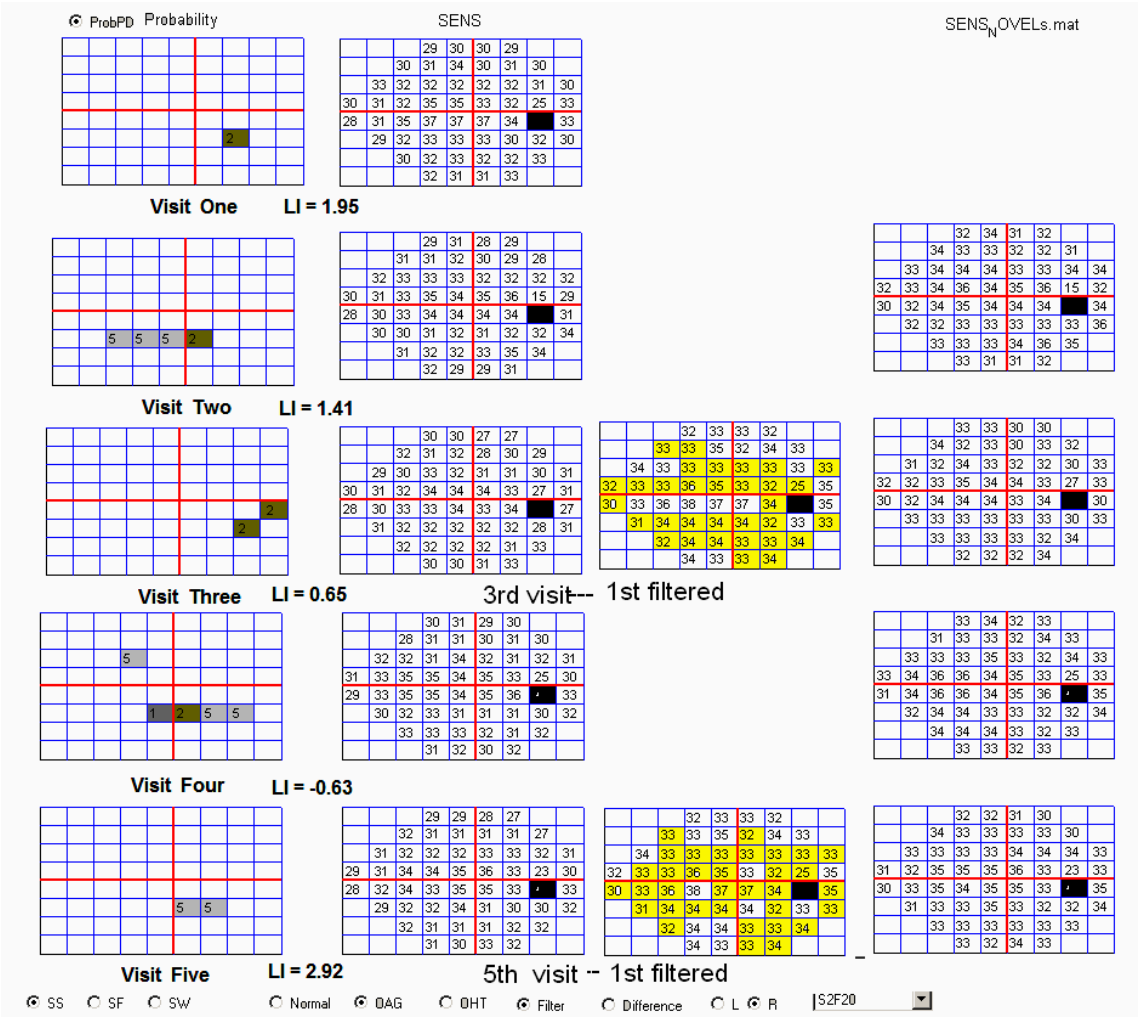

Figure 5.12 Graphical representation of filtering results, for the right eye of a glaucoma patient's visual field (with mild defects), for all visits and the SITA Standard algorithm. The first from the left column illustrates the Total Deviation probability values, the second column the raw sensitivity values and the third column the sensitivity values after applying the adaptive hybrid (SENSNovels.mat) filter. The 1st visit filtered outcome can be compared with the 3rd visit raw and with the 5th visit raw sensitivity chart, where the matching locations of the visual field are shaded yellow.

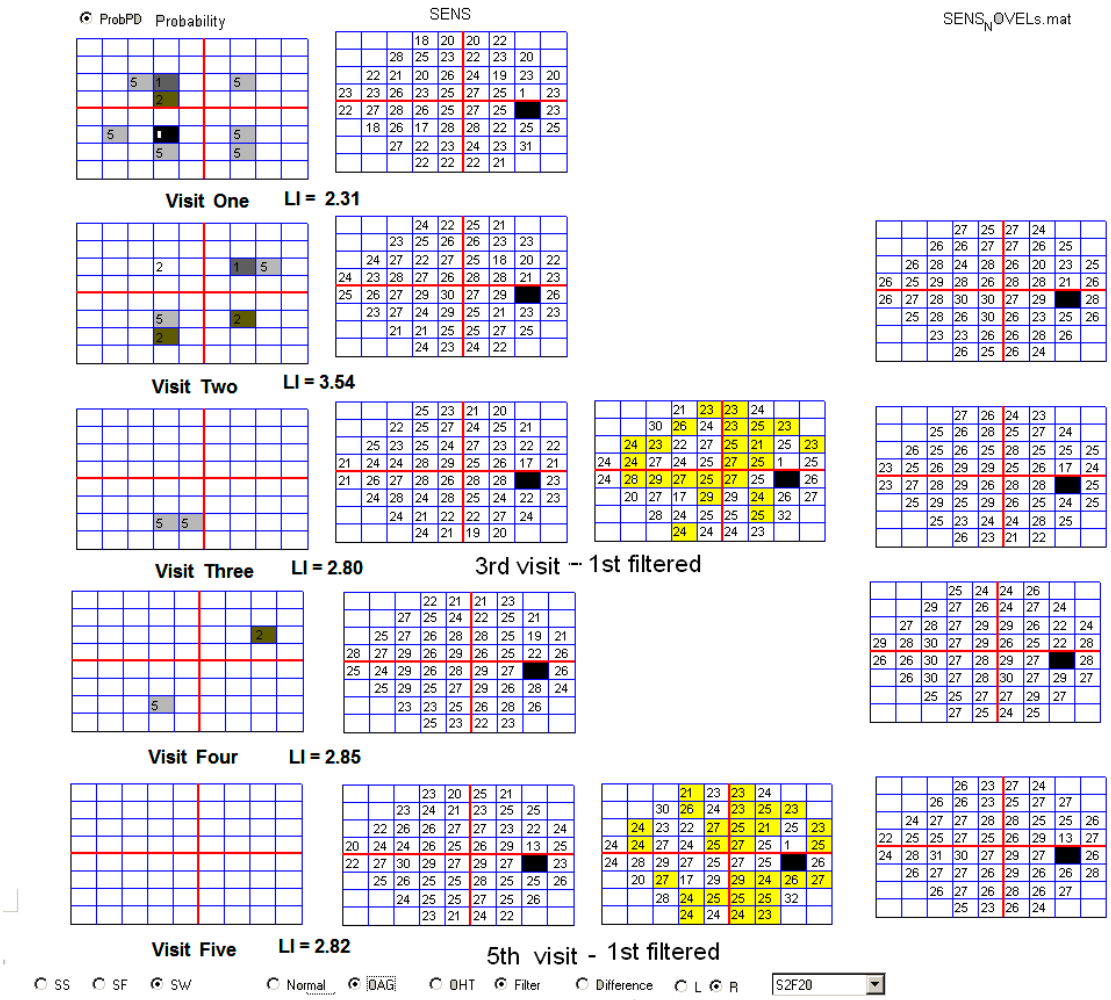

Figure 5.13 Graphical representation of filtering results, for the right eye of a glaucoma patient's visual field (with mild defects), for all visits and the SITA SWAP algorithm. The first from the left column illustrates the Total Deviation probability values, the second column the raw sensitivity values and the third column the sensitivity values after applying the adaptive hybrid (SENSNovels.mat) filter. The 1st visit filtered outcome can be compared with the 3rd visit raw and with the 5th visit raw sensitivity chart, where the matching locations of the visual field are shaded yellow.

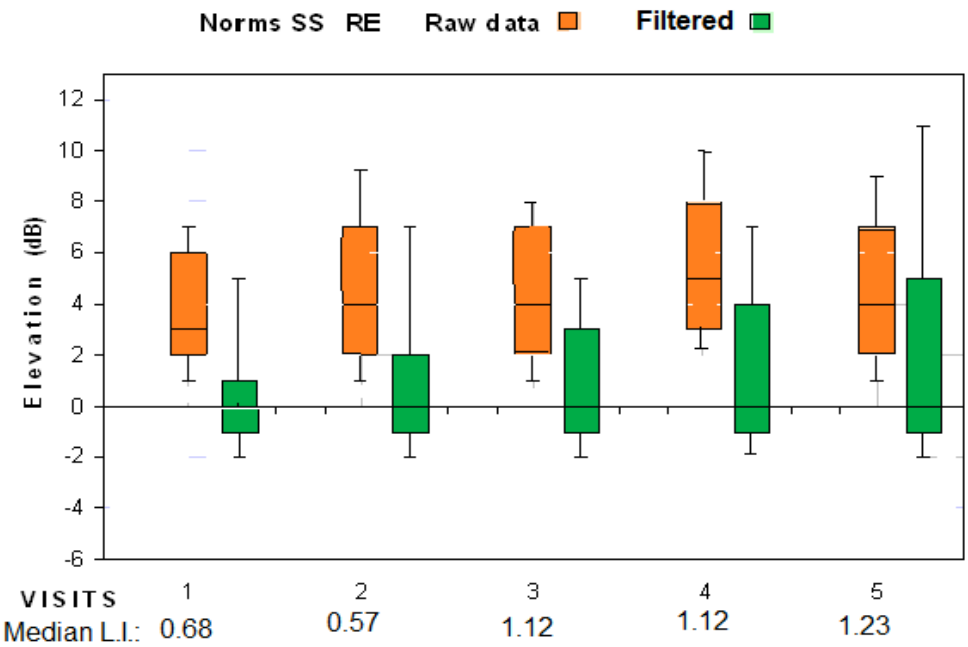

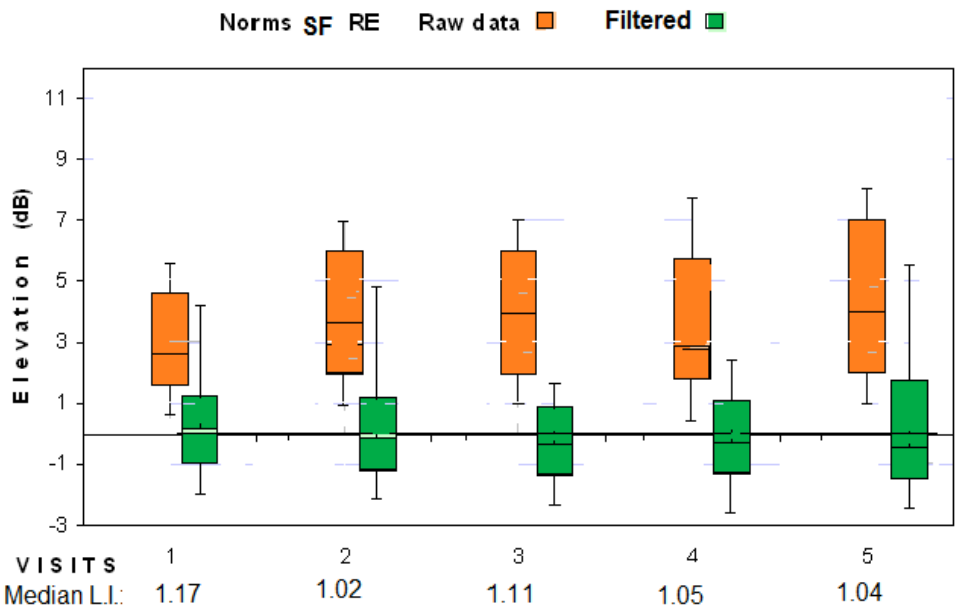

Figure 5.14. Graphical illustration of the discrepancy of sensitivity elevation for the right eye of normal subjects of raw data and data after the use of the adaptive filter, for SITA Standard (Top) and SITA Fast (bottom) strategies, at all five visits. Median L.I. is the median learning index at every visit.

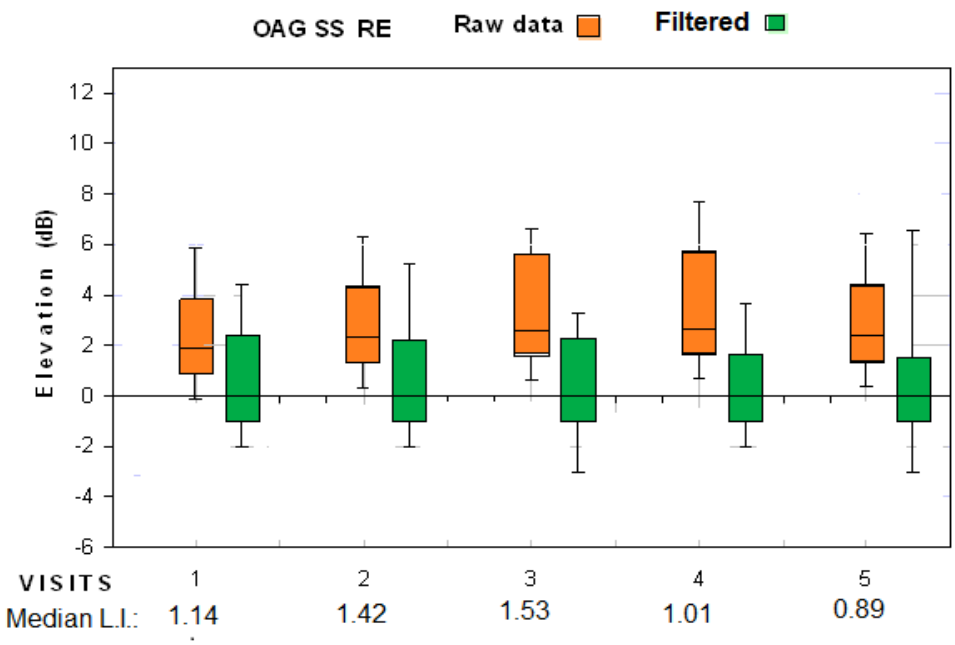

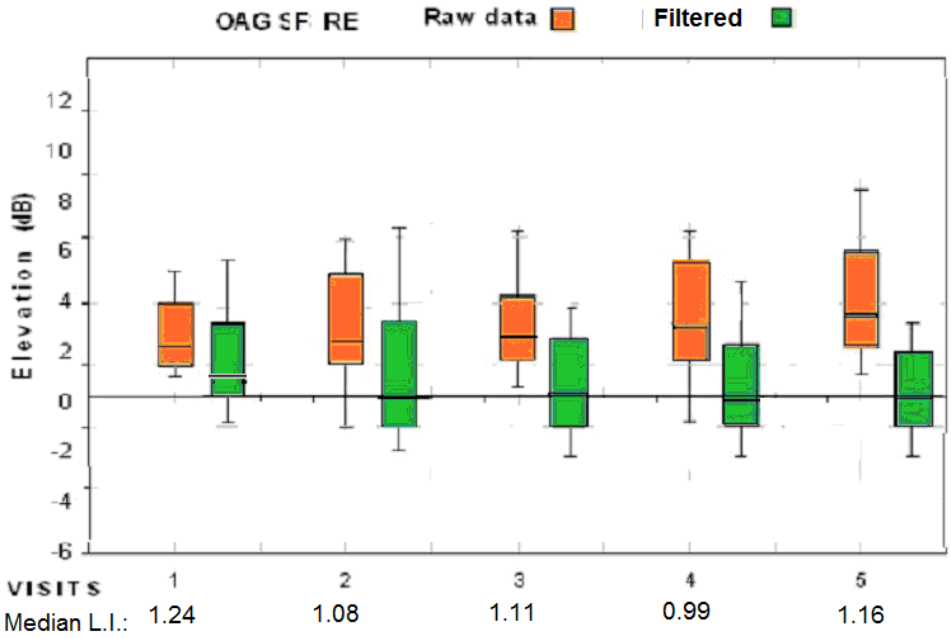

Figure 5.15 Graphical illustration of the discrepancy of sensitivity elevation for the right eye of OAG patients of raw data and data after the use of the adaptive filter, for SITA Standard (Top) and SITA Fast (bottom) strategies, at all five visits. Median L.I. is the median learning index at every visit.

5.8 Discussion

The learning effect is a key issue in many psychophysical tests. Commonly, it is believed that the individual experience manipulates the results of automated perimetry (Heijl, Lindgren and Olsson, 1987). A number of studies demonstrated that healthy and glaucomatous individuals could exhibit a learning effect with repeated standard automated perimetry testing for three of five sessions (Heijl and Bengtsson, 1996; Nordmann et al., 1998; Schimiti et al., 2002; Pierre-Filho et al., 2006;' Salvetat et al., 2007; Castro, Kawase and Melo Jr., 2008).

In the present study, results confirm that a visual field printout can be filtered to predict a close to the normal output of the field after three or five visits, if a special filter for the particular data could be designed. At the same time, findings suggest that the learning index might, in some patients, give a reasonable indication that the first visual field printouts are masked by a learning effect and that they may improve in subsequent sessions.

In previous similar studies (Crabb et al, 1995; 1997; Gardiner et al., 2004) observed that the median filter preserves the edges much better than the mean filter. Subsequently, taking into account the deployment of the optic nerve fibre layers of the retina in a similar design of the Garway-Heath and associates study (Garway-Heath et al., 2000) an Adaptive or Hybrid filter was designed again in MatLab and a promising issue of prediction of later test results was evident.

Evaluation between plots of sensitivity elevation discrepancy throughout the five visits and the learning index, easy could reveal that the learning index may be used as an indication of improvement in healthy individuals and in OAG patients. Of course it is important to emphasize that in these plots data comes only from the right eye of the examined Individuals, given that healthy group were naïve of SAP and as a result they would experienced minimum fatigue and glaucoma patients, as experienced in perimetry would have the least fatigue effect on the learning index.

5.9 Conclusions

One of the difficulties for the clinician is the tenacity of an unstable psychophysical behaviour in variability (signal and noise) of the visual fields. The result from one test suggests that the patient is normal (no glaucoma), while the result from the other test shows that the same patient may be abnormal (having glaucoma).

In present study, an alternative way of dealing with noisy data was introduced. A method of filtering the visual field results would be contemporary adaptive hybrid filters. This is a promising approach to identify and eliminate measurement noise in the visual field tests and to predict, after filtering the first examination outcome, the likely visual field outcome of the third or the fifth visit.

The median or mean filters were initially used but in preserving details both of the filters have quite serious problems. The comparative performances are showing that the median filter completely eliminates very fine details while the

mean filter blurs them but leaves something of the detail. The median filtered visual field looks markedly better. The main reason is that the remaining error is spread differently over the entire visual field for the mean. The mean filter leaves a small annoying blob of each impulse, while the median filter appears to handle the impulses very well.

The early indication of glaucoma gives the clinician the opportunity for efficient treatment, comfort for the patient and minimal financial expanses for both the individual and the state or private insurance company. Although the past years a large amount of information has been obtained concerning the visual fields behaviour, the future gold standard of glaucoma test, is not yet available for the glaucoma patients at hand.

SECTION C: DISCUSSION OF THE THESIS

6 CHAPTER SIX - Discussion of the Thesis

6.1 General discussion

Visual field testing is the most complete and diagnostically essential method of visual assessment for glaucoma, other optic nerve diseases and damage to the central visual pathways. Perimetry is the systematic measurement of the visual field function. In normal subjects, the retest variability of perimetry remains low (Heijl, Lindgren and Olsson, 1987; Wall et al., 2001). However, retest variability increases substantially with moderate visual field damage identified by SAP (Wall et al., 1999; Henson et al., 2000; Kutzko, Brito and Wall, 2000).

This high variability extensively limits early and reliable determination of visual field change. Thus, it is of critical importance to develops trustworthy methods to quantitatively discriminate progression of glaucomatous visual field loss from long-term variability. Such techniques are needed for the better clinical management of patients, and for the clinical research of glaucomatous optic nerve damage (Wall, 2004).

Perimetric variability occurs on many levels. First, it occurs on a neuronal level. Since, in most methods, the subject is required to respond to a sensory visual system stimulus, usually by pressing a response button, a variety of variables need to be controlled to achieve a reliable test. Initially, the patient must be instructed properly (Werner et al, 1989). Other cognitive factors are subject motivation and the effects of visual fatigue. Besides the variability from

cognitive factors and neuronal firing rates, characteristics of the test methodology such as stimulus properties and testing strategy are essential.

Since automated perimetry hands over the stimulus presentation control and response recording to a computer, variability due to technique differences among perimetric examiners has been reduced. In spite of greater control of stimulus parameters with automated instrumentation, variability of conventional automated perimetry in areas of visual field damage remains high (Werner et al, 1989; Wall et al., 1996; Smith, Katz and Quigley, 1996)).

Werner suggested that clinicians should not make decisions about glaucoma progression in glaucomatous subjects without at least six visual field results in hand. After a learning period of a number of visual fields, results of normal subjects retested four to five times over a one-month period present stabilized improvement (Werner et al, 1989).

However, the situation is different for automated perimetry results of individuals that present with optic nerve damage. Therefore, the most clinically important regions are ones in which determination of sensitivity change is most difficult, since these are defective locations (Flammer, Drance and Schulzer, 1983; Flammer et al., 1984; Flammer, 1985; Werner , Ganiban and Balazsi, 1991; Wall, 2004).

Several studies have reported learning effects both in glaucoma and in healthy individuals. As a result, a change in the threshold sensitivity can be expected

between the first two sessions of perimetry performed by an inexperienced individual.

In the present thesis, three groups of individuals were investigated for learning effect and the likelihood of a learning index establishment, in three different studies. These groups comprised by the normal individuals, the open angle glaucoma patients and the ocular hypertensive subjects. Normal individuals were categorized on the basis of normal findings from the clinical examination. The normal individuals (according to Castelberg , 2010) had no experience in any type of perimetry before their first test and a normal appearance of the field was defined after Morgan and colleagues (2005). The glaucoma patients and the OHT individuals, according to the Castelberg thesis, were experienced in SAP and naïve to SITA SWAP. Individuals with OAG were categorized on the basis of an optic nerve head, viewed by stereo-observation, characteristic of the disease including generalized or focal thinning of the neuro-retinal rim, disc asymmetry, changes in the lamina cribrosa, pallor, vessel changes or disc margin haemorrhage. The severity of the visual field loss for the individuals with OAG was graded, post hoc, on the appearance of the eye with the more severe loss recorded with the SITA Standard algorithm at the last visit of the study protocol. Individuals with OHT were categorized on the basis of a central corneal thickness-corrected IOP of ≥22mmHg in both eyes. The individuals from these two groups were expected to learn only in SITA SWAP where the pathway tested is different to that tested with SAP.

Olsson and colleagues (1997) were the first to develop a learning index (LI) in order to facilitate the differentiation between such disturbances that may be due

merely to lack of perimetric experience, and those due to true visual field loss. This learning index, which had to be sensitive to the mid-peripheral field disturbances, was devised following the results of a study investigating trained and untrained to perimetry normal individuals (Olsson, Asman and Heijl, 1997).

Although in the succeeding years many studies and published results mentioned the existence of the learning effect in different types of perimetry, none of them attempted to develop a similar index. As a consequence, the aim of this study was to establish a possible learning index and to investigate the behaviour of the index, in the normal population, glaucoma patients, and individuals with OHT. At the same time, a second aim was to search for different or alternative methods to Olsson's method and to investigate the likelihood of using this index, from a clinical point of view.

Therefore, in this study the untrained group consisted of normal individuals at the first test session and the trained group of the same individuals at the fifth test session, as they had already done 5 tests to both eyes

As the first approach to develop the LI, the design that was used in this study was very similar to Olsson's design. The equation used for the LI calculation by Olsson's colleagues was the same used in the new study and the normalisation factor K was exactly the same. The only difference between the two methods was that Olsson used Full Threshold 30-2 program output data and in the new study all the output data came from 24-2 program and SITA Standard, SITA Fast and SITA SWAP algorithms. Therefore, Olsson's study used data from a

greater number of locations for the calculation of the Learning Index, but these locations were in the periphery of the central field. Additionally, this study used data from 5 test sessions instead of the 3 test sessions used by Olsson's method.

Checking the distributional assumptions for the Learning Index to ensure that only the appropriate parametric or non-parametric descriptive tests and analyses were used, the normality of data distribution was tested by plotting the histogram of data distribution and the Bell Curve for all cohorts, all strategies for both eyes. As was expected, the plots show some data that follows it closely, but not perfectly (which is usual). As a result, the most appropriate parametric descriptive tests and analysis could be used for these data.

One-way repeated measures ANOVA analysis was carried out to test the hypothesis that the LI did not change significantly across visits for any of the tests and in any of the participant groups. The findings indicate that there was no statistically significant variation in LI across visits. for no significant difference in LI over time. Possible reasons for the absence of any significant difference in mean LI are, for the left eye, the fatigue resulting from always testing the left eye second and, with SWAP, the lack of experience of all subjects with this method and the difficulty of the algorithm employed in this method.

The common outcome of the effort to develop a learning index that could be indicative of the learning level of individuals, during repeated perimetric tests is

far from a simple task. Since the visual field test is a psychophysical function and incorporates a great number of factors, these generate potentially contradictory results which confound the utility of the index.

It is difficult to make firm conclusions about how the LI varies with severity of visual field damage, given the lack of consistency in the association between eyes and large variation in the magnitude (slope) of the association across conditions.

An optional design to develop the LI was then incorporated in a new study, which included the integration of the GHT test pattern into the complete pattern design of the basic method. This design was expected to offer a more valid and constant index for learning, particularly for the glaucoma and OHT individuals. Therefore, the tested locations of the visual field were grouped following the GHT pattern and all the tests replicated for all cohorts and strategies in order to consider the results with the original design outcome.

In a quick overview of the results, SITA Standard illustrated a similar behaviour for normal individuals but increased variability for glaucoma patients and OHT individuals. For the SITA Fast algorithm, the normal individuals illustrated low LI values, but the glaucoma patients showed unexpected variability. The OHT individuals illustrated very low LI values, most likely due to their previous experience and the decrease of test duration. For the SITA SWAP algorithm and for normal cohort more variability for right eye results is noticeable in all

visits most likely due to the difficulty for the blue on yellow test. For OAG and OHT individuals, the high levels of inconsistency do not permit the LI evaluation.

For normal individuals the paired samples t-test between the two methods, for all algorithms and both eyes, does not identify any statistically significant difference ($p>0.05$) and the linear regression, in general, demonstrates a rather weak association between the two methods. For glaucoma patients the paired samples t-test gave also similar results for all algorithms, for both eyes, denoting no significant ($p>0.05$) difference but very weak association in Bland Altman linear regression, between the two methods. Finally for ocular hypertensive individuals the paired samples t-test did not identify any statistically significant difference for all algorithms and both eyes and the linear regression again showed rather weak association between. So, from a clinical point of view the GHT pattern method has nothing to propose to the attempt of building up a learning index for perimetry.

As a consequence the study attempted to investigate another pattern, to develop a learning index. Although this No Eyelid pattern follows the initial method of complete visual field pattern, excludes the first upper row five locations values. The problem of Ptosis is common in the age of individuals having perimetry. As a result in many cases the eyelid covers a portion of the superior visual field producing erratic results.

Normal individuals demonstrated a slight decreasing of LI mean values for SITA Standard and SITA Fast algorithms, illustrated a reduced amount of variability,

although for SITA SWAP exhibited more variability for both eyes, as it was expected due to the difficulty of the specific algorithm. Glaucoma patients demonstrated more discrepancy of LI results for SITA Standard algorithm, likely due to the defective locations that cannot learn and for SITA Fast demonstrated unexpected major variability for both eyes. Finally, results for the SITA SWAP algorithm continued to exhibit increased variation, probably owing to the difficulty of the specific test. Ocular hypertensive individuals exhibited poor LI results for SITA Standard and SITA Fast algorithm and an overall reduced amount of learning, probably because they were experienced in perimetry. In contrast for SITA SWAP considerable variability in results was observed.

In order to compare the No Eyelid pattern method with the original complete pattern method, the Bland and Altman plots were implemented. These plots show that the majority of the points are scattered without any obvious trend or pattern, above and below zero, which suggests that there is no consistent bias of one approach versus the other (of course, there could be hidden biases that this plot does not show up). The presentation of the 95% limits of agreement does not provide power to the judgement that the two methods of measurement agree, as the range between these two limits is quite large. From a clinical point of view, the No Eyelid method do not appear to offer any benefits in the development of an effective Learning Index.

In order to investigate the learning near the defective locations of the visual field in moderate glaucoma patients a new study was carried out. An example of case series included two male glaucoma patients at the age of 70s and the

selected locations were in the inner border area of the defective locations. The chosen algorithm was SITA SWAP, although this algorithm is normally rather difficult for the patient. In contrast, numerous researchers have suggested the SWAP algorithm as a more sensitive algorithm to locate early changes of glaucoma defects (Racette and Sample, 2003; van der Schoot, 2010).

Furthermore, these patients were experienced with SAP, so they faced the least difficulty due to the algorithm, compared to other individuals performing perimetry for the first time. The right eye was selected, as it was always the first eye tested in all visits, so it was expected to have the least amount of fatigue. Locations that exist near a defective area were evaluated for visit 1,3 and 5, respectively. The damaged areas of these visual fields were likely not to show any improvement, as defective locations cannot see and consequently cannot learn.

It is difficult to draw conclusions from just two cases, however, the findings provide proof of concept that the LI can be calculated in a particular area of interest in the visual field. A more definitive study is required before one can formally assess the utility of this approach for clinical practice.

The present study includes also a novel approach. This is the filtering of visual field printout, with the purpose to predict from the first visit the visual field output that could be acquired after three or five visits, if a special filter for the particular data could be designed. Spatial filtering is a widely employed image processing

technique used to improve the quality of digital information and may be applied to perimetric test printout.

In previous studies many investigators proposed numerous types of filters in an attempt to eliminate noise and improve the useful signal of visual field data (Fitze et al., 1995; Crabb et al., 1995; 1997). Gardiner and associates (2004) proposed a spatial filter to be applied to the visual field output data. The filter complied with the rules of the accepted physiological shape of the retinal nerve fibre layer (Gardiner et al., 2004).

In this advanced method to evaluate perimetric learning by repeated test sessions, different types of filters have been applied to the first visit printout in order to simulate the third or fifth visit printout by filtering the noise, which probably at the first test mostly contains the learning effect. Additionally, benefits from post-test filtering of the data are assembled without any extra patient testing or alteration to the perimetric process.

Conversely, bearing in mind the deployment of the optic nerve fibre layers of the retina, in a similar design to the Garway-Heath and associates study design (Garway-Heath et al., 2000), an Adaptive or Hybrid filter was designed again in the MatLab environment and a promising issue of prediction of later test results was evident.

Furthermore, the outcome suggests that the learning index might, in some patients, give a reasonable indication that these first are masked by a learning

effect and that they may improve in subsequent sessions. These results are, in general, compatible with the results published for SAP (Wood et al., 1987; Heijl, Lindgren and Olsson, 1989; Wild et al., 1989) and for SWAP (Wild, Moss and O'Neill, 1996; Rossetti et al., 2006; Gardiner, Demirel and Johnson, 2008; Zhong et al., 2008; Fogagnolo et al., 2010).

6.2 Conclusions

The present learning index design, from a clinical point of view, is unlikely to become a useful index for automated perimetry. Such a conclusion is based upon the outcome of the numerous tests and the statistical analysis that followed the calculation of LI by the complete pattern method in chapter 3.

Visual field test as a psychophysical measurement includes a lot of variability that produces noisy outcomes, which are difficult to evaluate. The inconsistency of the tested individuals influences also the stability of the LI. So, the application of LI in moderate or severe glaucoma patients is not clinically practical.

Although the method studied in this thesis is unsuitable for clinical practice, there is still a need for some measure of learning in perimetry. Development of an alternative approach is warranted. A method of filtering the visual field results would be a promising approach by identifying and eliminating measurement noise in the visual field test results. The comparative performances of different design filters showed that if a future design could combine an adaptive weighted filter with a specific modern algorithm.

The results of the GHT and the No Eyelid studies lead to the impression that there was no significant improvement in LI results in order to serve the purposes of the development of a learning index using these methods for the design.

The early indication of the glaucoma combined to a warning index about the prognosis of a perimetric test outcome, gives also the clinician the opportunity

for efficient treatment, comfort for the patient and minimal financial expenses for both the individual and the state or private insurance company. Although over the past years, a large amount of information has been obtained from clinical research concerning the visual fields for glaucoma prognosis, the future for the glaucoma patient, is still contentious.

6.3 Strengths and weaknesses of the research

The major strengths of the research were the robust control over the exact schedule of a weekly separation of the five visits within each of the three studies and of the consistent instructions given to each individual. The analysis makes use of patients' own data, without the requirement to compare with normative databases. Therefore the individual learning indices within groups and instruments can be easily compared. However, as each of the instruments measures sensitivity on different scales (i.e. 30dB for SAP does not equate to 30dB for SWAP, etc.), it is less straightforward to compare between instruments.

Test-retest variability in SAP and SWAP sensitivity has previously been shown to be high, and this variability increases with depth of defect. Therefore, the ability to detect any true change in the visual field (e.g. true progression or a learning effect) becomes more difficult in participants with established sensitivity loss. This is an ongoing dilemma in research into detection of progression in perimetry, and despite several attempts to overcome this problem in recent literature, high variability remains a confounder when calculating the learning index. It was outside the scope of the current PhD to

develop an improved algorithm for measuring the learning effect, however, but rather the data demonstrate an evaluation of the current technique. It was assumed in this study that true sensitivity loss did not occur between visits, as any true sensitivity loss could be conflated with the effects of learning. Although disease progression between visits cannot be ruled out completely, there were no obvious cases in which clinically significant sensitivity loss occurred between visits.

The research was limited by the data available from the Castelberg study. Although it was known that the normal observers were naïve to perimetry, the experience of the OHT and glaucoma groups was less clear. The lack of a criterion for naivety (or significant experience) in the Castelberg study, nor specific details about the number of tests that the participants had previously undertaken meant that a criterion for separating participants into groups according to level of experience and a sub-analysis of participants in each of these groups was not possible.

To the author's knowledge, it remains the most extensive evaluation of a learning index for automated perimetry within the age range representative of those attending secondary and tertiary eye care.

\

6.4 Overall conclusion of the research and future work.

The overall conclusion of this study, about the establishment of a Learning Index (LI) following the proposed design by Olsson and colleagues (1997), is that this method is definitely not realistic and that it is without clinical benefit. Some modified methods also failed to establish themselves as clinically useful. The Learning index (LI) is unlikely to become the index of choice for automated perimetry.

Conversely, the method of filtering the visual field results potentially may be a promising approach to identify and eliminate measurement noise of the visual field output. The construction of a similar index to that reported in this thesis would be useful but very difficult to achieve.

The development of 'better' threshold algorithms has long been attempted. There is no easy answer to whether further investigation will yield significant results. Potentially, the intense data collection at a large number of locations throughout the field in a larger cohort of subjects (visually healthy and glaucomatous) would be required for a better index establishment. The incorporation of fatigue also may be required to form a robust index enough to simulate procedures of glaucoma prognosis

The low signal to noise ratio associated with perimetric testing suggest that improvements will always be difficult to make where either previous perimetric tests results are utilised in retesting or structural measures are used to inform

and focus perimetric testing (Turpin et al, 2009) may provide more reliable perimetric results.

As an overall research conclusion and bearing in mind that the utility of this particular technique in clinical practice is very limited, there is still merit in devising and developing in the future some form of learning index - just not this one.

REFERENCES

Acton, J. H. and V. C. Greenstein (2013). "Fundus-driven perimetry (microperimetry) compared to conventional static automated perimetry: similarities, differences, and clinical applications." Can J Ophthalmol **48**(5): 358-363.

Acton, J. H., J. M. Gibson and R. P. Cubbidge (2012). "Quantification of visual field loss in age-related macular degeneration." PLoS One **7**(6): e39944.

Airaksinen, P. J., A. Tuulonen, J. Välimäki and H. I. Alanko (1990). "Retinal nerve fiber layer abnormalities and high-pass resolution perimetry." Acta Ophthalmol (Copenh) **68**(6): 687-689.

Alencar, L. M. and F. A. Medeiros (2011). "The role of standard automated perimetry and newer functional methods for glaucoma diagnosis and follow-up." Indian J Ophthalmol **59 Suppl**: S53-58.

Anderson, A. J. (2003). "Spatial resolution of the tendency-oriented perimetry algorithm." Invest Ophthalmol Vis Sci **44**(5): 1962-1968.

Anderson, A. J., C. A. Johnson and J. S. Werner (2011). "Measuring visual function in age-related macular degeneration with frequency-doubling (matrix) perimetry." Optom Vis Sci **88**(7): 806-815.

Anderson, A. J., N. H. Shuey and M. Wall (2009). "Rapid confrontation screening for peripheral visual field defects and extinction." Clin Exp Optom **92**(1): 45-48.

Anderson, A. J. and A. M. McKendrick (2007). "Quantifying adaptation and fatigue effects in frequency doubling perimetry." Invest Ophthalmol Vis Sci **48**(2): 943-948.

Anderson AJ. and Johnson CA (2006) “Comparison of the ASA, MOBS and ZEST threshold methods” Vision research 46 (**15**), 2403-2411

Anderson, A. J., C. A. Johnson, M. Fingeret, J. L. Keltner, P. G. Spry, M. Wall and J. S. Werner (2005). "Characteristics of the normative database for the Humphrey matrix perimeter." Invest Ophthalmol Vis Sci **46**(4): 1540-1548.

Anderson A J, and Johnson C A (2002) Mechanisms isolated by frequency-doubling technology Perimetry. Invest Ophthalmol Vis Sci 43: 388-401.

Anderson D R, and Patella V M (1999). “Automated Static Perimetry”. Washington: CV Mosby.

Anderson, D.R. and Knighton, R.W.(1988) Perimetry and acute perimetry.Book Chapter In: Perspectives in Glaucoma. M.B. Shields, I.P. Pollack and A.E. Kolker, eds. Slack, Inc., Thorofare, NJ, pp.59-70.

Ang, G. S., M. Shunmugam and A. Azuara-Blanco (2010). "Effect of cataract extraction on the glaucoma progression index (GPI) in glaucoma patients." J Glaucoma **19**(4): 275-278.

Artes, P. H., N. O'Leary, D. M. Hutchison, L. Heckler, G. P. Sharpe, M. T. Nicolela and B. C. Chauhan (2011). "Properties of the statpac visual field index." Invest Ophthalmol Vis Sci **52**(7): 4030-4038.

Artes, P. H. and B. C. Chauhan (2005). "Longitudinal changes in the visual field and optic disc in glaucoma." Prog Retin Eye Res **24**(3): 333-354.

Artes, P. H., D. M. Hutchison, M. T. Nicolela, R. P. LeBlanc and B. C. Chauhan (2005). "Threshold and variability properties of matrix frequency-doubling technology and standard automated perimetry in glaucoma." Invest Ophthalmol Vis Sci **46**(7): 2451-2457.

Artes, P. H., A. Iwase, Y. Ohno, Y. Kitazawa and B. C. Chauhan (2002). "Properties of perimetric threshold estimates from Full Threshold, SITA Standard, and SITA Fast strategies." Invest Ophthalmol Vis Sci **43**(8): 2654-2659.

Asman, P., J. M. Wild and A. Heijl (2004). "Appearance of the pattern deviation map as a function of change in area of localized field loss." Invest Ophthalmol Vis Sci **45**(9): 3099-3106.

Asman, P. and A. Heijl (1992a). "Glaucoma Hemifield Test. Automated visual field evaluation." Arch Ophthalmol **110**(6): 812-819.

Asman, P. and A. Heijl (1992b). "Evaluation of methods for automated Hemifield analysis in perimetry." Arch Ophthalmol **110**(6): 820-826.

Astola J, and Kuosmanen P (1997) Fundamentals of nonlinear Digital Filtering. CRC Press

Atchison D. (1987) Effect of defocus on visual field measurement Ophta.& Physiol. Optics (**7**) 3; pp 259-265

Baez KA, McNaught AI, Dowler JG, Poinoosawmy D, Fitzke FW and Hitchings RA. (1995) Motion detection threshold and field progression in normal tension glaucoma. British Journal of Ophthalmology 5;79:125-128

Baraniuk R., (2003) Signals and Systems, The Connexion Project, Houston, USA

Barkana, Y., E. Bakshi, Y. Goldich, Y. Morad, A. Kaplan, I. Avni and D. Zadok (2012). "Characterization and comparison of the 10-2 SITA-standard and fast algorithms." ScientificWorldJournal **2012**: 821802.

Barkana, Y., Y. Gerber, R. Mora, J. M. Liebmann and R. Ritch (2006). "Effect of eye testing order on automated perimetry results using the Swedish Interactive Threshold Algorithm standard 24-2." Arch Ophthalmol **124**(6): 781-784.

Bartz-Schmidt KU, Weber J, (1993) Comparison of spatial thresholds and intensity thresholds in glaucoma Int Ophthalmol **17**: 171-178

Bebie, H., J. Flammer and T. Bebie (1989). "The cumulative defect curve: separation of local and diffuse components of visual field damage." Graefes Arch Clin Exp Ophthalmol **227**(1): 9-12

Bebie, H., F. Fankhauser and J. Spahr (1976). "Static perimetry: accuracy and fluctuations." Acta Ophthalmol (Copenh) **54**(3): 339-348.

Bengtsson, B. and A. Heijl (2008). "A visual field index for calculation of glaucoma rate of progression." Am J Ophthalmol **145**(2): 343-353.

Bengtsson, B. and A. Heijl (2006). "Diagnostic sensitivity of fast blue-yellow and standard automated perimetry in early glaucoma: a comparison between different test programs." Ophthalmology **113**(7): 1092-1097.

Bengtsson, B. and A. Heijl (2000). "False-negative responses in glaucoma perimetry: indicators of patient performance or test reliability?" Am J Ophthalmol **130**(5): 689.

Bengtsson, B. and A. Heijl (1998). "SITA Fast, a new rapid perimetric threshold test. Description of methods and evaluation in patients with manifest and suspect glaucoma." Acta Ophthalmol Scand **76**(4): 431-437.

Bengtsson B, Lindgren A, Heijl A, Lindgren G, Asman P, and Patella M (1997) Perimetric probability maps to separate change caused by glaucoma from that caused by cataract. Acta Ophthalmol Scand. 75: 184-188.

Bengtsson B, Olsson J, and Heijl A (1997) A new generation of algorithms for computerised threeshold perimetry,SITA. Acta Ophthalmol Scand. 75: 368-375.

Benjumeda A., (2006) “Visual field Progression in Glaucoma . A review” - Universitat de Sevilla- Facultat de Medicina, Spain

Bergin, C., T. Redmond, N. Nathwani, G. M. Verdon-Roe, D. P. Crabb, R. S. Anderson and D. F. Garway-Heath (2011). "The effect of induced intraocular straylight on perimetric tests." Invest Ophthalmol Vis Sci **52**(6): 3676-3682.

Bernardi L, Costa V P, and Shiroma L O (2007) Flicker perimetry in healthy subjects: influence of age and gender, learning effect and short-term fluctuation. Arq Bras Oftalmol. **70**: 91-99.

Bettelheim FA and Chylack LT (1985). Light scattering of whole excised human cataractous lenses. Relationships between different light scattering parameters.Experimental Eye Research, **41**, 19-30.

Bizios D**,** Heijl A and Bengtsson B (2011) Integration and fusion of standard automated perimetry and optical coherence tomography data for improved automated glaucoma diagnostics BMC Ophthalmology

Blumenthal, E. Z., P. A. Sample, C. C. Berry, A. C. Lee, C. A. Girkin, L. Zangwill, J. Caprioli and R. N. Weinreb (2003). "Evaluating several sources of variability for standard and SWAP visual fields in glaucoma patients, suspects, and normals." Ophthalmology **110**(10): 1895-1902.

Blumenthal EZ, Sample PA, Zangwill L, Lee AC, Kono Y and Weinreb RN (2000). Comparison of Long-term variability for standard and Short-wavelength Automated Perimetry in stable glaucoma patients. Am J Ophthalmol. 129, 309-313.

Boland, M. V. and H. A. Quigley (2011). "Evaluation of a combined index of optic nerve structure and function for glaucoma diagnosis." BMC Ophthalmol **11**: 6.

Bowd C, Zangwill LM, Berry CC, Blumenthal EZ, Vasile C, Sanchez-Galeana C, Bosworth CF, Sample PA, and Weinreb RN. (2001) Detecting Early Glaucoma by Assessment of Retinal Nerve Fiber Layer Thickness and Visual Function IOVS*,* Vol. 42, No. 9

Brenton RS and Phelps CD (1986). The normal visual field on the Humphrey Field Analyzer. Ophthalmologica, **193**, 56-74.

Broadway D., (2012). “Visual field testing for glaucoma - a practical guide”- Community Eye Health. **25**(79-80): 66–70.

Brusini, P., M. Zeppieri, C. Tosoni, L. Parisi and M. L. Salvetat (2010). "Optic disc damage staging system." J Glaucoma **19**(7): 442-449.

Brusini P., Salvetat ML, Parisi L., Zeppieri M., (2005) Probing glaucoma visual damage by rarebit perimetry Br J Ophthalmol ;89:180-184 doi:10.1136/bjo

Buerki E and Monhart M., (2007) “An Update to Octopus Perimetry”, Touch Briefings, DOI: 10.17925/EOR.2007.00.01.20

Budenz, D. L., P. Rhee, W. J. Feuer, J. McSoley, C. A. Johnson and D. R. Anderson (2002). "Sensitivity and specificity of the Swedish interactive threshold algorithm for glaucomatous visual field defects." Ophthalmology **109**(6): 1052-1058.

Burgansky-Eliash, Z., G. Wollstein, A. Patel, R. A. Bilonick, H. Ishikawa, L. Kagemann, W. D. Dilworth and J. S. Schuman (2007). "Glaucoma detection with matrix and standard achromatic perimetry." Br J Ophthalmol **91**(7): 933-938

Cahill KV, Bradley EA, Meyer DR, Custer PL et al., (2011) Functional Indications for Upper Eyelid Ptosis and Blepharoplasty Surgery Ophthalmology Vol 18 pp. 2510-2517

Capris, P., S. Autuori, E. Capris and M. Papadia (2008). "Evaluation of threshold estimation and learning effect of two perimetric strategies, SITA Fast and CLIP, in damaged visual fields." Eur J Ophthalmol **18**(2): 182-190.

Carroll JN and Johnson CA. (2013). “Visual Field Testing: From One Medical Student to Another:. EyeRounds.org.

Casson EJ, Johnson CA and Shapiro LR (1993a). A longitudinal comparison of Temporal Modulation Perimetry with white-on-white and blue-on-yellow perimetry in ocular hypertension and early glaucoma. J Opt Soc Am A Opt Image Sci Vis. 10, 1792-1806.

Casson EJ, Johnson CA and Nelson-Quigg JM (1993b). Temporal Modulation Perimetry: the effects of aging and eccentricity on sensitivity in normals. Invest Ophthalmol Vis Sci. 34, 3096-3102.

Casson EJ, James B, Rubinstein A, Haggai A (2000) Clinical comparison of frequency doubling technology perimetry and Humphrey perimetry Br J Ophthalmol ; **85** :360–362

Casson EJ and Johnson CA (1992). Temporal Modulation Perimetry in glaucoma and ocular hypertension. Perimetry Update 1992/93. 443-451.

Castelberg C.A., (2010) . *Evaluation of two novel perimetric techniques for the detection of open angle glaucoma: An in-depth analysis.* PhD Thesis, Cardiff University.

Castro D P E, Kawase J, and Melo J L S (2008) Learning effect of standard automated perimetry in healthy individuals. Arq Bras Oftalmol. **71**: 523-528.

Cello, K. E., J. M. Nelson-Quigg and C. A. Johnson (2000). "Frequency doubling technology perimetry for detection of glaucomatous visual field loss." Am J Ophthalmol **129**(3): 314-322.

Centofanti, M., P. Fogagnolo, F. Oddone, N. Orzalesi, M. Vetrugno, G. Manni and L. Rossetti (2008). "Learning effect of humphrey matrix frequency doubling technology perimetry in patients with ocular hypertension." J Glaucoma **17**(6): 436-441.

Chaglasian, M (2013) **"**Glaucoma Progression: New ideas in an evolving area". East Coast Optometric Glaucoma Symposium, USA

Chauhan, B. C. and P. H. House (1991). "Intratest variability in conventional and high-pass resolution perimetry." Ophthalmology **98**(1): 79-83.

Chauhan, B. C., P. H. House, T. A. McCormick and R. P. LeBlanc (1999). "Comparison of conventional and high-pass resolution perimetry in a prospective study of patients with glaucoma and healthy controls." Arch Ophthalmol **117**(1): 24-33.

Chauhan, B. C., R. P. LeBlanc, T. A. McCormick and J. B. Rogers (1993a). "Comparison of high-pass resolution perimetry and pattern discrimination perimetry to conventional perimetry in glaucoma." Can J Ophthalmol **28**(7): 306-311.

Chauhan, B. C., R. N. Mohandas, J. H. Whelan and T. A. McCormick (1993b). "Comparison of reliability indices in conventional and high-pass resolution perimetry." Ophthalmology **100**(7): 1089-1094.

Chauhan, B. C., J. D. Tompkins, R. P. LeBlanc and T. A. McCormick (1993c). "Characteristics of frequency-of-seeing curves in normal subjects, patients with suspected glaucoma, and patients with glaucoma." Invest Ophthalmol Vis Sci **34**(13): 3534-3540.

Christoforidis B J, (2011). "Volume of visual field assessed with kinetic perimetry and its application to static perimetry". Clinical Ophthalmology **5**: 535–541

Contestabile, M. T., A. Perdicchi, S. Amodeo, V. Recupero and S. M. Recupero (2007). "The influence of learning effect on frequency doubling technology perimetry (Matrix)." J Glaucoma **16**(3): 297-301.

Crabb DP, Gardiner SK., Fitzke FW, Hitchings RA (2003) A new spatial filter for visual field data p.31 Perimetry Update 2002/2003 Edited by D.Henson and M.Wall, The Kugler Publications, The Hague, Netherlands

Crabb, D.P., Fitzke, F.W., McNaught, A.I., Edgar, D.F. and Hitchings, R.A. (1997). Improving the prediction of visual field progression in glaucoma using spatial processing. Ophthalmology, ***104***(3), pp. 517–524.

Crabb D.P., Edgar D.F., Fitzke F.W., McNaught A.I. and Wynn, H.P. (1995). New approach to estimating variability in visual-field data using an image-processing technique British Journal of Ophthalmology, ***79***(3), pp. 213–217

Cubbidge R (2005). "Visual Fields". : Elsevier. Birmingham, UK

Dacey, D. M. and B. B. Lee (1994). "The 'blue-on' opponent pathway in primate retina originates from a distinct bistratified ganglion cell type." Nature **367**(6465): 731-735.

Daly, S. J. and R. A. Normann (1985). "Temporal information processing in cones: effects of light adaptation on temporal summation and modulation." Vision Res **25**(9): 1197-1206.

Davidson, S. I. and T. Akingbehin (1980). "Compliance in ophthalmology." Trans Ophthalmol Soc U K **100**(Pt 2): 286-290.

De Jong, L. A., C. E. Snepvangers, T. J. van den Berg and C. T. Langerhorst (1990). "Blue-yellow perimetry in the detection of early glaucomatous damage." Doc Ophthalmol **75**(3-4): 303-314.

Denniss, J., A. M. McKendrick and A. Turpin (2013). "Towards Patient-Tailored Perimetry: Automated Perimetry Can Be Improved by Seeding Procedures With Patient-Specific Structural Information." Transl Vis Sci Technol **2**(4): 3.

Dersu I I, and Thaly D (2007) Letter to the Editor. Ophthalmology 114: 1031-1032.

Drance M S, and Anderson D R (1985) “Automatic Perimetry in glaucoma: a practical guide”. New York: Grune & Stratton.

Dul MW (2013) Optimizing Contrast Sensitivity Perimetry for Clinical Use J Ophthalmic Vis Res. 8(1): 74–76.

Ennis, F. A. and C. A. Johnson (2002). "Are high-pass resolution perimetry thresholds sampling limited or optically limited?" Optom Vis Sci **79**(8): 506-511.

Fankhauser, F. (1979). "Problems related to the design of automatic perimeters." Doc Ophthalmol **47**(1): 89-139.

Faubert, J., & Bellavance, F. (2003). Temporal modulation visual fields, normal aging,
Parkinson's disease and methyl-mercury in the James Bay Cree: a feasibility study. Arquivos Brasileiros de Oftalmologia, **66**, 77-91.

Feghali JG, Bocquet X, Charlier J, Odom JV. (1991) Static flicker perimetry in glaucoma and ocular hypertension. Curr Eye Res.;10(3):205-12.

Fisher R.F. (1967) The influences of orbital contours and lid ptosis on the size of the peripheral visllal field Vision Res. Vol. 7. pp. 671-678**.**

Fitzke FW*,* Crabb DP, McNaught AI, et al. (1995) Image processing of computerised visual field data.: Br J Ophthalmol*;79:*207*–12*

Flammer J, Drance S, and Zulauf M (1984) Differential Light Threshold. Arch Ophthalmol 102: 704-706.

Flanagan, J. G., J. M. Wild and G. E. Trope (1993). "Evaluation of FASTPAC, a new strategy for threshold estimation with the Humphrey Field Analyzer, in a glaucomatous population." Ophthalmology **100**(6): 949-954.

Fogagnolo, P., L. Tanga, L. Rossetti, F. Oddone, G. Manni, N. Orzalesi and M. Centofanti (2010). "Mild learning effect of short-wavelength automated perimetry using SITA program." J Glaucoma **19**(5): 319-323.

Fogagnolo P, Rossetti L, Ranno S, Ferreras A, Orzalesi N. (2008) Short-wavelength automated perimetry and frequency-doubling technology perimetry in glaucoma. Prog Brain Res;173:101-24.

Francis, B. A., K. Singh, S. C. Lin, E. Hodapp, H. D. Jampel, J. R. Samples and S. D. Smith (2011). "Novel glaucoma procedures: a report by the American Academy of Ophthalmology." Ophthalmology **118**(7): 1466-1480.

Frisén, L. (2013). "Rapid assessment of neurovisual integrity using multiple rarebits." Ophthalmology **120**(9): 1756-1760.

Frisén, L. (2002). "New, sensitive window on abnormal spatial vision: rarebit probing." Vision Res **42**(15): 1931-1939.

Frisén, L. (1993). "High-pass resolution perimetry. A clinical review." Doc Ophthalmol **83**(1): 1-25.

Frisén, L. (1988). "Perimetric variability: importance of criterion level." Doc Ophthalmol **70**(4): 323-330.

Frisén, L. (1987). "High-pass resolution targets in peripheral vision." Ophthalmology **94**(9): 1104-1108.

Frisén, L. (1986). "Vanishing optotypes. New type of acuity test letters." Arch Ophthalmol **104**(8): 1194-1198.

Frisén, L. and C. Jensen (2008). "How robust is the optic chiasm? Perimetric and neuro-imaging correlations." Acta Neurol Scand **117**(3): 198-204.

Frisén, L. and F. Nikolajeff (1993). "Properties of high-pass resolution perimetry targets." Acta Ophthalmol (Copenh) **71**(3): 320-326.

Fujimoto, N., K. Minowa, O. Miyauchi, T. Hanawa and E. Adachi-Usami (2002). "Learning effect for frequency doubling perimetry in patients with glaucoma." Am J Ophthalmol **133**(2): 269-270.

Funkhouser, A. T., F. Fankhauser and R. A. Weale (1992). "Problems related to diffuse versus localized loss in the perimetry of glaucomatous visual fields." Graefes Arch Clin Exp Ophthalmol **230**(3): 243-247.

Gardiner SK, Demirel S and Johnson CA. (2008) Is There Evidence for Continued Learning Over Multiple Years in Perimetry? Optom Vis Sci. **85** (11); 1043–1048.

Gardiner S K, Demirel S, and Johnson C A. (2006) Modeling the sensitivity to variability relationship in perimetry Vision Res 46(11):1732-45.

Gardiner SK, Johnson CA and Cioffi GA (2005). Evaluation of the structure-function relationship in glaucoma. Invest Ophthalmol Vis Sci. **46**, 3712-3717.

Gardiner SK., Crabb DP,Fitzke FW, Hitchings RA (2004) Reducing noise in suspected glaucomatous visual fields by using a new spatial filter. Vision Research 839 - 848

Garway-Heath, D. F., J. Caprioli, F. W. Fitzke and R. A. Hitchings (2000a). "Scaling the hill of vision: the physiological relationship between light sensitivity and ganglion cell numbers." Invest Ophthalmol Vis Sci **41**(7): 1774-1782.

Garway-Heath, D. F., D. Poinoosawmy, F. W. Fitzke and R. A. Hitchings (2000b). "Mapping the visual field to the optic disc in normal tension glaucoma eyes." Ophthalmology **107**(10): 1809-1815.

Ghate, D., B. Bondarchuk, S. Sanders, S. Deokule and S. Kedar (2014). "The ability of healthy volunteers to simulate a neurologic field defect on automated perimetry." Ophthalmology **121**(3): 759-762.

Glass, E., M. Schaumberger and B. J. Lachenmayr (1995). "Simulations for FASTPAC and the standard 4-2 dB full-threshold strategy of the Humphrey Field Analyzer." Invest Ophthalmol Vis Sci **36**(9): 1847-1854.

Glovinsky, Y., H. A. Quigley and G. R. Dunkelberger (1991). "Retinal ganglion cell loss is size dependent in experimental glaucoma." Invest Ophthalmol Vis Sci **32**(3): 484-491.

Gonzalez de la Rosa, M., M. Gonzalez-Hernandez, M. Sanchez-Garcia, R. Rodriguez de la Vega, T. Diaz-Aleman and A. Pareja Rios (2013). "Oculus-Spark perimetry compared with 3 procedures of glaucoma morphologic analysis (GDx, HRT, and OCT)." Eur J Ophthalmol **23**(3): 316-323.

González de la Rosa M, González-Hernández M, García-Feijoo J et al (2011) Comparación del rango de medida de defectos entre la perimetría estandar blanco/blanco y la perimetria Pulsar. Arch Soc Esp Oftalmol **86**:113–117

Gonzalez de la Rosa M, Gonzalez-Hernandez M, Diaz-Aleman T (2009) Linear regression analysis of the cumulative defect curve by sectors and other criteria of glaucomatous visual field progression. Eur J Ophthalmol **19**:416–424

Gonzalez de la Rosa G, Hernandez G, Estevez A, Aleman D, and Plasencia A (2007) Diagnostic Capability of Pulsar, FDT and HRT-II in glaucoma suspects. Arch Soc Esp Oftalmol **82**: 413-422.

Gonzalez de la Rosa, M. and A. Pareja (1997). "Influence of the "fatigue effect" on the mean deviation measurement in perimetry." Eur J Ophthalmol **7**(1): 29-34.

Gonzalez de la Rosa M, Martinez A, Sanchez M, Mesa C, Cordoves L, and Losada MJ (1996) “Accuracy of the Tendency-Oriented Perimetry (TOP) in the Octopus 1-2-3 Perimeter”. In: Wall M, and Wild JM [eds.] Perimetry Update 1996/97. Amsterdam/ New York Kugler Publ., pp. 119-223.

Gonzalez-Hernandez M, Garcia-Feijoo J, Sanchez Mendez M, Gonzalez de la Rosa M (2004) Combined spatial, contrast and temporal functions perimetry in mild glaucoma and ocular hypertension. Eur J Ophthalmol 14:514–522

Gonzalez-Hernandez M, Rios A, Rodriguez M, de la Rosa M (2000) Combined spatial resolution and contrast perimetry in normal subjects. In: Wall M, Mills RP (Hrsg) Perimetry update 2000/2001. Kugler Publ., The Hague, S 109–114

Graham, S. L. and S. M. Drance (1995). "Interpretation of high-pass resolution perimetry with a probability plot." Graefes Arch Clin Exp Ophthalmol **233**(3): 140-149

Graves D., (2013) „Visual Field Testing: How to Avoid Fixation Losses“ Ophthalmic Professional, Volume: 2 , Issue: April 2013, page(s): 26 27

Greve, E. L. (1973). "Single and multiple stimulus static perimetry in glaucoma; the two phases of perimetry. Thesis." Doc Ophthalmol **36**: 1-355.

Guthauser U and Flammer J (1988). Quantifying visual field damage caused by cataract. American Journal o f Ophthalmology, **106**, 480-484.

Haas A*,* Flammer J *&* Schneider U *(*1986*):* Influence of age on the visual fields of normal subjects. Am J Ophthalmol **101***:* 199–203*.*

Hackett, D. A. and A. J. Anderson (2011). "Determining mechanisms of visual loss in glaucoma using Rarebit perimetry." Optom Vis Sci **88**(1): 48-55.

Hamill, T. R., R. B. Post, C. A. Johnson and J. L. Keltner (1984). "Correlation of color vision deficits and observable changes in the optic disc in a population of ocular hypertensives." Arch Ophthalmol **102**(11): 1637-1639.

Harrington, DO.and Drake, MV. (1990). “The visual fields: text and atlas of clinical perimetry”. St. Louis, Mosby

Hart WM Jr and Gordon MO (1983). “Calibration of the Dicon Auto Perimeter 2000 compared with that of the Goldmann perimeter”. Am J Ophthalmol. 96, 744-750.

Harwerth, R. S., J. L. Wheat, M. J. Fredette and D. R. Anderson (2010). "Linking structure and function in glaucoma." Prog Retin Eye Res **29**(4): 249-271.

Harwerth, R. S. and J. L. Wheat (2008). "Modeling the effects of aging on retinal ganglion cell density and nerve fiber layer thickness." Graefes Arch Clin Exp Ophthalmol **246**(2): 305-314.

Harwerth R S, Vilupuru A S, Rangaswamy N V, and Smith E L (2007) The relationship between nerve fiber layer and perimetry measurements. Investigative Ophthalmology & Visual Science 48: 763-773.

Harwerth R, Quigley H. (2006) Visual field defects and retinal ganglion cell losses in patients with glaucoma. Arch Ophthalmol.;124:853–859.

Harwerth RS, Carter-Dawson L, Smith EL, Barnes G, Holt WF and Crawford MLJ. (2004) Neural losses correlated with visual losses in clinical perimetry. Investigative Ophthalmology and Visual Science;45:3152-3160.

Harwerth RS, Crawford MLJ, Frishman LJ, Viswanathan S, Smith EL and Carter-Dawson L (2002). Visual field defects and neural losses from experimental glaucoma. Progress in Retinal and Eye Research, 21, 91-125

Harwerth, R. S., E. L. Smith and M. Chandler (1999). "Progressive visual field defects from experimental glaucoma: measurements with white and colored stimuli." Optom Vis Sci **76**(8): 558-570.

Harwerth, R. S., L. Carter-Dawson, F. Shen, E. L. Smith and M. L. Crawford (1999). "Ganglion cell losses underlying visual field defects from experimental glaucoma." Invest Ophthalmol Vis Sci **40**(10): 2242-2250.

Havvas, I., D. Papaconstantinou, M. M. Moschos, P. G. Theodossiadis, V. Andreanos, P. Ekatomatis, I. Vergados and D. Andreanos (2013). "Comparison of SWAP and SAP on the point of glaucoma conversion." Clin Ophthalmol **7**: 1805-1810.

Heijl, A. (1989). "Visual field changes in early glaucoma and how to recognize them." Surv Ophthalmol **33 Suppl**: 403-404; discussion 409-411.

Heijl, A. (1985). "Computerised perimetry." Trans Ophthalmol Soc U K **104 (Pt 1)**: 76-87.

Heijl A (1977) Time changes of contrast thresholds during automatic perimetry. Acta Ophthalmol. Scand. **55**: 696-708.

Heijl, A. (1976). "Automatic perimetry in glaucoma visual field screening. A clinical study." Albrecht Von Graefes Arch Klin Exp Ophthalmol **200**(1): 21-37.

Heijl A*,* Bengtsson B. and Patella A., (2012*). "*Effective Perimetry" - Zeiss Visual Field Primer, 4th Edition.

Heijl A, Lindgren A, and Lindgren G (1990) "Extended empirical statistical package for evaluation of single and multiple fields in glaucoma: Statpac 2". Perimetry Update 1990/91. Amsterdam: Kugler Publ. 1991. 303-315.

Heijl, A., G. Lindgren and J. Olsson (1987). "Normal variability of static perimetric threshold values across the central visual field." Arch Ophthalmol **105**(11): 1544-1549.

Heijl A, and Bengtsson B (1996) The Effect of Perimetric Experience in Patients With Glaucoma. Arch Ophthalmol. 114:: 19-22.

Heijl A, and Drance S M (1983) Changes in differential threshold in patients with glaucoma during prolonged perimetry. Br J Ophthalmol **67**: 512-516.

Heijl, A. and C. E. Krakau (1977). "A note of fixation during perimetry." Acta Ophthalmol (Copenh) **55**(5): 854-861.

Heijl, A. and C. E. Krakau (1975a). "An automatic static perimeter, design and pilot study." Acta Ophthalmol (Copenh) **53**(3): 293-310.

Heijl, A. and C. E. Krakau (1975b). "An automatic perimeter for glaucoma visual field screening and control. Construction and clinical cases." Albrecht Von Graefes Arch Klin Exp Ophthalmol **197**(1): 13-23.

Henson DB (1998). "Visual Fields". paperback ed. Oxford: Oxford University Press.

Henson, D. B. and T. Emuh (2010). "Monitoring vigilance during perimetry by using

pupillography." Invest Ophthalmol Vis Sci **51**(7): 3540-3543.

Henson, D. B., S. Chaudry, P. H. Artes, E. B. Faragher and A. Ansons (2000). "Response variability in the visual field: comparison of optic neuritis, glaucoma, ocular hypertension, and normal eyes." Invest Ophthalmol Vis Sci **41**(2): 417-421.

Henson DB, Morris EJ (1993) Effect of uncorrected refractive errors upon central visual field testing. Ophthal Physiol Opt. **13** 339

Henson, D. B., B. C. Chauhan and A. Hobley (1988). "Screening for glaucomatous visual field defects: the relationship between sensitivity, specificity and the number of test locations." Ophthalmic Physiol Opt **8**(2): 123-127.

Hirasawa, K., N. Shoji, A. Okada, K. Takano and S. Tomioka (2014). "Evaluation of stimulus velocity in automated kinetic perimetry in young healthy participants." Vision Res **98**: 83-88.

Hitchings, R. A. (2009). "Glaucoma: an area of darkness." Eye (Lond) **23**(9): 1764-1774.

Hong S, Na K, Kim C Y, and Seong G J (2007) Learning effect of Humphrey Matrix perimetry. Can J Ophthalmol **42**: 707-711.

Hood DC, Anderson SC, Wall M and Kardon RH. (2007a) Structure versus function in glaucoma: an application of a linear model. Investigative Ophthalmology and Visual Science;**48**:3662-3668.

Hood D C, and Kardon R H (2007b) A framework for comparing structural and functional measures of glaucomatous damage. Progress in Retinal and Eye Research **26**: 688-710.
Horani, A., S. Frenkel, C. Yahalom, M. D. Farber, U. Ticho and E. Z. Blumenthal (2002). "The learning effect in visual field testing of healthy subjects using frequency doubling technology." J Glaucoma **11**(6): 511-516.

Hudson, C., J. M. Wild and E. C. O'Neill (1994). "Fatigue effects during a single session of automated static threshold perimetry." Invest Ophthalmol Vis Sci **35**(1): 268-280.

Hutchings N, Hosking SL, Wild JM and Flanagan JG (2001). Long-term fluctuation in Short-wavelength Automated Perimetry in glaucoma suspects and glaucoma patients. Invest Ophthalmol Vis Sci. 42, 2332-2337.

Iester M, Perdicchi A, Capris E, Siniscalco A, Calabria and Recupero SM (2008). Comparison between discriminant analysis models and 'Glaucoma Probability Score' for the detection of glaucomatous optic nerve head changes. J Glaucoma. **17**, 535-540.

Iester M, Altieri M, Capris P, Vittone P, Zingiriam M, Traverso CE: (2002) Different perimetric techniques to detect early glaucomatous defects. Acta Ophthalmol Suppl 236: 22-24,

Jampel HD,. Francis BA, Singh K, Lin SC, Hodapp E, Samples JR, Smith SD. (2011) Novel *glaucoma* procedures: a report by the *American Academy of Ophthalmology.* Ophthalmology.;118(7):1466–80.

Johnson, C. A. (2013). "Psychophysical factors that have been applied to clinical perimetry." Vision Res **90**: 25-31.

Johnson C.A., (2008) Chapter 9: “Detecting functional changes in the Patient’s vision: Visual Field Analysis”, Clinical Glaucoma Care Ed. Samples J & Schacknow P, Springer ISBN-978-1-4614-4171-7

Johnson C.A. (2006). “Visual field variability”. Optometric Glaucoma Society E-Journal. 1(2):13.

Johnson, C. A. (1993). "Modern developments in clinical perimetry." Curr Opin Ophthalmol **4**(2): 7-13.

Johnson, C. A., M. Wall and H. S. Thompson (2011). "A history of perimetry and visual field testing." Optom Vis Sci **88**(1): E8-15.

Johnson, C. A. and S. J. Samuels (1997). "Screening for glaucomatous visual field loss with frequency-doubling perimetry." Invest Ophthalmol Vis Sci **38**(2): 413-425.

Johnson, C. A., J. D. Brandt, A. M. Khong and A. J. Adams (1995). "Short-wavelength automated perimetry in low-, medium-, and high-risk ocular hypertensive eyes. Initial baseline results." Arch Ophthalmol **113**(1): 70-76.

Johnson, C. A., A. J. Adams, E. J. Casson and J. D. Brandt (1993a). "Blue-on-yellow perimetry can predict the development of glaucomatous visual field loss." Arch Ophthalmol **111**(5): 645-650.

Johnson, C. A., A. J. Adams, E. J. Casson and J. D. Brandt (1993b). "Progression of early glaucomatous visual field loss as detected by blue-on-yellow and standard white-on-white automated perimetry." Arch Ophthalmol **111**(5): 651-656.

Johnson C, Adams C, Lewis R, and Adams J. (1988) Fatigue effects in automated perimetry. Applied Optics **27**: 1030-1038.

Joson, P. J., M. E. Kamantigue and P. P. Chen (2002). "Learning effects among perimetric novices in frequency doubling technology perimetry." Ophthalmology **109**(4): 757-760.

Kalaboukhova, L., V. Fridhammar and B. Lindblom (2006). "Glaucoma follow-up by the Heidelberg retina tomograph--new graphical analysis of optic disc topography changes." Graefes Arch Clin Exp Ophthalmol **244**(6): 654-662.

Kammer JA (2011) The Cost-effective Use of Diagnostic Technologies Glaucoma Today - Early Spring Issue

Kanski J.and Bowling B,, (2011). ”Clinical Ophthalmology“, Elsevier- Saunders, Edinburg, UK

Kass MA, Heuer DK, Higginbotham EJ et al. (2002): The Ocular Hypertension Treatment Study: a randomized trial determines that topical ocular hypotensive medication delays or prevents the onset of primary open-angle glaucoma. Arch Ophthalmol **120**: 701–713

Katz J (1998) “Scoring Systems for Measuring Progression of Visual Field Loss in Clinical Trials of Glaucoma Treatment”. Ophthalmology **106**: 391-395.

Katz, J., H. A. Quigley and A. Sommer (1995). "Repeatability of the Glaucoma Hemifield Test in automated perimetry." Invest Ophthalmol Vis Sci **36**(8): 1658-1664.

Katz, J., A. Sommer and K. Witt (1991). "Reliability of visual field results over repeated testing." Ophthalmology **98**(1): 70-75.

Katz, J., J. M. Tielsch, H. A. Quigley and A. Sommer (1995). "Automated perimetry detects visual field loss before manual Goldmann perimetry." Ophthalmology **102**(1): 21-26.

Kelly, D. H. (1981). "Nonlinear visual responses to flickering sinusoidal gratings." J Opt Soc Am **71**(9): 1051-1055.

Keltner, JL., Johnson CA, Quigg JM, et al, (2000) Confirmation of Visual Field Abnormalities in the Ocular Hypertension Treatment Study Arch Ophthalmol. 118(9):1187-1194.

Keltner, JL. and CA. Johnson (1995). "Short-wavelength automated perimetry in neuro-ophthalmologic disorders." Arch Ophthalmol **113**(4): 475-481.

Kerrigan-Baumrind, L. A., H. A. Quigley, M. E. Pease, D. F. Kerrigan and R. S. Mitchell (2000). "Number of ganglion cells in glaucoma eyes compared with threshold visual field tests in the same persons." Invest Ophthalmol Vis Sci **41**(3): 741-748.

Kiernan J. and Rajakumar R.,(2014). “The Human Nervous System: An Anatomical Viewpoint“. Editors Walters Lippincott ISBN-13: 978-1451173277

King-Smith, P. E., S. S. Grigsby, A. J. Vingrys, S. C. Benes and A. Supowit (1994). "Efficient and unbiased modifications of the QUEST threshold method: theory, simulations, experimental evaluation and practical implementation." Vision Res **34**(7): 885-912.

Kirwan J F , Hustler A, Bobat H, Toms L, Crabb D P and McNaught A I**2014)** Portsmouth visual field database: an audit of glaucoma progression - Eye 28, 974–979;

Knox GW. (1945) Investigations of flicker fusion. I. The effect of practice, under the influence of various attitudes, on the CFF. Journal of General Psychology,;33:121-129.

Kocabeyoglu, S., S. Uzun, M. C. Mocan, B. Bozkurt, M. Irkec and M. Orhan (2013). "Comparison of visual field test results obtained through Humphrey matrix frequency doubling technology perimetry versus standard automated perimetry in healthy children." Indian J Ophthalmol **61**(10): 576-579.

Kook M, Yang S, Kim S, Chung J, Kim S, and Tchah H (2004) Effect of cataract extraction on frequency doubling technology perimetry. Am J Ophthalmol **138**: 85-90.

Krueger D. (2013) Vigabatrin associated visual field loss (VAVFL) - White paper - Tuberous Sclerosis Alliance.

Kulkarni, C., U. R. Chaudhuri and A. Jagathesan (2013). "Bilateral acute angle-closure glaucoma following treatment with topiramate for headache." Neurol Ther

2(1-2): 57-62.

Kulze J., Stewart W, Sutherland S, and Sutherland S (1990) Factors associated with a learning effect in glaucoma patients using automated perimetry. Acta Ophthalmol 68: 681-686.

Kutzko K E, Brito C F, and Wall M (2000) Effect of Instructions on Conventional Automated Perimetry. Invest Ophthalmol Vis Sci **41**: 2006-2013.

Lachenmayr BJ (1994). The role of temporal threshold criteria in psychophysical testing in glaucoma. Curr Opin Ophthalmol. **5**, 58-63.

Lachenmayr BJ and Gleissner M (1992). Flicker perimetry resists retinal image degradation. *I*nvest Ophthalmol Vis Sci. **33**, 3539-3542.

Lachenmayr BJ and Drance (1992). Diffuse field loss and central visual function in glaucoma. Ger J Ophthalmol. 1, 67-73.

Lachenmayr, B. J., S. M. Drance, B. C. Chauhan, P. H. House and S. Lalani (1991b). "Diffuse and localized glaucomatous field loss in light-sense, flicker and resolution perimetry." Graefes Arch Clin Exp Ophthalmol **229**(3): 267-273.

Lachenmayr, B. J., S. M. Drance, G. R. Douglas and F. S. Mikelberg (1991a). "Light-sense, flicker and resolution perimetry in glaucoma: a comparative study." Graefes Arch Clin Exp Ophthalmol **229**(3): 246-251.

Lamparter J, Aliyeva S, Schulze A, Berres M, Pfeiffer N, Hoffmann E. (2013) Standard Automated Perimetry versus Matrix Frequency Doubling Technology Perimetry in Subjects with Ocular Hypertension and Healthy Control Subjects Plos/One

Lamparter J; Russel RA, Schulze A; Schuff AC; Pfeiffer N; Hoffmann E (2012) Structure-function relationship between FDF, FDT, SAP, and scanning laser ophthalmoscopy in glaucoma patients. Invest Ophthalmol Vis Sci 7;53(12):7553-9

Lamparter J, Schulze A, Schuff A, Berres M, Pfeiffer N, and Hoffman E. (2011) Learning Curve and Fatigue Effect of Flicker Defined Form perimetry Am J Ophthalmol*;***151**:1057–1064.

Lamparter J; Schulze A; Schuff AC; Pfeiffer N; Hoffmann EN. (2010) Learning Curve of Flicker Defined Form Perimetry Investigative Ophthalmology & Visual Science, Vol.51

Landers, J., A. Sharma, I. Goldberg and S. Graham (2006). "Topography of the frequency doubling perimetry visual field compared with that of short wavelength and achromatic automated perimetry visual fields." Br J Ophthalmol **90**(1): 70-74.

Landers, J., A. Sharma, I. Goldberg and S. Graham (2007). "A comparison of global indices between the Medmont Automated Perimeter and the Humphrey Field Analyzer." Br J Ophthalmol **91**(10): 1285-1287.

Lee, J. M., N. Cirineo, M. Ramanathan, K. Nouri-Mahdavi, E. Morales, A. L. Coleman and J. Caprioli (2014). "Performance of the visual field index in glaucoma patients with moderately advanced visual field loss." Am J Ophthalmol **157**(1): 39-43.

Lennie, P. (1980). "Parallel visual pathways: a review." Vision Res **20**(7): 561-594.

Leske M, Heijl A, Hussein M, Bengtsson B, Hyman L, and Komarof f E (2003) Factors for glaucoma progression and the effect of treatment: the early manifest glaucoma trial. Arch Ophthalmol **121**: 48-56.

Livingstone, M. S. and D. H. Hubel (1987). "Psychophysical evidence for separate channels for the perception of form, color, movement, and depth." J Neurosci **7**(11): 3416-3468.

Liu C, Bayer A, Cosgrove SE, Daum RS, et al., (2011) Clinical practice guidelines by the infectious diseases society of america for the treatment of methicillin-resistant Staphylococcus aureus infections in adults and children. Clin Infect Dis. 1;52(3):e18-55.

Longhin, E., E. Convento, E. Pilotto, G. Bonin, S. Vujosevic, O. Kotsafti and E. Midena (2013). "Static and dynamic retinal fixation stability in microperimetry." Can J Ophthalmol **48**(5): 375-380.

McBride, J and Rowe, FJ (2014) Review of the Use of SWAP and FDT for the Early Detection of Visual Field Loss. Ophthalmology Research: *An International Journal*. pp. 78-95.

Maddess, T. and M. R. Ibbotson (1992). "Human ocular following responses are plastic: evidence for control by temporal frequency-dependent cortical adaptation." Exp Brain Res **91**(3): 525-538.

Madea H, Nakamura M, and Negri A (2000) “New perimetric threshold test algorithm with Dynamic strategy and Tendency-Oriented Perimetry (TOP) in glaucomatous eyes”. Eye. **14**: 747-751.

Mahneke A. (1957) Flicker-fusion thresholds; comparison between the continuous and the discontinuous method. Acta Ophthalmologica;35:53-61.

Malik, R., W. H. Swanson and D. F. Garway-Heath (2012). "'Structure-function relationship' in glaucoma: past thinking and current concepts." Clin Exp Ophthalmol **40**(4): 369-380.

Malik R; Swanson WH; White E; Shewry J; Garway–Heath DF (2006) “Scaled–Stimulus Perimetry: Scaling Stimulus Size by Ganglion Cell Density Reduces the Normal Variation of Sensitivity Across Test Locations”. Investigative Ophthalmology & Visual Science, Vol.**47**, 3974.

Markowitz, S. N. and S. V. Reyes (2013). "Microperimetry and clinical practice: an evidence-based review." Can J Ophthalmol **48**(5): 350-357.

Marín-Franch, I. and W. H. Swanson (2013). "The visualFields package: a tool for analysis and visualization of visual fields." J Vis **13**(4).

Marmor MF, Kellner U, Lai TY, et al. (2011) Revised recommendations on screening for chloroquine and hydroxychloroquine retinopathy. Ophthalmology;**118**:415–22.

Martin, L. M. and A. L. Nilsson (2007). "Rarebit perimetry and optic disk topography in pediatric glaucoma." J Pediatr Ophthalmol Strabismus **44**(4): 223-231.

Martinez, G. A., P. A. Sample and R. N. Weinreb (1995). "Comparison of high-pass resolution perimetry and standard automated perimetry in glaucoma." Am J Ophthalmol **119**(2): 195-201.

Martinez A, Pareja A, Mantolan C, Sanchez M, Cordoves L, and Gonzalez de la Rosa M (1996) "Results of the Tendency-Oriented Perimetry (TOP) in normal population". Vision Res Sup Jermov*. 36, 153.*.

Matsumoto C, Takada S, Okuyama S, Arimura E, Hashimoto S and Shimomura Y. (2006) Automated flicker perimetry in glaucoma using Octopus 311: a comparative study with the Humphrey Matrix. Acta Ophthalmologica Scandinavica;**84**:210-215.

Matsuo, H., G. Tomita, Y. Suzuki and M. Araie (2002). "Learning effect and measurement variability in frequency-doubling technology perimetry in chronic open-angle glaucoma." J Glaucoma **11**(6): 467-473.

Mayer MJ, Ward B, Klein R, Talcott JB, Dougherty RF and Glucs A. (1994) Flicker sensitivity and fundus appearance in pre-exudative age-related maculopathy. Investigative Ophthalmology and Visual Science; 35:1138-114

Mayer MJ, Spiegler SJ, Ward B, Glucs A and Kim CB. (1992a) Foveal flicker sensitivity discriminates ARM risk from healthy eyes. Investigative Ophthalmology and Visual Science; 33:3143-3149.

Mayer MJ, Spiegler SJ, Ward B, Glucs A and Kim CB. (1992b) Mid-frequency loss of foveal flicker sensitivity in early stages of age-related maculopathy. Investigative Ophthalmology and Visual Science;33:3136-3142.

McBride, J and Rowe, FJ (2014) "Review of the Use of SWAP and FDT for the Early Detection of Visual Field Loss". Ophthalmology Research: An International Journal. pp. 78-95.

McCoy, A. N., H. A. Quigley, J. Wang, N. R. Miller, P. S. Subramanian, P. Y. Ramulu and M. V. Boland (2014). "Development and validation of an improved neurological hemifield test to identify chiasmal and postchiasmal lesions by automated perimetry." Invest Ophthalmol Vis Sci **55**(2): 1017-1023.

McKendrick A (2005) "Recent developments in perimetry: test stimuli and procedures". Clin Exp Optom*.* 88: 73-80.

McKendrick A and Turpin A. (2005) "Combining Perimetric Suprathreshold and Threshold Procedures to Reduce Measurement Variability in Areas of Visual Field Loss". Optom Vis Sci 82:43–51)

Medeiros, F. A., R. Lisboa, R. N. Weinreb, C. A. Girkin, J. M. Liebmann and L. M. Zangwill (2012a). "A combined index of structure and function for staging glaucomatous damage." Arch Ophthalmol **130**(9): 1107-1116.

Medeiros, F. A., L. M. Zangwill, C. Bowd, K. Mansouri and R. N. Weinreb (2012b). "The structure and function relationship in glaucoma: implications for detection of progression and measurement of rates of change." Invest Ophthalmol Vis Sci **53**(11): 6939-6946.

Medeiros, F. A., L. M. Zangwill, L. M. Alencar, P. A. Sample and R. N. Weinreb (2010). "Rates of progressive retinal nerve fiber layer loss in glaucoma measured by scanning laser polarimetry." Am J Ophthalmol **149**(6): 908-915.

Menon V, Jain D, Saxena R, Sood R. (2009) Prospective evaluation of visual function for early detection of ethambutol toxicity. Br J Ophthalmol;**93**(9):1251-4

Meyer, J. H. and J. Funk (1995). "High-pass resolution perimetry and light-sense perimetry in open-angle glaucoma." Ger J Ophthalmol **4**(4): 222-227.

Michaelides M, Stover NB, Francis PJ, Weleber RG. (2011) Retinal toxicity associated with hydroxychloroquine and chloroquine. Arch Ophthal.;**129**:30–39
Midena, E. (2006). "Microperimetry." Arch Soc Esp Oftalmol **81**(4): 183-186.

Midena E. (1989) Psychophysics and visual aging. Metabolic, Pediatric and Systemic Ophthalmology ;12:28-31.

Miglior S*,* Zeyen T*,* Pfeiffer N*,* Cunha-Vaz J*,* Torri V *&* Adamsons I *(*2005*):* Results of the European Glaucoma Prevention Study*.* Ophthalmology **112***:* 366–375*.*

Monhart M,, (2009) “Technical description of the new EyeSuite perimetry functions”. EyeSuite Perimetry New Functions Description*,* Haag-Streit AG

Monhart M, Buerki E, Bebié H, and Palmowski-Wolfe A (2006). “Calculation of the abnormal response area as an indicator of visual field changes”. Invest Ophthalmol Vis Sci. **47**: 3982.

Morales, J., M. L. Weitzman and M. González de la Rosa (2000). "Comparison between Tendency-Oriented Perimetry (TOP) and octopus threshold perimetry." Ophthalmology **107**(1): 134-142.

Montolio FGJ; Wesselink C; Gordijn M; Jansonius NM, (2012) Factors That Influence Standard Automated Perimetry Test Results in Glaucoma: Test Reliability, Technician Experience, Time of Day, and Season. Investigative Ophthalmology & Visual Science, Vol.**53**, 7010-7017

Morgan, J. E., H. Uchida and J. Caprioli (2000). "Retinal ganglion cell death in experimental glaucoma." Br J Ophthalmol **84**(3): 303-310.

Morrison JC, and Pollack IP (2003) "Glaucoma: Science and Practice" Publisher: Thieme | ISBN: 0865779155

Nayak BK,and Dharwadkar S (2014) “Interpretation of autoperimetry” - J Clin Ophthalm & Research Vol 2 (**1**) 31-59

Ng M, Racette L, Pascual JP, Liebmann JM, Girkin CA, Lovell SL, Zangwill LM, Weinreb RN, Sample PA. (2009). “Comparing the full-threshold and Swedish interactive thresholding algorithms for short-wavelength automated perimetry“ Invest Ophthalmol Vis Sci. ;50(4):1726-33.

Nevalainen J., Paetzold J., Papageorgiou E., Sample P. et al., Pamela A. (2009) Specification of progression in glaucomatous visual field loss, applying locally

condensed stimulus arrangements Graefe's Archive for Clinical and Experimental Ophthalmology , 247:1659

Newkirk, M. R., S. K. Gardiner, S. Demirel and C. A. Johnson (2006). "Assessment of false positives with the Humphrey Field Analyzer II perimeter with the SITA Algorithm." Invest Ophthalmol Vis Sci **47**(10): 4632-4637.

Nilsson, M., O. Abdiu, C. G. Laurell and L. Martin (2010). "Rarebit perimetry and fovea test before and after cataract surgery." Acta Ophthalmol **88**(4): 479-482.

Nordmann, J. P., F. Brion, P. Hamard and D. Mouton-Chopin (1998). "[Evaluation of the Humphrey perimetry programs SITA Standard and SITA Fast in normal probands and patients with glaucoma]." J Fr Ophtalmol **21**(8): 549-554.

Nouri-Mahdavi, K., N. Nassiri, A. Giangiacomo and J. Caprioli (2011). "Detection of visual field progression in glaucoma with standard achromatic perimetry: a review and practical implications." Graefes Arch Clin Exp Ophthalmol **249**(11): 1593-1616.

Nowomiejska, K., R. Vonthein, J. Paetzold, Z. Zagorski, R. Kardon and U. Schiefer (2005). "Comparison between semiautomated kinetic perimetry and conventional Goldmann manual kinetic perimetry in advanced visual field loss." Ophthalmology **112**(8): 1343-1354.

O'Leary N, Artes PH, Hutchison DM, Nicolela MT, Chauhan BC. (2012) Rates of retinal nerve fibre layer thickness change in glaucoma patients and control subjects. Eye. **26**: 1554-62

Oleszczuk JD, Bergin C and Sharkawi E. (2012) Comparative resilience of clinical perimetric tests to induced levels of intraocular straylight. Investigative Ophthalmology and Visual Science;**53**:1219-1224

Olson, J. A., A. T. Purdie and R. J. Coleman (2002). "Tangent screens are still useful in the assessment of vigabatrin induced visual field defects." Br J Ophthalmol **86**(8): 931-932.

Olsson J, Asman P, and Heijl A (1997). “A perimetric learner’s index”. Acta Ophthalmol Scand. 75: 665-668.

Olsson J, Heijl A, Bengtsson B, and Routzen H (1992) “Frequency-of-seeing in computerized perimetry:. In: Mills RP. [ed.] Perimetry Update *1992/1993*. Amsterdam/New york: Kugler Publications, pp. 551-556.

Okuyama S, Matsumoto C, Iwagaki A., Takada S and Otori T, (1999) Comparison of Threshold pupil perimetry and suprathreshold pupil perimetry Perimetry Update 1998/1999, pp. 187–191. Kugler Amsterdam/New York.

Oppenheim A. and Verghese G. (2010) Signals, systems and inference, MIT Class Notes, USA

Oztürk, F., G. F. Yavas, T. Küsbeci and S. S. Ermis (2008). "A comparison among Humphrey field analyzer, Microperimetry, and Heidelberg Retina Tomograph in the evaluation of macula in primary open angle glaucoma." J Glaucoma **17**(2): 118-121.

Pan, F. and W. H. Swanson (2006). "A cortical pooling model of spatial summation for perimetric stimuli." J Vis **6**(11): 1159-1171.

Pieron H. (1962) Neurophysiological mechanisms of critical flicker frequency and harmonic phenomena. Journal of the Optical Society of America;52:475-475

Pierre-Filho П.P, P.R. Gomes, E. T. Pierre and L. M. Pierre (2010). "Learning effect in visual field testing of healthy subjects using Humphrey Matrix frequency doubling technology perimetry." Eye (Lond) **24**(5): 851-856.

Perez CA, Gil-Arribas L, Ferreras A, Otin S, Altemir I, Fernadez S, Julvez IP, Fuertes I, (2010b) Relationship between flicker FDF perimetry and standard automated perimetry Acta Ophthalmologica Vol. 88

Perez CA, Ferreras A, Le Pablo, Pajarin AB, Polo V. (2010a) Relationship between the automated classification of Heidelberg retina tomograph and main indices of short-wavelength automated perimetry Acta Ophthalmologica Vol. 87

Phipps JA, Dang TM, Vingrys AJ and Guymer RH. (2004) Flicker perimetry losses in age-related macular degeneration. Investigative Ophthalmology and Visual Science ;45:3355-3360.

Phipps JA, Guymer RH and Vingrys AJ. (1999) Temporal sensitivity deficits in patients with high-risk drusen. Australian and New Zealand Journal of Ophthalmology ;27:265-267.

Pierre-Filho P de T, Gomes PR, Pierre ET and Pierre LM (2010) Learning effect in visual field testing of healthy subjects using Humphrey Matrix frequency doubling technology perimetry Eye; 24, 851–858

Pineles, S. L., N. J. Volpe, E. Miller-Ellis, S. L. Galetta, P. S. Sankar, K. S. Shindler and M. G. Maguire (2006). "Automated combined kinetic and static perimetry: an alternative to standard perimetry in patients with neuro-ophthalmic disease and glaucoma." Arch Ophthalmol **124**(3): 363-369.

Punjabi O.S., Lin S.C., and Stampe R.L. (2006). “Advances in Mapping the Glaucomatous Visual Field: From Confrontation to Multifocal Visual Evoked Potentials”. The Internet Journal of Ophthalmology and Visual Science. Volume 4 Number 1

Prasad, S. and S. L. Galetta (2011). "Anatomy and physiology of the afferent visual system." Handb Clin Neurol **102**: 3-19.

Quigley, H. A., G. R. Dunkelberger and W. R. Green (1989). "Retinal ganglion cell atrophy correlated with automated perimetry in human eyes with glaucoma." Am J Ophthalmol **107**(5): 453-464.

Racette L.; Tafreshi A.; Liebmann JM.; Girkin CA; Lalezary M.; Zangwill LM; Weinreb RN; Sample PA. (2008) Visual Function Specific Perimetry to Identify Glaucomatous Visual Loss Using Three Different Definitions of Visual Field Abnormality Investigative Ophthalmology & Visual Science, Vol.**49**, 1157.:

Rao, H. L., U. K. Addepalli, R. K. Yadav, N. S. Choudhari, S. Senthil and C. S. Garudadri (2014). "Factors affecting the ability of the spectral domain optical

coherence tomograph to detect photographic retinal nerve fiber layer defects." PLoS One **9**(12): e116115.

Rao, G. N., R. Khanna and A. Payal (2011). "The global burden of cataract." Curr Opin Ophthalmol **22**(1): 4-9.

Redmond T, O'Leary N, Hutchison DM, Nicolela MT, Artes PH, Chauhan BC. (2013) Visual field progression with frequency-doubling matrix perimetry and standard automated perimetry in patients with glaucoma and in healthy controls. JAMA Ophthalmol .;**131**(12):1565-72.

Redmond T. and Anderson R.S. (2011).” Visual Fields: Back to the Future”. Optometry in Practice Volume 12 Issue 1 11 – 20

Rhodes M.J..(2013). “Pilot Study Looking at the Size andVariation of the Blind Spot Scotoma in Adults Measured on the Octopus 900 Field Analyser”. Ophthalmology Research,***1*** *(1) 38-50*

Rhodes L.A., McGwin G., Huisingh C.E.,,Owsley C., Girkin C.A. (2014). “Glaucoma - screening, risk factors, and outcomes”. ARVO 2014 Annual Meeting Abstracts

Rossetti, L., P. Fogagnolo, S. Miglior, M. Centofanti, M. Vetrugno and N. Orzalesi (2006). "Learning effect of short-wavelength automated perimetry in patients with ocular hypertension." J Glaucoma **15**(5): 399-404.

Rowe, F. J. and A. Rowlands (2014). "Comparison of diagnostic accuracy between Octopus 900 and Goldmann kinetic visual fields." Biomed Res Int **2014**: 214829.

Ruelle D., (1987). Diagnosis of dynamical systems with fluctuating parameters. Proc. R. Soc. London. A 413, 5-8

Sabel, B. A., P. Henrich-Noack, A. Fedorov and C. Gall (2011). "Vision restoration after brain and retina damage: the "residual vision activation theory"." Prog Brain Res **192**: 199-262.

Saigal, R (2011) Learning effects and artefacts in automated perimetry Optometry Today; Vol. **51** Issue 22, p56

Salvetat, M. L., M. Zeppieri, L. Parisi and P. Brusini (2007). "Rarebit perimetry in normal subjects: test-retest variability, learning effect, normative range, influence of optical defocus, and cataract extraction." Invest Ophthalmol Vis Sci **48**(11): 5320-5331.

Sanabria, O., W. J. Feuer and D. R. Anderson (1991). "Pseudo-loss of fixation in automated perimetry." Ophthalmology **98**(1): 76-78.

Saunders, R. M. (1975). "The critical duration of temporal summation in the human central fovea." Vision Res **15**(6): 699-703.

Scherrer, M., J. C. Fleischhauer, H. Helbig, K. Johann Auf der Heide and F. K. Sutter (2007). "Comparison of tendency-oriented perimetry and dynamic strategy in octopus perimetry as a screening tool in a clinical setting: a prospective study." Klin Monbl Augenheilkd **224**(4): 252-254.

Schiefer, U., J. P. Pascual, B. Edmunds, E. Feudner, E. M. Hoffmann, C. A. Johnson, W. A. Lagrèze, N. Pfeiffer, P. A. Sample, F. Staubach, R. G. Weleber, R. Vonthein, E. Krapp and J. Paetzold (2009). "Comparison of the new perimetric GATE strategy with conventional full-threshold and SITA standard strategies." Invest Ophthalmol Vis Sci **50**(1): 488-494.

Schiefer U, Paetzold J , Krapp E, Nevalainen J and Besch D (2007). “Correlating nerve fibre layer defects spatially with functional loss”. Eye , 21, S25–S28

Schiefer, U., J. Pätzold and F. Dannheim (2005). "[Conventional perimetry I: introduction--basics]." Ophthalmologe **102**(6): 627-644; quiz 645-626.

Schimiti RB, Avelino RR, Kara-Jose N & Costa VP (2002):Full-threshold versus Swedish Interactive Threshold Algorithm (SITA) in normal individuals undergoing automated perimetry for the first time.Ophthalmology **109**:2084–2092.

Searle AT, Wild J, Shaw D E, and O'Neil E C (1991) Time-related variation in normal automated static perimetry. Ophthalmology 98: 701-707.

Sekhar, G. C., T. J. Naduvilath, M. Lakkai, A. J. Jayakumar, G. T. Pandi, A. K. Mandal and S. G. Honavar (2000). "Sensitivity of Swedish interactive threshold algorithm compared with standard full threshold algorithm in Humphrey visual field testing." Ophthalmology **107**(7): 1303-1308.

Shaarawy TM, Sherwood MB, Hitchings RA, Crowston JG (2009) “Glaucoma” - Elsevier Health Science Philadelphia: Saunders Limited;

Shapley, R. (1990). "Visual sensitivity and parallel retinocortical channels." Annu Rev Psychol **41**: 635-658.

Sharma A, Goldberg I, Graham St. and Mohsin M. (2000) “Comparison of the Humphrey Swedish Interactive Thresholding Algorithm (SITA) and full threshold strategies”. J Glaucoma **9**: 20-27.

Sherafat H, Spry PG, Waldock A, Sparrow JM and Diamond JP (2003). Effect of a patient training video on visual field test reliability. British Journal of Ophthalmology**,** **87**, 153-156.

Shirakashi, M., H. Abe, S. Sawaguchi and S. Funaki (1997). "Measurement of thickness of retinal nerve fiber layer by scanning laser polarimetry and high-pass resolution perimetry in patients with primary open-angle or normal-tension glaucoma." Acta Ophthalmol Scand **75**(6): 641-644.

Shirakashi, M., S. Funaki, H. Funaki, K. Yaoeda and H. Abe (1999). "Measurement of retinal nerve fibre layer by scanning laser polarimetry and high pass resolution perimetry in normal tension glaucoma with relatively high or low intraocular pressure." Br J Ophthalmol **83**(3): 353-357.

Siddiqui MA, Khairy HA and Azuara-Blanco A. (2007) Effect of cataract extraction on SITA perimetry in patients with glaucoma. Journal of Glaucoma;**16**:205-208.

Spry PG, Johnson CA, SL M, and Cioffi GA (2005) Psychophysical investigation of ganglion cell loss in early glaucoma. J Glaucoma. **14**: 11-19.

Spry, P. G., C. A. Johnson, A. M. McKendrick and A. Turpin (2001). "Variability

components of standard automated perimetry and frequency-doubling technology perimetry." Invest Ophthalmol Vis Sci **42**(6): 1404-1410.

Spry P, and Johnson C (2002) Identification of Progressive Glaucomatous Visual Field Loss. Survey of Ophthalmology **(47)**: 158-173.

Stanojcic, N., M. Wilkins, C. Bunce and A. Ionides (2010). "Visual fields in patients with multifocal intraocular lens implants and monovision: an exploratory study." Eye (Lond) **24**(11): 1645-1651.

Stavrou EP and Wood JM. (2005) Central visual field changes using flicker perimetry in Type 2 diabetes mellitus. Acta Ophthalmologica Scandinavica 83:574-580.

Strouthidis N, Scott A, Viswanathan A, Crabb D, and Garway-Heath (2007) Monitoring glaucomatous visual field progression: The effect of a novel spatial filter.. Invest Ophthalmol Vis Sci. **48**: 251-257.

Strouthidis N; Vinciotti V; Tucker A; Gardiner S; Crabb D ; Garway-Heath D, (2006) Structure and Function in Glaucoma: The Relationship between a Functional Visual Field Map and an Anatomic Retinal Map Investigative Ophthalmology & Visual Science Vol.**47**, 5356-5362

Swanson, W. H. (2013). "Stimulus size for perimetry in patients with glaucoma." Invest Ophthalmol Vis Sci **54**(6).

Swanson, W. H., V. E. Malinovsky, M. W. Dul, R. Malik, J. K. Torbit, B. M. Sutton and D. G. Horner (2014). "Contrast sensitivity perimetry and clinical measures of glaucomatous damage." Optom Vis Sci **91**(11): 1302-1311.

Swanson WH, Sun H, Lee BB, Cao D. (2011) Responses of primate retinal ganglion cells to perimetric stimuli. Invest Ophthalmol Vis Sci;**52**:764-771.

Swanson, W.H., Dul,M.W.and S E.Fischer (2005). "Quantifying effects of retinal illuminance on frequency doubling perimetry." Invest Ophthalmol Vis Sci **46**(1): **235-240.**

van der Schoot, J., N. J. Reus, T. P. Colen and H. G. Lemij (2010). "The ability of short-wavelength automated perimetry to predict conversion to glaucoma." Ophthalmology **117**(1): 30-34.

Tate G.W. (1985) Physiological basis for perimetry. In: Drance SM, Anderson DR (eds) Automatic perimetry in Glaucoma: A practical guide, pp 1-28. Orlando, Florida, Grune & Stratton.

Thompson, H.S., and Wall, M., (2010). "A history of perimetry". Imaging and Perimetry Society (IPS).

Todorova MG, Palmowski-Wolfe AM., Schoetzau A., Flammer J and Monhart MJ (2013). "A Comparison between the Pulsed Rising Amplitude Perimetry and the Normal Staircase Strategy in Standard Automated Perimetry". J Clin Exp Ophthalmol **4**:283.

Turpin A, Artes PH; McKendrick AM (2012) The Open Perimetry Interface: An enabling tool for clinical visual psychophysics Journal of Vision , Vol.12, 22

Turpin, A., A. M. McKendrick, C. A. Johnson and A. J. Vingrys (2003). "Properties of perimetric threshold estimates from full threshold, ZEST, and SITA-like strategies, as determined by computer simulation." Invest Ophthalmol Vis Sci **44**(11): 4787-4795.

Van Coevorden RE, Mills RP, Chen YY and Bamebey HS (1999). Continuous visual field test supervision may not always be necessary. Ophthalmology, **106**, 178-181.

Van der Schoot, J., N. J. Reus, T. P. Colen and H. G. Lemij (2010). "The ability of short-wave-length automated perimetry to predict conversion to glaucoma."Ophthalmology **117**(1):30-34.

Vingrys AJ and Pesudovs K. (1999) Localized scotomata detected with temporal modulation perimetry in central serous chorioretinopathy. Australian and New Zealand Journal of Ophthalmology;27:109-116

Vislisel, J. M., C. K. Doyle, C. A. Johnson and M. Wall (2011). "Variability of rarebit and standard perimetry sizes I and III in normals." Optom Vis Sci **88**(5): 635-639.

Vonthein, R., S. Rauscher, J. Paetzold, K. Nowomiejska, E. Krapp, A. Hermann, B. Sadowski, C. Chaumette, J. M. Wild and U. Schiefer (2007). "The normal age-corrected and reaction time-corrected isopter derived by semi-automated kinetic perimetry." Ophthalmology **114**(6): 1065-1072.

Wabbels, B. K., S. Diehm and G. Kolling (2005). "Continuous light increment perimetry compared to full threshold strategy in glaucoma." Eur J Ophthalmol **15**(6): 722-729.

Wabbels, B. K. and S. Wilscher (2005). "Feasibility and outcome of automated static perimetry in children using continuous light increment perimetry (CLIP) and fast threshold strategy." Acta Ophthalmol Scand **83**(6): 664-669.
Wall, M. (2004). "What's new in perimetry." J Neuroophthalmol **24**(1): 46-55.

Wall, M., C. K. Doyle, T. Eden, K. D. Zamba and C. A. Johnson (2013a). "Size threshold perimetry performs as well as conventional automated perimetry with stimulus sizes III, V, and VI for glaucomatous loss." Invest Ophthalmol Vis Sci **54**(6): 3975-3983.

Wall, M., C. K. Doyle, K. D. Zamba, P. Artes and C. A. Johnson (2013b). "The repeatability of mean defect with size III and size V standard automated perimetry." Invest Ophthalmol Vis Sci **54**(2): 1345-1351.

Wall, M., K. R. Woodward, C. K. Doyle and G. Zamba (2010). "The effective dynamic ranges of standard automated perimetry sizes III and V and motion and matrix perimetry." Arch Ophthalmol **128**(5): 570-576.

Wall, M., K. R. Woodward, C. K. Doyle and P. H. Artes (2009). "Repeatability of automated perimetry: a comparison between standard automated perimetry with stimulus size III and V, matrix, and motion perimetry." Invest Ophthalmol Vis Sci **50**(2): 974-979.

Wall, M., R. J. Maw, K. E. Stanek and B. C. Chauhan (1996). "The psychometric function and reaction times of automated perimetry in normal and abnormal areas of the visual field in patients with glaucoma." Invest Ophthalmol Vis Sci **37**(5): 878-885.

Walsh J T (2011) “Ophthalmology Monographs” Vol.3*:* Visual Fields, Examination and Interpretation. New York: Oxford University Press.

Walsh J T (1978) *“*Neuro-Ophthalmology: Clinical Signs and Symptoms*”*. 4th ed. Baltimore: Williams & Wilkins.

Wang YZ, and Henson DB. (2012) “Diagnostic Performance of Visual Field Test Using Subsets of the 24-2 Test Pattern for Early Glaucomatous Field Loss”, OVS*,* Vol. 54, No. **1**

Weijland A, Fankhauser F., Bebie H., Flammer J., (2004). “Automated Perimetry” - Visual Field Digest 05/06 Haag-Streit AG ISBN 3-033-00108-

Weber J, and Klimaschka T (1995) “Test time and efficiency of the dynamic strategy in glaucoma perimetry”. Ger J Ophthalmol. 4.: 25-31.

Weber, J. and S. Rau (1992). "The properties of perimetric thresholds in normal and glaucomatous eyes." Ger J Ophthalmol **1**(2): 79-85.

Werner E, (2011). The Medical Textbook - Chapter 214 – “Visual Field Perimetry in Glaucoma”. Ophthalmology*;* World Press

Werner E, Krupin T, Adelson A, and Feitl M (1990) Effect of patient experience on the results of automated perimetry in glaucoma suspect patients. Ophthalmology*. .* 97: 44-48.

Werner E, Adelson A, and Krupin T (1988) Effect of patient experience on the results of automated perimetry in clinically stable glaucoma patients. Ophthalmology*. .* 95: 764-767.

Wild JM, Kim S L, Pacey I E, and Cunliffe I A (2006) Evidence for a Learning Effect in Short-Wavelength Automated Perimetry. *Ophthalmology* 113: 206-215.

Wild, J. M. (2001). "Short wavelength automated perimetry." Acta Ophthalmol Scand **79**(6): 546-559.

Wild, J. M., I. E. Pacey, S. A. Hancock and I. A. Cunliffe (1999a). "Between-algorithm, between-individual differences in normal perimetric sensitivity: full threshold, FASTPAC, and SITA. Swedish Interactive Threshold algorithm." Invest Ophthalmol Vis Sci **40**(6): 1152-1161.

Wild JM, Pacey I, O’Neill E, and Cunliffe I (1999b) “The SITA perimetric threshold algorithms in glaucoma”. Invest Ophthalmol Vis Sci*.* 40, : 1998-2009. .

Wild, J. M., R. P. Cubbidge, I. E. Pacey and R. Robinson (1998). "Statistical aspects of the normal visual field in short-wavelength automated perimetry." Invest Ophthalmol Vis Sci **39**(1): 54-63.

Wild, J. M., A. E. T. Searle, M. Dengler-Harles, E. C. O'Neill, (1991) Long-term follow-up of baseline learning and fatigue effects in the automated perimetry of glaucoma and ocular hypertensive patients. Acta Ophthalmologica, 69: 210–216.

Wild J.M, Dengler-Harles' M., Searle A.E.T, O'Neill E.C, and Crews S. J (1989) The influence of the learning effect on automated perimetry in patients with suspected glaucoma. Acta Ophthalmol 67: 537-545.

Wood M, Wild J M, Hussey M K, and Crews S j (1987) Serial examination of the normal visual field using Octopus automated projection perimetry. Evidence of a learning effect. Acta Ophthalmol 65: 326-333.

Wu, Ling-Ling; Suzuki, Yasuyuki; Kunimatsu, Shiho; Araie, Makoto; Iwase, Aiko; Tomita, Goji (2001) Frequency Doubling Technology and Confocal Scanning Ophthalmoscopic Optic Disc Analysis in Open-angle Glaucoma With Hemifield Defects Journal of Glaucoma Volume 10 - Issue 4 - pp 256-260

Yaqub, M. (2012). "Visual fields interpretation in glaucoma: a focus on static automated perimetry." Community Eye Health **25**(79-80): 1-8.

Zeppieri, M., P. Brusini, L. Parisi, C. A. Johnson, R. Sampaolesi and M. L. Salvetat (2010). "Pulsar perimetry in the diagnosis of early glaucoma." Am J Ophthalmol **149**(1): 102-112.

Zeppieri, M., S. Demirel, K. Kent and C. A. Johnson (2008). "Perceived spatial frequency of sinusoidal gratings." Optom Vis Sci **85**(5): 318-329.

Zulauf, M., P. Fehlmann and J. Flammer (1996). "[Perimetry with normal Octopus technique and Weber 'dynamic' technique. Initial results with reference to reproducibility of measurements in glaucoma patients]." Ophthalmologe **93**(4): 420-427.

Zulauf M, Fehlmann P, and Flammer J (1994) “Efficiency of the standard Octopus bracketing procedure compared to that of the ‘Dynamic strategy’ of Weber”. In: Mills RP and Wall M [ed.] Perimetry update 1994/95*. Amsterdam/ New York: Kugler Publications, 1995. 422-437*